Fakultät für Maschinenwesen

Lehrstuhl für Anlagen- und Prozesstechnik

New Routes for Efficient and Sustainable Oxymethylene Ethers Synthesis

Mohamed Kamal Ouda Salem

"The first step to knowledge is to know we are ignorant"

Socrates 470 to 390 B.C.

This cumulative thesis is composed from the following peer reviewed research articles as first author

- Paper 1: Ouda, M.; Yarce, G.; White, R. J.; Hadrich, M.; Himmel, D.; Schaadt, A.; Klein, H. et *al.* (**2017**): Poly(oxymethylene) dimethyl ether synthesis – a combined chemical equilibrium investigation towards an increasingly efficient and potentially sustainable synthetic route. In: *React. Chem. Eng. 2017,* 2, S. 50–59. DOI: 10.1039/C6RE00145A.

- Paper 2: Ouda, M.; Mantei, F. K.; Elmehlawy, M.; White, R. J.; Klein, H.; Fateen, S.-E. K. (**2018**): Describing oxymethylene ether synthesis based on the application of non-stoichiomsetric Gibbs minimisation. In: *React. Chem. Eng. 2018*, 3, S. 277-292. DOI: 10.1039/C8RE00006A.

- Paper 3: Ouda, M.; Mantei, F. K.; Hesterwerth, K.; Bargiacchi, E; Klein, H.; White, R. J. (**2018**): A hybrid description and evaluation of Oxymethylene dimethyl ethers synthesis based on endothermic dehydrogenation of methanol. In: *React. Chem. Eng. 2018*, 3, S. 676-695. DOI: 10.1039/C8RE00100F.

Foreword

This thesis was written during my time as a scientific assistant at the Fraunhofer institute for solar energy systems ISE and as PhD student at the institute of plant and process technology at the technical University of Munich APT-TUM. A lot of people in both institutes contributed directly and indirectly to this work. I would like to express my appreciation and gratitude for everyone of them.

Special thanks to my supervisor Prof. Dr.-Ing. Harald Klein for his trust to supervise this work and his support along this journey which will impact my whole life. His presence and readiness to help was something to learn besides the scientific exchange that I enjoyed.

Thanks for Prof. Dr.-Ing. Matthias Kraume for taking over the second supervision.

Thanks for Dr. Achim Schaadt and Dr. Robin White for their supervision at the Fraunhofer institute for Solar energy systems ISE and for their continouos support and orientation. Many thanks to Dr. Christopher Hebling, the head of Hydrogen-technologies division at Fraunhofer ISE for the trust and support on the personal and professional levels.

Many thanks to all the co-authors and my students who did great work and gave me the chance to learn new things and widen my horizons.

Special thanks to my colleagues and friends Christoph Hank, Valentine Leible, Lara Theiss, Kläre Chlinsmann, Max Hadrich, Florian Rümmeler, Robert Szolak, Anand Kakadyia, Johannes Full, Florian Nestler, Malte Otromke, Monika Bosilij and Tom Smolinka for their support: Working with you was more than great.

My partner and very special supporter Carla: very grateful for your sincere care and support in the good and very hard times.

Freiburg, den 01.07.2019   M. Ouda

Kurzfassung

Die C1-Oxygenate Oxymethylendimethylether (OME) sind ein interessanter Dieselersatz, der bei der Verbrennung in Dieselmotoren auch unter realen Fahrbedingungen eine deutliche Reduzierung der PM-Emissionen ermöglicht. OME werden auch als attraktive "grüne" Lösungsmittel und CO_2-Absorber untersucht. Sie werden auf Basis von Methanol (MeOH) hergestellt, so dass ein auf fossilen oder erneuerbaren Energiequellen basierender Rohstoff verwendet werden kann. In dieser Arbeit wird ein einfaches, skalierbares und praktikables OME-Syntheseverfahren (im weiteren Textverlauf bezeichnet als direkte OME-Synthese) eingeführt, welches ausschließlich auf dem Rohstoff MeOH basiert. Die Synthese erfolgt in zwei Schritten, der endothermen katalytischen Dehydrierung von MeOH zu wasserfreiem Formaldehyd (FA) und Wasserstoff (H_2). Dieses wasserfreie Produkt wird in einem zweiten Schritt direkt in den OME-Synthesereaktor eingeführt, was zu einer sehr hohen Ausbeute von 14% g $g^{-1}_{product}$ führt. Die Prozesssimulation wurde in einer hybriden Simulationsplattform implementiert, die die Vorteile der Verwendung von selbst entwickelten Reaktormodellen mit kommerziell verfügbaren Algorithmen kombiniert.

Das kombinierte chemische und Phasengleichgewicht der OME-Synthesereaktion wurde durch die Lösung der Gleichgewichtsbeziehungen mit dem Newton-Raphson-Ansatz beschrieben. Versuche im Batch-Autoklaven mit MeOH und para-Formaldehyd (p-FA) wurden mit DW50X2 und Amberlyst 36 Katalysatoren bei unterschiedlichen Temperaturen und Feedverhältnissen durchgeführt. Die Ergebnisse wurden für die Validierung des in Matlab® implementierten OME-Reaktormodells verwendet. Parametrische Studienergebnisse zeigten, dass eine sehr hohe OME$_{3-5}$ Ausbeute bei einem FA/MeOH-Molverhältnis von 1,8-2, einer Temperatur von 60 °C und dem geringsten Wassergehalt im Feed erreicht werden konnte. Die Ergebnisse zeigten zudem, dass die Temperatur die Gleichgewichtsreaktion nicht wesentlich beeinflusst.

Basierend auf den bisherigen Ergebnissen wurde die Prozessleistung des wichtigsten Prozessschrittes, der endothermen MeOH-Dehydrierung zu FA und H_2, definiert. Zur Prüfung der Dehydrierungsreaktion wurde eine kontinuierliche Versuchsanlage aufgebaut. Für dieses kinetisch gesteuerte Reaktionssystem wurde ein ringförmiger Gegenstromreaktor entwickelt. Die Tests wurden mit Na_2CO_3 bei T = 650-700 °C, mit einer MeOH-Feedkonzentration <10 vol.% und $GHSV$ zwischen 7-35×10^3 h^{-1} durchgeführt. Die beste Prozessleistung wurde mit 40% MeOH-Umsatz bei >90% FA-Selektivität erzielt. Diese Prozessleistung lag in der Nähe der gewünschten Ergebnisse. Jedoch verringerte sich die Katalysatorselektivität gegenüber FA nach einigen Stunden im Betrieb, während die MeOH-Umsatz zunahm. Die Katalysatorentwicklungen für dieses Reaktionssystem und die Skalierung der innovativen Reaktorkonzepte sollen weiter untersucht werden. Dennoch wurden die Ergebnisse aus den stationären Tests dieser Reaktion zur Ermittlung experimenteller Reaktionsratenkonstanten bei 690 °C

verwendet und ein einfaches globales kinetisches Modell dieses Reaktionssystems abgeleitet.

Die Ausbeute an OME-Produkten wird durch das chemische Gleichgewicht und die Rückführung von Nicht-Reaktanten begrenzt. Zudem werden andere OME-Fraktionen als die des gewünschten OME-Wunschproduktes für eine zufriedenstellende Prozessausbeute unerlässlich. Die Modellierung dieses komplexen Reaktionsgleichgewichtssystems mit 32 Komponenten, die an 29 gleichzeitigen Reaktionen teilnehmen, unter Berücksichtigung der Rückführung ist herausfordernd. Die OME-Gleichgewichtszusammensetzung unter Berücksichtigung der Rückführung wurde dann durch die Anwendung des nicht-stöchiometrischen Gibbs-Ansatzes zur ungehinderten Minimierung unter Verwendung eines stochastischen globalen Optimierers beschrieben. Dieses Modell wurde mit Hilfe von Trioxan (TRI) und Methylal (OME_1) als Feed über den Amberlyst 36 Katalysator validiert. Die Modellergebnisse ermöglichten es das optimale FA/MeOH-Feedmolverhältnis von 1,8 zu definieren, was die gewünschte endgültige OME_{3-5}-Produktverteilung bei einer sehr hohen Ausbeute von 80,3 Gew.% (MeOH zu OME_{3-5}) und einem minimalen Rückführungsverhältnis von ca. 2,8 $mol_{recycle}$ mol^{-1}_{feed} ergibt. Die Ergebnisse des OME-Reaktionsgleichgewichtsmodells wurden zusammen mit den Ergebnissen des globalen kinetischen Reaktormodells der FA-Synthese sowohl in der Matlab®-Software implementiert als auch in eine CHEMCAD®-Plattform integriert, in der alle Komponenten des Prozessfließbildes enthalten sind. Die Integration erfolgte durch die Einbindung eines benutzerdefinierten Excel®-VBA-Blocks in CHEMCAD®, welcher die beiden Programme miteinander kommunizieren lässt. Ein physikalisches Stoffdatenmodell wurde in CHEMCAD® implementiert und die rigorosen Destillationskolonnen-Algorithmen zur Trennung der OME-Produktmischung verwendet. Die Integration der Prozesswärme erfolgte mit der Software PinCH 2.0. Für die Datenaufbereitung der PinCH-Ergebnisse wurde ein VBA-Code zur Stromdatenextraktion, Prozessstromsegmentierung nach Phasenänderung und Wärmekapazitätsauswertung entwickelt. Schließlich wurde ein einfaches Produktionskostenmodell implementiert und die Prozesskennzahlen definiert. Nach der Integration der Prozesswärme konnte der Dampfverbrauch um 16,1% und der Kühlwasserverbrauch um 30,4% gesenkt werden.

Bei einer jährlichen Produktionskapazität von 35 kt OME_{3-5} beträgt die Gesamtprozessausbeute MeOH bis OME_{3-5} 80,3%, die Prozessenergieeffizienz 71,7%, der spezifische Dampfverbrauch 2,31 MWh pro t OME_{3-5} und die Produktionskosten 903 US\$ pro t OME_{3-5} (0,16 €ct./kWh). Die MeOH-Kosten sind mit 47% des Produktionskostenanteils der größte Anteil, gefolgt von den Energiekosten mit 22,3% und der Produktionskapazität. Bei einer großen jährlichen Produktionskapazität von 1000 kt und MeOH-Feedkosten von 300 US\$ pro t betragen die geschätzten Produktionskosten nach dem in dieser Arbeit beschriebenen Verfahren 599 US\$ pro t OME_{3-5} (0,10 €ct./kWh). Dies stellt die niedrigsten Produktionskosten im

Vergleich zum verfügbaren Literaturprozess dar und zeigt das Potenzial des vorgestellten OME-Produktionsprozesses. Das im Rahmen dieser Arbeit entwickelte Hybridmodell ermöglicht eine zuverlässige und robuste Prozessbewertung und kann bei korrekter Definition der Prozesskomponenten und -parameter für verschiedene Prozesskonzepte eingesetzt werden.

Abstract

The C1-oxygenates oxymethylene dimethyl ethers (OME) are attracting interest as potential diesel substitutes as they offer significant emission reductions upon combustion (e.g. particulate matter, NOx *etc*.), as well as being potentially attractive low vapour pressure "green" solvents (e.g. in CO_2 capture applications). They are synthesized based on methanol (MeOH), which can be source from fossil (e.g. via steam methane reforming) or renewable (e.g. CO_2 hydrogenation) feedstocks. In this thesis a potentially scalable and feasible OME synthesis process (denoted heron as the "direct OME synthesis") is described based on the endothermic catalytic dehydrogenation of MeOH to yield anhydrous Formaldehyde (FA) and H_2, followed by a low temperature acid catalyzed OME synthesis step. Anhydrous FA is directly introduced to the OME synthesis reactor which leads to very high single path target product OME_{3-5} yield of 14% [g $g^{-1}_{product}$]. The process flow sheet was implemented *via* a hybrid simulation platform combining the merits of using "in-house" developed reactor models together with commercially available software and algorithms.

The combined chemical and phase equilibrium of the OME synthesis reaction was described by solving the equilibrium relations using Newton-Raphson approach. Experiments in batch autoclave using MeOH and para-formaldehyde (p-FA) feed were carried out using commercial DW50X2® and Amberlyst 36® catalysts at different temperatures and feed ratios. The results were used to validate the OME reactor model implemented in Matlab®. Parametric study results showed that very high OME_{3-5} yield could be achieved at FA/MeOH molar ratio 1.8-2, temperature of 60 °C and the least water content in the feed. Additionally, the results emphasized that the temperature is not significantly influencing the equilibrium reaction.

Based on the previous results, the performance of the key process step of MeOH endothermic dehydrogenation to FA and H_2 was defined. A continuous test setup was constructed for testing the dehydrogenation reaction. An annular counter current reactor was developed for this kinetic controlled reaction system. Tests were carried out using Na_2CO_3 at T = 650-700 °C, with MeOH feed concentration <10 vol.% and GHSV between 7-35 $\times 10^3$ h^{-1}. The best performance achieved was 40% MeOH conversion at >90% FA selectivity. This performance was in the vicinity of the desired results; however the catalyst selectivity towards FA was reducing after several hours on stream while the MeOH conversion was increasing. Catalyst developments for this reaction system and scaling up the innovated reactor concepts are to be further investigated. Nevertheless, the results obtained from steady state tests of this reaction were used for extraction of experimental reaction rate constants at 690 °C and implement a simple global kinetic model of this reaction system.

OME product yield is limited by the chemical equilibrium and recycle of non-reactants and OME fractions other than the desired OME product is essential for achieving satisfying process yield. Modelling this complex reaction equilibrium system involving 32 components participating in 29 simultaneous reactions while considering recycling is cumbersome. The OME equilibrium composition considering recycle was then described by adopting non-stoichiometric Gibbs unconstrained minimization technique using stochastic global optimizer. This model was validated against batch experimental data set using trioxane (TRI) and methylal (OME_1) as the feed over Amberlyst 36® catalyst. The model results enabled defining the optimum FA/MeOH feed molar ratio of 1.8 which results in the desired final OME_{3-5} product distribution at a very high yield of 80.3 wt.% (MeOH to OME_{3-5}) and minimum recycle ratio of *ca.* 2.8 [$mol_{recycle}$ mol^{-1}_{feed}]. The OME reaction equilibrium model results together with the FA global kinetic reactor model results were both implemented using Matlab® software and integrated in a CHEMCAD® platform were all the process flow sheet components are included. The integration was done by including a user-defined Excel® unit in CHEMCAD® which interfacing the two software *via* a VBA node. A physical property model was implemented in CHEMCAD® and the rigorous separation columns algorithms were used for separating the OME product mixture. The process heat integration was done using PinCH 2.0 software. A VBA code for stream data extraction, process streams segmentation according to phase change and heat capacities evaluation was developed for data preparation for PinCH software. Finally, a simple production cost model was implemented and the process key performance indicators were defined. After the process heat integration, the steam consumption was reduced by 16.1% and cooling water consumption was reduced by 30.4%.

At annual production capacity of 35 kt OME_{3-5}, the overall process yield MeOH to OME_{3-5} is 80.3%, the process energy efficiency is 71.7%, the specific steam consumption is 2.31 MWh/t OME_{3-5} and the production cost is 951.5 US$ per t OME_{3-5} (0.16 €ct./kWh). The MeOH cost is the major production cost factor with 47% of the production cost share followed by the energy cost of 22.13% and then the production capacity. At large annual production capacity of 1000 kt and MeOH feed cost of 300 US$ per t, the assessed production cost using the process described in this work is US$ 598.7 per t OME_{3-5} (0.10 €ct./kWh). This represents the lowest production cost in comparison with the available literature process and demonstrates the potential of the presented OME production process. The hybrid model developed in the frame of this thesis allows reliable and robust process evaluation and can be applied for different process concepts once the process components and parameters are correctly defined.

Table of Contents

List of Tables

List of Figures

Nomenclature

Abbreviations

Abbreviations	Full Name
A-36	Amberlyst®-36
A-46	Amberlyst®- 46
$E_{process}$	Total energy required for production process
FA	Formaldehyde
GHGE	Green House Gas Emissions
HF	Polyoxymethylene hemiformals
LHV	Lower Heating Value
MEFO	Methyl Formate
MeOH	Methanol
MG	Polyoxymethylene glycols
NO_x	Nitrous oxides
NRS	Newton-Raphson
OME	Oxymethylene Ethers
OME_n	Oligomer of OME of chain length n
PM	Particulate Matter
POMDE	Poly-Oxymethylene Dimethyl Ethers
p-FA	Paraformaldehyde
SGO	Stochastic Global Optimizer
TRI	Trioxane
VBA	Visual Basics for Applications
VLE	Vapor-Liquid- Equilibrium
VLLE	Vapor-Liquid-Liquid-Equilibrium
VOC	Volatile Organic Compounds

Symbols and Indices

Symbol or Index	Name	Unit
γ_i	Activity coefficient	-
f^l_i	Fugacity of component i in liquid phase	bar
f^v_i	Fugacity of component i in vapor phase	bar
G^t	Gibbs free energy	J/mol
G_i^0	Gibbs free energy at standard conditions	J/mol
K	Equilibrium constant	-
μ_i	chemical potential of species i	J/mol
v_i	Stoichiometric coefficient	-
n_i	Molar amount	mol
P	Pressure	bar
P_i^{sat}	Saturation pressure	bar
R	Gas constant	J/mol.K
T	Temperature	K
t	Metric tonnes	t
w_i	Mass fraction of component i	
x_i	Molar fraction liquid phase	-
y_i	Molar fraction gas phase	-
N_{io}	Initial Feed	mol

1 Introduction

1.1 Context

According to international renewable energy agency (IRENA) report, three earths are needed to satisfy the growing raw materials, water and energy demands of our modern society (+80% Energy, +55% water and +60% food demand growth by 2050 relative to 2015 with 8.2 billion global population by 2050).[1] Fossil fuels are of the main pillars where modern economy depends on to produce materials, in agriculture, in water economy and to generate the required energy.[2] Anthropogenic exploration, extraction and combustion of fossil fuels contributes significantly to emissions of greenhouse gases (GHG) and consequently to global warming (GW) phenomena.[2] In this context world leaders committed themselves (most recently in the frame of COP 23) to undertake mitigation actions to limit the increase of the global average temperature well below 2 °C relative to the pre-industrial levels.[3,4] On the global level, CO_2 emissions are of the main addressed contributors to the GHG level increase and consequently to GW.[5] GHG emissions reduction targets of 40% relative to 1990 levels were set by the European Union (EU) till 2030.[2] In Germany, a greenhouse gas neutral concept was introduced by the German Environmental Agency (UBA) where technical reduction measures were defined for the different GHG emissions contributing sectors.[3] In 2016 the German cabinet adopted the climate change action plan 2050 with a reduction target of 80 to 95% lower GHG emissions than the levels of 1990.[2] The sectorial contribution to these GHG emissions have been dissected with relation to corresponding reduction targets up to 2050 (Figure 1).[2]
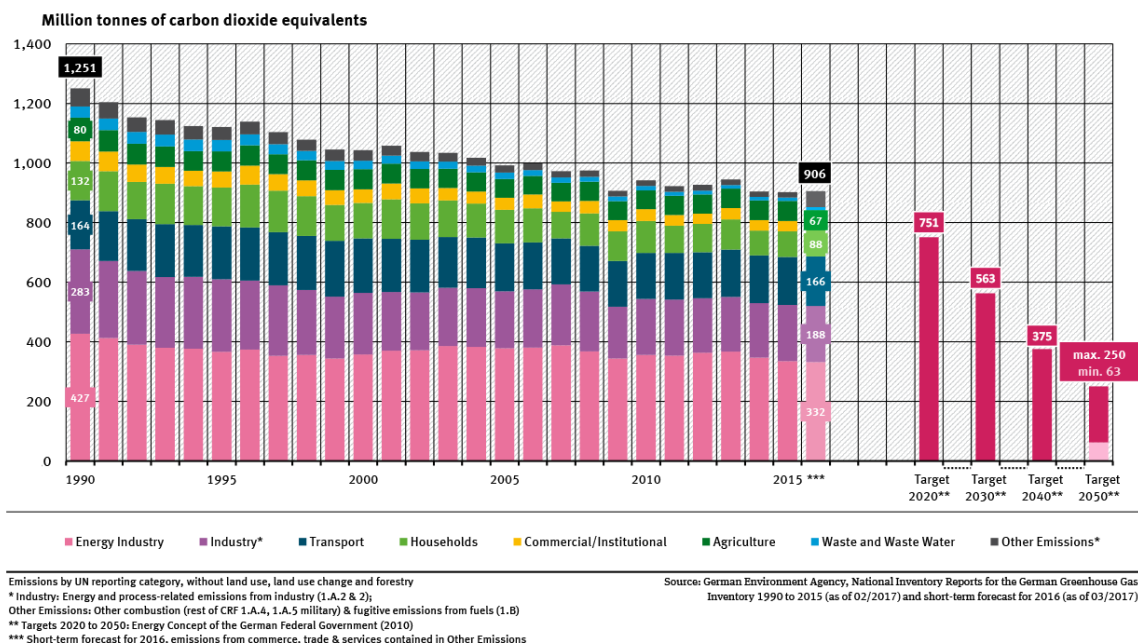
Figure 1 Sectorial CO_2 emissions in Germany from 1990 till 2016 with the emission reduction milestones till 2050.[6]

The energy industry is one of the main contributing sectors to the GHG emissions with 36% share in 2016. Primary energy consumption in Germany reduced by 10% between 1990 and 2016 due to energy efficiency and energy saving measures together with the increase of the renewable energy (RE) share.[2] Using and generating energy is mainly based on combustion of fossil fuels with a small share to nuclear based generators and other power generation forms. This energy generation and use trend harm the environment not only due to the GHG emissions form combustion processes, rather from extraction of the raw materials, transporting to energy generation plants were also water pollution or earth surface damage are considered.[7] The current RE electricity generation share in Germany is 31.7% (2016) with the long term target of having 80% RE electricity share by 2050.[7] RE supply offers several advantages as security of supply and de-fossilization of the energy industry sector; however the intermittence characteristic of RE systems is still challenging aspect for electrical grid management. Energy storage technologies that are capable for robust energy storage in large scale and for long durations are imperative to be developed along with expansion of RE capacities (RE power generation of 210 TWh with 38.5% share of net electricity generation in 2017).[8] Several mechanical, electro-chemical and thermal energy storage solutions are established or under development for short and moderate term electricity storage and also for limited take-up capacities.[8] Chemical energy storage based on electricity conversion *via* water electrolysis to H_2 and O_2 followed by conversion of H_2 to different energy carriers of interest is a promising option for long term and seasonal storage capacities. Together with the benefits of different sector coupling and storage in unlimited capacities, chemical energy storage creates opportunities for increased flexibility and optimization of the power generation system.[8]

On the other hand the transport sector is one of the most primary energy consumers with 30% share of the primary energy consumption and contributes to 20% of the net CO_2 emissions.[9] In the last two and half decades as shown in Figure 1, the transport sector is the only sector in Germany with no net CO_2 emission reduction contribution. The European Commission amended reduction targets for the CO_2 emissions of the transport sector of less than 60% by 2050 relative to that of 1990.[10] On the local emissions side the Euro emissions norms (most recent Euro 6d-TEMP)[11] were reduced almost by hundred folds between Euro 1 and Euro 6 regarding the NO_x and fine particulate matter PM emissions. Half million premature deaths in European cities where directly related to the latter.[11,12] This urban mobility local emission issue is becoming a heavy public debate and some legislations are under discussion regarding completely prohibiting combustion engine based drive trains in big cities or only allowance to drive for certain periods of the day or with special permits.[13] The transport sector constitutes mainly of road fright and road passengers with *ca.* 82% of primary energy consumption share and *ca.* 90% of net CO_2 emissions. (Figure 2 a and b).[9,14] According to EU study for energy, transport and GHG till 2050, diesel fuel consumption is projected to be constant or increases in Europe till 2050 (Figure 2c) as a preferred drive train with high combustion efficiency and relatively lower market price in comparison with gasoline.[15,16]
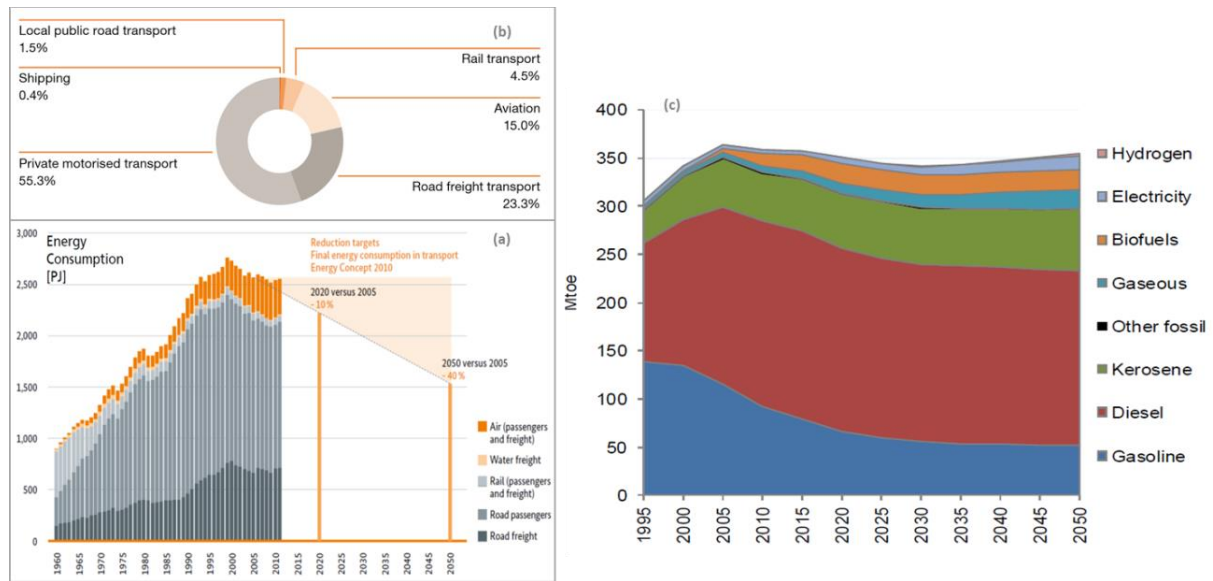
Figure 2 (a) Total primary energy consumption of different mobility sector mode of transport;[9] (b) CO_2 emissions by mode of transport;[17] (c) Final energy demand by fuel type up to 2050 according to EU trends.[15]

With the fast growing transport sector with more than 1.2 billion private vehicles on the roads worldwide with growth rates approaching human beings, solutions leading to CO_2-neutral mobility with limited or no local emissions are necessary.[18] Several potential alternatives for tackling the mobility sector challenges are addressed as follows:

1. Optimization of combustion engine (in-engine measures or exhaust gas treatment systems)
2. Switching to electrical drive train with batteries or H_2 fuel cells
3. Using biofuels with drop-in capability
4. Using synthetic fuels as an active substance in internal combustion engines.[18–20]

The optimization of the combustion engine is an ongoing R&D aspect where automobile industry invests a lot of effort and resources in the previous decades to cope with the amended local emission targets without a net reduction in globally discussed CO_2 targets.[9] Low hanging fruits regarding this aspect have been collected and expensive exhaust gas treatment systems are getting complicated.[11,20] The electrification of the transport sector is strongly addressed solution for de-fossilization of the sector and achieving CO_2 neutrality as mentioned in the mobility and fuels strategy (MFS) of the German government report with referring to the rail transport sector transition to 100% renewable electricity by 2050. This sector represents 2.3% of primary energy consumption of the transport sector.[9]

For urban mobility and with regard to local emissions targets reduction, e-mobility represents an attractive -yet expensive- option. However, it is important to note that high energy density liquid fuels (e.g. diesel) will continue to play a very important role as energy carriers for certain mobility modes (e.g. heavy duty transport, agriculture, ships).[18,21,22] On the other hand considering the transition of private transport in

Germany to electric driven train, 295 TWh of electricity will be needed. With the German current power mix CO_2 emission figures, almost same CO_2 net emissions based on fossil road fright will be emitted (1.51×10^8 t_{CO2}). [18] Considering the governmental support to introduce e-mobility in Germany and reach a target of 1 million electric vehicles (EV) in the market by 2020, only 25,502 EV where registered in Germany by the beginning of 2016.[17] This is interesting to be correlated to the driving culture. Generally, introducing new technology in the private transport market is rather not preferred by users and takes usually much time for adaptation and acceptance (Figure 3).[23]

For the third alternative, biofuels showed technical feasibility and applicability in the current infrastructures; however the availability of sustainable biomass resources and the discussion of "tank or plate" lead to several uncertainties of this option.[9] Last but not least in this discussion, synthetic or designer fuels with drop-in characteristics are considered a very promising alternative.[14] A synthetic fuel that is combusting with lower local emissions must also fulfil the following criteria:

1. CO_2 "quasi" neutrality
2. Sustainability with regard to unlimited availability
3. As low environmental/ecological impact as possible
4. Economic efficiency
5. Functionality and best possible integrity with existing technologies (i.e. retrofitting).[24]
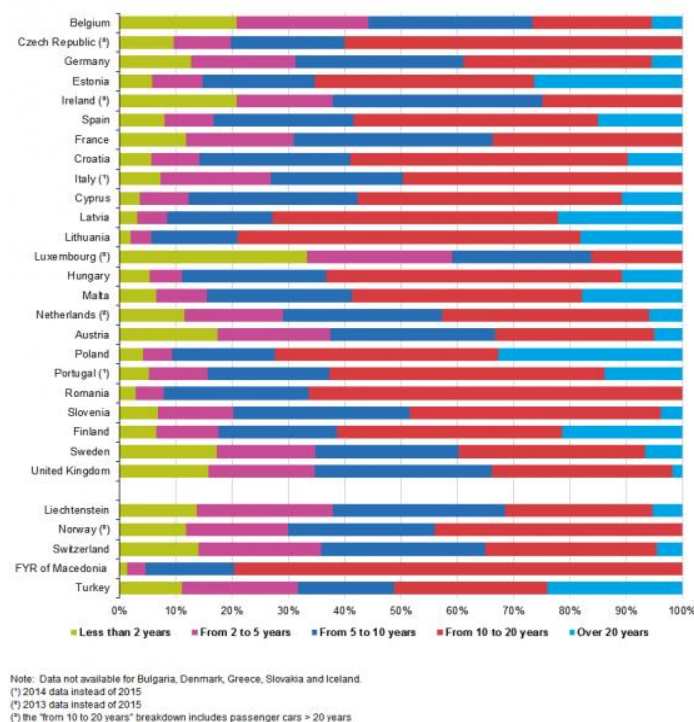
Figure 3 Passenger cars by age in EU 2015.[23]

In this context, C_1-oxygenates represents interesting candidates as synthetic fuels. Methanol (MeOH), Dimethyl Carbonate (DMC) and Methyl Formate (MeFO) represents candidates for gasoline engines, while Dimethyl ether (DME) and Oxymethylene dimethyl ethers (OME) are interesting fuels for diesel engine.[19]

MeOH is the key building block for the C_1-oxygenates as well for many different chemicals, intermediates and energy carriers. It is one of the most important chemical industry commodities with worldwide production capacity exceeding 80 Mt per year (2016).[25,26] MeoH is conventionally produced from synthesis gas (syngas) which is basically produced from the gasification of any carbon source. Mega-MeOH plants with annual production capacities exceeding 1000 kt are operating worldwide based on the coal to liquid (CtL, mainly in China) or gas to liquid (GtL, mainly in Middle East) technologies as depicted in Figure 4. The synthesis takes place in a heterogeneously catalysed reaction (Cu-Zn-Al/Zr oxides) at high temperature (200-350 °C) and high pressure (50-250 bar). From the most important MeOH chemical derivatives are FA, olefins, methylamines and methyl acrylate. Besides MeOH is a very important chemical, it has very high energy density of 22.7 MJ kg^{-1} with 12 wt.% of H_2. This nominates MeOH as an attractive energy carrier.[27]

MeOH can also be synthesized *via* the direct hydrogenation of waste/captured CO_2, with H_2 being provided by RE powered water splitting (e.g. via electrolysis). This approach falls under the general description of "*Carbon Capture & Utilisation*", although in Germany it is more commonly referred to as "*Power-to-Liquids*" (PtL; Figure 4). When CO_2 (from biogenic sources, industrial waste or ultimately from air) is used as the carbon source, a drop-in renewable energy carrier is produced which offers an option for achieving (as near as possible) CO_2 neutral fuels and chemicals. Therefore, PtL technologies offer a chemical energy storage option for stable, sustainable and flexible modern electricity grids with expanded RE power generation capacities; and a possibility for producing synthetic fuels with CO_2 neutral emissions capabilities and reduced local emissions.[3]
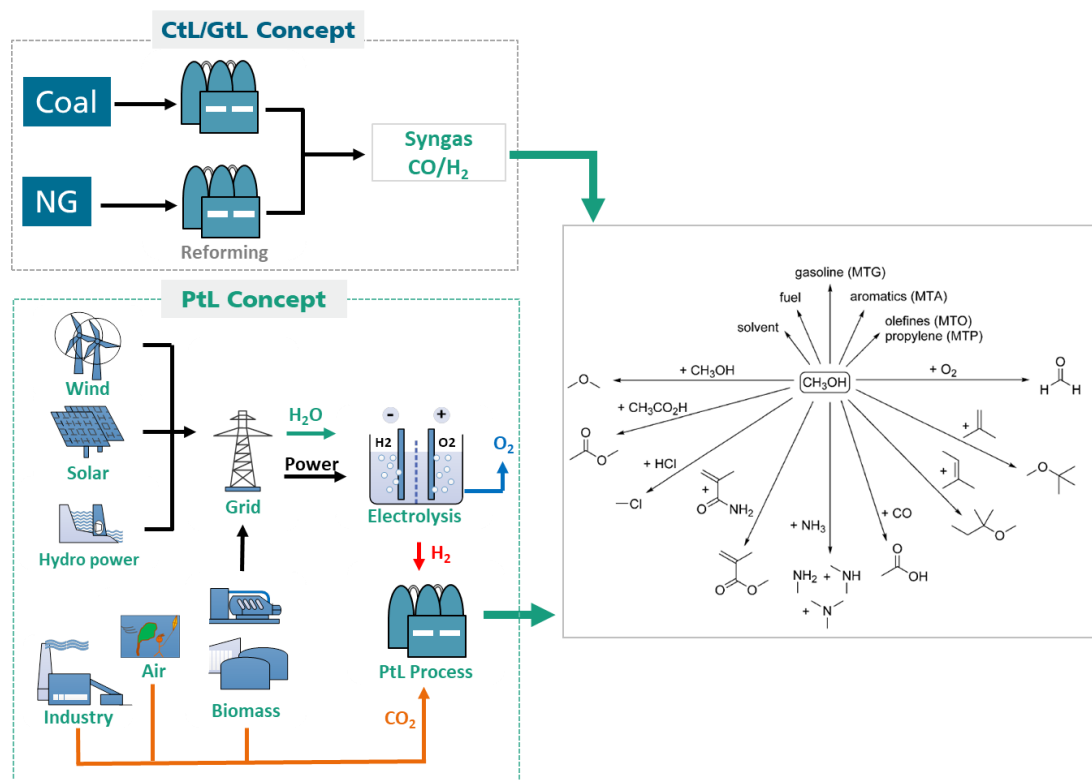
Figure 4 Different synthesis pathways to methanol as C1-Chemistry building block. CtL: Coal to Liquid; GtL: Gas to Liquid; PtL: Power to Liquid. (right) MeOH derivatives diagram as presented by Klankermayer et al.[25]

1.2 Oxymethylene dimethyl ethers – OME

Polyoxymethylene dimethyl ethers (also known in literature as POMDME, PODE, DMM_n, Molecular formula: $H_3CO-(CH_2O)_n-CH_3$, OME for short chains with $n \leq 8$, Figure 5) represent a class of chemical compounds that can contribute to the aforementioned sectors. OME contains more than 40 wt.% oxygen and no direct C-C bonds (e.g. as in classical hydrocarbon fuels), which leads to improved combustion properties at lower fuel to air ratios. The combustion of $OME_{n \leq 5}$ is typically soot free, indirectly reducing NO_x emissions.[11,28,29] OME have similar thermochemical properties to conventional diesel, are diesel miscible and have a higher Cetane number.[30,28] They are believed to be non-hazardous to human health or the environment, whilst a low vapour pressure and liquid state, provides the option to drop them in to existing infrastructure.[31,32]

Figure 5 OME chemical structure[33]

Due to the molecular structure, several OME fractions and mixtures acquire interesting thermo-physical and chemical properties that made them suitable for several applications. The physical properties of OME fractions vary according to the chain length. OME_1 (Methylal, dimethoxymethane or known commercially as Solvalid®) is a

commercial market product with wide range of applications as solvent for paint strippers, cleaning and polishing chemicals, blowing agent and as reagent in pharmaceutical synthesis.[34] Several OME fractions were also investigated as promising CO_2 absorbents in theoretical studies and also recently experimentally by Schappals et al.. It was concluded that OME_2, OME_3 and OME_4 are interesting physical CO_2 absorbents against commercially available candidates.[35,36]

OME were also investigated as a fuel in direct oxidation fuel cells as alternative for MeOH. $OME_{n>1}$ fractions has low vapor pressure, are non-toxic and have higher H_2 content per mole than MeOH; which are all interesting properties for this application.[37,38] Blending OME to diesel fuel is already implemented in China for increasing diesel fuel quality.[39] Other applications for OME in China are as wood coatings, coil coating, as an additive for oil solvent #100 and #200, as replacement for Methoxy Propyl Acetate (PMA), Ethylene glycol monoethyl ether acetate (CAC) solvents and in paint, ink and textile industries.[40]

The reported thermo-physical, chemical, thermodynamic and fuel properties of OME in public domain are summarized in Table 1. Pure OME component properties as well OME_{3-5} mixture and diesel DIN EN590 properties are tabulated. OME_{3-5} mixture has been identified as suitable diesel blend or alternative and will be in focus of the properties discussion.[14] The oxygen content of OME is significant and as aforementioned this reflects on the complete combustion of these oligomers when applied as fuels. Most of OME fractions have densities higher than diesel fuel standards set by DIN EN590; this can impact on the fuel atomization which indirectly reflects on the combustion process.[14] On the other hand this density property could present a logistic advantage in case of spillages during marine transportation. OME_{3-5} melting point almost fulfils the requirements of the DIN EN590 and the boiling point of OME_{3-5} is in appropriate range to be applied without pressurizing the combustion engine.[14] According to Liu et al. and Münz et al. OME mixtures evaporates faster than diesel and enables more targeted fuel injection leading to higher combustion efficiency.[19,41] Viscosity and lubricity are important properties for applying certain fuel in combustion engines. OME_{3-5} lubricity confines with the DIN standards limitations while the viscosity of this mixture is less than the DIN EN590 range of 2-4.5 mm^2 s^{-1}. This could be overcome by additives.[28] OME are advantageous against diesel fuel regarding Cetane number; a value describes the self-ignition quality of the fuel. For compression combustion engines, high Cetane numbers are desired for good combustion quality.[14]

OME fractions have lower volumetric energy content in comparison to diesel due to the high inter-molecular oxygen content.[20] Münz et al. and Härtl et al. demonstrated strategies for fuel injection to compensate for the OME lower calorific value.[19,20] Several OME fractions have been tested in single diesel engine cylinder in static test rigs and also in multiple cylinders and under real drive conditions. Härtl et al. and Gaukel et al. reported on the combustion of OME_1, OME_2 and a mixture of OME_{3-6} in diesel engine.[28,42] Using OME_1 with additives and OME_2 as blends with diesel fuel showed

reductions of NO_x at low PM emissions (< 1 mg kWh^{-1} which is much lower than the Euro 6 limitations).[28] Also using OME_{3-6} fractions as diesel blends as well as pure components showed significant PM reductions.[28] Richter et *al.* tested OME_{3-6} fractions in single cylinder diesel engine and emphasized the low PM emissions of OME fractions and the potential to to override the NO_x-soot trade-off allowing measures to reduce the NO_x emissions (e.g. increasing exhaust gas recycle EGR).[43] Iannuzzi et *al.*, Liu et *al.* and Sun et *al.* also investigated the combustion and the emissions resulting from applying OME in diesel engines confirming the local emission reduction potential using OME as diesel additive or alternative.[41,44–47,47–49] Recently Tan et *al.* investigated the sooting characteristics of OME blends with diesel. The effect of oxygen content of OME against the chain length was explained. It was interesting to notice that the soot reduction was rather depending on the oxygenate decomposition mechanism and the type of radicals formed while decomposition and not only the oxygen content.[50]

Schemme et *al.* summarized the work related to OME testing in diesel engines in the recent decade.[14] These investigations concluded that it is better to use OME as pure fuel and not as an additive. OME showed good material compatibility and low toxicity which make them applicable in the current infrastructure. New norms would be required to apply OME in current diesel engines or additives should be used to adjust OME properties within the DIN EN590 norms.[14] Regarding material compatibility, Härtl et *al.* discussed the effect of applying OME on the sealing materials and recommended using Ethylen-Propylen-Diene-monomer rubber (EPDM) as sealing material.[20] In real drive test using pure OME_{3-5} as a fuel for a test vehicle with minimal injection system adjustment, Münz et *al.* concluded 60% PM emission reduction using OME compared to conventional diesel with PM emission of 6×10^{11} # km^{-1} which is far below the Euro 6 norm.[19]

For process evaluation of OME synthesis, standard thermodynamic properties are required. Standard enthalpy of formation and standard Gibbs free energy data for some OME fractions are given in Table 1. Several reaction equilibrium and thermodynamic properties have been evaluated experimentally.[51–54] Also Himmel et *al.* reported on ab-initio thermodynamic investigation where standard properties for OME were theoretically evaluated.[55] Some temperature dependent properties (vapor pressure, heat capacities, etc) are currently not available in literature. This was overcome by estimations of the missing properties using UNIFAC, Joback or CHETAH 9.0 ASTM thermodynamic calculator software. CO_2 absorption properties presented as Henry's constant demonstrates the applicability of some OME fractions against commercial CO_2 physical absorbents are also listed.[36]

Table 1 Thermo-physical, chemical and fuel properties of OME[20,30,36,53,56,57]

	Unit	DME	OME$_1$	OME$_2$	OME$_3$	OME$_4$	OME$_5$	OME$_6$	OME$_{3-5}$	Diesel
CAS no.			109-87-5	628-90-0	13353-03-2	13353-03-5	13352-76-6	13352-77-7	-	68476-34-6
Molecular Formula		C$_2$H$_6$O	C$_3$H$_8$O$_2$	C$_4$H$_{10}$O$_3$	C$_5$H$_{12}$O$_4$	C$_6$H$_{14}$O$_5$	C$_7$H$_{16}$O$_6$	C$_8$H$_{18}$O$_7$		C$_n$H$_{1.9 \times n}$
Thermo-physical Properties										
Molecular Weight		46.1	76.1	106.1	136.2	166.2	196.2	226.2	166.2	
O-content	wt.%	34.7	42.1	45.2	47.0	48.1	48.9	49.5	48.8	≤ 0.7
Density	kg m^{-3}	0.668	0.868	0.971	1.035	1.079	1.111	1.135	1.070	0.82-0.84
Melting Point	°C	-141	-105	-70	-43	-10	18	45.8	-16	-20
Boiling Point	°C	-25	42	105	156	202	242	273	155-242	170-390
Viscosity (40 °C)	mm^2 s^{-1}	>0.1	0.58$^{(20°C)}$	0.66$^{(20°C)}$	1.08	1.72	2.63	-	1.89	2-4.5
Lubricity (60 °C)	μm	-	759	545$^{(20°C)}$	534	465	437	-	514	<460
Surface tension		-	20.4	27	28.8	30.7	32.6	-	-	-
Auto ignition point	°C	-	237	230	235	235	240	-	-	-
Henry's Constants	MPa	-	-	5.06$^{(40°C)}$	4.8$^{(40°C)}$	4.68$^{(40°C)}$	-	-	-	-
Thermodynamic Properties										
Standard enthalpy h^o_{fi}	kJ mol^{-1}	-	-379.8	-553.5	-727.2	-900.9	-1074.7	-1248.4	-	-
Standard Gibbs energy G^o_{fi}	kJ mol^{-1}		-207.12	-316.79	-426.46	-536.13	-645.8	-755.48	-	-
Fuel Properties										
■ LHV	kWh kg^{-1}	7.5	6.5	5.4	5.4	5.3	5.1	4.9	5.4	11.8
■ Cetane number		55	29	63	67	76	90	-	70-100	>51
■ Diesel Equivalent	L L^{-1}	1.96	1.75	1.75	1.75	1.73	1.72	-	1.8	1

1.3 Problem definition and thesis objectives

Due to their interesting thermo-physical and intrinsic combustion properties, OME has high potential as diesel fuel alternative, "green" solvents or as CO_2 absorbent. The greatest hindrance for introducing OME into the market is the lack of energy efficient, economically feasible and a scalable industrial process for the synthesis of OME with a certain chain length. A new process concept for sustainable and efficient OME synthesis is to be developed in this thesis. The potential of OME synthesis *via* the two step process namely (1) methanol endothermic dehydrogenation to anhydrous formaldehyde and (2) reacting of the non-converted MeOH with anhydrous FA directly to OME is to be investigated. This route theoretical evaluation showed production cost benefits and energy efficient synthesis potential. For the process evaluation against the literature described processes, a hybrid simulation platform is to be implemented. The complex OME reaction equilibrium system and the literature not well known MeOH endothermic dehydrogenation kinetic models are to be described and integrated to the simulation platform.

A continuous test stand should be developed for the experimental investigation of the high temperature endothermic MeOH dehydrogenation to FA. Special reactor concept should be developed to achieve high FA selectivity. The influence of the operational parameters and the catalyst system on the final FA yield should be clarified. A batch reaction unit for the OME reaction should be constructed and used for the model validation. Several selective catalysts for the OME synthesis would be investigated for evaluating the OME reaction equilibrium. The analytical methods for the complex experimental systems under investigations should be designed, calibrated and coupled to the test apparatus.

The experimental outcomes are to be used for validation the developed reaction models. An interface and convergence algorithms between the developed reaction models and the commercial simulation platform should be implemented. A process heat integration tool and ultimately a cost evaluation model for the hybrid described are to be also integrated. With the aid of the developed hybrid simulation platform, process design and key performance indicators of the new synthesis route should be described.

This work was performed at the Fraunhofer Institute for Solar Energy Systems ISE (FhISE), as supported by the Institute of Plant and Process technology, Faculty of Mechanical Engineering at the Technical University of Munich (TUM-MW-APT). Aspects of the work were also performed in collaboration with the "HyCO$_2$ project" of the Leistungszentrum Nachhaltigkeit Freiburg.[58]

2 State-of-the-Art

2.1 OME in literature

OME were discovered in 1859 by the Russian chemist Alexander Mikhailovic Butlerov. By the beginning of the twentieth century Auerbach and Barschel had successfully synthesized longer chains OME (POM) via polymerisation of FA over an acid catalyst.[59] Properties of POM were first systematically investigated by Staudinger et *al.* in 1920.[60] In the middle of the twentieth century, several developments took place regarding longer chain POM synthesis, notably by DuPont.[16] The main applications for POM were in thermoplastic resins, electronic parts and in automobile industry.[59] In the last decade of the 20th century, short chain OME (n = 1-8) are being recognized as interesting diesel fuel substitutes or additives by Moulton and Naegeli.[61] In this period investigations to improve diesel combustion properties and related emissions using oxygenates were intensive.[61] Consequently, several motor tests using different fractions of OME (mainly OME_1) and blends of OME (n = 2-6) were carried out.[16] The main contributors to this early work were Ford Motor Company and Eni SpA.[62,63]

From 1998 till early beginning of 21st century, BP Corporation intensively investigated different synthesis routes of OME from different feeds. Different applications of OME at this time were also investigated; most prominent was using OME fractions for CO_2 absorption and as alternative fuel for direct oxidation fuel cells from Arkema (Table 3). Afterwards, BASF investigated the synthesis from MeOH, OME_1, Dimethyl Ether (DME) and different FA sources untill 2011. The main contributions were on the process development and the simplification of the purification and downstream steps. Since 2009 and due to Chinese prominent role as Coal-to-Liquid or Gas-to-Liquid (CtL/GtL) technology leader, the main progress on OME research and development is being done in China leaded by China Petroleum & Chemical Corporation (SINOPEC). In 2015, Schandong Yuhuang Chemical Co. commissioned a 30 kt per annum OME_{3-8} synthesis plant in China. Similar demonstration plants in terms of capacity are being commissioned or constructed in China (Figure 6).[16,24,60,64–66] An overview of the patents related to OME synthesis processes from different feeds *via* different synthesis technologies and OME various patented applications are given in Table 2 and Table 3.

Table 2 OME synthesis processes patents based on different feed systems

Feed	Year	Organization	Patent Identifier
OME₁/TRI	2008 - 2011	BASF	US20070260094 WO2006045506 DE102009039437 US20100056830
	2017	Nanjing Guochang Chemical Technology Co., Ltd	CN205886832U
		CHINA Univ OF Petroleum Beijing	CN106495996 A
		Changzhou University	CN105294406B
	2016	Shenyang University of Chemical Technology	CN105833907 A
	2014	China Petroleum & Chemical Corporation	CN102372615B
OME₁/P-FA	2017	China Petroleum & Chemical Corporation	CN106588585A
		JIANGSU SUCCESS RESIN CORP	CN106311328A
		Jiangsu Kaimao Petrochemical Technology Co., Ltd	CN106397143A
	2016	Shandong Yuhuang Chemical Co., Ltd.	US9266990 B2
		China Petroleum & Chemical Corporation	CN103420817 B
	2015	Suzhou Ossote New Material Co., Ltd	CN104610026A
	2011	China Petroleum & Chemical Corporation	CN102295734A
MeOH/ P-FA	2017	China Petroleum & Chemical Corporation	CN104230685B
		Kerry Environmental Protection Technology Co Ltd	CN106518641A
	2016	Shaanxi Henghua Energy Technology Co., Ltd	CN105601479 A
	2015	Lanzhou Institute of Chemicl Physics	CA2847372A1
		Jiangsu Kaimao Petrochemical Technology Co., Ltd	CN103880615B
	1999-2001	BP Corp North America Inc	US6160174A US6166266A US6350919B1 US6392102B1 US6265528B1
	2006 -2008	BASF SE	WO2007051658A1 WO2006134088A1 US20080207954 A1
	2014	Shanghai Pan Ma Chemical Engineering Technology Co., Ltd	CN104016839A
		Lanzhou Institute of Chemicl	US20140114092A1

		Physics	
	1999-2000	BP Corp North America Inc	US6350919B1
			WO2000029365A2
	2011	China Petroleum & Chemical Corporation	CN102040490A
MeOH/TRI	2011	Chinese Academy of Sciences	US20110313202A1
	2010	China Petroleum & Chemical Corporation	CN101768057A
	2010		CN101768058A
DME/TRI	2008-2011	BASF	WO2006134081
	1998	BP Corp North America Inc	US6160174A

Table 3 OME Applications Patents

Application	Year	Organization	Patent Identifier
Fuel Cell	2006	Arkema	US20080138690 A1
	2005		FR2881750A1
Engine test	2012	MAN AG	US8298303 B2
	2003	Eni S.p.A	EP1422285A1
	2015	Sichuan Province Air Investment Co., Ltd	CN104449898A
			CN104449896A
			CN104498114A
	2016	Shanghai Zhongmao New Energy Application Co., Ltd	CN106118760 A
		Guangxi Fengtai Energy Technology Co., Ltd	CN104232180 B

In Europe and specifically in Germany, research on OME in motor applications and synthesis processes is back in focus since 2008 leaded by University of Kaiserslautern TU KL, Karlsruhe Institute of Technology KIT and Technical University of Munich TUM.[28,32] Noticeably, the introduction of the synthesis process concept based on MeOH and FA as commercial feeds by Schmitz et *al.* from TU KL in cooperation with the newly founded OME-technologies GmbH.[67] Also the production of OME based on woody biomass introduced by Zhang et *al.* in cooperation with Sauer et *al.* from KIT (with the Bioliq® technology experience). In this work, the technical and the preliminary process economic metrics of this path were defined.[68,69]

Since 2017, OME Technologies GmbH and Ineos Paraform announced their cooperation for production of OME on ton scale in Europe.[24] On the engine research side, Härtl et *al.*, Feiling et *al.* investigations are duly acknowledged and the OME testing in real driving conditions by Münz et *al.* from TU Darmstadt is an important milestone in the OME research history.[19,20,43] Recently, Schemme et *al.* and Baranowski et *al.* did a review work regarding OME catalytic synthesis in the former while the latter reported on the potential role of OME as a PtL electrofuel candidate that represents a promising solution for the troubled mobility sector.[16,64]

Methanol-to Clean-Diesel plant, in Dongying, Shandong province. [Photo by Wang Qian/chinadaily.com.cn]

Figure 6 The Shandong Yuhuang Chemical Co. "MeOH-to-Clean Diesel" plant in Shandong province (Left) and the Jiangsu Kaimao Chemical Technology Co. Ltd. Plant (right), located in Jiangsu province, both in China.

Figure 7 illustrates the progress on OME research worldwide regarding patented technologies and publications. Over the last decade, the research interest of OME in Europe and worldwide increased significantly as reflected by the issuing of patents and publication of research articles. In the last few years, OME application and testing in diesel engine, catalytic developments, and standardization of OME properties for different applications and evaluation of the ecological impacts of the synthesis process are in the focus of the research community.

Accompanying the academic interest, also OME activities in Germany within federal government co-financed projects with industry and academia (i.e. Carbon2Chem and Kopernikus P2X projects) are increasing. The target is to produce OME in Europe *via* a carbon neutral and sustainable process in contrast to the Chinese approach based on coal as the carbon source.[16,24,70,71]

Regarding the economics of OME synthesis, Schmitz et *al.* assessed the OME production cost based on OME1 and trioxane (TRI) commercial feed for a large scale production plant.[69] The production cost showed a break-even point with diesel price (without taxation) at specific conditions but the technical feasibility of the described process on refinery scale and the process energy efficiency are still low. The technical feasibility of these processes at this production scale is still under investigation. Research and development on scaling up OME synthesis technologies and defining suitable market entry mechanism are still essential.

The ecological impact of OME_1 when applied as diesel additive was investigated in a well-to-wheel analysis by Deutz et *al.*. OME_1 blends of 24 wt.% to diesel could reduce the GW impact by 22% and also significantly reduce the NO_x and soot emissions in comparison to fossil diesel fuel.[72] Also in a preliminary well-to-wheel analysis comparing different CO_2 emission per driven km from different PtL fuels in comparison with fossil

fuels showed the potential of OME for net CO_2 emission reduction against fossil diesel fuel.[73]
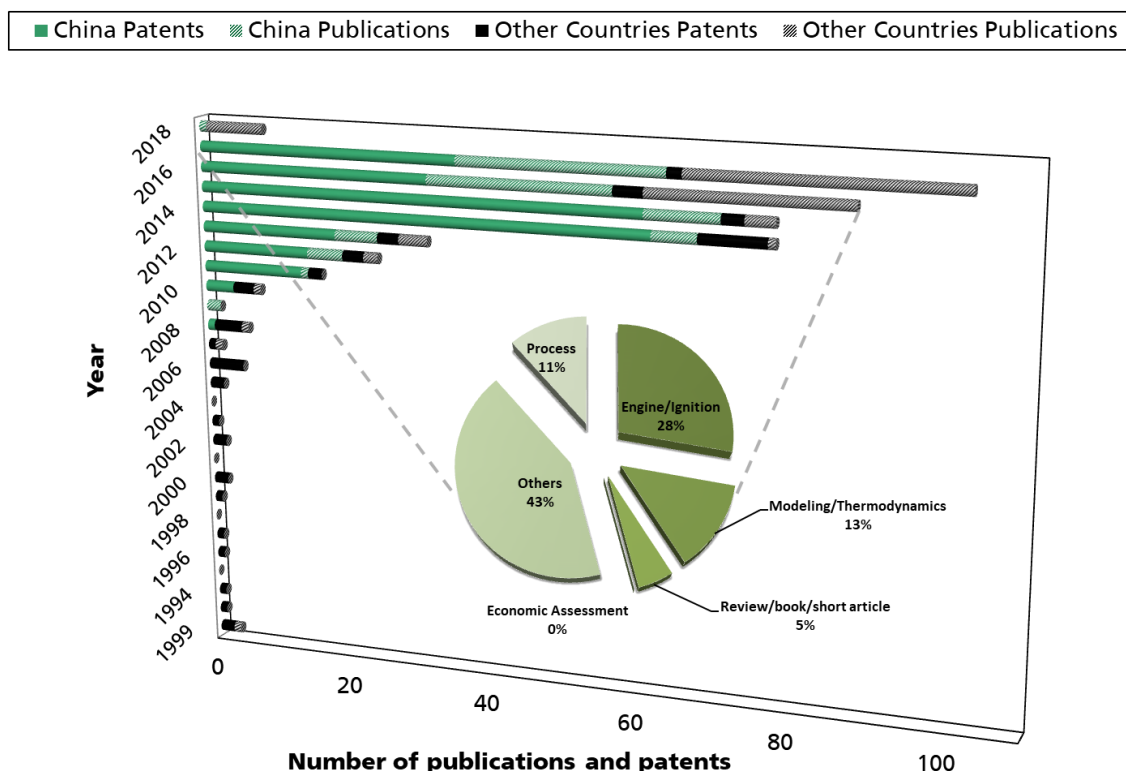
Figure 7 Research progress on OME synthesis and applications and the breakdown of the contributions by research field in 2017 (pie chart)

Literature Gap:

The available reports and patents in the public domain describe process concepts, synthesis apparatus, product purification or water management concepts for single or more components in the OME process chain. All contributions considering MeOH and FA feed systems are having water in the process feed with limited FA/MeOH feed molar ratio of ≤ 1.6 mol mol^{-1} in aqueous or methanolic solution due to solubility issues. Therefore, describing the OME synthesis system in the range of the anhydrous FA/MeOH feed ratio of 1.8-2 mol mol^{-1} where this thesis is investigating cannot be described by literature available data and own process models should be developed for this purpose. Additionally, a whole process concept detailed flow sheet description with the single component models, process convergence followed by process energy integration and economical evaluation in a single platform and complementary the experimental validation of process main components is lacking.

2.2 OME synthesis processes and mechanisms

OME is synthesized based on MeOH as a feedstock, thus fossil raw materials (natural gas, coal) as well as renewable feed stock (H₂ and CO₂ as industrial waste, from biogass production or ultimately from air) can be used. For OME synthesis, a FA source (formalin, p-FA, trioxane) and a methyl capping group supplier (MeOH, Methylal, DME) are required for OME synthesis. Acetalization, addition, trans-acetilization or condensation reactions take place according to the feed components as explained by Burger et. *al.*[52] and Zhao et *al.* explaining the mechanisms of OME synthesis.[74] Established processes for OME synthesis are based on complex synthesis steps (reactive distillation, extraction, etc.), are having low synthesis efficiency (η_{eff}<52 %; where $\eta_{eff} = \frac{(\dot{m}_i\ LHV_i)_{product}}{(\dot{m}_i\ LHV_i)_{feed}+E_{process}}$)[1] or based on expensive feedstocks.[16,32,53,75] In the following section the synthesis routes and mechanisms for OME synthesis from different feedstocks are discussed. Current synthesis routes that are described on research or industrial level are illustrated in Figure 8.
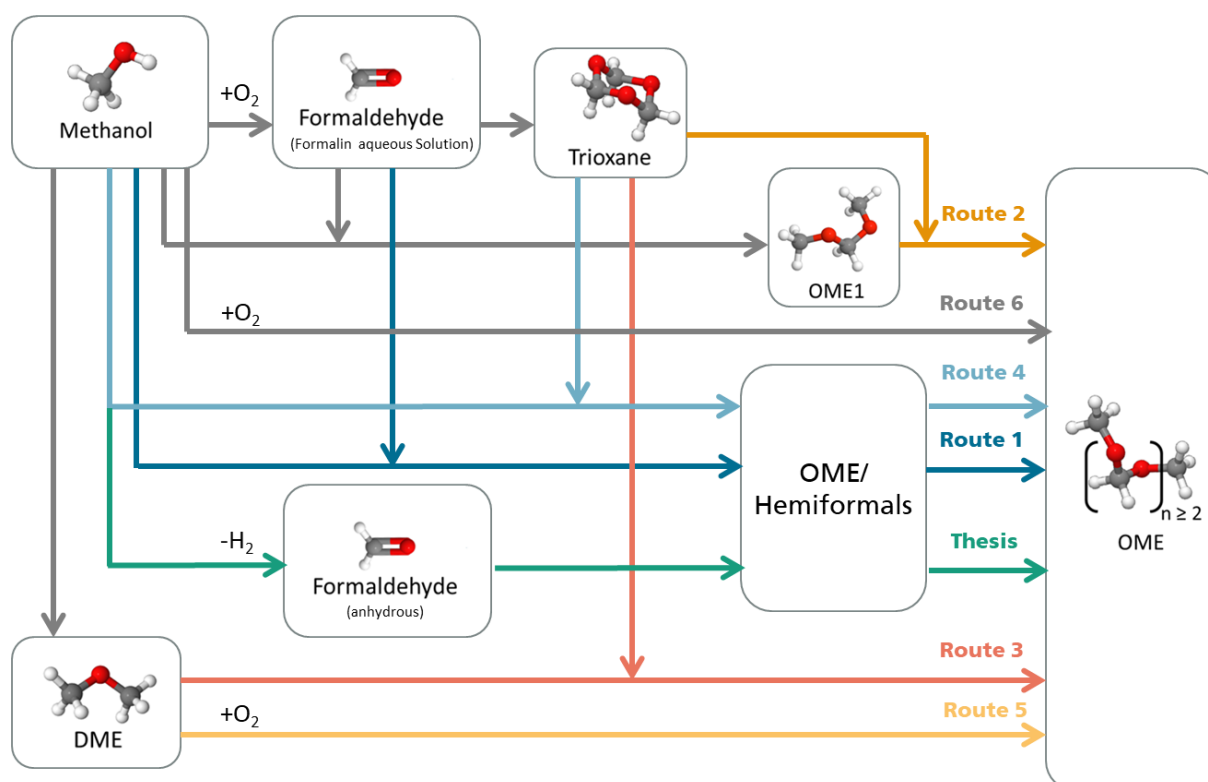
Figure 8 Different OME synthesis routes starting from MeOH

The synthesis route 1 based on MeOH and formaldehyde (formaldehyde originated from aqueous formalin solution or p-FA solid powder as depicted in Figure 8) represents economic attractiveness. It is a complex chemistry route but with simple process design and both MeOH and formalin are commodity feedstocks. Formalin or p-FA are synthesized commercially from MeOH. The former is produced *via* the silver catalyst

---

[1] η_{eff} is process efficiency, $\dot{m}_i$ is the mass flow rate of component i, LHV_i is the lower heating value of component i and $E_{process}$ is the energy consumption in the process

based process from BASF or the FORMOX process. In these processes, MeOH is partially oxidized over Ag based catalyst or metal oxide based catalyst to produce selectively formalin aqueous solution (FA concentration 37-55 wt.%) as shown in reaction 1. p-FA could by synthesized by energy intensive vacuum distillation of formalin.[76,77]

$$CH_3OH + \frac{1}{2} O_2 \rightleftharpoons CH_2O + H_2O \qquad\qquad \Delta H_R^{298} = -159 \; kJ \; mol^{-1} \qquad \text{(Reaction 1)}$$

With MeOH as the methyl capping group supplier and formalin or p-FA as the FA sources in the feed, OME synthesis proceeds *via* the aqueous synthesis mechanism. MeOH reacts with FA to form methyl hemiformal (HF) which proceeds through sequential growth mechanism of FA units to higher hemiformals followed by the acetilization of HF with MeOH in acidic medium to OME and stoichiometric H_2O (reaction 2-5). Thus the H_2O in the FA supplier in the feed is thermodynamically not favorable and shifts the equilibrium towards the feed.[60]

$$CH_3OH + CH_2O \rightleftharpoons HO(CH_2O)CH_3 \qquad\qquad (HF_1) \qquad\qquad \text{(Reaction 2)}$$

$$HO(CH_2O)_{n-1}CH_3 \;\; + CH_2O \rightleftharpoons HO(CH_2O)_nCH_3 \qquad\qquad \text{(Reaction 3)}$$

$$CH_3OH + HO(CH_2O)CH_3 \overset{H^*}{\rightleftharpoons} CH_3O(CH_2O)CH_3 + H_2O \qquad (OME_1) \qquad \text{(Reaction 4)}$$

$$CH_3O(CH_2O)_{n-1}CH_3 + CH_2O \overset{H^*}{\rightleftharpoons} CH_3O(CH_2O)_nCH_3 \qquad \begin{array}{l} \Delta H_R^{298} \\ = -25.2 \; kJ \; mol^{-1} \end{array} \qquad \text{(Reaction 5)}$$
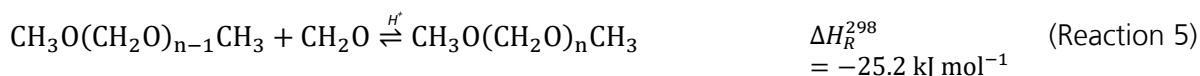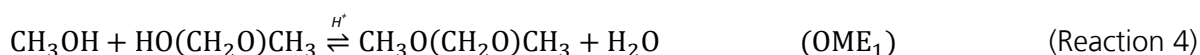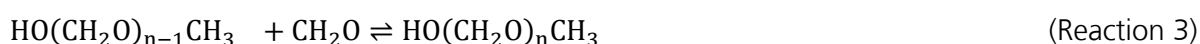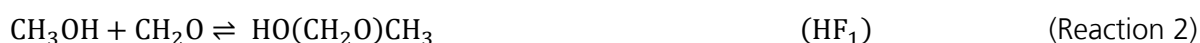
Those are equilibrium reactions which mainly depend on the concentration of FA and are shifting to longer chain lengths with an increasing FA feed concentration.[52] The OME formation reactions are slightly exothermic reactions (ΔH_R^{298} = –25.2 kJ mol^{-1}) and take place at mild conditions (T = 50–90 °C), the temperature is not significantly influencing the reaction equilibrium.[78] The presence of FA and H_2O leads to the consumption of FA to produce Methylene glycols (MG) as shown in reactions 6 and 7.[53]

$$H_2O + CH_2O \rightleftharpoons HO(CH_2O)H \qquad\qquad (MG_1) \qquad\qquad \text{(Reaction 6)}$$

$$HO(CH_2O)_{n-1}H + CH_2O \rightleftharpoons HO(CH_2O)_nH \qquad\qquad \text{(Reaction 7)}$$

HF and MG formation reactions occur at any pH value and without a catalyst. The equilibrium of these reactions is far on the side of the product.

The dissolution and behavior of FA in polar solvents as H_2O and MeOH has been investigated in several studies due to the importance of their influence while dealing with a FA containing systems. Basically a free monomeric FA in an aqueous or methanolic FA solution is negligible rather FA is chemically bounded in the form of HF or MG. The degree of polymerization of FA to these unstable intermediates depends on the FA concentration the solution type and the solution or reaction temperature as depicted in Figure 9.[79] For the description of synthesis of FA containing systems, the understanding of these interactions is imperative. Hahnstein et *al.,*

Albert et *al.* and Kuhnert et *al.* explained the phase and reaction equilibrium of this system which was applied further by Burger et *al.* for describing the OME synthesis equilibrium.[52,80,81]
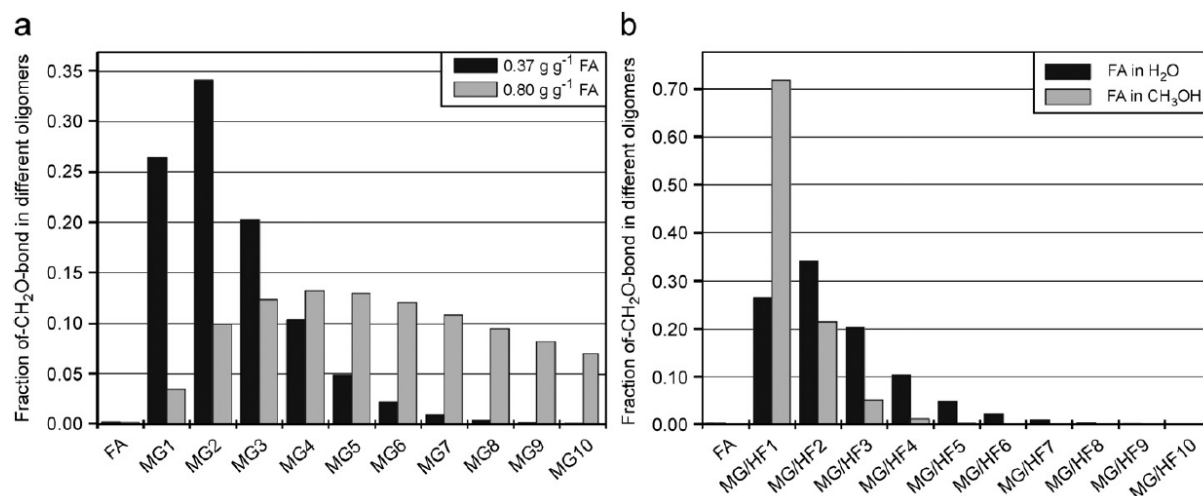
Figure 9 Distribution of FA (a) in water at different FA concentrations; (b) in different solvents at same concentration according to studies by Kuhnert et *al.*[79]

Trimerization of FA to TRI or the condensation of MeOH to DME and the formation of methyl formate (MEFO) *via* the Tishchenko reaction are also potential side reactions (reactions 8-10). The choice of the catalyst system can influence the side product formation as discussed by Schmitz et *al.* were side products formation was detected using Amberlyst36® catalyst while only traces of these side products were detected using Amberlyst-46® catalyst.[51,78]

$$3\,CH_2O \overset{H^+}{\rightleftharpoons} (CH_2O)_3 \qquad\qquad (TRI) \qquad\qquad (Reaction\ 8)$$

$$2\,CH_3OH \overset{H^+}{\rightleftharpoons} CH_3OCH_3 + H_2O \qquad\qquad (DME) \qquad\qquad (Reaction\ 9)$$

$$2\,CH_2O \rightleftharpoons HCOOCH_3 \qquad\qquad (MEFO) \qquad\qquad (Reaction\ 10)$$
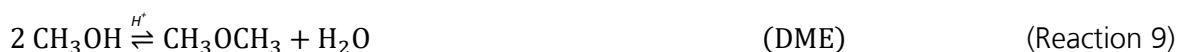
This synthesis route was intensively investigated in literature. As shown in the intellectual property overview in Figure 6. Several patents regarding catalysts, equipment and reactor types, synthesis processes and synthesis mechanisms are available. The work of BP Corporation, BASF SE and SINOPEC contributed significantly to the process development and the product separation. The kinetics of OME synthesis over cation exchange resin catalyst (Amberlyst-46®), several Brønsted acid catalysts (i.e. DOWEX 50W, H-BEA 25) and over Zr-Al$_2$O$_3$ catalyst using MeOH and FA feed system were reported by Schmitz et *al.*, Oestreich et *al.* and Zhang et *al.* respectively.[33,51,82] The equilibrium of this complex reaction system was described by Schmitz et *al.* and the multi-phase reaction equilibrium modelling details of this systems are also reported in this thesis (attached publication[53]).[54,78] Recently Schmitz et *al.* described a process concept for OME synthesis based on MeOH and formalin with water separation using adsorption or membranes with zeolites. The results showed process energy efficiency enhancement potential.[75]
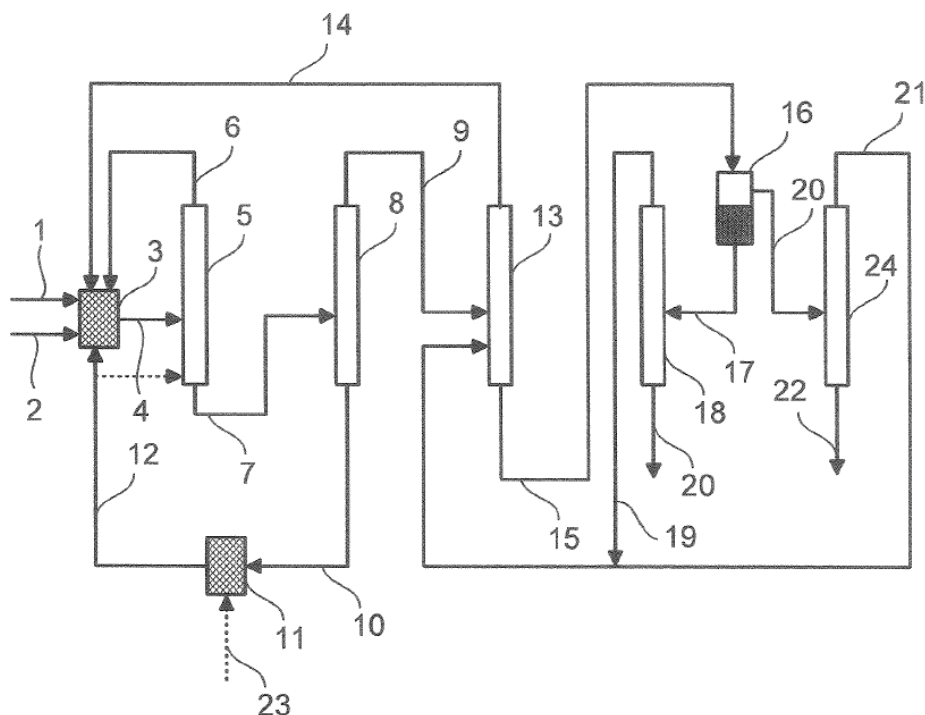
Figure 10 OME synthesis process from MeOH and FA based on BASF SE technology as described in the patent US007700809B2. (3) OME reactor; (5) Distillation Column 1; (8) Distillation Column 2; (11) OME synthesis reactor; (13) Distillation Column 3; (18) Distillation Column 4; (16) Aqueous phase separator; (24) Distillation Column 5. Feed streams 1 and 2 consists of MeOH and FA; product streams 20 of OME_{3-4} and 22 is H_2O.[83]

This synthesis route challenge is the OME reactor product work up. The OME reactor product constitutes of more than 30 components in equilibrium with azeotropic behavior between H_2O, FA, MeOH, OME_2 and TRI. Usually, a reactive distillation in several columns is required to achieve the separation of the desired OME_{3-5} product from H_2O, non-reacted MeOH and FA and other OME fractions and the side products HF and MG. Figure 10 illustrates the complexity of the synthesis process based on this route. Considering only MeOH as the starting material, a FA synthesis plant should be included in Figure 10 to represent the whole process chain. The presence of H_2O in the reactor feed limits the single path yield of the desired product. With 10 wt.% H_2O, a maximum of 8 wt.% of OME_{3-5} yield in the product can be achieved.[11,54] In this thesis an anhydrous FA is used as the feed with MeOH which significantly enhance the product yield (up to 14 wt.% OME_{3-5} single path yield can be achieved with anhydrous feed) and the whole process efficiency. This will be discussed later in detail.

A benchmark synthesis route is based on OME_1 and TRI (route 2). This route is characterized by simple reaction chemistry and significantly easier OME product work up compared to route 1. Both OME_1 and TRI are commercially available but with limited market capacity and high production cost.[24,75] MeOH is the initial feed stock for TRI and OME_1. The synthesis of TRI proceeds through the conversion of MeOH to FA as aforementioned, followed by the trimerization of FA over strong acid catalyst to TRI followed by energy intensive extraction and concentration steps.[84] OME_1 is synthesized *via* the homogeneous acid catalyzed reaction of FA with MeOH followed by reactive

distillation (Figure 11).[69,85] The OME synthesis using this feed proceeds through anhydrous mechanism. This comprise the possible ring opening and dissociation of TRI to FA, the sequential growth of OME fractions by addition of FA and the trans-acetalization reaction of TRI with OME fractions (reactions 5, 8, 11 and 12).[52,60,86]

$$(CH_2O)_3 + CH_3OCH_2OCH_3 \overset{H^+}{\rightleftharpoons} CH_3O(CH_2O)_4CH_3 \qquad \text{(Reaction 11)}$$

$$CH_3O(CH_2O)_nCH_3 + CH_3O(CH_2O)_mCH_3 \qquad \text{(Reaction 12)}$$
$$\rightleftharpoons CH_3O(CH_2O)_{n-\Delta n}CH_3 + CH_3O(CH_2O)_{m+\Delta n}CH_3$$

The reaction kinetics and thermodynamics of this synthesis route are completely described.[52] Burger et *al.* described the flow sheet and the synthesis process based on this feed.[87] OME synthesis based on TRI and OME_1 over several catalyst systems were reported. The work from Wu et *al.* and Xue et *al.* to synthesize OME over ZSM-5 zeolite catalyst showed efficient synthesis with high OME_{3-5} selectivity and at high conversion.[88,89] Wu et *al.* also investigated the synthesis using this feed over Brønsted acid ionic liquids where 91% OME_{3-8} selectivity was reached at 170 °C.[90] Schmitz et *al.* assessed the production cost of this route. However the educts OME_1 and TRI are expensive, at high production capacity OME synthesis based on this route showed economic competitiveness against diesel fuel.[69] The synthesis process flow sheet based on route is depicted in starting from OME_1 and TRI feed. Considering the initial synthesis blocks to produce these intermediates, the process complexity is evident.
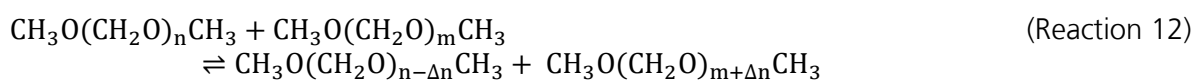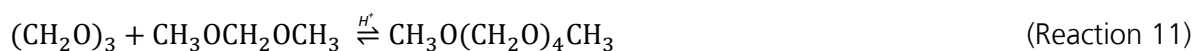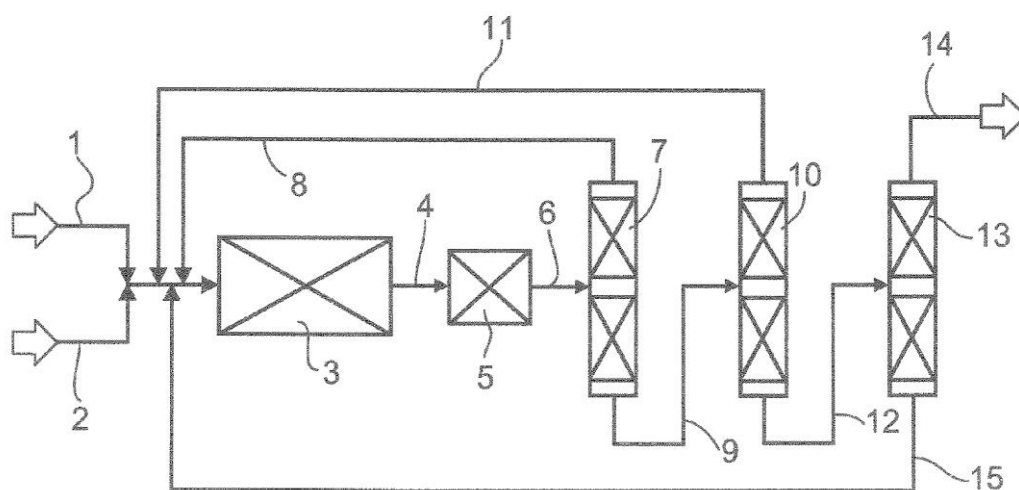

Figure 11 OME synthesis process from OME_1 and TRI based on BASF SE technology as described in the patent US20070260094A1. (3) OME reactor; (5) Anion exchange resin bed; (7) Distillation Column 1; (10) Distillation Column 2; (13) Distillation Column 3. Feed streams 1 and 2 consists of OME_1 and TRI; product stream 14 of OME_{3-4}[91]

Several other synthesis routes are investigated conceptually or experimentally in lab or mini-plant scale. Haltenort et *al.* reported recently on the OME synthesis based on DME and TRI.[29] This synthesis route (route 3) proceeds through anhydrous OME synthesis mechanism where DME is converted to OME via the addition of FA molecules

(reaction 13). The thermodynamic potential of this route is rather high considering the initial feeds to produce DME from CO or CO_2 hydrogenation is thermodynamically favorable than MeOH.

$$n\,CH_2O + CH_3OCH_3 \overset{H^+}{\rightleftharpoons} CH_3O(CH_2O)_nCH_3 \qquad \text{(Reaction 13)}$$

DME is however in gaseous form under normal OME reaction conditions. The reactions Gibbs free energy under these conditions do not favor the OME formation. Experimental investigations for this reaction system over H-BEA 25 catalyst were done in laboratory autoclave under vacuum and reduced temperatures to keep DME in the liquid phase. OME_{3-5} product yield of 8.2 wt.% was reached at 13.9% DME conversion.[29]

Reacting MeOH and TRI leads to aqueous OME synthesis mechanism as previously discussed (Route 4). However, it is not attractive to use the expensive TRI feed together with MeOH which will lead to water and side product formation during OME synthesis, still the potential of increased OME single path yield using a dry FA source as TRI is of academic interest and mainly in China. This approach is similar to this thesis approach since a dry FA source is used in both cases but contrarily the thesis approach offers a simple two steps OME synthesis process. Fang et *al.* and Wang et *al.* investigated this synthesis routes over different catalyst systems namely graphene oxides and zeolites. The aim of the studies was to define the operational parameters where the maximum OME target product yield and the least side products are formed.[92,93]

The direct partial oxidation of methanol or DME over bifunctional catalysts combining acid and redox properties to OME was also investigated (route 5 and 6). Mostly short chains OME_1 or OME_2 are the products of this reaction routes. The early work on this synthesis possibility was introduced by Hagen et *al.* from BP Amoco. DME undergoes (oxi-)dehydrogenation to produce a mixture of MeOH, H_2O and FA which reacts in-situ over the acidic active sites further to OME or which is introduced in a second step to acidic catalyst where higher OME can be synthesized *via* a combination of anhydrous and aqueous synthesis mechanisms (route 5).[94–97] Also the direct oxidation of MeOH was investigated with the aim to produce OME_1 (route 6).[98,99] Liu et *al.* revealed the potential of the direct MeOH oxidation to produce OME_1 at higher rates than DME oxidation.[100] A concept for revamping FA synthesis plants towards OME_1 synthesis plants using same catalyst and technology while adjusting the operational parameters was introduced by Thavornprasert et *al.*. In this review work, several catalysts for this synthesis routes were introduced together with the operational parameters. Importantly high MeOH concentrations in air up to 40 vol.% can be fed over commercial FeMo catalyst at $T = 200\text{-}300\ °C$ and OME_1 yield of 4.6 kg h^{-1} kg$_{cat}^{-1}$.[101]

Based on the work of Klankermayer et *al.* were formic acid, FA, MeOH and several other products were synthesized over multi-functional catalysts in a multi-step insitu reaction mechanisms from CO_2 and H_2, there is a future perspective for a single-pot OME synthesis with a maximized "*drop-in*" solution potential.[102]

Direct OME synthesis process concept

The direct OME synthesis based on MeOH and anhydrous FA is not yet discussed in literature. In this thesis, the potential of this route is investigated. The synthesis mechanism is similar to route 1 but with no water in the feed (Figure 12). This increases the OME target product per path yield, enhance the OME equilibrium distribution and suppress side product formation. In this synthesis path MeOH is endothermically dehydrogenatied at high temperatures (>650 °C) to FA with H_2 as a side product as shown in reaction 14.

$$CH_3OH \rightleftharpoons CH_2O + H_2 \qquad\qquad \Delta H_R^{298} = +85 \text{ kJ mol}^{-1} \qquad \text{(Reaction 14)}$$

In addition secondary competing reactions occur:[77]

$$CH_3OH \rightleftharpoons CO + 2H_2 \qquad\qquad \Delta H_R^{298} = +105 \text{ kJ mol}^{-1} \qquad \text{(Reaction 15)}$$

$$CH_3OH \rightleftharpoons C + H_2O + H_2 \qquad\qquad \Delta H_R^{298} = -31 \text{ kJ mol}^{-1} \qquad \text{(Reaction 16)}$$

Next to the competing reactions, FA is thermodynamically unstable and can convert into several compounds like HCOOH, CH_4, CO and CO_2 which are all thermodynamically favored.[77] Therefore, the reaction temperature should be sufficiently high, an effective, selective and active catalyst should be used, the residence time in the reactor should be short to minimize further conversions of FA leaving the reactor and the product needs to be cooled down fast to limit the decomposition of FA.[77] With selective FA synthesis at moderate MeOH conversion, the product of this reaction step is then mixed with the recycle stream from the OME reactor prior to be converted in OME reactor to higher OME (Reactions 1-7). The process simplified flow diagram of this synthesis concept is shown in Figure 12.
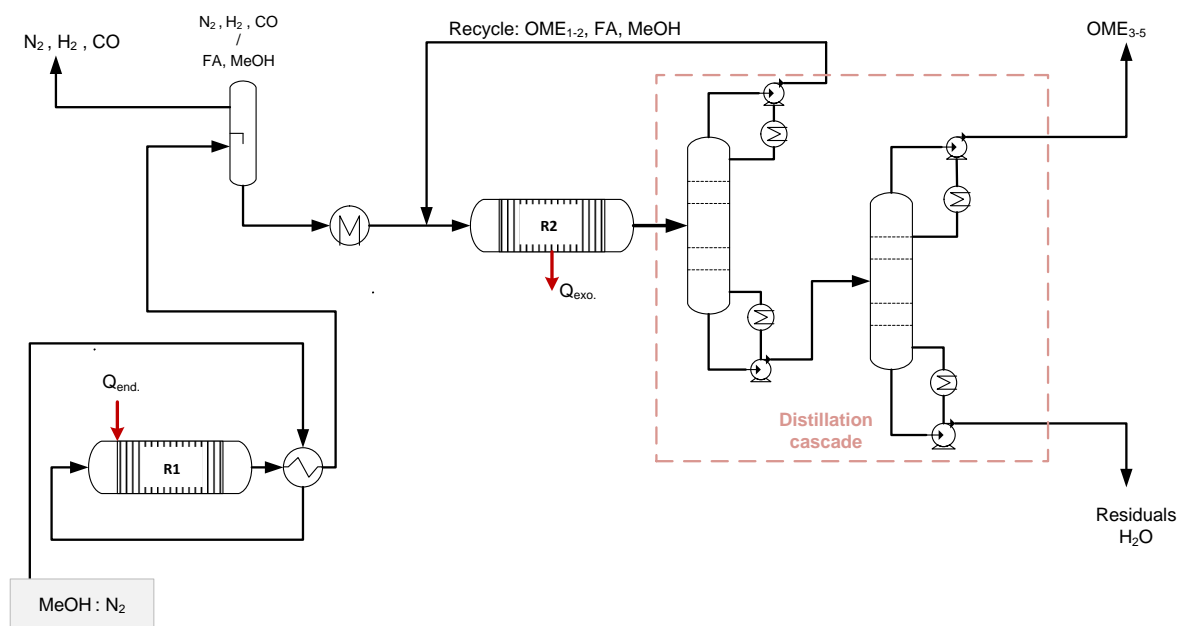
Figure 12 Conceptual simplified Process flow diagram of the direct OME synthesis based on MeOH and anhydrous FA as introduced in this thesis.

The work up of the product is still challenging due to the water formation during the OME synthesis reactions and the consequent HF and MG formation. On the other hand this concept offers several advantages from which: the simple process design, potentially high synthesis efficiency, valuable H_2 as side product and using the commodity chemical MeOH is the main feedstock with simple synthesis technology allows easy process scale-up.

2.3 Catalysts and kinetics

The two steps synthesis described in this work converts MeOH *via* catalytic reactions to OME. In the first reaction step, selective MeOH endothermic dehydrogenation to FA and H_2 at high temperature occurs. This is a kinetic controlled reaction were short residence time is desired (<0.01 s) to avoid the conversion of MeOH to the thermodynamically favored side products (CO, CH_4, MEFO and HCOOH) or the further conversion of the highly active FA to further dehydrogenation products.[77] Therefore, the choice of catalysts for this system is very crucial and significantly influence the selectivity to FA and the conversion of MeOH. The MeOH and FA product of the first reaction step are then converted over acidic catalysts to OME in a second reaction step. These reactions occur at mild temperatures and proceeds to thermodynamic equilibrium generally in acidic medium. The choice of the catalyst here reflects on the selectivity of the target products and the ability to suppress side product formation. Furthermore, the rate of OME formation and the OME chain length distribution depends on the acidity and the surface properties of the catalyst. In the following an overview of the catalyst systems investigated for anhydrous FA synthesis and for OME synthesis is introduced.

.

2.3.1 Anhydrous FA synthesis

More than 90% of the world formaldehyde is produced by the catalytic oxidation of MeOH which yield an aqueous solution of FA. Mostly FA is used as intermediate to produce other chemicals as aminophenol or important polyacetal resins *via* condensation reactions.[77,103] The presence of water in the feed shifts the equilibrium towards the feed. Same as in the case of OME synthesis as previously explained (reaction 2-10). Concentrating FA to p-FA or trimerization to anhydrous TRI can be achieved by complex and energy intensive procedures.[76,77] Therefore, production of anhydrous FA *via* MeOH dehydrogenation with the highly valuable H_2 as the side product is attractive.

Since 1960 several investigations to identify selective catalysts for the anhydrous FA synthesis have been expended. For the OME synthesis under investigation in this thesis, FA selectivity higher than 90% is needed at MeOH conversion higher than 67%; this was defined based on simulation results as explained later. Hence, catalysts that can be operated in the vicinity of these conditions were of special interest. Employing the transition metals copper, zinc, silver and indium showed interesting results. When the reaction occurs in the absence of oxygen in both the reaction feed and the catalyst, MeOH dehydrogenation proceeds very slowly and needs extremely high temperatures (650-750°C). From the transition metals, ZnO mixtures with SiO_2 and Z13X showed very high selectivity (>94%) at conversion up to 66%. However, the oxygen containing catalysts were subjected to rapid deactivation under the harsh reducing reaction environment.[77] In 2003 Ren et. *al*. reported the superior performance of complete MeOH conversion and very high FA selectivity on $Ag-Mg-SiO_2-Al_2O_3$ multi-phase catalyst however no further contributions were made public based on this system since then.[104]

Oxygen containing compounds of group IA elements showed improved catalytic performance. Sauer et *al*. investigated the $NaAlO_2$ and $LiO_2.NaAlO_2$ catalyst systems for the MeOH dehydrogenation reaction at temperatures up to 900 °C and FA yield of 70% was achieved.[103] Su et *al*. and Zaza et *al*. investigated the Na_2CO_3 catalyst for this reaction at temperatures up to 700 °C. The carbonate based catalysts are initially deactivated due to coking of MeOH and sintering of the catalyst material before a steady state selective FA production can be achieved. Selectivity higher than 90% was achieved at low conversions of 14%. Increasing the conversion was accompanied by decreased selectivity.

Improving Na_2CO_3 catalyst with supporting the catalyst on charcoal was also investigated and showed enhancements on the catalyst activity. This was explained by Renken et *al*. due to the H_2 spillover from the carbonate to the carbons which accelerate the rate determining step.[77,105] Zeolites were also investigated for the MeOH dehydrogenation significantly the work from Tchistovskaya et *al*. over modified ZSM-5 catalyst with Cs and Na. Over this catalyst system a complete conversion of MeOH was achieved at FA selectivity of 65%.[77]
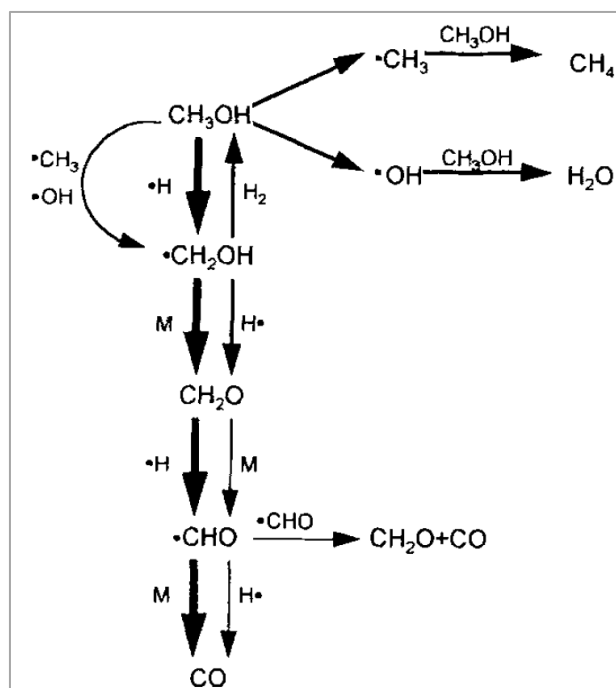
Figure 13 Reaction chain mechanism of radical MeOH dehydrogenation to FA. (M) is a colliding species. [59]

Kinetic models and reaction mechanism for MeOH dehydrogenation over Ag based catalyst, $NaAlO_2$ catalyst and Na_2CO_3 catalysts were discussed in literature however these results are very specific and only applicable in the discussed reactor arrangements.[77,103,106] The radical chain reaction postulated by Sauer et *al.* is depicted in Figure 13.[103] The proposed mechanism covered mainly the gas phase radical reactions. Complementary to this work, Zaza et *al.* explained the mechanism over Na_2CO_3 catalysts where catalyst surface reactions are also described. The importance of the catalyst surface reaction was emphasized by the authors as it accounts for more than half the total conversion of MeOH.[106]

2.3.2 OME synthesis

Several catalysts have been investigated for OME synthesis for different feed systems. Mainly Brønsted acidic catalysts were used in homogeneous and heterogeneous systems and also in batch and flow reactor arrangements.[16] Generally an efficient catalyst for this system is the one that has high selectivity to the target products, high activity to maximize the conversion of the educts, the ability to suppress side product formation and stability during long time operation. For homogeneous catalysis mineral acids as H_2SO_4, HCOOH and Ionic liquids (ILs) have been investigated. Among the carboxyl, carbonyl, hydroxyl and sulfonic acid groups, the latter showed the best performance for OME homogeneous catalysis.[16] As reported by Wang et *al.* best performance for mineral acid catalysts was over H_2SO_4 catalyst with TRI conversion of 72.2% and 19.3% OME_{2-8} selectivity.[107] OME synthesis over ILs showed several advantages due to the tunability of the physical and acidic property of the solvent. Wu et *al.* demonstrated the potential of using ILs with alkanesulfonic acid groups for the synthesis from TRI and OME_1.

Conversion of TRI of 91.18% with OME_{3-8} selectivity of 70.9% were reached.[90] Wang et *al.* investigated the mechanism of OME formation and recently the kinetics of OME synthesis over ILs.[108,109]

Homogeneous catalysts showed activity and uniformity of distribution for OME synthesis but their separation from the reaction mixture and their corrosive nature are challenging aspects. Ion exchange resins are mostly used for heterogeneous OME catalysis. They have well defined active sites and can be easily separated from the reaction mixture. However, the thermal stability and leaching of active species in polar solutions are drawbacks of these catalysts.[16] The surface area, diffusion to the active sites in the bulk and micro pores of this resins are influencing parameters for the activity and selectivity of ion exchange resins. Oestreich et *al.* investigated the kinetics of OME synthesis over DW50x2® ion exchange resins with different particle size and also over Amberlyst-36® catalyts.[33]

Burger et *al.* investigated the effect of distribution of sulfonic acid group on the catalyst bulk and micro pores on the side product formation when comparing Amberlyst-36®and Amberlyst-46® catalysts. The latter showed no side product formation which was explained by the absence of active sites in the micro pores where FA may accumulate and leads to side product formation.[52] Zheng et *al.* investigated NKC-9 ion exchange resins for OME synthesis using OME_1 and pFA. Conversion of pFA 84.6% and 36.6% OME_{3-5} selectivity were reported.[110] Zeolites, solid acid carbons, solid super acid catalysts and supported ILs were also used for OME synthesis.[16] Mostly zeolites and solid acid carbons exhibit thermal stability and tuneability of the acidity of the former by adjusting the Si/Al ratio is advantageous.[16,111,112]

Zhao et *al.* explained *t*he influence of the acidic group nature and strength on the OME synthesis using molecular sieves with various Si/Al ratios by the reaction of methanol and trioxane. They identified that short OME chains are formed mostly in presence of weak acidic sites, while longer OME chains are preferably synthesized by the use of medium strength acidic sites, which also improve OME_{3-5} yields. [113] A summary of the reported literature for OME synthesis based in different routes, the feeds of each route and the catalyst systems that has been used in each route is presented in Table 4.

Kinetic models for OME synthesis based on different feeds and over different catalyst systems were introduced. For the synthesis from MeOH and FA system, the work from Schmitz et *al.*, Zhang e*t al. and* the extended model introduced Oestreich et *al.*, covered the kinetic aspect over different catalyst systems.[33,51,82] Schmitz et *al.* described the synthesis over Amberlyst 46 catalyst at 90 °C and FA/MeOH ratio of 0.86 g g^{-1} using an exponential approach. Zheng et *al.* described the kinetics of this system over HD-S ion exchange resin in a fixed bed reactor, T = 40-80 °C and WHSV of 1.35-9.95 h^{-1}. The system was described with a fourth order Runge-Kutta method.[82] Oestreich et *al.* extended the work from Zheng et *al.* by including the etherification of HF with MeOH and not only the OME_1. Also other educts like OME_{1-3} were included considering the

recycle strategies with the corresponding etherification reactions. Several Brønsted acidic catalysts were investigated while the ion exchange resin DW50x2® was employed since it showed the highest activity. A hyperbolic based model was introduced with experimental validation at FA/MeOH ratios of 0.5-1.5 g g^{-1}, T = 40-120 °C and H_2O content up to 23 wt.%.[33]

Table 4 Literature overview for reported OME synthesis based on different feeds and different types of catalysts used

	Feed	Catalyst	Year
Anhydrous routes	OME_1+TRI	A46[a52], CT175[a114], [PY.BS][HSO_4^-][b90], ZSM-5[c89], C_{10}-AS-50[c115], BEA25[c60], A36[a54,60]	2012 – 2015
	OME_1+$FA_{an.}$	trimethyloxonium salts[55,116]	2017
	DME+$FA_{an.}$	H-BEA 25[c29]	2017
Aqueous routes	OME_1+pFA	NKC-9[a110,117], H_2SO_4[74], A36[a54,60]	2013 – 2015
	MeOH+TRI	A36[a54,60], MCM-22[c113], ZSM-5+P_2O_5[c118], PVP-HPAs[92], SO^{2-}/Fe_2O_3[119], GO[d93]	2011 – 2016
	MeOH+pFA	γ-Al_2O_3+4%ZrO_2[82]	2015
	MeOH+Formalin	HD-S[a120], A46[a78], D50WX2[a54,121], A36[a33,54,60]	2011 – 2017

[a]Ion exchange resins, [b]Acid Ionic Liquids, [c]Zeolite, [d]Graphene oxide

3 Methodology

Work flow and problem tackling strategies

The strategies to realize the process concept under investigation in this thesis and develop a robust tool to evaluate this process are presented in this chapter. Two working layers or platforms were developed in parallel within the frame of this work as depicted in Figure 14. An experimental platform constitutes of lab-scale testing facilities for process main components testing and model validation. In this platform mainly a continuous anhydrous FA synthesis reactor and batch OME synthesis reactor are developed together with the corresponding analytics. In the simulation platform, the reactor unit models and the product separation by distillation are implemented. The complementary tools as the physical property model, the node for connecting various software interfaces in the same simulation platform, process heat integration and finally the cost modelling tools have been consolidated in the simulation tool, which is called later on a "hybrid model".
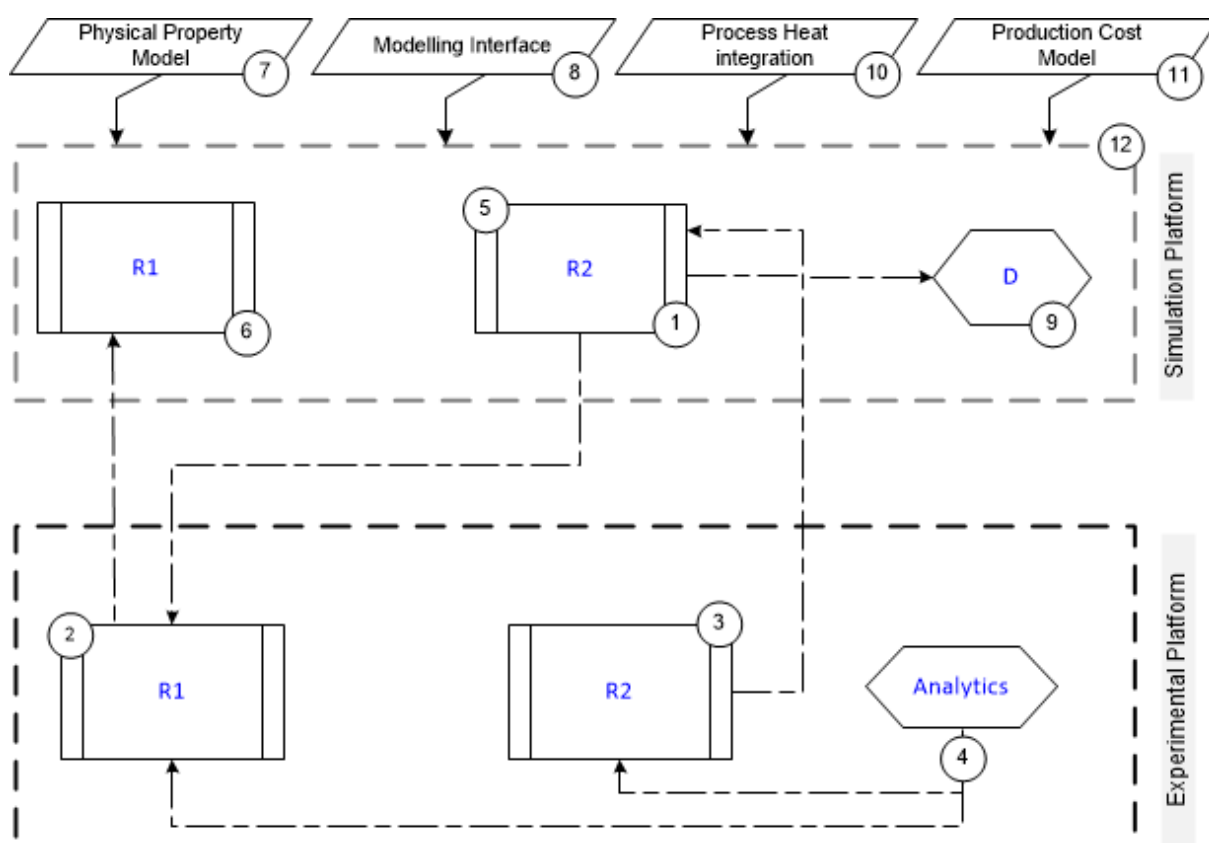
Figure 14 Work flow diagram with the interactions between different work layers and process components. R1: Anhydrous FA synthesis reactor; R2: OME Synthesis reactor; D: Distillation Cascade. Numbering refers to the order of the task within the frame of this thesis.

3.1 OME synthesis reactor modelling

The research progress in this work started by the OME synthesis reactor modelling. The objective was to describe this complex system based on MeOH and anhydrous FA feed

and define the optimum conditions of this unit to maximize the OME_{3-5} target product yield. The multi-phase chemical equilibrium model was developed and implemented in Matlab® for the description of this system. For the OME system, several contributions investigating the vapor-liquid equilibrium VLE lead to reliable description of the non-ideality of the system in the liquid phase using the UNIFAC method. The vapor phase of this system is considered ideal and only formation of short chain MG and HF are considered. The stoichiometric chemical equilibrium approach was adopted. The reaction system comprises 32 components (MeOH, FA, H_2O, OME_{1-8}, HF_{1-10}, MG_{1-10} and TRI) that are contributing simultaneously in 29 reactions (reactions 2-8 considering the different fractions of OME, HF and MG).

To assess such a thermodynamic problem for a multi-component complex system, reaction conditions (mainly T and P), the amount of chemical species entering and leaving the system and the considered components should be defined. Including or excluding a single compound can significantly influence the equilibrium composition. Hence, a good knowledge with the system under investigation is important. Catalyst choice also influences the side product formation as previously discussed in section 2.3.

For the stoichiometric chemical equilibrium model, experimental reaction equilibrium constant ($K_{eq,j}$) were adopted from Schmitz et *al.* at certain temperature range.[78] The Gibbs-Helmholtz approach was used to assess the $K_{eq,j}$ values at other T within the investigated range (T= 60-105 °C). The chemical equilibrium problem was solved using an algorithm adopted from O'Connell.[2] Newton-Raphson approach was used to find the number of moles of each component at equilibrium meeting the equilibrium criteria by equating the chemical potential to zero while conserving the atomic balance constraint.[122]

After evaluating the chemical equilibrium composition, the phase equilibrium calculations are initiated by assuming reaction occurring in one phase and a vapor fraction. Iterations are done till the components compositions that leads to reaction equilibrium composition in the liquid phase which is having equal gas phase fugacity. This is explained in details in attached publication.[54] Chemical-phase equilibrium criteria relations that are simultaneously solved are described as follows:

Reaction Eqm.: $\quad \sum_i^C v_{ij}\mu_i = 0 \qquad j = 1,2,\dots\dots,R \qquad$ (1)

Phase Eqm.: $\quad f_i^l = f_i^v$

$$x_i \gamma_i P_i^s = y_i P \qquad i = 1,2,\dots\dots,C \qquad (2)$$

Where μ_i is the chemical potential of component i, v_{ij} is the stoichiometric coefficient of every component i in reaction j, $f_i^{v,l}$ is the fugacity of i components in a certain phase, y_i and x_i are the mole fractions in vapour and liquid phase respectively, P is the total pressure, P_i^s is the saturation pressure of component i, and γ_i is the activity coefficient of i components in liquid phase.

With the model successful convergence and preliminary validation from literature experimental data, a parametric study was done varying the reaction T, the feed H_2O content and the FA/MeOH mass ratio. It was concluded that a H_2O free feed at FA/ME composition 1.8-2 mol mol^{-1} at the lowest T are the optimum conditions for single path highest OME$_{3-5}$ yield (0.14 g$_{OME3-5}$ g$^{-1}_{product}$). These conditions were the basics for developing and operating the test stand for anhydrous FA synthesis.

3.2 Anhydrous FA synthesis continuous test setup

The defined FA/ME molar ratio desired for optimum OME synthesis was then translated into target performance of this experimental test setup. Therefore, MeOH conversion U_{MeOH} of more than 67% with FA selectivity S_{FA} of more than 90% were targeted. The MeOH endothermic dehydrogenation reaction occurs at elevated temperatures (higher than 700 °C) for considerable conversion of MeOH.[76] On the other hand, high temperatures promote the pyrolysis of MeOH and enhance the thermodynamically favored reaction of MeOH to CO and H_2 (reaction 15). Therefore, the system under investigation is a kinetic controlled system where a selective catalyst and reactor design with specific prerequisites should be met for satisfactory anhydrous FA product yield.[103] These prerequisites are: (a) fast heating of educts to avoid pyrolysis of MeOH, (b) fast reaction over the catalytic species (residence time less than 0.01 s),[76] (c) fast quenching of the products to avoid further conversion of the thermodynamically unstable FA to CO and H_2 and (d) maintaining the stream containing the FA product in a stable temperature range (usually between 100-150 °C) to avoid the very non-stable monomeric FA from polymerization.[76,103]

A continuous flow test setup was developed to investigate this key reaction step for the described process. The conception, design, safety study, procurement, construction, commissioning and operating the continuous test setup was one of the major tasks of this thesis. In the following a brief description of the test setup and its components is given.

3.2.1 Continuously operated test setup

The process flow diagram of the test setup is shown in Figure 15. The test setup consists of three main sections namely: (1) the feeding section, (2) the reaction section and (3) the analytical section. In the feeding section, argon (Ar), nitrogen (N_2), hydrogen (H_2) and air are the available feed gases from in house supply at Fraunhofer ISE. H_2 is mainly used for leakages testing and was connected when needed in the N_2 or Ar lines for this purpose. Ar and N_2 were used for flushing the test stand and as carrier gases. Air was

used for catalyst regeneration and for partial oxidation testing. Feed lines are constructed as follows: a pressure regulator (DM) after each feed gas source was mounted followed by a mass flow controller (MFC; MKS-Multi gas controller 647B/C). Magnetic valves (MV; 2/2 ways solenoid valve from Bürkert) were then constructed allowing the remote control of the gas feeding and automatic response in case of emergency. Back flow valves (RV; Hylock) were then installed to prevent the back mixing of the feed gases. The orientation of the feed gases either towards the saturator (B2), reactor 1 (R1), reactor (R2) or towards the analytical section is regulated by the three way valves V-24, V-12 and V-25 (Hylock).

MeOH can be introduced to the test setup by saturation in carrier gas. For this purpose, a saturator with two temperature zones was integrated in the test setup. The MeOH reservoir T was controlled using a heating coil with T regulator. The upper part of the saturator is a double pipe heat exchanger where the saturated gas flows in the inner tube while a cooling medium supplied from a cryostat flows in the outer tube. The saturation T is monitored using a resistance temperature detector (Pt-100) and displayed on an external data acquisition device (Agilent 34970A) for minimal T readings error. The saturation P is also monitored using a digital P transmitted (Wika) and displayed in the LabVIEW monitoring and control program. The saturation of MeOH is also a function of the residence time of the flowing gas through the saturator. After the controlled saturation of MeOH in the carrier gas, the feed gas can be introduced for the analytical section where the steady state concentration can be detected. After the saturator, all the lines towards the reaction section should be heated to avoid MeOH condensation. All lines were heated using heating coils (Horst) which are controlled using external T regulators (PI regulators; Gefran/Eberle) that are manually set according to the test purpose.
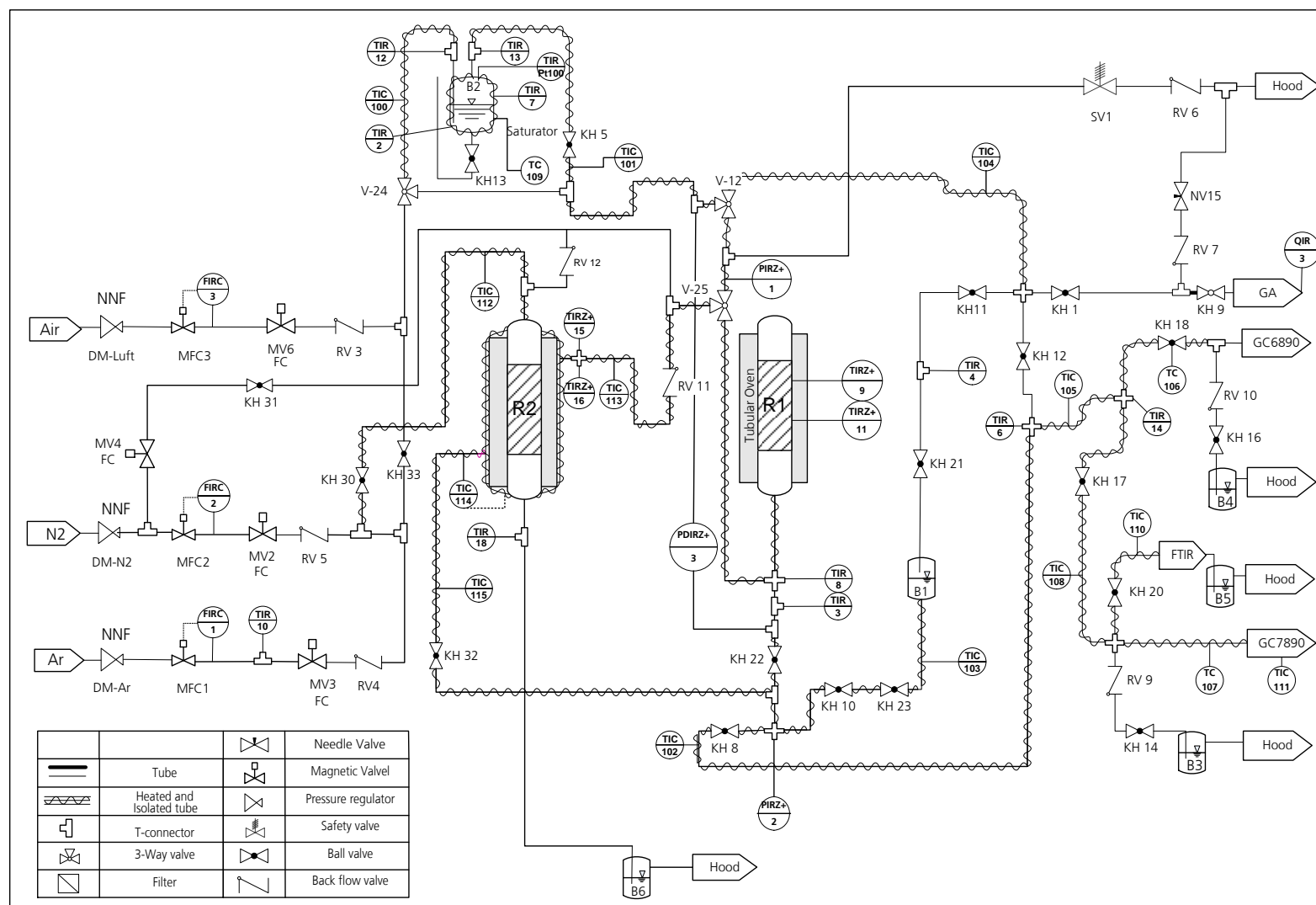
Figure 15 Process flow diagram for the continuously operated anhydrous FA synthesis test stand

In the reaction section two reactors were constructed. R1 is used for the endothermic high T MeOH dehydrogenation test and heated in an electrically heated tubular oven (Carbolite HST12/600) with a programmable T ramp up to 1200 °C (reactor description in attached publication[123]). A double pipe stainless steel reactor (R2) heated with electrically heating jacket was also constructed for testing partial oxidation reactions, benchmark tests using commercial FA synthesis catalysts and for testing pre- or post-catalytic dissociation reactions of FA and MeOH. The pressure before and after the reactors was monitored using digital pressure transmitters PIRZ1 and 2 and a differential pressure sensor PDIRZ 3. The product T should be kept higher than 100 °C to avoid FA polymerization. Hence, all product lines after the reaction section are electrically heated and isolated. A safety valve SV1 was installed in the reactor feeding line preventing pressure rise events than the desired limits.

The analytical section constitutes of two gas chromatographs (GC), gas analyzer (GA) and a Fourier Transfer Infrared Spectrophotometer (FTIR). The Agilent GC 6890A with CP-Sil 5CB (30 m × 8 µm) capillary column and a thermal conductivity detector (TCD) was suitable for MeOH and FA peak separation. An Agilent GC 7890A Poraplot-Q capillary column (30m x 530 µm x 20 µm) and TCD for identification of the other components that were not detected or well separated from other products by the GC6890A (H_2, CO, CO_2 and H_2O). An ABB GA with a Caldos 17 and Uras 14 modules was used for the online detection of H_2, CO, CO_2 and CH_4. The product gas from the reactor was split between the GC and GA lines using the valve arrangement (KH8, KH10 and KH22). The product stream towards GA was first washed in a Na_2SO_3 solution (B1) to washout the FA and then introduced to internal cooler in GA operated at 5 °C prior being filtered and directed to the GA non-dispersive infrared detectors. This preparation is essential since GA available detectors are not suitable for condensable gases present in the product samples. GA measurements allow online monitoring of the test progress which is displayed on the LabVIEW program. The rest of the product is directed towards GCs where discrete analysis (11 minutes per chromatogram using the developed method within this thesis) was done. The rest of the product gas was washed in Na_2SO_3 solution (B3 and B4) before being discharged in the fume hood exhaust gas lines. The test stand pressure was regulated *via* a pressure sink regulated using a needle valve (N15).

Feed gases flow rates, magnetic valves setting and electrical safety allowance for reactors heating were controlled using a monitoring and control LabVIEW program. Also all the T, P and online GA readings were monitored using a LabVIEW program. 19 external T regulators with corresponding thermocouples (mainly N-type from TC Direct) are installed for achieving the steady state desired T in the whole test setup sections.

The test setup is installed in two neighboring fume hoods with air ventilation to avoid the escape of the gases from test setup to the laboratory environment. Gas sensors for CO and H_2 are installed in the fume hood and connected to a gas alarm device. MeOH

and gas product washing solution are filled in the corresponding reservoirs before test start and without any gas flow or heating the lines. During test procedure manual valves adjustments could be done by opening the fume hood sliding door. Feed gases supply are controlled *via* MVs which allows the shutdown of the process feed in case of emergency. Manually open MVs are also installed to allow the introduction of flushing inert gases in case of emergency.

A safety concept was initially defined (PAAG) and translated as shutdown criteria for the LabVIEW control program (i.e. *T* or *P* rise over pre-defined limits). A liquid collecting plate is installed under the test setup to avoid the spread of liquids in case of leakages. The test stand 220 V electrical power supply can be completely cut through emergency button. However, 12 V supply for MVs is still available in case of emergency. Grounding of the test stand electrically heated lines and test setup components for avoiding static charges are also done as part of electrically approval test from the technical department of Fraunhofer ISE. Only trained personnel were allowed to operate the test stand after attending three levels of safety trainings and only with the corresponding lab safety equipment. A photographic presentation of the test setup and a schematic of the LabVIEW interface are presented in appendices 7.1 and 7.2.

3.2.2 Catalytic investigation

A literature review for this reaction catalysts was done as introduced in section 2.3. Initially Ag-MgO-SiO$_2$-Al$_2$O$_3$ catalyst was synthesized at FhISE chemistry labs according to the method reported by Ren et *al.* with claimed complete U_{MeOH} at very high S_{FA}.[124] A tubular glass reactor from a previous project was used for this purpose which was heated in electrical oven. The reactor was integrated in a continuous flow test stand as described in attached publication[123].

After commissioning the test setup, tests over similar conditions (T = 600°C, $GHSV$ = 10,000 h^{-1} and MeOH concentration in feed *ca.* 20 wt.%) as Ren et *al.* were carried out.[124] Highest selectivity reached in this reactor type was 18.4% at U_{MeOH} of 41%. It was visually clear that much of the MeOH feed was coked (reaction 16) before it reached the catalyst bed in the long reactor tube going along the tubular oven. Hence, a new reactor concept was designed with the aim of satisfying the aforementioned reactor criteria.

This innovative reactor type was called Annular Counter Current Reactor (ACCR) and is described in detail in attached publication[123]. However, the temperature profile was enhanced and less coke formation were noticed using the new reactor type, the performance of this catalyst type did not significantly improved. *T, GHSV* and MeOH concentration in the feed were varied with the highest S_{FA} reached of 30% at 16.4% U_{MeOH}. Therefore, this catalyst was phased out and the literature search started once more.

The next candidate was the Na_2CO_3 catalyst. This group IA sodium based catalyst showed interesting performance as explained previously in section 2.3.1. Na_2CO_3 is cheap, abundant and can be produced as industrial waste. Su et *al.* investigations of the mechanisms and performance using Na_2CO_3 and Na_2CO_3 supported on charcoal for selective anhydrous FA synthesis emphasized the potential of this catalyst system. More than 50 experiments were pursued at different parameters namely *T*, particle size, feed concentration and *GHSV*. The purpose is to achieve the target reaction performance and investigate the stability of the catalyst at these conditions. Best achieved performance was U_{MeOH} of 40% with more than 90% S_{FA}. More MeOH conversion can be achieved either by increasing the residence time or the reaction *T*, both parameters variation was accompanied by reduction in selectivity. Important to mention also that this performance was achieved at low MeOH concentration between 5-6 wt.%.

Additionally, the results were strongly deviating by shut down and restarting the test setup. This was preliminary explained by strong catalyst surface property change using scanning electron microscopy SEM technique. In spite of that Na_2CO_3 catalyst has interesting economic and sustainability benefit and performed in the vicinity of the desired performance, the catalyst characterization and deeper understanding were not in the frame of this thesis. The catalyst optimization to reach the target performance is to be carried out with project partner. Experimental results extracted from these runs were used for the implementation of a global kinetic model as explained later on.

3.3 OME batch synthesis reactor

For the extended validation of the process model using FA and MeOH feedstock or other feeds, a batch OME synthesis reactor was used. An old autoclave from Carl Roth® with stainless steel 500 mL reactor cylinder was revamped and reconstructed according to the OME synthesis reaction needs. The autoclave cylinder is installed in housing with electrical heating jacket and sits on a magnetic stirring disc. The feed and product flow lines and the concept behind their installation are described in attached publication[53]. This batch reactor was used for testing several catalysts namely Amberlyst-36®, DW50x2®. Mainly thermodynamic reaction equilibrium data were extracted but also kinetic tests were carried out for basic comparison between different catalysts. The validation of the extended OME reaction model using TRI and OME_1 feed was also carried out using the batch autoclave reactor. A photographic presentation of the test setup is presented in appendix 7.3.

3.4 Analytics

In the experimental platform in this work, two main synthesis were considered namely: the anhydrous FA synthesis taking place in the gas phase and the OME synthesis taking place mainly in the liquid phase. The objective was to develop the suitable analytical techniques for precise quantitative analysis of the different components in different phases as illustrated in Table 5. Gas chromatography, online gas analysis and volumetric titration where the techniques used for the considered components mixture qualitative

and quantitative analysis. Two GCs with TCD detectors were connected to the continuous anhydrous FA test stand for gas phase components analysis. As shown in Table 5, several components can be detected by both GCs. However, the separation of FA, MeOH and H_2O was not possible using the GC7890 with poraplot Q column.

Table 5 Overview of the analytical techniques used for different system components analysis

Technique	GC		GA	GC	Titration
Detector	TCD		Uras14/Caldos17	FID	
Model	6890	7890	ABB	7890	
Phase	Gas			Liquid	Liquid
Method	Ref.[54]	Ref.[54]		Ref.[53]	SSM - Walker[125]
FA Synthesis					
N_2	✓	✓			
Ar	✓	✓			
H_2		✓	✓		
CO		✓	✓		
CO_2		✓	✓		
CH_4		✓	✓		
CH_3OH	✓	✓			
H_2O	✓	✓			
DME	✓	✓			
CH_2O	✓	✓			
OME Synthesis					
CH_3OH				✓	
CH_2O					✓
OME_n				✓	
H_2O					
TRI				✓	

Also separation of H_2O and DME peaks in the GC7890 was not possible without interfering with other components peaks. For these reasons GC6890 with CP-SIL5CB capillary column suitable for FA, MeOH, DME and H_2O system separation was employed. Moreover, this column was not suitable for separating the CO, CO_2 and H_2 peaks. Several methods were developed to achieve this peak separation on both GCs. Mainly the varying parameters were the oven T ramping, the column pressure and the split ratio. With this configuration, all components can be discretely detected using both GCs. Simultaneously, the anhydrous FA synthesis product mixture was continuously analyzed using an ABB GA equipped with a Caldos 17 and Uras 14 modules. Those make continuous measurement of components in gaseous phase based on non-dispersive infrared absorption and thermal conductivity respectively. GA was used for the online detection of H_2, CO, CO_2 and CH_4. An online product gas absorption section

was constructed for the FA complete absorption and analysis when needed according to the titration method described by Walker.[125]

For the OME liquid phase samples analysis from batch experiments, GC with Flame Ionization Detector was used (GC-FID). Methods for analyzing mixtures with high concentration of FA in the end product or for product mixtures with high water content were adopted from literature and modified to achieve all component separation tasks.[52,78] FA liquid phase analysis was done based on a Na_2SO_3 volumetric titration method, using 1M HCl (aq) as titre and thymolphtalein as indicator.[125]

For the gas phase components calibration mainly saturation of components MeOH, H_2O, OME_1 or using calibration gas mixtures cylinders was used. For liquid phase calibration, standard mixtures samples were prepared using internal standard and a solvent. Calibration of $OME_{n>5}$ was done using extrapolation based on the linearity of the number of carbon atoms of OME fractions to the area per mass fraction of the components. More information about the analytical equipment and the methods used for achieving the quantitative analysis tasks are given in the publications in appendices 7.5, 7.6 and 7.7.

3.5 Extending OME synthesis reactor model

OME synthesis model was then improved by adopting a non-stoichiometric Gibbs minimization approach (NSGM) using stochastic global optimizer (SGO) solver. This development was done for extended description of OME reaction system not only in a single path but rather when considering recycling the non-reacted components and other OME fractions than the desired ones. The modelling algorithm previously discussed adopted from O'Conell started by initialization step.[2] An initial guess is required for the whole system components equilibrium composition that is matching the atomic balance constraint and in a suitable range of each component that do not mislead the systematic solver. An initialization algorithm was developed for finding the equilibrium composition of the considered components when only MeOH, FA and possibly H_2O are the system feed. When considering the recycling of non-reacted components and other OME fractions, the numerical solver in this case has an inherent initialization difficulty.

Applying the NSGM with the objective function of minimizing the total Gibbs free energy in eqn (3) have several advantages which are: it only requires the knowledge of which components are participating in the system, the Gibbs energy of formation at the reaction *T*, no need for an accurate initial guess and it is a simple and scalable method once the system is well defined. The description of the model algorithm based on NSGM is presented in attached publication[53]

$$G^t = \sum_i^N n_i G_i^0 + RT \sum_i^N n_i ln X_i \gamma_i \qquad (3)$$

Where G^t= total Gibbs free energy, N = number of species present in the reacting mixture, n_i= number of moles of component i, R = gas constant, T = temperature, X_i = molar fraction in the liquid phase, γ_i = activity coefficient of component i in the liquid phase and the index 0 refers to the standard state.

OME synthesis reaction with recycle was implemented considering ideal separation units after the OME synthesis reactor. Thus, the reaction equilibrium was converged in Matlab®, equilibrium compositions were defined followed by splitting the product stream into final OME_{3-5} and water product and recycling the rest of components to be mixed with the fresh FA and MeOH feed. Separation factor vector a_i was defined in the algorithm where each component split rate is defined. The optimum feed molar ratio of FA/MeOH corresponding to minimum recycle ratio and desired OME_{3-5} product composition distribution was defined at 1.8 mol mol^{-1}.

At this level of knowledge, the process material balance could be evaluated. The MeOH dehydrogenation reactor is considered as stoichiometric reactor operating at the desired U_{MeOH} and S_{FA} supplying the OME reactor with FA and MeOH at 1.8 mol mol^{-1}. The overall process yield of MeOH/OME_{3-5} and important process key performance indicators could be defined (i.e. reactors yield, recycle ratios,etc).

3.6 Anhydrous FA synthesis global kinetic model

The next step for improving the simulation platform was to transform the experimental results of the anhydrous FA synthesis into a global kinetic model. For the Na_2CO_3 catalyst considered in this work, this kinetic data for the dehydrogenation reaction were not available in literature. Three main reactions are considered in this model. Reaction rate constants K_j values for the main contributing reactions were evaluated experimentally at T = 690 °C using the annular counter current reactor ACCR. K_j for the MeOH pyrolysis to carbon was evaluated from previously published experimental results over similar catalyst system.[126] An ideal plug flow reactor model was adopted with some assumptions as discussed in attached publication.[123] The equation system is implemented in Matlab® whereby at a certain feed concentration C_{Ao} and given residence time, the concentration of each component C_i in the product stream can be evaluated.

3.7 Physical property model

At this point of modelling maturity, the whole process flow sheet detailed simulation is of interest. This comprises of including the heating and cooling equipment, detailed description of the separation equipment and including auxiliary units. The software CHEMCAD® Version 5.2.0 is the available flow sheet simulation program at the hydrogen technology division at Fraunhofer ISE. CHEMCAD® contains a variety of models for various process units, the possibility to implement user generated models and cost functions for most of the units. For starting a simulation, the chemical

components have to be chosen from a built-in library which contains physio-chemical and thermodynamic properties for more than 1900 components. Additionally, the user can implement own defined components and property models.

The interest for investigating OME_n, HF_n and MG_n only increased recently, thus these components were not included in the built-in component library and have been added manually to the component library. A dataset of OME_{1-8} properties have previously been reported.[46] This dataset provides parameters for the correlation of the vapor pressure P_i^s, enthalpy of vaporization h_i^v, heat capacity of ideal gas C_{p_i}, standard enthalpies of formation $h_{f_i}^o$, liquid molar density ρ_i and the critical temperature T_c. In addition, values for the molar mass M, specific gravity, standard Gibbs energy of formation $G_{f_i}^o$ (evaluated from the reaction rate constants as discussed in attached publication[53]). For some of the added properties, regressions have been necessary to convert the temperature dependencies from one equation to another form of equation as used by CHEMCAD®. These were evaluated using a natural regression tool based in CHEMCAD®, with good agreements found with comparison to original values.

For consistency, FA and TRI have also been included as new components, even though they already existed in the CHEMCAD® database. The molecular weight, boiling temperature T_b and the molecular structure have been implemented, as well as the UNIFAC parameters from Kuhnert et al.[47] counting for the non-ideality in the liquid phase. CHEMCAD® facilitates the calculation of unknown properties based on group contribution methods, (e.g. Joback and UNIFAC), which act as good first estimation but however lead to relatively large errors as described previously by Poling et al.[48] In particular for the $G_{f_i}^o$ evaluation, high inaccuracies may result as a consequence of the logarithmic relationship with the equilibrium constant K_{eq}, and therefore these methods have not been used.

For HF_n and MG_n, there are very few properties available in the literature. Therefore, to still use the commercial software CHEMCAD® to solve the separation task after the reaction unit, some assumptions had to be made. First, as described by Schmitz et al.[51], the OME reactions reach equilibrium for MeOH, FA, H_2O, OME_{1-8} and TRI and HF_{1-10} and MG_{1-10}. Second as stated by Hahnenstein et al.[127], the degradation reactions of HF and MG are slow in comparison to typical residence times in separation equipment. Third, $HF_{n>1}$ and $MG_{n>1}$ stay in the liquid phase. According to Albert et al.[128] „there is no experimental evidence for the presence of substantial amounts of poly(oxymethylene) glycols or poly(oxymethylene) hemiformals in the gas phase". Therefore, the process considers the equilibrium composition to be achieved in the reactor and further changes so slowly in comparison to the separation residence time that this change can be neglected. Furthermore, $HF_{n>1}$ and $MG_{n>1}$ completely split to the bottom stream.

The minimum required properties for the distillation calculation comprise the dependency of vapor pressure on temperature, the dependency of the heat capacity on

temperature and for HF_1 and MG_1 the enthalpy of vaporization. Liu et *al.*[129] published a physicochemical model for VLE in mixtures of FA with MeOH and FA with H_2O to describe the enthalpy changes upon vaporization. From this model heat capacities for HF_{1-10} and MG_{1-10} could be extracted. However, since the considered temperature range of 323 to 363 K for FA with H_2O and 312 to 347 K for FA with MeOH is comparatively small to the temperatures reached in the distillation unit, the extrapolation of these relations led partially to negative heat capacities. Therefore, the heat capacities of $HF_{n>1}$ and $MG_{n>1}$ have been assumed to be equal to the heat capacity of the corresponding OME, whereby the heat capacity of HF_{9-10} and MG_{9-10} has been assumed to be equal to OME_8. The extracted relations for HF_1 and MG_1 were used, since they will mainly stay in the vapor phase and therefore exposed much smaller temperatures in the distillation separation units. Albert et *al.*[128] furthermore published relations for the vapor pressure depending on temperature for HF_1 and MG_1 for the temperature range of 293 to 413 K. However, for $HF_{n>1}$ and $MG_{n>1}$ no vapor pressure relations could be found. But since they are assumed to stay in the liquid phase their vapor pressure has been assumed to be equal to the vapor pressure of OME_8.

3.8 Modelling interface

After implementing the physical and thermodynamic properties model of OME in the CHEMCAD® platform, the developed reactor models in Matlab® are to be integrated. The reason not using CHEMCAD® algorithms for describing the reactor units was the weak agreement between results from the CHEMCAD®, Gibbs and equilibrium reactors modules and the experimental and theoretical product compositions as explained in Ouda et *al.*[123], an alternative Microsoft Excel®-based unit was developed to include the reaction code developed in Matlab® using NSGM. In this context, Microsoft Excel® offers the possibility to open and run a Matlab® code *via* the use of a "*Visual Basic for Applications*" VBA add-on, as well as exchanging matrices and single values, as long as both programs are installed within the same operating system.

The Excel® unit allows creating a tunnel were a set of com interfaces to the CHEMCAD® simulation can be exchanged. This is very advantageous since the topology of a flowsheet can be retrieved (e.g. stream and units data can be extracted or altered). The extracted results from Matlab® using VBA can be translated to the CHEMCAD® format and introduced in the CHEMCAD® platform. The development of the Microsoft Excel®-based VBA unit is significant here as it enables the combination of the functionality of CHEMCAD® and the flexibility and calculation speed of Matlab®. Running the Matlab® code through the VBA node does not alter the results as long as the input/output variables (as defined in each platform) are translated correctly via VBA. Calculations using the VBA node as interfaced between the two software platforms needed more computational time than those performed with Matlab® directly.

3.9 Product separation – rigorous distillation units

Within the simulation layer, at this stage the task was switching from the Matlab® single reactor models to the CHEMCAD® platform using the aforementioned modelling interface. The anhydrous FA synthesis reactor kinetic model and the OME equilibrium reactor model were integrated by adding the corresponding Excel® units. The heat exchange equipment and pressure compensation units were implemented from CHEMCAD® unit library. The OME reactor product was so far separated and recycled within the reactor model in Matlab® using the ideal separation factor a_i. This complex mixture separation was then extended using rigorous separation column units in CHEMCAD® as follows.

The OME reaction model in Matlab® was adjusted for single path convergence and the product was introduced to a distillation cascade that was allocated based on the work of Stroefer et *al.* were similar equilibrium mixtures were separated.[130] For such complex mixtures separation with considerable non-ideality in the liquid phase (considered by implementing UNIFAC models as previously discussed), the problem starts first as a simple design case were reduced models are used for initial parameterization of the separation column. The shortcut column unit (SHOR) from CHEMCAD® was used for this purpose using Fenske-Underwood-Gilliland method were the light and heavy key components, minimum reflux ratio are sufficient for obtaining estimated column parameters. The results of the design case are then used for the rating case where rigorous distillation column unit (SCDS) is implemented.

Employing SCDS unit, the separation of complex multi component systems using the MESH equations can be achieved. The SCDS unit was converged using the simultaneous method (SC) as a solver (i.e. Naphthali-Sandholm method) which was better suited for non-ideal mixtures than other global Newton models.[131] The specifications of the condenser and reboiler should be defined as convergence objective functions. The reflux ratio as the condenser specification and the reboiler temperature as the reboiler specification were selected. Pressure drop within the column was accounted according to Henley and Seader with 6.9 mbar per distillation stage, 345 mbar for the condenser.[132] The iteration limit of SCDS column was extended from the default maximum of 20 iterations to 100 iterations to achieve convergence. A built in profile generation algorithm in CHEMCAD® was selected for generating the initial T-profile. Also default convergence tolerance values from CHEMCAD® were chosen.

Extracting the data from the SHOR column unit allowed the initialization and convergence of the SCDS column unit. SCDS columns in the process flow sheet were consequently converged using the methodology described here untill the final products OME_{3-5} and H_2O were separated and the rest of components were recycled to the OME reactor Excel®-unit. The reaction equilibrium model was then re-compiled and the loop for adjusting the SCDS columns continued until steady state was reached. More details about the distillation algorithm convergence are discussed in attached publication.[123]

3.10 Process heat integration

With the process flowsheet implemented in CHEMCAD® platform, the next development step was the process heat integration. For this purpose PinCH 2.0 software was used. Pinch software accepts Excel® spreadsheet data and therefore can be interlinked with the flowsheet topology of CHEMCAD®. Initially, a developed VBA code will extract streams data (each stream initial and final T) from CHEMCAD®, segment each stream at predefined T intervals, flash the stream and run a phase change check. If no phase change occurs, an average C_p would be evaluated and the stream data would be delivered to the Excel® spreadsheet feeding the PinCh software. If phase change occurs within the T range, the stream can be split into various segments with sensible and latent heat (within phase change) regions. The phase change is then assumed to occur isothermally and the latent heat is extracted using a CHEMCAD® function. The sensible heat sections average C_p are calculated as no phase change segments. These streams data are also then exported to PinCH *via* the Excel® unit.

For the definition of the heat transfer coefficient, the heat transition coefficient was used according to Towler *et al*.[133] and doubled, thus the internal and external heat transfer coefficients are assumed to be equal, while the influence of heat conductivity is neglected. Mass flow and pressure level were taken from CHEMCAD®. After the definition of the process streams the utility streams were defined. Therefore, cooling water at 25 °C with an increase of additionally 10 °C was defined as cold utility and steam at 80 bar was assumed as hot utility. The heat exchanger network (HEN) is then constructed with the target of maximizing the process heat recovery at the least cost. The composite and the grand composite curves can then be generated. After the HEN allocation was defined in PinCH software, the process flow sheet was accordingly updated and the whole flow sheet convergence loop repeated.

3.11 Process production cost assessment modelling

The last but not least step for simulation platform development was the cost assessment model integration. This basic cost evaluation model was implemented in the CHEMCAD® platform as an Excel® unit. A VBA code was developed which allowed the extraction of material streams and energy demand of the process units. Within the Excel® file, a simple production cost model was constructed. The capital costs (CAPEX) and the operational costs (OPEX), which constitutes mainly of variable cost of production (VCP) and fixed cost of production (FCP), are evaluated as follows. Regarding CAPEX, a capital investment of 1 million ton annual capacity plant which was used by Schmitz et *al.* was adopted in this work.[69] To adjust the CAPEX to the considered capacity in this work, a power law with a capacity factor, also called six-tenths rule due to the regression coefficient of 0.6 was used.

For the OPEX, VCP are basically MeOH raw material cost and the process energy cost. The former is provided by the material balance while the latter is calculated from the

process energy demand as evaluated in this work. The process energy is supplied by high pressure steam, natural gas, cooling water and electricity. The FCP are evaluated using a factorial method as discussed by Baerens.[134] Several CAPEX or OPEX cases can be evaluated using the developed tool with slight changes in the user defined parameters.

3.12 Hybrid process model

With the integration of the production cost assessment model, the simulation platform in CHEMCAD® is completely defined and is called the hybrid model. Several outputs at different scenarios could be retrieved from this robust tool. (1) Material and energy stream tables, (2) process key performance indicators KPIs, (3) process energy efficiency, (4) allocation of process energy consumption and (5) production cost can be extracted from the hybrid model. Importantly, the effect of technology development or altering on the overall process or on single units or modules can be swiftly investigated. Also the hybrid model tools (i.e. heat integration, cost assessment) are developed to be flexible for process flow sheet changes. Thus with a proper process definition, the developed hybrid model can be considered a scalable and tunable process simulation tool.

4   Synoptic discussion

There is a perspective market for OME as diesel alternative or as a green solvent; however OME need to be made available to launch these markets. The OME synthesis process is the bottle neck of the OME value chain. This thesis focus was to produce OME in the most economical way using simple and scalable technology. The thesis focus thus lies in the technical sphere as highlighted in Figure 16. The feedstock was for instance fossil MeOH in order to compare the process with conventional OME synthesis processes. Water management is one of the major issues towards efficient OME synthesis. The direct OME synthesis introduced in this work based on anhydrous FA (pre-OME synthesis step water management) allowed significant enhancements achieving overall process OME_{3-5} yield of 80.3 wt.%, synthesis energy efficiency of 71.7% and production cost 598.7 US$per t (at high production capacities of *ca.* 1000 kt/a).
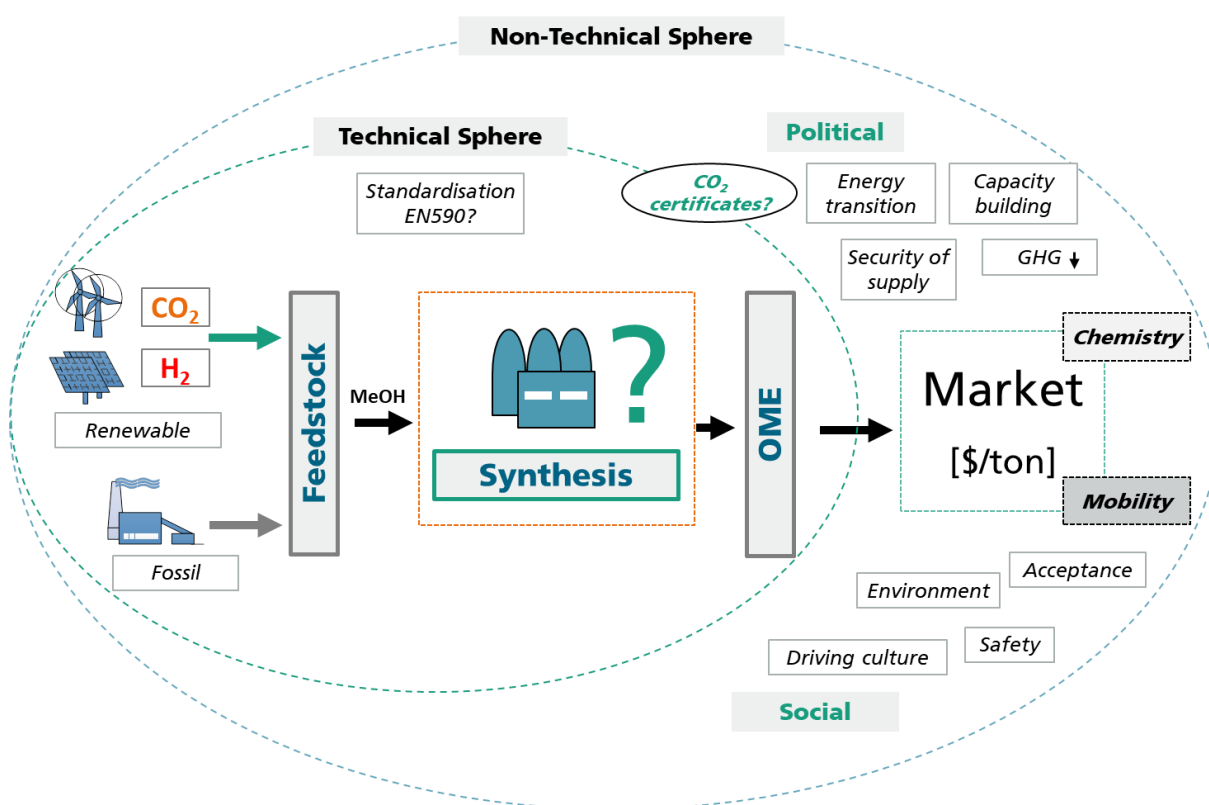
Figure 16 Description of the non-technical and technical spheres regarding OME production possibilities. TRL: Technology Readiness Level; MRL: Market Readiness Level; VOC: Volatile Organic Compounds; PM: Particulate Matter.

Additionally, if the water management pre the OME synthesis step as introduced in this thesis -using anhydrous FA feed- is coupled with post OME synthesis water management concepts by adsorption or extraction as introduced by Schmitz et al.[75] or Arnold et al.[2] respectively, significant process energy efficiency improvement can be achieved with considerable production cost reduction (attached publication[123]). Several synergies with other existing processes or technologies (e.g. heat integration with the MeOH synthesis, high temperature recovery from steel industry) were considered which

showed substantial process energy efficiency enhancement potential. Considering an optimistic scenario combining the aforementioned process developments, the best process performance was at overall process OME_{3-5} yield of 80.3 wt.%, synthesis energy efficiency of 76.9% and production cost 539 US$ per t (production capacity *ca.* 1000 kt/a). Other literature processes could produce OME at synthesis energy efficiency of 52% and best cost of 615 US$ per t.[53,69]

If OME are to be introduced as an energy vector or a chemical that could contribute to a net CO_2 reduction and achieve the GHG emission reduction targets, a sustainable feedstock should be used for the OME synthesis. This sustainable (denoted hereon as *"green"*) MeOH can be produced using PtL technology by hydrogenation of CO_2 as presented in section 1.1. Assuming an ideal synthesis process is employed with the highest possible MeOH to OME_{3-5} theoretical yield of 87 wt.% and no external energy consumption, With green MeOH cost ranging between 653 and 1557 US$ per t, the OME_{3-5} production cost is 751 and 1791 US$ per t.[135] A rather high cost compared to the fossil diesel (460-870 US$ per t, production cost without taxation).[69] Therefore, an efficient synthesis process can only enhance the OME competitiveness in a fossil based economy and other measures should be introduced allowing the transition to a renewable economy. There are still some technical developments on the production side that needs to be done to improve the technology readiness level (TRL) of OME synthesis; however the introduction of OME to the market is not only a technical issue. The interactions between the technical and non-technical aspects are illustrated in Figure 16.

Along with the process technical feasibility, suitable market and legislative frames should persist for the introduction of OME in the current market structure. Promising technologies as introduced in this work need to be scaled up and demonstrated to produce sufficient OME for market initiation. Currently, developments and OME engine testing are being done in the automobile industry based on imported OME from China - which is containing impurities that could lead to hazardous emissions- or on batch small OME quantities with high purity synthesized in Germany; which are not enough for market initiation.[32,136–138] Chemical manufacturers should make efficient production processes available on large scale for market initiation and establishment. Nonetheless there is skepticism about which technology, which OME fractions, under which standards and for which application this should be produced. There is no market if there is no OME, and there is no OME if no market exists. This chicken and egg problem needs to be solved for launching OME market. The linkage between the academia, automobile manufacturers, chemical industry and political bodies as the main stakeholders should be coordinated. Within such consortiums, the TRL should be improved, the specific OME fractions for certain applications should be defined, the standardization of these fractions should be carried out and the OME market supply and demand should be coordinated. The OME production should be done in Europe and the final product should be standardized for the European market. Political incentives, standardization of E-fuels and governmental financial schemes are the main deciding

factors for introducing synthetic fuels into the market. Several technologies and products have been introduced to the market under the umbrella of such schemes as the solar PV systems financial schemes (e.g. feed in tariffs), infrastructural and financial support for electric mobility market introduction and introducing biodiesel as diesel blend.[1,9,17,18,21,22,139] Also the social acceptance aspect should be considered alongside the R&D in the early phases. Tremel et *al.* evaluated this aspect regarding MeOH, Fischer-Tropsch (FT) products and other liquid fuels. The results showed that FT fuels are the most socially accepted candidates due to their applicability in the current infrastructure and similarity to the familiar fuels.[140] This social acceptance is projected to be positive for OME considering their compatibility with the infrastructure, safety and the driving culture previously discussed in section 1.1.

Härtl et *al.*[136] and Wilharm et *al.*[137] discussed the challenges and scenarios towards the introduction of OME to the market. Regarding applying OME as diesel fuel, it is recommended to use OME as pure fuel and not as blends with diesel. This is beneficial regarding reduced engine emissions but also considering other factors as the non-miscibility of OME in diesel with low water content, the unknown interaction with diesel being chemically not defined and the non-compliance of OME-diesel blends with the EN590 standards. Diesel market in Germany only is consuming *ca.* 30 Mt per annum while the whole world OME production capacity is still in the range 30-40 kt per annum, therefore, it is recommended of using pure OME for limited market applications (e.g. public transport, motor saw, local maritime transport, agriculture machinery, stationary generators, etc) using dedicated OME engines. Short term goals for OME supply of 5 kt per annum are defined to supply the R&D and market launching demand. Consequently a long term OME production and market development plan was proposed which proceeds through step-wise shifting from batch OME synthesis in Europe (mainly in Germany at production cost of 16-26 US$/DEQ at capacity <1 kt per annum; DEQ: diesel equivalent quantity) and OME importing from China, towards pilot OME production scale (5 kt per annum, with production cost of 5.3 US$/DEQ, operating by 2023) and at this stage introducing green MeOH as feedstock along with the development towards large-scale production (cost depends on green MeOH, operating by 2030).[136]

Together with production capacity increase, OME standardization for the target market should be achieved. In this context, ASG analytic has a REACH permission to distribute up to 350 t per annum OME to supply OME for R&D purposes in Europe. For that permission several standardization efforts regarding defining a specification for OME$_{3-5}$ fraction as a fuel were carried out. A complete REACH registration allowing handling amounts more than 1000 t per annum requires the definition of all toxicological and environmental data.[137] Complementary to this scenario and based on the understandings and OME developments witnessed in the frame of this work, the chemistry market (e.g. solvents or CO_2 absorbents) represents a matching candidate regarding the demand capacities and the product market value. In this market, fossil

based OME can be currently competitive using the synthesis technology described in this work even at low production capacities (product market value 1-3 US$/kg).[141] Considering some cost reduction benefits from the legislative side, the competitiveness of "green" OME in the chemistry sector can prevail. OME need to be produced by a chemical manufacturer at the first place, this makes the chemistry market more potential launching market.

OME market introduction could also be alleviated by considering the several potential benefits for the different stakeholders using OME as fuel alternative or a chemical. When these benefits are wrapped in business cases and translated as production cost benefits, OME market introduction should be possible. In the following some of the most prominent benefits are elaborated. For OME producers, OME can be produced using PtL technology with a "*drop-in*" characteristic allowing net CO_2 reduction which can be reflected as production cost benefit. On the OME distribution and storage side, there are potential benefits regarding the environmentally benign, interesting physical properties and non-hazardous OME properties (OME are also water compatible and rapidly biodegradable).[138] This can allow storage and distribution of OME using simple technologies and within the available infrastructure. There are also several benefits in the utilization phase when considering OME as diesel fuel alternative in the mobility sector. The automobile manufacturers are seeking using alternative fuels as active substance to confine with the amended emissions regulations avoiding the increased cost of including exhaust gas treatment complex and expensive systems.

On the other hand, legislations concerning local emissions -specifically NO_x and PM2.5 emissions- as the air quality directive 2008/50/EC, Fuel Quality Directives (98/70/EC and 2009/30/EC and the regulation (EC) No 715/2007 represent a possibility for a political initiative to facilitate the introduction of "green" OME into the market (e.g. tax reduction, CO_2 cost). Similarly, OME introduction in the chemistry sector to replace some solvents, CO_2 absorbents, etc. can be driven by the legislations which only permitted some hazardous chemicals to be used by trained personnel as dichloromethane (DCM) or similar legislations as the Volatile Organic Compound (VOC) solvent emissions directive 1999/13/EC where the replacement of solvents with high VOC emissions with rather environmentally benign alternatives is promoted. There are several benefits on the political aspects to facilitate introducing such green alternatives to the market from which: (1) they provide a feasible lever to achieve the national and international GHG reduction targets, (2) can offer the security of supply since they can be produced based on local renewable energy resources, (3) can provide chances for sustainable economy growth with several capacity and job building potential and (4) offer sector coupling possibilities which enhances achieving the energy transition targets.[18,21,24,39,138,142]

In the light of this discussion the current status, challenges and opportunities towards introducing OME to the market have been elaborated. Together with developing technically, economically and ecologically efficient process; social and political aspects

should be considered for successful market initiation. The biggest obstacles towards OME market initiation next to an efficient OME production process are the definition and standardization of certain OME fraction for a specific application. For the fuel market standardization is undergoing for the OME_{3-5} fraction and a market introduction scenario is defined. Pure OME_{3-5} fraction is preferred to be used in limited markets using dedicated OME engines. Considering the chemistry sector, there is a perspective potential for introducing OME for some applications with higher market value than the fuel sector. Generally for green OME market introduction, incentives need to be done to facilitate the scale-up of efficient synthesis processes. Also the cost benefit of GHG saving must be made accessible for fuel, producers and OEM.

5   Summary and Conclusions

Oxymethylene ethers (OME) are a novel class of oxygenates that have interesting thermo-physical properties making them attractive as a diesel fuel substitute, solvents and CO_2 absorbents. In this work a new OME synthesis process based on methanol as the only feedstock is introduced. The two steps direct synthesis starts with MeOH endothermic dehydrogenation to produce a mixture of anhydrous formaldehyde, H_2 and non-reacted MeOH, followed by converting the product of this step in a second reactor to higher OME. The theoretical efficiency of the direct OME synthesis process starting from hydrogenation of CO_2 to MeOH and followed by the synthesis of 1 kg OME_4 was evaluated at 87% which was advantageous compared to the conventional synthesis pathway using TRI and OME_1 feed with 67% theoretical process energy efficiency. Additionally, a CAPEX reduction potential was foreseen due to the direct process simplicity. The combined chemical and phase equilibrium model was developed where the complex OME reaction equilibrium considering 29 reactions involving 32 components were considered. A Newton-Raphson approach was used for the convergence of the equilibrium problem. Experiments in batch autoclave were carried out using the feed MeOH and FA to validate the implemented model. Two catalyst systems were used for these tests namely Amberlyst-36® and D50WX2®. Different feed compositions and synthesis temperatures were tested. The model showed strong agreement with the experimental results from this work and also with previously published data sets. The model was used to study the effect of temperature, FA/MeOH ratio and the presence of H_2O in the OME reactor feed. The results showed that the temperature variation did not significantly influence the system while a maximum yield of the target product OME_{3-5} can be reached at FA/MeOH molar ratio 1.8-2. The water content in the feed significantly influence the equilibrium yield of the target product, at 10 wt.% H_2O in the feed the OME_{3-5} yield is *ca.* 8 wt.% while with anhydrous feed the OME_{3-5} yield is 14 wt.%. Therefore, an anhydrous FA/MeOH feed can considerably enhance the process performance.

From the results of this equilibrium model, the desired FA/MeOH was defined and translated into experimental performance for the MeOH endothermic dehydrogenation reactor to produce this mixture. MeOH conversion >69% with FA selectivity >90% were targeted to reach FA/MeOH = 1.8-2 mol mol^{-1}. A continuous test setup was designed and constructed to test the catalytic endothermic dehydrogenation of MeOH. An Annular Counter Current Reactor ACCR was specially designed to meet the prerequisites of this kinetic controlled reaction and Na_2CO_3 was the selected catalyst. More than 52 test runs were carried out studying the effect of temperature, GHSV, MeOH concentration in the feed and catalyst particle size variation. Best results achieved were at MeOH conversion of 40% with FA selectivity >90%. However, the duration tests showed increasing of conversion trend while the selectivity was decreasing with time. After 60 hours on stream, the MeOH conversion was *ca.* 65% while the FA selectivity was *ca.* 70%. Material preliminary SEM analysis showed structural changes

between the original and used catalyst after short time on stream. Optimization of Na_2CO_3 catalyst or the choice of another catalyst system and the scale up of the reactor concept are aspects that should be further investigated. The results of the experimental investigation however enabled the extraction of data to evaluate the reaction rate constants of the main contributing reactions and implement a simple global kinetic model.

The OME synthesis reactor model was improved to include the recycle of the non-reacted components and OME fractions other than the desired OME_{3-5} product and to account more accurately for the non-ideality of the reacting mixture. The recycle calculations at this stage were considered using ideal separation by defining separation factor vector accounting for each component. Activity based reaction equilibrium constant relations were adopted and a non-stoichiometric Gibbs minimization (NSGM) approach was employed using a stochastic global optimizer (cuckoo solver) for the convergence of the complex reaction system with recycle. Important advantage of this Gibbs energy minimization approach is the lack of a dependence of the problem solution on a good starting point for iterations. The alternative methodology which would rely on the solution of a set of non-linear equations resulting from the condition of dG = 0 by using a Newton–Raphson approach or a similar numerical method, has an inherent initialization difficulty.

Experimental runs using the feed system TRI and OME_1 over Amberlyst-36® catalyst were carried out to validate the implemented model. Three feed ratios were tested each at three different temperatures. Also the model results were compared to experimental data sets from literature for the TRI/OME_1 system and also for the FA/MeOH system. The model results showed very good agreement to the experimental results. The model was then used to run parametric study defining favored operational points for the higher OME synthesis step. The most influencing parameter is the FA/MeOH molar ratio in the feed. Minimum recycle ratio of 3 was reached with FA/MeOH ratio 1.8. Importantly, the model showed that even though several FA/MeOH molar ratios in the range 1.6-2 showed low recycle ratios, the end product OME_{3-5} distribution at equilibrium is significantly influenced by the feed ratio. A desired end product distribution was reached at FA/MeOH = 1.8 mol mol^{-1}. The equilibrium with recycle model did not converge at 1.4>FA/MeOH>2.2 molar ratios. This provides a word of caution for the practical synthesis regarding achieving a steady-state recycle process in these ranges.

The two main synthesis reactors were then implemented into the commercial simulation platform CHEMCAD®. The MeOH endothermic dehydrogenation reactor global kinetic model implemented in Matlab® was integrated in CHEMCAD® using an Excel® unit *via* a VBA node. Similarly, the OME equilibrium NSGM model was also integrated in the CHEMCAD® platform using the VBA node. The physical property model for the OME reaction components was defined using thermodynamic and physical properties defined from literature data or using estimation methods. The product separation using rigorous distillation units was then implemented using

CHEMCAD® SCDS tower algorithms. UNIFAC model parameters were defined for the distillation columns to account for the non-ideality of the liquid phase. Reduced short-cut column models were used to obtain the initiation data of the rigorous SCDS models. Four columns were employed for the separation task. Also two ideal phase separators were implemented to allow the separation of HF_1 and the higher MG_n and HF_n. Due to the similar vapor pressure of OME_2 and H_2O, The column separating these components is quiet complex with 80 theoretical stages, reflux ratio of 4 and 19.6% consumption of the total process heating duty.

A heat integration task was then carried out for the whole process flow sheet. PinCH 2.0 software was used for this task. Process stream data were extracted to Excel® program using VBA code. All process streams undergoing heat exchange processes were segmented to check phase change events and calculate average heat capacities. The results were then imported to PinCH 2.0 where a heat exchanger network was constructed allowing maximum process heat recovery. After the process heat integration, the steam consumption was reduced by 16.1% and cooling water consumption was reduced by 30.4%.

After the heat integration task, the whole process is completely defined on one platform which was further called the process "hybrid model". A simple cost calculation model was then developed adopting the CAPEX from literature OME synthesis process and evaluating the OPEX as variable and fixed cost of production (VCP and FCP). By extracting the material and energy balance data from the hybrid process model, the VCP can be calculated using utilities and raw materials cost from literature. The FCP were calculated using factorial method from the CAPEX as discussed by Baerens et al..[134]

The key performance indicators for the described process were evaluated. At annual production capacity of 35 kt OME_{3-5}, the overall process yield MeOH to OME_{3-5} is 80.3 wt.%, the process energy efficiency is 71.7%, the specific steam consumption is 2.31 MWh/t OME_{3-5} and the production cost is 951.5 US$ per t OME_{3-5} (0.16 €ct./kWh). The MeOH cost is the major production cost factor with 47% of the production cost share followed by the energy cost of 22.13% and the production capacity. Considering several process developments namely operating the endothermic MeOH dehydrogenation reactor at high MeOH feed concentration up to 20%, synergy between the process described in this thesis and adopting post OME synthesis reactor water management using adsorption technology as described by Schmitz et al.[75] and at MeOH feed cost of 300 US$/t, OME can be produced at 820.3 US$ per t OME_{3-5} (0.14 €ct./kWh). The available literature process based on TRI and OME_1 production cost was assessed at refinery annual production capacities of 1 million t with MeOH feed cost of 300 US$ per t. The OME production cost was 615 US$ per t OME_{3-5} (0.11 €ct./kWh) at synthesis energy efficiency of 52%.[69] At this large annual production capacity and same MeOH feed cost, the assessed production cost using the process described in this work is US$ 598.7 per t OME_{3-5} (0.10 €ct./kWh). This represents the lowest production cost in comparison with the available literature process.[32,53] Figure 17 illustrates the

production cost of different energy carriers against their carbon footprint as presented by Maus et *al..*[138] These cost projections for fossil based OME agrees with the assessment done in this work. Considering green MeOH as a feed with cost of 653 US$/t[135], a production cost of US$ 1045.4 per t OME$_{3-5}$ (0.18 €ct./kWh) is projected based on the direct OME synthesis technology described in this work.

In a well-to-wheel preliminary assessment, Hank et *al.* illustrated that green OME $CO_{2-eq.}$ emissions per km of driven distance is almost 30% less than fossil diesel emissions.[73] The cost benefit of the CO_2 reduction should be considered to improve the competitiveness of such sustainable fuels or chemicals.
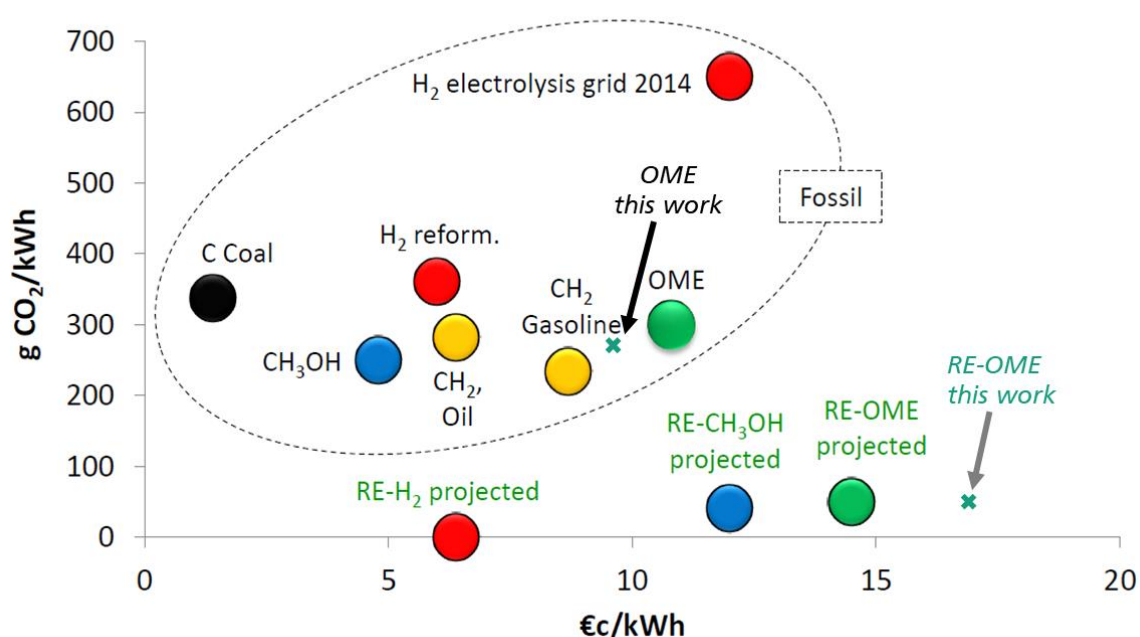
Figure 17 Production cost and carbon footprint of fossil and renewable energy carriers and fuels as introduced by Maus et *al.*[138]

In conclusion, this work introduced the concept for direct OME synthesis based on endothermic MeOH dehydrogenation to anhydrous FA. The process concept is scalable since it is based on MeOH and using simple synthesis technologies. Process flow sheet assessment using the hybrid model developed in the frame of this work showed economic benefit at high synthesis energy efficiency. Several synergies and scenarios were investigated which highlighted the potential of more production cost improvements. Nevertheless, developments are still needed regarding stable catalytic performance of the MeOH endothermic dehydrogenation reaction. Importantly, the results presented in this thesis elaborate the potential of the described process to enhance the production costs of OME once it is successfully scaled up. The hybrid process model developed in the frame of this work presents for the first time an integrated platform where OME synthesis technologies can be robustly evaluated.

Extending the economic model to account for sizing and costing of the process equipment and consequently the process detailed CAPEX is under development. Coupling of life cycle assessment (LCA) tool in the hybrid model is a foreseen development for extending the KPIs including process ecological metrics along with the techno-economic metrics.

6   Bibliography of the literature and other information sources used in this thesis

1.   International Renewable Energy Agency, ed., *Renewable Energy in the Water, Energy and Food Nexus*, 2015.
2.   Federal Ministry for the Environment, Nature Conservation and Building and Nuclear Safety, eds., *Climate Action Plan 2050 – Principles and goals of the German government's climate policy*, Druck- und Verlagshaus Zarbock GmbH & Co. KG, 2016.
3.   W. W. Patrick Schmidt, ed., *Power-to-Liquids: Potentials and Perspectives for the Future Supply of Renewable Aviation Fuel*, 2016.
4.   http://www.cop-23.org/ (last accessed July 2018).
5.   S. Spiecker and C. Weber, *Energy Policy*, 2014, **65**, 185.
6.   German Environment Agency, ed., *Submission under the United Nations Framework Convention on Climate Change and the Kyoto Protocol 2017: National Inventory Report for the German Greenhouse Gas Inventory 1990 – 2015*, 2017.
7.   German Environment Agency, ed., *Data on the Environment: Indicator report*, 2017.
8.   F. Ausfelder, C. Beilmann, M. Bertau, S. Bräuninger, A. Heinzel, R. Hoer, W. Koch, F. Mahlendorf, A. Metzelthin, M. Peuckert, L. Plass, K. Räuchle, M. Reuter, G. Schaub, S. Schiebahn, E. Schwab, F. Schüth, D. Stolten, G. Teßmer, K. Wagemann and K.-F. Ziegahn, *Chemie Ingenieur Technik*, 2015, **87**(1-2), 17.
9.   Bundesministerium für Verkehr, Bau und Stadtentwicklung, *The Mobility and Fuels Strategy of the german government (MFS): New pathways for energy*, 2013.
10. European Commission, *White paper: Roadmap to a Single European Transport Area - Towards a competitive and resource efficient*, Brussels, Belgium, 2011.
11. B. Niethammer, S. Wodarz, M. Betz, P. Haltenort, D. Oestreich, K. Hackbarth, U. Arnold, T. Otto and J. Sauer, *Chemie Ingenieur Technik*, 2018, **90**(1-2), 99.
12. O. Deutschmann and J.-D. Grunwaldt, *Chemie Ingenieur Technik*, 2013, **85**(5), 595.
13. https://www.theguardian.com/environment/2018/feb/27/german-court-rules-cities-can-ban-diesel-cars-to-tackle-pollution (last accessed March 2018).
14. S. Schemme, R. C. Samsun, R. Peters and D. Stolten, *Fuel*, 2017, **205**, 198.
15. Directorate-General for Energy, the Directorate-General for Climate, ed., *EU Reference Scenario 2016 Energy, transport and GHG emissions Trends to 2050*, 2016.
16. C. J. Baranowski, A. M. Bahmanpour and O. Kröcher, *Applied Catalysis B: Environmental*, 2017, **217**, 407.
17. P. Hockenos, The energy transition and Germany's transport sector: Car giant Germany struggles to ignite Energiewende in transportation. https://www.cleanenergywire.org/dossiers/energy-transition-and-germanys-transport-sector.
18. R. Schlögl, *Angew. Chem.*, 2017, **129**(37), 11164.
19. M. Münz, A. Mokros, D. Töpfer and C. Beidl, *MTZ Worldw*, 2018, **79**(3), 16.
20. M. Härtl, K. Gaukel, D. Pélerin and G. Wachtmeister, *MTZ worldwide*, 2017, **78**(2), 52.
21. Robert Schlögl, ed., *CO2 to Fuels –Chemical Perspectives: 193–264*, 37. Internationales Wiener Motorensymposium, Vienna, 2016.
22. K. Wagemann and F. Ausfelder, eds., *White Paper: E-Fuels -Mehr als eine Option*, 2017.

23. http://ec.europa.eu/eurostat/statistics-explained/index.php/File:Figure_4_Passenger_cars_by_age,_2015_.png (last accessed March 2018).

24. E. Jacob and W. Maus, *MTZ worldwide*, 2017, **78**(3), 52.

25. J. Klankermayer, S. Wesselbaum, K. Beydoun and W. Leitner, *Angewandte Chemie (International ed. in English)*, 2016, **55**(26), 7296.

26. M. Berggern, *Methanol to Energy - Challenges and Opportunities: 4th Methanol Technology and Policy Commercial Congress*, Frankfurt an Main, 2017.

27. M. Bertau and F. Asinger, *Methanol: The basic chemical and energy feedstock of the future Asinger's vision today*, Springer, Heidelberg, 2014.

28. Dr.-Ing. M. Härtl, K. Gaukel, D. Pélerin and G. Wachtmeister, *MTZ worldwide*, 2017, **78**(2), 52.

29. P. Haltenort, K. Hackbarth, D. Oestreich, L. Lautenschütz, U. Arnold and J. Sauer, *Catalysis Communications*, 2018, **109**, 80.

30. L. Lautenschütz, D. Oestreich, P. Seidenspinner, U. Arnold, E. Dinjus and J. Sauer, *Fuel*, 2016, **173**, 129.

31. E. Jacob and W. Maus, eds., *Synthetic Fuels–OME1: A Potentially Sustainable Diesel Fuel: 325-347*, 35. Wiener Motorensymposium, Vienna, 2014.

32. E. Jacob and W. Maus, *MTZ Worldw*, 2017, **78**(3), 52.

33. D. Oestreich, L. Lautenschütz, U. Arnold and J. Sauer, *Chemical Engineering Science*, 2017, **163**, 92.

34. https://www.ineos.com/show-document/Render/?grade=DMM93&bu=INEOS+Paraform&documentType=Technical+Data+Sheet&docLanguage=EN (last accessed March 2018).

35. J. Burger, V. Papaioannou, S. Gopinath, G. Jackson, A. Galindo and C. S. Adjiman, *AIChE J.*, 2015, **61**(10), 3249.

36. M. Schappals, T. Breug-Nissen, K. Langenbach, J. Burger and H. Hasse, *J. Chem. Eng. Data*, 2017.

37. N. Wakabayashi, K. Takeuchi, H. Uchida and M. Watanabe, *J. Electrochem. Soc.*, 2004, **151**(10), A1636.

38. K. Kakinuma, I.-T. Kim, Y. Senoo, H. Yano, M. Watanabe and M. Uchida, *ACS applied materials & interfaces*, 2014, **6**(24), 22138.

39. K. Gaukel, D. Pélerin, M. Härtl, G. Wachtmeister, J. Burger, W. Maus and E. jacob, eds., *The fuel OME2: An Example to Pave the Way to Emission-Neutral Vehicles with Internal Combustion Engine*.

40. http://www.prechems.com/showpro.asp?id=1136 (last accessed March 2018).

41. J. Liu, H. Wang, Y. Li, Z. Zheng, Z. Xue, H. Shang and M. Yao, *Fuel*, 2016, **177**, 206.

42. M. Härtl and E. Jacob, eds., *The Fuel OME2: An Example to Pave the Way to Emission-NeutralVehicles with Internal Combustion Engine: 224-252*, 37. Internationales Wiener Motorensymposium, Vienna, 2016.

43. A. Feiling, M. Münz and C. Beidl, *ATZextra worldwide*, 2016, **21**(11), 16.

44. S. E. Iannuzzi, C. Barro, K. Boulouchos and J. Burger, *Fuel*, 2016, **167**, 49.

45. H. Liu, Z. Wang, J. Wang, X. He, Y. Zheng, Q. Tang and J. Wang, *Energy*, 2015, **88**, 793.

46. J. Liu, H. Shang, H. Wang, Z. Zheng, Q. Wang, Z. Xue and M. Yao, *Fuel*, 2017, **193**, 101.

47. W. Sun, G. Wang, S. Li, R. Zhang, B. Yang, J. Yang, Y. Li, C. K. Westbrook and C. K. Law, *Proceedings of the Combustion Institute*, 2017, **36**(1), 1269.

48. H. Yang, X. Li, Y. Wang, M. Mu, X. Li and G. Kou, *Scientific reports*, 2016, **6**, 37611.
49. H. Yang, X. Li, Y. Wang, M. Mu, X. Li and G. Kou, *Aerosol Air Qual. Res.*, 2016, **16**(10), 2560.
50. Y. R. Tan, M. L. Botero, Y. Sheng, J. A.H. Dreyer, R. Xu, W. Yang and M. Kraft, *Fuel*, 2018, **224**, 499.
51. N. Schmitz, J. Burger and H. Hasse, *Industrial & Engineering Chemistry Research*, 2015, **54**(50), 12553.
52. J. Burger, E. Ströfer and H. Hasse, *Industrial & Engineering Chemistry Research*, 2012, **51**(39), 12751.
53. M. Ouda, F. K. Mantei, M. Elmehlawy, R. J. White, H. Klein and S.-E. K. Fateen, *React. Chem. Eng.*, 2018, **3**(3), 277.
54. M. Ouda, G. Yarce, R. J. White, M. J. Hadrich, D. Himmel, A. Schaadt, H. Klein, E. jacob and I. Krossing, *Reaction Chemistry & Engineering*, 2017, **2**(1), 50.
55. D. Himmel, R. J. White, E. Jacob and I. Krossing, *Sustainable Energy & Fuels*, 2017.
56. D. Deutsch, D. Oestreich, L. Lautenschütz, P. Haltenort, U. Arnold and J. Sauer, *Chemie Ingenieur Technik*, 2017, **89**(4), 486.
57. J. Burger, E. Strofer and H. Hasse, *Chemical Engineering Research and Design*, 2013, **91**, 2648.
58. http://www.leistungszentrum-nachhaltigkeit.de/en/pilot-projects/hyco2/ (last accessed April 2018).
59. S. Lüftl, V. P.M. and S. Chandran, *Polyoxymethylene Handbook: Structure, Properties, Applications and their Nanocomposites*, John Wiley & Sons, Inc, 2014.
60. L. P. Lautenschütz, *Neue Erkenntnisse in der Syntheseoptimierungoligomerer Oxymethylendimethylether aus Dimethoxymethan und Trioxan: INAUGURAL-DISSERTATION*, 2015.
61. D. N. D. Moulton, *Diesel fuel having improved qualities and method of forming*(US5746785A).
62. D. SanFilippo, R. Patrini and M. Marchionna, *Use of an oxygenated product as a substitute of gas oil in diesel engines*(EP1422285 A1), 2004.
63. K. D. Vertin, J. M. Ohi, D. W. Naegeli, K. H. Childress, G. P. Hagen, C. I. McCarthy, A. S. Cheng and R. W. Dibble, *Methylal and Methylal-Diesel Blended Fuels for Use in Compression-Ignition Engines*, 1999.
64. S. Schemme, R. C. Samsun, R. Peters and D. Stolten, *Fuel*, 2017, **205**, 198.
65. H. Shang, Z. Hong, Z. YE, J. Xiang and Z. Xue, *Method for producing polyoxymethylene dimethyl ethers from feedstock of concentrated formaldehyde*(US20160168307A1).
66. http://www.kaimao-chem.com/products.html (last accessed April 2018).
67. http://www.ome-technologies.de/fileadmin/omet/OMETechnologiesGmbH_Jan2017.pdf (last accessed April 2018).
68. X. Zhang, A. O. Oyedun, A. Kumar, D. Oestreich, U. Arnold and J. Sauer, *Biomass and Bioenergy*, 2016, **90**, 7.
69. N. Schmitz, J. Burger, E. Ströfer and H. Hasse, *Fuel*, 2016, **185**, 67.
70. https://www.bmbf.de/de/mit-abgas-das-klima-retten-3044.html (last accessed March 2018).
71. https://www.kopernikus-projekte.de/projekte/power-to-x (last accessed April 2018).
72. S. Deutz, D. Bongartz, B. Heuser, A. Kätelhön, L. Schulze Langenhorst, A. Omari, M. Walters, J. Klankermayer, W. Leitner, A. Mitsos, S. Pischinger and A. Bardow, *Energy Environ. Sci.*, 2018, **11**(2), 331.

73. M. Ouda, C. Hank, R. White, A. Schaadt, H. Klein and H.-M. Henning, *Energiewirtschaftliche Tagesfragen*, 2018, **2018**(3), 44.
74. Y. Zhao, Z. Xu, H. Chen, Y. Fu and J. Shen, *Journal of Energy Chemistry*, 2013, **22**(6), 833.
75. N. Schmitz, E. Ströfer, J. Burger and H. Hasse, *Industrial & Engineering Chemistry Research*, 2017, **56**(40), 11519.
76. G. Reuss, W. Disteldorf, A. O. Gamer and A. Hilt, Formaldehyde.
77. S. Su, P. Zaza and A. Renken, *Chem. Eng. Technol.*, 1994, **17**(1), 34.
78. N. Schmitz, F. Homberg, J. Berje, J. Burger and H. Hasse, *Industrial & Engineering Chemistry Research*, 2015, **54**(25), 6409.
79. C. Kuhnert, *Dampf-Flüssigkeits-Gleichgewichte in mehrkomponentigen formaldhydhaltigen [formaldehydhaltigen] Systemen*, Shaker, Aachen, 2004.
80. I. Hahnenstein, H. Hasse, C. G. Kreiter and G. Maurer, *Industrial & Engineering Chemistry Research*, 1994, **33**(4), 1022.
81. C. Kuhnert, M. Albert, S. Breyer, I. Hahnenstein, H. Hasse and G. Maurer, *Industrial & Engineering Chemistry Research*, 2006, **45**(14), 5155.
82. J. Zhang, M. Shi, D. Fang and D. Liu, *Reaction Kinetics, Mechanisms and Catalysis*, 2014, **113**(2), 459.
83. E. Stoefer, H. Hasse, S. Blagov, *Process for preparing polyoxymethylene dimethyl ethers from methanol and formaldehyde*(Pat. US 7,700,809 B2), 2010.
84. T. Grützner, H. Hasse, N. Lang, M. Siegert and E. Ströfer, *Chemical Engineering Science*, 2007, **62**(18-20), 5613.
85. P. Hasse, J.-O. Drunsel, J. Burger, U. Schmidt, M. Renner and S. Blagov, *Process for the production of pure methylal*, Google Patents(WO2012062822A1), 2012.
86. T. J. Goncalves, U. Arnold, P. N. Plessow and F. Studt, *ACS Catalysis*, 2017, **7**(5), 3615.
87. J. Burger, E. Ströfer and H. Hasse, *Chemical Engineering Research and Design*, 2013, **91**(12), 2648.
88. Z. Xue, H. Shang, Z. Zhang, C. Xiong, C. Lu and G. An, *Energy Fuels*, 2017, **31**(1), 279.
89. J. Wu, H. Zhu, Z. Wu, Z. Qin, L. Yan, B. Du, W. Fan and J. Wang, *Green Chem*, 2015, **17**(4), 2353.
90. Q. Wu, M. Wang, Y. Hao, H. Li, Y. Zhao and Q. Jiao, *Industrial & Engineering Chemistry Research*, 2014, **53**(42), 16254.
91. E. Ströfer, H. Schelling, H. Hasse and S. Blagov, *Method for producing polyoxymehtylene dimethyl ethers from trioxan and dialkylethers*(US20080207955 A1), 2008.
92. X. Fang, J. Chen, L. Ye, H. Lin and Y. Yuan, *Sci. China Chem.*, 2015, **58**(1), 131.
93. R. Wang, Z. Wu, Z. Qin, C. Chen, H. Zhu, J. Wu, G. Chen, W. Fan and J. Wang, *Catal. Sci. Technol.*, 2016, **6**(4), 993.
94. G. P. Hagen and M. J. Spangler, *Preparation of polyoxymethylene dimethyl ethers by catalytic conversion of dimethyl ether with formaldehyde formed by oxy-dehydrogenation of dimethyl ether*(US5959156 A1), 1999.
95. G. P. Hagen and M. J. Spangler, *Preparation of polyoxymethylene dimethyl ethers by acid-activated catalytic conversion of methanol with formaldehyde formed by oxy-dehydrogenation of dimethyl ether*(US6265528 B1), 2001.
96. G. P. Hagen and M. J. Spangler, *Preparation of polyoxymethylene dimethyl ethers by catalytic conversion of formaldehyde formed by oxidation of dimethyl ether*(US6392102 B1), 2002.

97. G. P. Hagen and M. J. Spangler, *Preparation of polyoxymethylene dialkane ethers, by catalytic conversion of formaldehyde formed by dehydrogenation of methanol or dimethyl ether*(US6350919 B1), 2002.

98. G. P. Hagen and M. J. Spangler, *Preparation of polyoxymethylene dimethyl ethers by catalytic conversion of dimethyl ether with formaldehyde formed by oxidation of methanol*(US6166266 A1), 2000.

99. G. P. Hagen and M. J. Spangler, *Preparation of polyoxymethylene dimethyl ethers by catalytic conversion of dimethyl ether with formaldehyde formed by oxy-dehydrogenation of methanol*(US6160174 A1), 2000.

100. H. Liu and E. Iglesia, *The Journal of Physical Chemistry B*, 2003, **107**(39), 10840.

101. K.-a. Thavornprasert, M. Capron, L. Jalowiecki-Duhamel and F. Dumeignil, *Catalysis Science & Technology*, 2016, **6**(4), 958.

102. J. Klankermayer, S. Wesselbaum, K. Beydoun and W. Leitner, *Angew. Chem.*, 2016.

103. Jörg Sauer and Gerhard Eming, *Chem. Eng. Technol.*, 1995(18), 284.

104. L.-P. Ren, W.-L. Dai, X.-L. Yang, Y. Cao, H. Li and K.-N. Fan, *Applied Catalysis A: General*, 2004, **273**(1-2), 83.

105. S. Su, M. R. Prairie and A. Renken, *Applied Catalysis A: General*, 1993, **95**(1), 131.

106. P. Zaza, H. Randall, R. Doepper and A. Renken, *Catalysis Today*, 1994, **20**(3), 325.

107. R. Wang, Z. Wu, Z. Qin, C. Chen, H. Zhu, J. Wu, G. Chen, W. Fan and J. Wang, *Catalysis Science & Technology*, 2016, **6**(4), 993.

108. D. Wang, F. Zhao, G. Zhu and C. Xia, *Chemical Engineering Journal*, 2018, **334**, 2616.

109. F. Wang, G. Zhu, Z. Li, F. Zhao, C. Xia and J. Chen, *Journal of Molecular Catalysis A: Chemical*, 2015, **408**, 228.

110. Y. Zheng, Q. Tang, T. Wang, Y. Liao and J. Wang, *Chemical Engineering & Technology*, 2013, **36**(11), 1951.

111. J. Wu, H. Zhu, Z. Wu, Z. Qin, L. Yan, B. Du, W. Fan and J. Wang, *Green Chemistry*, 2015, **17**(4), 2353.

112. X.-J. Gao, W.-F. Wang, Y.-Y. Gu, Z. Zhang, J.-F. Zhang, Q. Zhang, N. Tsubaki, Y.-Z. Han and Y.-S. Tan, *ChemCatChem*, 2018, **10**(1), 273.

113. Q. ZHAO, H. WANG, Z. Qin, Z.-w. WU, J.-b. WU, W.-b. FAN and J.-g. WANG, *Journal of Fuel Chemistry and Technology*, 2011, **39**(12), 918.

114. L. Wang, W.-T. Wu, T. Chen, Q. Chen and M.-Y. He, *Chemical Engineering Communications*, 2014, **201**(5), 709.

115. W. H. Fu, X. M. Liang, H. Zhang, Y. M. Wang and M. Y. He, *Chem. Commun.*, 2015, **51**(8), 1449.

116. A. Peter, S. M. Fehr, V. Dybbert, D. Himmel, I. Lindner, E. Jacob, M. Ouda, A. Schaadt, R. J. White, H. Scherer and I. Krossing, *Angewandte Chemie International Edition*, 2018.

117. Y. Zheng, Q. Tang, T. Wang and J. Wang, *Chemical Engineering Science*, 2015, **134**, 758.

118. G. Xiaochen, Y. Weimin, L. Yi and G. Huanxin, *11th European Congress on Catalysis – EuropaCat-XI*, 2013.

119. H. Li, H. Song, L. Chen and C. Xia, *Applied Catalysis B: Environmental*, 2015, **165**, 466.

120. J. Zhang, D. Fang and D. Liu, *Industrial & Engineering Chemistry Research*, 2014, **53**(35), 13589.

121. U. Arnold, L. Lautenschütz, D. Oestreich and J. Sauer, *New OME synthesis pathways*, 2014.

122. J. P. O'Connell and J. M. Haile, *Thermodynamics: Fundamentals for applications*, Cambridge University Press, New York, 2005.

123. M. Ouda, F. Mantei, K. Hesterwerth, E. Bargiacchi, H. Klein and R. J. White, *React. Chem. Eng.*, 2018(3), 676.
124. L.-P. Ren, W.-L. Dai, Y. Cao, H. Li and K. Fan, *Chem. Commun.*, 2003(24), 3030.
125. J. F. Walker, *Formaldehyde*, Reinhold Publ. Corp, New York, 1964.
126. S. Su, *Catalytic dehydrogenation of methanol to formaldehyde on sodium carbonate*, Dissertation, 1991.
127. I. Hahnenstein, M. Albert, H. Hasse, C. G. Kreiter and G. Maurer, *Industrial & Engineering Chemistry Research*, 1995, **34**(2), 440.
128. Albert, Hahnenstein, Hasse, Maurer, *AIChE J.*, 1996, **42**(6), 1741.
129. Y.-Q. Liu, H. Hasse and G. Maurer, *AIChE J.*, 1992, **38**(11), 1693.
130. E. Ströfer, H. Hasse and S. Blagov, *Process for preparing polyoxymethylene dimethyl ethers from methanol and formaldehyde*, 2010.
131. H. Z. Kister, *Distillation Design*, McGraw-Hill Education, 1992.
132. E. J. Henley and J.D. Seader, *Equilibrium-stage separation operations in chemical*, John Wiley and Sons Ltd, 1981.
133. G. Towler and R. Sinnott in *Chemical Engineering Design*, Elsevier, 2013, p 1047.
134. M. Baerns, A. Behr, A. Brehm, J. Gmehling, H. Hofmann, U. Onken, A. Renken, K.-O. Hinrichsen and R. Palkovits, *Technische Chemie*, Wiley-VCH-Verl., Weinheim, 2013.
135. C. Hank, S. Gelpke, A. Schnabl, R. J. White, J. Full, N. Wiebe, T. Smolinka, A. Schaadt, H.-M. Henning and C. Hebling, *Sustainable Energy Fuels*, 2018, **30**(1), 1019.
136. M. Härtl and G. Wachmesiter, *Methanol derived synthetic fuels for diesel and spark ignited engines. 4th Methanol Technology and Policy Commercial Congress*, Frankfurt an Main, 2017.
137. T. Wilharm and E. Jacob, *First steps towards the market launch of OME diesel 4th Methanol Technology and Policy commercial congress*, Frankfurt an Main, 2017.
138. E. Jacob and W. Maus, *Novel methods of synthesis for diesel fuel OME*.
139. REN21, ed., *Renewables 2015 Global Status Report*, Paris, 2015.
140. A. Tremel, P. Wasserscheid, M. Baldauf and T. Hammer, *international journal of hydrogen energy*, 2015, **40**(35), 11457.
141. P. Dunn, A. Wells and M. Williams, *Green chemistry in the pharmaceutical industry*, Wiley-VCH, 2010.
142. E. Jacob, *4th Methanol Technology and Policy Commercial Congress*, 2017.
143. M. Baerns, A. Behr, A. Brehm, J. Gmehling, K.-O. Hinrichsen, H. Hofmann, R. Palkovits, U. Onken and A. Renken, *Technische Chemie*, Wiley-VCH Verlag GmbH & Co. KGaA, Weinheim, 2013.

7 Appendix

7.1 Graphical Presentation of anhydrous FA synthesis test stand
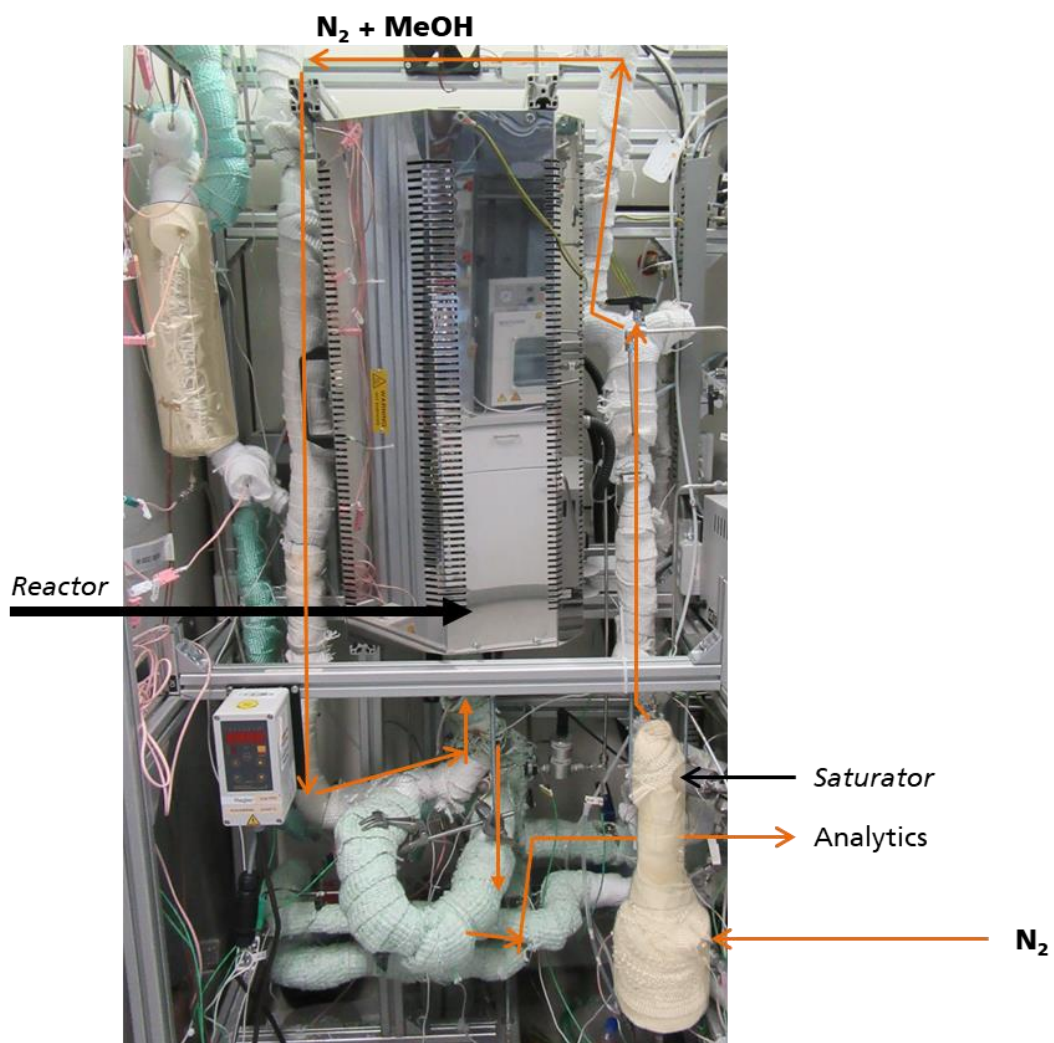
Figure 18 Anhydrous FA synthesis test stand

7.2 Continuous Test stand LabVIEW monitor and control program
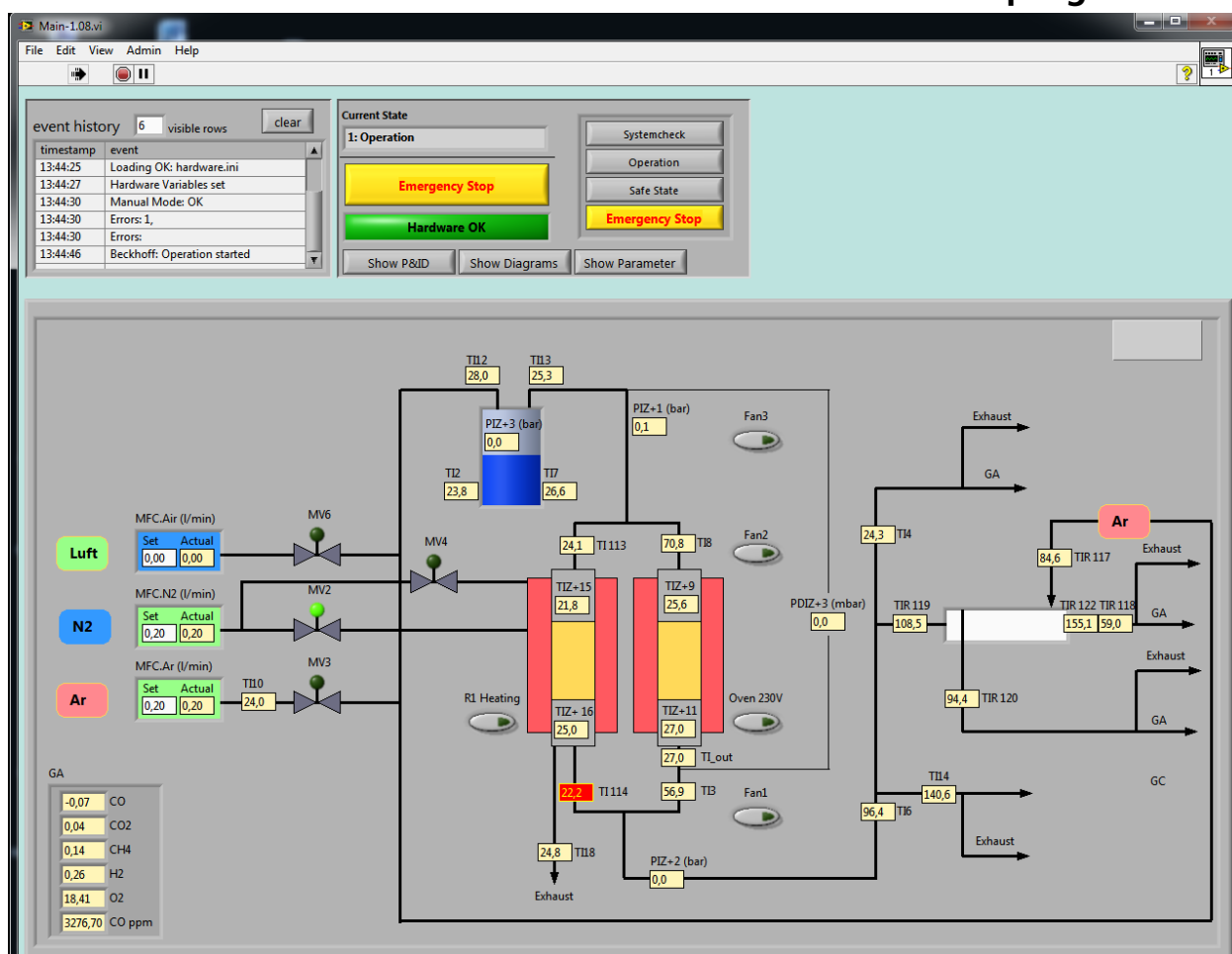
Figure 19 LabVIEW monitoring and control program for the continuous anhydrous FA synthesis teststand

7.3 Graphical Presentation of batch OME synthesis test stand

Figure 20 Batch OME synthesis test stand

7.4 Copyright and permission royal society of chemistry

- Author reusing their own work published by the Royal Society of Chemistry

You do not need to request permission to reuse your own figures, diagrams, etc, that were originally published in a Royal Society of Chemistry publication. However, permission should be requested for use of the whole article or chapter <u>except if reusing it in a thesis</u>. If you are including an article or book chapter published by us in your thesis please ensure that your co-authors are aware of this.[2]

- Confirmation by email from the Royal Society of Chemistry

Permission is granted to reproduce your article in your thesis as long as it is fully acknowledged and includes a link back to the article on our website. Please ensure that all authors are aware that it is being included.

If you have any further questions, please let me know.

Kind regards,

Allison Holloway
Publishing Assistant – Journals
Royal Society of Chemistry
Thomas Graham House
Science Park, Milton Road
Cambridge, CB4 0WF, UK
If replying directly, please ensure you cc the relevant journal inbox.

---

[2] https://www.rsc.org/journals-books-databases/journal-authors-reviewers/licences-copyright-permissions/

7.5 Paper 1: Poly(Oxymethylene) Dimethyl Ether Synthesis - A combined chemical equilibrium investigation towards an increasingly efficient and potentially sustainable synthetic route

M. Ouda, G. Yarce, R. J. White, M. Hadrich, D. Himmel, A. Schaadt, H. Klein, E. Jacob and I. Krossing

7.5.1 Summary of the paper

Polyoxymethylene dimethyl ethers (denoted hereon as OME) are potential sustainable fuels (e.g. as a diesel substitute). The greatest hindrance for introducing OME into the market is the lack of energy efficient, economically feasible and a scalable industrial process for the synthesis of OME with a certain chain length. The endothermic catalytic dissociation of methanol (MeOH or CH_3OH) to anhydrous formaldehyde (FA or H_2CO) and H_2 was investigated in literature, however was not regarded as attractive path since the handling of anhydrous FA as end product is challenging. Additionally, the anhydrous FA synthesis was not advantageous from the economics point of view against the conventional synthesis processes with aqueous FA as end product. In this paper, the fundamental analysis of a potentially, sustainable OME synthesis process based on anhydrous FA is presented. To the best of my knowledge, this process concept is not yet investigated in literature. A theoretical efficiency evaluation carried in this work indicates that the proposed anhydrous route is potentially more attractive than the conventional OME synthesis (i.e. based on dimethoxymethane and trioxane). The introduced OME synthesis proceeds *via* two process steps namely (1) methanol endothermic dehydrogenation to anhydrous formaldehyde and (2) reacting of the non-converted MeOH with anhydrous FA directly to OME was investigated. The focus of this work was on the second step of the higher OME synthesis to identify the requirements and reaction conditions in methanol dehydrogenation step. For this purpose, a multicomponent thermodynamic vapour-liquid equilibrium model, based on CH_3OH as the educt and source of H_2CO for OME synthesis, is described. A thermodynamic equilibrium mathematical model for this complex (i.e. a 29 reaction network) equilibrium system is presented, capable of solving the sequential chemical and phase equilibrium, importantly considering all components in the reaction system including the intermediate products poly(oxymethylene) hemiformals and poly(oxymethylene) glycols. A batch reaction system was designed and commissioned to validate the implemented model. The equilibrium investigations were carried out over two commercial catalysts that were discussed in literature. The presented findings reliably describe the synthesis equilibrium with respect to the experimentally obtained results. The model defines the optimum required feed ratio of the methanol dehydrogenation step which is FA/MeOH = 1.9 g g^{-1}. Based on this evaluation, the reaction performance of the first step was defined in terms of desired MeOH conversion and FA selectivity. These results were the basis for literature research to identify potential catalysts for the methanol dehydrogenation reaction which allow achieving this desired performance.

7.5.2 Overview of the contributions in this work

I was significantly involved in the essential phases of brainstorming and in the elaboration of all parts of the work. From the (1) initial concept of the work, (2) the process theoretical stoichiometric evaluation, (3) process potential definition investigation and (4) understanding the considered reaction network. Additionally, identifying (5) the two phase interactions, literature research for selecting the suitable model to describe the combined chemical and phase equilibrium of such reaction network. Implementation of the model in Matlab® was done together with my master student and co-autor Gabriel Yarce. (6) The design, safety study, procurement and construction of the test setups namely, (a) glass components setup for feed preparation and (b) batch autoclave for running the reactions was done by me with the assistance of my master students Gabriel Yarce and Max Hadrich. (7) The analytical concept, calibration of analytical equipment, evaluation sheets development was explicitly done by me. (8) Running the simulation cases and experimental tests was done with the assistance of Gabriel Yarce. Finally, writing the whole paper and doing the corresponding adjustments after the review process was explicitly my task. The rest of the co-authors contributed in the initial concept discussion phase, correction reading and adding some understandings in the process theoretical evaluation phase.

7.5.3 Paper as published in Peer-Reviewed journal

Poly(oxymethylene) dimethyl ether synthesis – a combined chemical equilibrium investigation towards an increasingly efficient and potentially sustainable synthetic route†

M. Ouda,[ab] G. Yarce,[a] R. J. White,*[a] M. Hadrich,[a] D. Himmel,[c] A. Schaadt,[a] H. Klein,[b] E. Jacob[d] and I. Krossing[ce]

Polyoxymethylene dimethyl ethers (denoted hereon as OME) are potential sustainable fuels (*e.g.* as a diesel substitute). In this paper, the fundamental analysis of a potentially, sustainable synthetic OME system is presented (*i.e.* based on CH_3OH synthesised from H_2 and recycled CO_2). In this context, a multicomponent thermodynamic vapour–liquid equilibrium model, based on CH_3OH as the educt and source of H_2CO for OME synthesis, is described. A thermodynamic equilibrium mathematical model for this complex (*i.e.* a 29 reaction network) CH_3OH–H_2CO equilibrium system is presented, capable of solving the sequential chemical and phase equilibrium, importantly considering all components in the reaction system including poly(oxymethylene) hemiformals and poly(oxymethylene) glycols. A theoretical efficiency evaluation indicates that the proposed anhydrous route is potentially more attractive than the conventional synthesis (*i.e.* based on dimethoxymethane and trioxane). To substantiate these theoretical investigations, a complimentary experimental batch OME synthesis is also presented, providing validation for the presented thermodynamic model. An initial kinetic analysis of the OME synthesis over different commercial catalysts is also highlighted. Our presented findings reliably describe the synthesis equilibrium with respect to our experimentally obtained results. The presented work supports further an operating OME synthesis framework based on CH_3OH and H_2CO and highlights the requirement for innovative process design regarding feed preparation, reactor technology, and product separation/fractions recycling.

Introduction

To counteract the negative impacts of greenhouse gas (GHG) emissions, the utilisation of CO_2 as a carbon source/precursor is of critical importance in the production of chemicals, materials and fuels, particularly if society is to successfully achieve GHG reduction targets at the global (*e.g.* COP21) and national levels (*e.g.* 80% reduction by 2050 in Germany, relative to 1990).[1] One of the most challenging sectors in this context is

the mobility sector, which accounts for *ca.* 23% of global energy-related CO_2 emissions (6.7 Gt (CO_2) in 2010).[2] Therefore liquids fuel production based on CO_2 (*e.g.* suitable for current and future mobility modes) could play an important role in reaching emission targets in transport applications provided they can be produced sustainably and integrated with renewable energies. In this context, there have been a number of recent reports describing the conversion CO_2 typically with H_2 (*e.g. via* thermo- or electrochemical routes), followed by upgrading if necessary, to produce high purity "clean" fuels and platform chemicals.[3–7] These products, typically oxygenates including methanol, dimethyl ether and more recently members of the poly(oxymethylene) dimethyl ether family (denoted hereon as MeOH, DME and OME respectively) are characterised by interesting intrinsic combustion properties (*e.g.* significantly reduced soot and particulate matter production), when employed in pure form or blended with conventional fuels.[8–10]

Regarding the low molecular weight oxygenates, MeOH, DME and dimethoxy methane (OME1) have potential disadvantages as fuels due to high vapour pressures and low

[a] Fraunhofer Institute for Solar Energy Systems ISE, Heidenhofstraße 2, 79110 Freiburg, Germany. E-mail: robin.white@ise.fraunhofer.de; Tel: +497614588519
[b] Institute of Process and Plant Technology, Technical University Munich, Boltzmannstraße 15, 85748 Garching, Germany
[c] Institute for Inorganic and Analytical Chemistry, Albert-Ludwigs-University Freiburg, Albertstraße 21, 79104 Freiburg, Germany
[d] Motors Emissions Concepts UG, Karwendelstraße 25, 82152 Krailling, Germany
[e] FMF - Freiburger Materialforschungszentrum, Stefan-Meier-Straße 21, D-79104 Freiburg, Germany
† Electronic Supplementary Information (ESI) available: Tables for thermodynamic standard properties sources from reported literature; thermodynamic phase and chemical equilibrium model parameters; experimental results for tests test-1 and test-2. See DOI: 10.1039/c6re00145a

viscosity, whilst conventional engines must typically be modified to use this fuels (*e.g.* to avoid vapour lock or injection system problems associated with DME use).[8,11] Conversely, OME oligomers (chemical formula $H_3C-O-(CH_2O)_n-CH_3$ where $n = 3–5$) have successfully been blended with conventional diesel at 5–30% vol. and the resulting mixed fuel used without engine modification.[12] Application of these fuel blends enhanced the cetane number and significantly reduced soot formation during combustion.[13–16] These use of these fuel blends also improved overall combustion efficiency, the result of enhanced air to fuel ratios, since the OME_n (where $n = 3–5$) fraction contains *ca.* 48% covalently incorporated oxygen.

Given the ability to control in principle the oligomer chain length and in turn the resulting liquid polarity, OME have also been considered as sustainable solvents (*e.g.* if they are sourced from captured CO_2/renewable H_2), complementing the current use of OME1 as a common industrial organic solvent. Along similar lines, OME_5 has been proposed, based on computation modelling studies to be particularly suitable for CO_2 absorption (*e.g.* from natural gas streams).[17] In addition, OMEs are known to present limited or no health or environmental hazards.[13,14]

The synthesis of OME requires a methyl end group supplier or capping source (*e.g.* MeOH, DME, OME1) and a formaldehyde (FA) monomer supplier (*e.g.* monomeric FA, poly(oxymethylene)glycols as a concentrated solution of FA in water, *para*-formaldehyde (*p*-FA), or trioxane (TRI)). Based on the selected feed, an aqueous or anhydrous synthesis route can be used, which highly influences the end product distribution and side product formation (Fig. 1). All routes are based on MeOH as the platform alcohol, which may be produced, amongst other pathways, through the direct hydrogenation of CO_2, where H_2 is supplied from renewable energy powered electrolysis.[3,4,6,18] Therefore, the optimisation of a complete MeOH-based, OME synthesis chain facilitates the

synthesis of quasi-CO_2-neutral OME (*e.g.* for fuel or chemical industry applications).

Current industrial synthesis routes (*e.g.* in China) to OME (where $n > 2$) are based on OME1 plus TRI or *p*-FA systems, with these precursors derived from conventional feedstocks (*e.g.* gas-to-liquid, coal gasification, *etc.*).[19–27] Using MeOH and FA directly in OME synthesis could potentially provide a more efficient route to OME, as the energy intensive synthesis of TRI, *p*-FA or OME1 could be avoided. In this context, previous reports by Zhang *et al.* demonstrate OME synthesis based on MeOH and FA over a Zr-modified γ-alumina catalyst in a fixed bed reactor, with the authors describing the kinetics of this system.[28,29] Likewise Burger *et al.* studied the thermodynamics and kinetics of this OME synthetic system over a Amberlyst®-46 catalyst in a batch reactor.[30,31] Complimentarily to these works, the following report describes a multiphase chemical equilibrium thermodynamic model for OME synthesis, that includes all components for a complex aqueous reaction system (Fig. 2). To assess and validate this developed model, batch autoclave experiments were also performed with results compared to those of previous reports. The presented results and the understanding derived from both a theoretical and experimental standpoint provides the fundamental basis for further improvements in OME synthesis as well as assisting continuous process development, importantly from a sustainable synthetic chain based on CO_2 and H_2.

Theory and background

Chemical reactions

The OME reaction system is a unique cascade based in the described case on two starting compounds, namely MeOH and FA and more than thirty components in equilibrium. The set of reactions that occur in this system and the corresponding distribution of components in each phase,

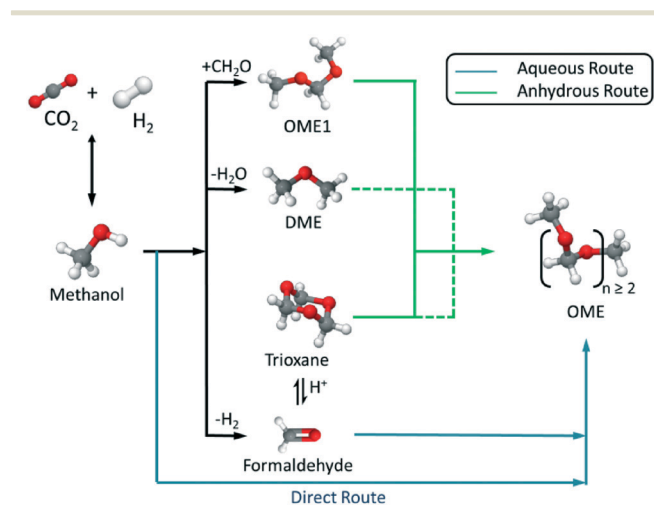**Fig. 1** Synthetic routes to polyoxymethylene dimethyl ethers (OME) based on the synthesis of CH_3OH from recycled CO_2 and sustainable H_2 *via* aqueous or anhydrous routes.
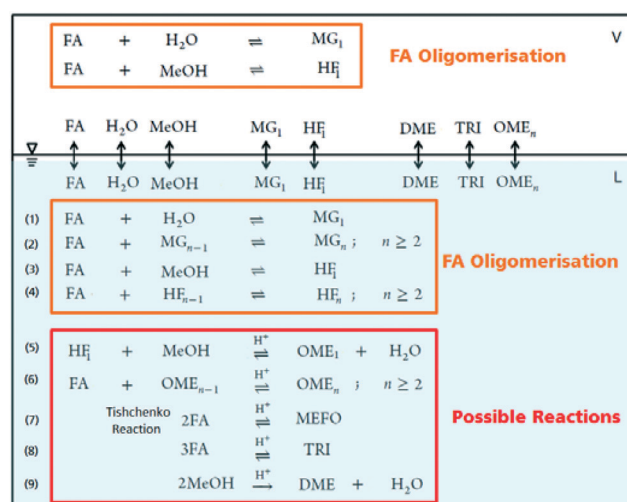

Fig. 2 OME synthesis reaction systems in liquid and vapour phases following a direct aqueous-based synthesis route.

following the direct aqueous-based synthesis route have been outlined (Fig. 2). In a previous report, Burger *et al.* explained the formation of poly(oxymethylene) hemiformals (denoted as HF_n) $HO–(CH_2O)_n–CH_3$ and poly(oxymethylene) glycols (denoted as MG_n) $HO–(CH_2O)_n–H$ in aqueous and methanolic FA solutions at values across the entire pH scale.[30] In the absence of a catalyst, the majority of monomeric FA is considered bound as either HF_n or MG_n, with the equilibrium lying strongly in favour of the products for eqn (1) to (4) (Fig. 2). However, HF_n and MG_n are known to be unstable (intermediates in this context) and can be expected to decompose relatively easily towards the reactants.

In contrast, the reactions governing OME formation only occur in acidic medium and a catalyst is required to establish an acceptable rate of reaction. In acidic medium, possible side reactions involving FA may also take place to yield methyl formate (MEFO) (eqn (7)) or TRI (eqn (8)). The formation of DME from MeOH is also known to be favoured using acidic conditions/catalysts (eqn (9)).[7c] In the gas phase, only reactions favouring short chain MG_1 and HF_1 formation are reported but other components exchanging between the gas and liquid phases may also influence the overall equilibrium composition distribution.

Reaction mechanism

Two reaction mechanisms are reported in literature for the aqueous phase synthesis of OME from MeOH and FA.[31] The reaction pathway is believed to proceed through an addition reaction between monomeric FA and OME oligomers as they are formed in acidic media (eqn (10) and (11)). Previous literature indicates that acetalisation of HF_n dominates for the OME chain growth as in eqn (3), (4) (Fig. 2) and (12).[31]

$$2\text{MeOH} + \text{FA} \underset{}{\overset{H^+}{\rightleftharpoons}} \text{OME}_1 + H_2O \qquad (10)$$

$$\text{OME}_{n-1} + \text{FA} \underset{}{\overset{H^+}{\rightleftharpoons}} \text{OME}_n \qquad (11)$$

$$HF_n + \text{MeOH} \underset{}{\overset{H^+}{\rightleftharpoons}} \text{OME}_n + H_2O \qquad (12)$$

Wang *et al.* analysed this mechanism using density functional theory (DFT) combined with experimental investigations over sulfonic acid functionalized ionic liquids.[32] It was reported that the formation of HF_1 is energetically favourable over other proposed pathways and that OME chain growth proceeds through addition of monomeric FA to the forming HF_{n-1} and terminating based on capping the formed carbocations with MeOH. During kinetic investigations, it was reported that the simultaneous formation of long chain OME was observed with no sign of delay due to sequential

chain growth,[31] and therefore an acetalisation mechanism is a more probable description of the system; an important consideration regarding the establishment of reliable equilibrium models based on a stoichiometric approach.

Theoretical efficiency

In evaluating the theoretical efficiency of an OME production process based on MeOH (*e.g.* derived from CO_2 and H_2) two routes are compared. 1) A standard or conventional route; this starts with MeOH synthesis followed by FA production *via* (partial) oxidation of MeOH (*i.e.* the FORMOX/BASF process) to yield aqueous solutions of FA.[33] The resulting solution is concentrated and trimerized over an acid catalyst to produce TRI in a complex energy intensive distillation process.[33,34] TRI or concentrated FA then reacts with MeOH to yield OME1. Finally, OME1 and TRI are selectively converted to higher OMEs ($n \geq 2$); 2) an alternative pathway, as adopted in this work, proceeds based on MeOH dehydrogenation to anhydrous FA, an excellent feed for direct OME synthesis. Using a basic thermodynamic evaluation (Fig. 3), the respective efficiencies of these routes are compared on a basis of 1 kg (OME_4) product. These calculations use the higher heating values (HHV) of the components and a simple stoichiometric evaluation. Even though the efficiency losses through the synthesis steps – *more pronounced in route 1 (conventional)* – are not regarded in this simplified calculation, the efficiency of route 2 (direct aqueous) is significantly higher. The direct synthesis of OME from MeOH and FA in route 2 requires 22% less H_2 than route 1, consequently enhancing the potential theoretical efficiency of route 2 by 20% (with respect to route 1). In addition, the technological simplicity and synthesis energy demand of route 2 is to be noted (*e.g.* as compared to route 1), providing further motivation to investigate this synthesis pathway.
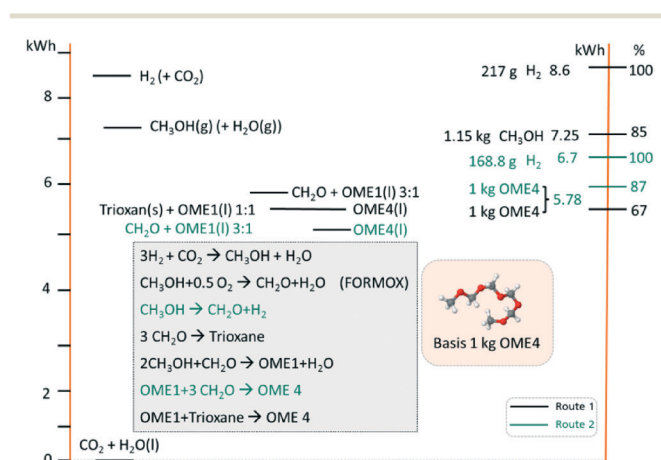
Fig. 3 Thermodynamic theoretical efficiency evaluation of proposed OME synthesis starting from CO_2 and H_2O (*i.e.* as H_2 source). Conventional route 1 (black) uses a partial oxidation (*i.e.* FORMOX) process and TRI, compared route 2 (green; *i.e.* the direct aqueous route) with FA production based on MeOH dehydrogenation and direct conversion to OME_4.

52 | *React. Chem. Eng.*, 2017, **2**, 50–59

This journal is © The Royal Society of Chemistry 2017

Multiphase model of the chemical equilibrium

The model algorithm

To solve chemical equilibrium challenges it is necessary to combine mass balances with reaction equilibria criteria. Stoichiometric methods described by O'Connell *et al.* are applied in this investigation.[35] In this case, a set of R reactions (29 reactions in the present work; Fig. 4) are solved for R-number extents of reactions (ξ) within an iterative loop, following a Newton–Raphson approach. For this algorithm the reactions have to be well specified through their stoichiometric coefficients (v). For a two phase reaction system approaching a chemical-phase equilibrium state, the following equilibrium criteria should be fulfilled (eqn (13) and (14)).

$$\text{Reaction Eqm.: } \sum_i^C v_{ij}\mu_i = 0,\ j = 1,\ 2,\ldots,R \tag{13}$$

$$\text{Phase Eqm.: } f_i^l = f_i^v$$
$$x_i\gamma_i P_i^s = y_i P,\ i = 1,\ 2,\ldots,C \tag{14}$$

where μ_i is the chemical potential of component i, v_{ij} is the stoichiometric coefficient of every component i in reaction j, $f_i^{v,l}$ is the fugacity of i components in a certain phase, y_i and x_i are the mole fractions in vapour and liquid phase respectively and γ_i is the activity coefficient of i components in liquid phase. At certain operating conditions (T, P and feed amount), the two equilibrium relations are sequentially solved, thus the chemical equilibrium compositions are also at vapour/liquid phase equilibrium (VLE). Taking into account the relatively low pressure, eqn (14) is developed considering an ideal behaviour of the gas phase as well as pressure independence of the fugacity in the liquid phase.

Model inputs

Expanding the chemical equilibrium criteria in eqn (13) towards the form of either eqn (15) or (16) highlights the required inputs needed to solve the problem. Eqn (15) and (16) are the same construction as eqn (13), but expanded in terms of the standard Gibbs energy of formation $\left(\Delta g_{if}^\circ\right)$ or the reac-

tion equilibrium constant ($\ln K_j$). Ψ_j represents the numerical value of the function in every iteration step, which must meet a value below a pre-set tolerance.

$$\sum_i^C v_{ij}\Delta g_{if}^\circ + RT\ln\prod_i^C a_i^{v_{ij}} = \psi_j,\ j = 1,\ 2,\ldots,R \tag{15}$$

$$-\ln K_j\left(T,[P^\circ]\right) + \ln\prod_i^C a_i^{v_{ij}} = \psi_j,\ j = 1,\ 2,\ldots,R \tag{16}$$

Solving the chemical equilibrium using the target function (eqn (15)), requires the definition of $\Delta g_{if}^\circ\left(T,P^\circ\right)$ for each component i corrected at T_{Reaction}. Thus, a temperature correction relation (defined as a function of the standard enthalpy of formation $\left(\Delta h_{if}^\circ\right)$ and the standard heat capacity $\left(\Delta C_{p_i}^\circ\right)$), needs to be solved to transfer Δg_{if}° from standard T to the reaction condition.

It is important to note that since thermodynamic data for higher OME ($n \geq 2$) nor HF_n and MG_n are currently defined in the literature, estimation of these values are provided based on functional group contributions first used to define the required properties (please refer to Table S1† for further details). Although estimation methods for the required properties are quite reliable, the small error associated for each property of each component accumulates and can significantly influence the equilibrium composition calculation. Poling *et al.* reported the sensitivity of K_j with deviations in Δg_j° due to the exponential relation between them.[36] On the other hand the equilibrium constant K_j is a function of temperature and can be determined experimentally (eqn (17); Table S2† for values of A and B constants used in calculation of K_j).[30,37]

$$\ln k\left(T\right) = A + \frac{B}{T} \tag{17}$$

For phase equilibrium calculations, eqn (14) can be solved as a normal flash calculation. The excess Gibbs energy of the liquid mixture is described by the modified UNIFAC group contribution method,[38] using the same UNIFAC-group distribution and interactions parameters as Hahnenstein *et al.*, and Schmitz *et al.*[39] The UNIFAC groups considered in this investigation are the following: $(CH_2O)_{FA}$, $(CH_2O)_{OME}$, H_2O, MeOH, OME1 and MG_1 along with OH, CH_2, CH_3O, and CH_2OH. Within these, the CH_2O corresponding to FA is different than the oxymethylene groups in the OME structure. There are 10 groups in total, thus all the compounds present in the mixtures are a molecular arrangement of these groups (Tables S3 and S4† for details concerning UNIFAC-group assignment and group interaction parameters (a_{mn})).
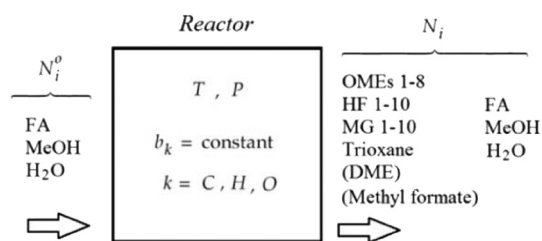

Fig. 4 The chemical equilibrium component system for a single phase OME aqueous route synthesis.

Modelling procedure

Fig. 4 illustrates the chemical equilibrium components in a single phase. The aim of the modelling is to find a combination of moles number (N_i) for every component i that meets the target function. N_i do not change arbitrarily, but is instead coupled through the stoichiometry of the reactions. The algorithm therefore solves for R-number of independent extents of reaction at kth step ($\Delta\xi_l^{(k)}$), from which the next moles number ($N_i^{(k+1)}$) can be obtained (i.e. eqn (18)) until the target function is fulfilled. These changes are moderated by the damping factor, ζ.

$$N_i^{(k+1)} = N_i^{(k)} + \zeta \sum_j^R v_{ij} \Delta\xi_j^{(k)} \qquad (18)$$

The elementary mass balance (b_k) represents the total amount of k = C, H and O atoms, which are constant throughout the whole calculation (i.e. the mass balance constraint), defined by the initial mole number (N_i^0), multiplied by the elementary matrix (a_{ki}) for k elements and i components (eqn (19)).

$$\sum_i^C a_{ki} N_i^\circ = \sum_i^C a_{ki} N_i = b_k \qquad (19)$$

With the pre-defined constraint and target functions, the algorithm functions through three steps: (1) an initialisation step – all input data is fed to the model and ε of the target function is defined. This step requires an initial estimation of the equilibrium composition N_i that agrees with the elementary mass balance b_k; (2) Iterative loop solving is used to find N_i that meets the target function 15 (or 16). The value of $\Delta\xi_l^{(k)}$ is computed using a Taylor series expansion of the target function for the $(K + 1)$th iteration and truncating after the linear term.

$$\psi_j^{k+1} = \psi_j^k + \sum_l^R \sum_i^C \sum_m^C v_{ij} \left(\frac{\partial \ln a_i}{\partial N_m}\right)^{(k)} \left(\frac{\partial N_m}{\partial \xi_l}\right) \Delta\xi_l^{(k)}$$

where the Hessian matrix ($R \times R$) Ω_{jl} is defined as follows giving eqn (20).

$$\Omega_{jl} = \sum_i^C \sum_m^C v_{ij} \left(\frac{\partial \ln a_i}{\partial N_m}\right)^{(k)} v_{ml}$$

$$0 = \psi_j^{k+1} = \psi_j^k + \sum_l^R \Omega_{jl} \Delta\xi_l^{(k)} \qquad (20)$$

Eqn (20) therefore can be then solved for R increments of $\Delta\xi_l^{(k)}$. Step (3) is a convergence, whereby the routine finally ends when all $\Psi_j (R \times 1) < \varepsilon$. A typical value for the tolerance could be between 10^{-4} and 10^{-5}. After the chemical equilibrium loop converges, the phase equilibrium loop starts. Coupling with the phase equilibrium calculation does not impact significantly on the thermodynamic consideration and requires minimal additional computational effort. The chemical-phase criteria (i.e. eqn (13) and (14)), are solved by assuming that the reactions occur in one phase only. This assumption is supported by the fact that the chemical potentials (μ_i) are combinations of fugacities, and the phase equilibrium criteria requires the same value of fugacity for each component in all phases.[35] The strategy to solve the chemical-phase calculation is described (Fig. 5). The initial mole number (N_i) overall compositions (z_i) estimation are generated by assuming reaction in one phase only and solving the previous single-phase reaction equilibrium calculation.

At the core of the iteration, the phase equilibrium is calculated by assuming a vapour fraction (V) as an initial estimation and then fitting the liquid and vapour compositions as a product of the Rachford-Rice equation.[35] After determining the phase equilibrium, the mole numbers (N_i) are distributed into the calculated liquid (N_i^l) and vapour (N_i^v) fractions, followed by a one-phase chemical equilibrium reaction performed considering an appropriate reaction phase to generate new N_i^v (or N_i^l) values. Thus new y_i (or x_i) are iteratively improved until the compositions do not vary more than the chosen tolerance (ε) conserving the elementary mass balance.

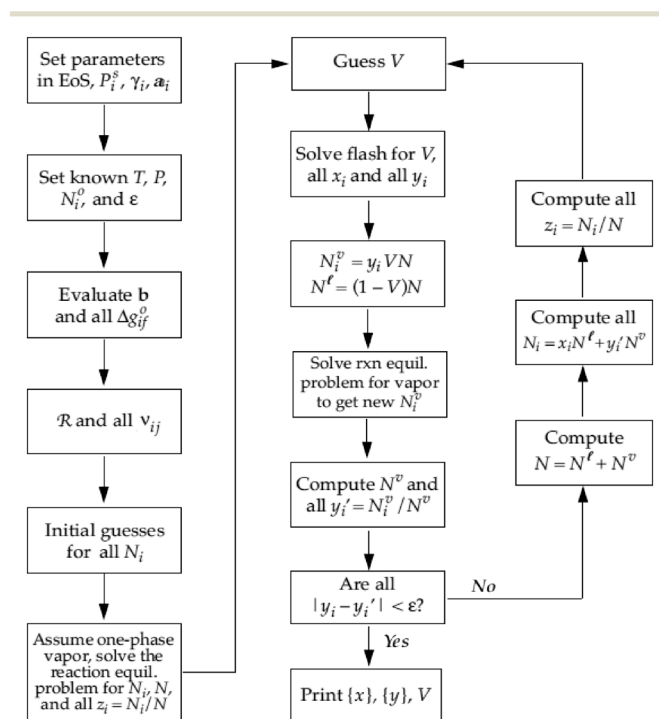
Fig. 5 Algorithm to compute chemical-phase equilibrium for several components i and reactions j at fixed T and P.[24]

54 | *React. Chem. Eng.*, 2017, **2**, 50–59

This journal is © The Royal Society of Chemistry 2017

Experimental

Chemicals and materials

Methanol (ROTISOLV®, purity >99.9%) and *para*-formaldehyde (n = 8–100, purity >95%) were purchased from Carl Roth GmbH. OME_1 (purity ≥99%) was purchased from Sigma Aldrich. $OME_{(n=2)}$ (purity = 98.6%), OME_3 (purity >99%), $OME_{(n=4)}$ (purity = 97%) were supplied by ASG Analytik Service GmbH. MEFO was purchased (97% purity (3% methanol)) from Alfa Aesar. Anhydrous sodium sulphite (Na_2SO_3; Bioultra grade, purity ≥98%) and 1.0 M HCl(aq) (Fluka standard grade solution) were purchased from Sigma Aldrich. All chemicals were used without further purification. Amberlyst™-36 (A36) (wet, D_p = 600–850 µm) was purchased from Rohm and Haas.[21] DOWEX™ 50WX2 (DW50X2) (D_p = 37–74 µm) was purchased from DOW chemicals. Catalysts were dried overnight at 100 mbar under vacuum at 70 °C before use. Reaction mixtures were prepared by dissolving *p*-FA in MeOH at a *p*-FA/MeOH ratio of 1.5 (g g^{-1}) corresponding to maximum FA solubility in methanolic solution. *p*-FA was dissolved by stirring and heating gradually for 4 h until reaching 80 °C. The solution was then left overnight at this temperature until a clear solution was obtained.[40]

Analysis

The quantitative analysis of the obtained product mixtures was performed using an Agilent 7890A gas chromatograph equipped with a flame ionisation detector (GC-FID) and auto sampler (0.4 µl sample volume). Samples were injected onto a DB-5 ms column (dimensions: 30 m × 250 µm × 0.5 µm) using He (g) as the carrier gas (flow: 4.1 mL min^{-1} at *ca.* 2 bar). The GC inlet temperature was set at 270 °C and operated in split mode (split ratio = 20). Chromatograms were obtained using a programmed oven temperature ramp (*i.e.* 35 to 270 °C, over 16 min). Calibration of the GC was achieved using pure $OME1$, $OME_{(n=2–4)}$ and standard mixtures of the pure components in MeOH. For MEFO, a 97% purity sample was used. OME_5 was calibrated based on extrapolation and relating the chromatogram area per mass fraction as a linear function of carbon number in the OME molecule.[30] As a complimentary qualitative analysis, an Agilent 6890A GC was also employed equipped with a CP-SIL5 (30 m × 8 µm) column and a Thermal Conductivity Detector (TCD). Samples were analysed using He as the carrier gas, an oven temperature ramp of 40 to 280 °C, and a column pressure ramp of 35–60 psi. FA was analysed based on a Na_2SO_3 volumetric titration method, using 1 M HCl(aq) as titre and thymolphthalein as indicator.[41] The absolute deviation between the FA content measured in this work and the available literature experimental measurements, as well as the simulation results was ≤2%.

Experimental setup

To perform the acid catalysed synthesis of OME, an autoclave with 500 mL volume was used, equipped with a stainless
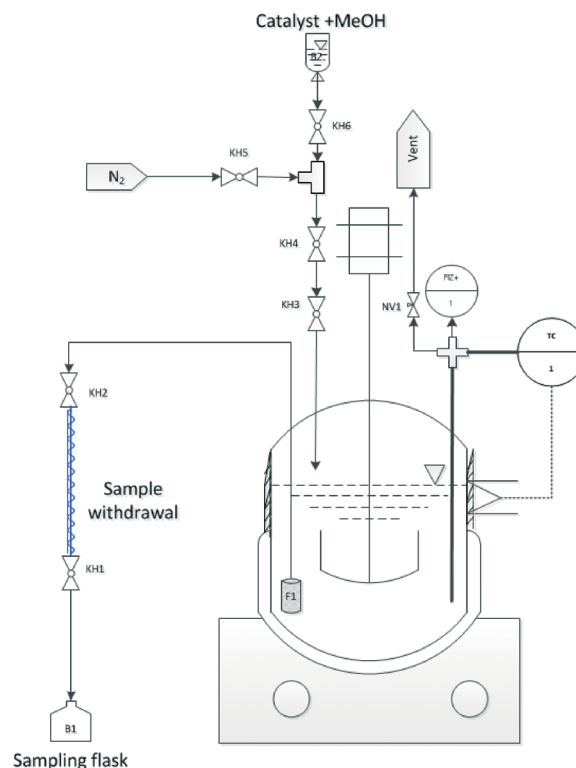
Fig. 6 Experimental setup used for OME synthesis equilibrium study *i.e.* (KH = Kugelhahn (german) / = BV = Ball Valve (BV) (english)).

steel reactor cylinder (P_{max} = 100 bar). Reaction temperature was controlled using a fixed electrical heating jacket and integrated thermocouple (*i.e.* K-type thermocouple; accuracy ± 1.5 K). An integrated magnetic stirrer was also used (Fig. 6). Pressure was measured using a diaphragm pressure indicator (accuracy ± 0.24 bar) a cylindrical sintered stainless steel (AISI 316TI) filter (F1) with 10 µm pore size is mounted on the sampling line and positioned near to the reactor base to assure sample withdrawal without catalyst particles. To cool the withdrawn samples, a quartz glass double jacket condenser connected to a thermal bath was used (cooling medium = Glysofor® (Wittig Umweltchemie)). A set of ball valves (BV) and needle valves (NV) was designed to allow feed and catalyst loading, sample withdrawal and pressure regulation in the reaction system (Fig. 6).

Experimental procedure

The feed mixture was prepared externally in an electrically heated glass flask with a magnetic stirrer and reflux condenser to assure a clear reactant solution. Prior to loading, the autoclave was pre-heated and flushed with N_2 until the reaction temperature of 80 °C was reached. The educts were then added to the autoclave reactor. The system was then sealed and brought to a steady state before initial sample withdrawal (t = 0 min). The catalyst (*e.g.* A36) was then loaded with *ca.* 10 mL MeOH in the loading line and introduced to the reactor using N_2 flow (at *ca.* 3 bar). Samples were withdrawn for analysis at defined time intervals under reactor pressures. A flush of 3 mL was dispensed before each

Table 1 Summary of the parameters of the experimental runs

Test #	Test 1	Test 2
Temperature (°C)	80	80
Pressure (bar)	3.5	3.1
Catalyst	D50WX2	A36
Cat. load (g g_{mix}^{-1})	0.5%	0.5%
Reactant mix. load (g)	200	200
p-FA/MeOH (g g^{-1})	1.5	1.5

Fig. 7 Comparison of the experimental chemical equilibrium compositions of test-1 and test-2 with previous simulation and values from ref. 30 and 40. Reaction conditions: FA/MeOH (g g^{-1}) = 1.5; 0.5% (0.1% for ref. 40) g g_{mix}^{-1} catalyst load; T = 80 °C (75 °C for ref. 30).

sample to rinse the sampling line. The reaction mixture was kept at constant T and stirring rate along the planned test interval ($t \geq 180$ minutes). Samples analysed after longer test intervals showed constant equilibrium compositions. Experiments were performed using the two commercially available acid catalysts (*i.e.* D50WX2 and A36; Table 1).

Results and discussion

Model validation

To validate the afore-described equilibrium model for OME synthesis, the set of experiments test-1 and test-2 (Table 1) were performed under the described reaction conditions. As comparative datasets, two previously published works performed at similar reaction conditions were selected; A) Burger *et al.* investigated the equilibrium experimentally under almost identical conditions, using Amberlyst®-46 as the catalyst (T = 75 °C, catalyst loading = 0.6% g g_{mix}^{-1}).[30] B) Arnold *et al.* also reported OME synthesis experiments under the same conditions as reported here, using DOWEX®-50WX2 as catalyst (loading = 0.1% g g_{mix}^{-1}).[40] In the current study, DME was excluded from the equilibrium mixture as it was not experimentally detected using the selected catalysts. The performance of the experiments under slightly higher pressure also aided to validate one phase and two phase simulations, as emphasised by an insignificant vapour fraction ($V \approx 0$). The previously reported experiments (*i.e.* ref. 30 and 40) varied in the reactor setup, feed preparation method and experimental procedure, but all examples equilibrium was established, enabling a fair comparison.

The equilibrium compositions from the developed model in comparison with the results obtained from experiments test-1 and test-2, along with previously published data are compared (Fig. 7 and 8). Based on a parity plot analysis, a good agreement between all the considered components with model results was observed, except for MeOH (Fig. 8). The starting measured concentration of MeOH in previously reported literature was also found to vary from the measured initial MeOH concentration as in this work. In the equilibrium mixture, MeOH is mainly bound in the form of the unstable HF$_n$. Depending on the analytical technique the free MeOH measured could vary (*e.g.* using GC), potentially providing an explanation for this observed deviation. Furthermore, the maximum arithmetic mean value of the absolute deviations between experimental measurements of OME in this work and previously published data did not exceed
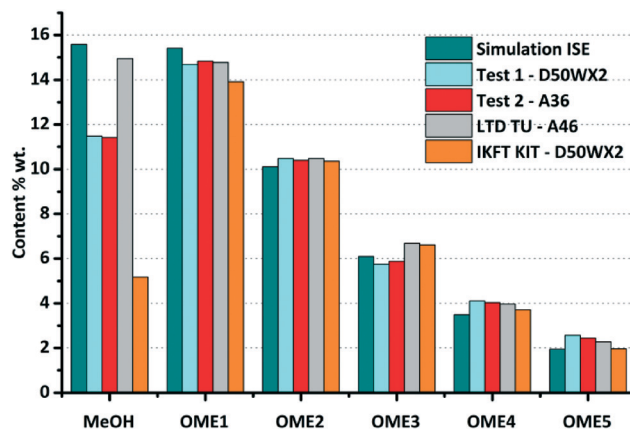
0.5 wt%. These preliminary results demonstrate that the constructed model can reliably be employed to describe the equilibrium composition of this reaction system under different conditions.

The reaction progress of experiments test-1 and test-2 are available as ESI† (test-1: Table S5, Fig. S1; test-2: Table S6, Fig. S2). The equilibrium compositions over D50WX2 were reached in *ca.* 20 min, while it took almost 1 h to be reached over the A36 catalyst. The observed higher reaction rates using the D50WX2 catalyst were attributed to the considerably smaller particle size and also the differing acid strengths/active site access (*e.g.* porosity).[40] It is considered that these results provide a good basis for the kinetic study of different catalytic systems (*i.e.* to be investigated in the future).

Parametric study

After the model validation, parametric studies were performed to determine the influence of T, feed ratio and H$_2$O
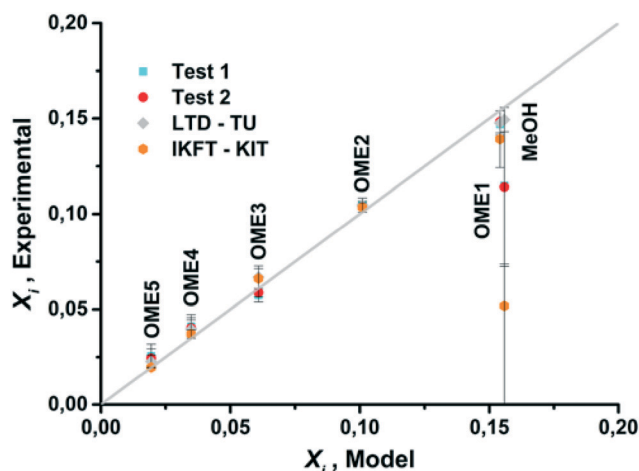
Fig. 8 Parity plot for mass fractions of OME1, OME$_{(n=2-5)}$ and MeOH for model and experimental results.
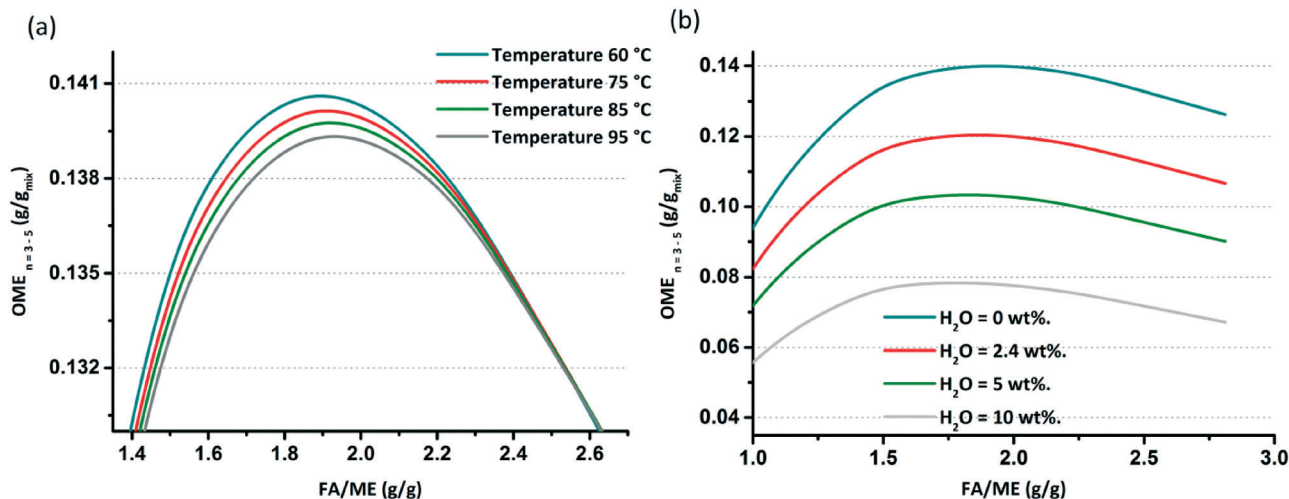
Fig. 9 (a) Effect of temperature increase on the OME (n = 3–5) composition at equilibrium. (b) Effect of water content in the feed (wt%) on the OME (n = 3–5) composition at equilibrium.

content in the feed on the equilibrium composition. The OME formation reactions are slightly exothermic ($\Delta h_j \approx -25$ mol^{-1}). Simulations for T indicate that the influence of this parameter on the equilibrium compositions at different FA/MeOH feed ratios are negligible regarding the production of OME$_{(n=3-5)}$, (*i.e.* when varying T by 35 °C; Fig. 9(a)).

The influence of H$_2$O content on the equilibrium composition distribution is more significant than T. Using an anhydrous feed doubles the target OME chain productivity when compared with a feed with a 10 wt% H$_2$O content. In an MeOH/p-FA feed, *ca.* 2.4 wt% H$_2$O is present, which limits the OME$_{(n=3-5)}$ yield (Fig. 9(b)). Referring to these results, the objective to achieve the highest OME$_{(n=3-5)}$ yield is defined to have a water free feed and operating as close as possible to a feed ratio of 1.9 FA/MeOH (g g^{-1}). To establish this reaction, an innovative process is required to control the appropriate feed composition; whilst an OME synthesis reactor is required that enables operation in the vicinity of theoretical maximum. The maximum yield at equilibrium of the target OME chain ($g_{OME_{(3-5)}}$ $g_{product}$$^{-1}$) under the optimum simulated conditions and anhydrous feed is *ca.* 14%, which is significantly low on an absolute basis. The main reasons for the low yield are (a) the limited conversion of MeOH and FA, since they also share equilibrium reactions to form MG$_n$ and HF$_n$, (b) most of the converted educts to OME are in the OME1 and OME$_{(n=2)}$ components (>35% $g_{OME_{(1-2)}}$ $g_{product}$$^{-1}$) and (c) the poor selectivity towards OME$_{(n=3-5)}$. It is proposed that the appropriate design and operation of a continuous process, which enables short OME oligomers to be recycled, supported by continuous H$_2$O and OME$_{(n=3-5)}$ separation will lead to significantly enhanced overall yield. Furthermore, complimentary catalyst development, particularly given the highly polar environment of the equilibrium reactions and the importance of the interaction between the growing OME chain and supported acid catalyst, will presumably aid to improve overall synthesis productivity.

Conclusions

In this paper, the development, design and validation of the synthesis of OME based on MeOH and FA was investigated (*e.g.* as derived from a CO$_2$ hydrogenation platform). The theoretical efficiency evaluation demonstrated that a proposed anhydrous route is potentially more attractive than a conventionally performed synthesis based on feeds of OME1 and TRI. A thermodynamic equilibrium mathematical model was developed and demonstrated to be capable of solving the sequential chemical and phase equilibrium, importantly considering all components in the reaction system including HF$_n$ and MG$_n$. The equilibrium constants required for model convergence were successfully derived based on experimental and published data. Batch reaction experiments were performed using an autoclave-based test setup to enable the validation of the developed model. Two commercial polymer supported (Brønsted; namely –SO$_3$H) acid catalysts were employed in the experimental evaluation of the equilibrium. Model results showed a strong and positive agreement with experimental results from this work and also with previously published datasets. After the model validation, a parametric study was performed to enable identification of the optimum operating conditions for OME synthesis, highlighting the significant impact of H$_2$O content in the educts feed to the reactor and the importance of employing an anhydrous feed for maximising the yield of OME$_{(n=3-5)}$. Conversely, reaction temperature was found not to significantly influence the reaction equilibrium. A feed FA/MeOH (g g^{-1}) ratio of approximately 1.9 was identified as potentially providing the highest yield of the target OME chain length (*i.e.* n = 3–5), although further work is required concerning process design if this high educt ratio is to be successfully achieved.

This study also highlights the operating framework for OME synthesis based on MeOH and FA and the necessity of innovative process regarding feed preparation, reactor

technology, product separation/fractions recycling and potentially new catalyst development. With this understanding, a concept for an efficient continuous process for OME synthesis is to be developed and tested, whilst alternative feed mixtures are also being investigated within the framework of OME synthesis. Importantly, the presented results, synthetic model and system relies on the use of MeOH as educt, as a source of FA and in turn OME, providing a potentially sustainable route to higher value, higher energy content fuels, based on CO_2 utilisation and renewable energy powered H_2 production.

Acknowledgements

References

1 (*a*) M. Mikkelsen, M. Jørgensen and F. C. Krebs, *Energy Environ. Sci.*, 2010, **3**, 43–81; (*b*) L. Mennicken, A. Janz and S. Roth, *Environ. Sci. Pollut. Res.*, 2016, **23**(11), 11386–11392; (*c*) J. Rogelj, M. den Elzen, N. Höhne, T. Fransen, H. Fekete, H. Winkler, R. Schaeffer, F. Sha, K. Riahi and M. Meinshausen, *Nature*, 2016, **534**, 631–639; (*d*) N. S. Lewis, *Energy Environ. Sci.*, 2016, **9**, 2172–2176.

2 (*a*) Intergovernmental Panel on Climate Change, *Climate Change 2014: Mitigation of Climate Change: Working Group III Contribution to the IPCC Fifth Assessment Report*, Cambridge University Press, Cambridge, UK, 2014; (*b*) *CO₂ Emissions from Fuel Combustion, Highlight Report*, International Energy Agency, Paris, France, 2015.

3 (*a*) F. Pontzen, W. Liebner, V. Gronemann, M. Rothaemel and B. Ahlers, *Catal. Today*, 2011, **171**(1), 242–250; (*b*) M. Aresta, A. Dibenedetto and A. Angelini, *Chem. Rev.*, 2014, **114**(3), 1709–1742; (*c*) A. J. Martín, G. O. Larrazábal and J. Pérez-Ramírez, *Green Chem.*, 2015, **17**, 5114–5130.

4 (*a*) H. Goehna and P. Koenig, *CHEMTECH*, 1994, **24**(6), 36–39; (*b*) M. Peters, B. Köhler, W. Kuckshinrichs, W. Leitner, P. Markewitz and T. E. Müller, *ChemSusChem*, 2011, **4**, 1216–1240; (*c*) E. Frei, A. Schaadt, T. Ludwig, H. Hillebrect and I. Krossing, *ChemCatChem*, 2014, **6**(6), 1721–1730.

5 (*a*) W. Wang, S. Wang, X. Ma and J. Gong, *Chem. Soc. Rev.*, 2011, **40**, 3703–3727; (*b*) G. A. Olah, *Angew. Chem., Int. Ed.*, 2013, **52**(1), 104–107.

6 (*a*) O.-S. Joo, K.-D. Jung, I. Moon, A. Y. Rozovskii, G. I. Lin, S.-H. Han and S.-J. Uhm, *Ind. Eng. Chem. Res.*, 1999, **38**(5), 1808–1812; (*b*) R. W. Dorner, D. R. Hardy, F. W. Williams and H. D. Willauer, *Energy Environ. Sci.*, 2010, **3**, 884–890.

7 (*a*) K.-W. Jun, W.-J. Shen and K.-W. Lee, *Bull. Korean Chem. Soc.*, 1999, **20**(9), 993–998; (*b*) T. Sakakura, J. C. Choi and H. Yasuda, *Chem. Rev.*, 2007, **107**(6), 2365–2387; (*c*) S. Abate, K. Barbera, G. Centi, P. Lanzafame and S. Perathoner, *Catal. Sci. Technol.*, 2016, **6**, 2485–2501.

8 J. Burger, M. Siegert, E. Ströfer and H. Hasse, *Fuel*, 2010, **89**(11), 3315–3319.

9 *Soot in Combustion Systems and Its Toxic Properties*, ed. J. Lahaye and G. Prado, Springer, Boston, MA, USA, 1983.

10 (*a*) W. Ying, L. Genbao, Z. Wei and Z. Longbao, *Fuel Process. Technol.*, 2008, **89**(12), 1272–1280; (*b*) B. Lumpp, D. Rothe, C. Pastötter, R. Lämmermann and E. Jacob, *MTZ Worldwide*, 2011, **72**, 198–203.

11 M. Werner and G. Wachtmeister, *MTZ Worldwide*, 2010, **71**(7–8), 70–72.

12 (*a*) Z. Wang, H. Liu, J. Zhang, J. Wang and S. Shuai, *Energy Procedia*, 2015, **75**, 2337–2344; (*b*) K. Gaukel, M. Härtl, G. Wachtmeister, J. Burger, W. Maus and E. Jacob, *The Fuel OME2: An Example of the pathway to Emission Neutral Vehicles with Internal Combustion Engine*, 37th Wiener Motorensymposium, Fortschritt-Berichte VDI, Reihe 12, Nr. 796, 2016.

13 A. Feiling, M. Münz and C. Beidl, *ATZextra Worldwide*, 2016, **21**(11), 16–21.

14 W. Maus, E. Jacob, M. Härtl, P. Seidenspinner and G. Wachtmeister, *Synthetic Fuels - OME1: A Potentially Sustainable Diesel Fuel*, 35th Wiener Motorensymposium, Fortschritt-Berichte VDI, Reihe 12, Nr. 777, 2014.

15 M. Härtl, P. Seidenspinner, E. Jacob and G. Wachtmeister, *Fuel*, 2015, **153**, 328–335.

16 R. Wang, Z. Wu, Z. Qin, C. Chen, H. Zhu, J. Wu, G. Chen, W. Fan and J. Wang, *Catal. Sci. Technol.*, 2016, **6**(4), 993–997.

17 J. Burger, V. Papaioannou, S. Gopinath, G. Jackson, A. Galindo and C. S. Adjiman, *AIChE J.*, 2015, **61**(10), 3249–3269.

18 (*a*) W. Wang, S. Wang, X. Ma and J. Gong, *Chem. Soc. Rev.*, 2011, **40**, 3703–3727; (*b*) E. V. Kondratenko, G. Mul, J. Baltrusaitis, G. O. Larrazábal and J. Pérez-Ramírez, *Energy Environ. Sci.*, 2013, **6**, 3112–3135; (*c*) A. Goeppert, M. Czaun, J. P. Jones, G. K. S. Prakash and G. A. Olah, *Chem. Soc. Rev.*, 2014, **43**, 7995–8048.

19 J. Burger, E. Ströfer and H. Hasse, *Ind. Eng. Chem. Res.*, 2012, **51**(39), 12751–12761.

20 W. H. Fu, X. M. Liang, H. Zhang, Y. M. Wang and M. Y. He, *Chem. Commun.*, 2015, **51**(8), 1449–1452.

21 L. Wang, W.-T. Wu, T. Chen, Q. Chen and M.-Y. He, *Chem. Eng. Commun.*, 2014, **201**(5), 709–717.

22 J. Wu, H. Zhu, Z. Wu, Z. Qin, L. Yan, B. Du, W. Fan and J. Wang, *Green Chem.*, 2015, **17**(4), 2353–2357.

23 Q. Wu, M. Wang, Y. Hao, H. Li, Y. Zhao and Q. Jiao, *Ind. Eng. Chem. Res.*, 2014, **53**(42), 16254–16260.

24 Y. Zhao, Z. Xu, H. Chen, Y. Fu and J. Shen, *J. Energy Chem.*, 2013, **22**(6), 833–836.

25 Y. Zheng, Q. Tang, T. Wang, Y. Liao and J. Wang, *Chem. Eng. Technol.*, 2013, **36**(11), 1951–1956.

26 Y. Zheng, Q. Tang, T. Wang and J. Wang, *Chem. Eng. Sci.*, 2015, **134**, 758–766.

27 (*a*) L. P. Lautenschütz, *New findings in the optimisation of oxymethylene diethylether oligomer synthesis from dimethoxymethane and trioxane/("Neue Erkenntnisse in der Syntheseoptimierung oligomerer Oxymethylen-dimethylether*

aus Dimethoxymethan und Trioxan"), *Dissertation*, University of Heidelberg, URN:nbn:de:bsz:16-heidok-192102, 2015; (*b*) L. Lautenschütz, D. Oestreich, P. Seidenspinner, U. Arnold, E. Dinjus and J. Sauer, *Fuel*, 2016, **173**, 129–137.

28 J. Zhang, M. Shi, D. Fang and D. Liu, *React. Kinet., Mech. Catal.*, 2014, **113**(2), 459–470.

29 J. Zhang, D. Fang and D. Liu, *Ind. Eng. Chem. Res.*, 2014, **53**(35), 13589–13597.

30 N. Schmitz, F. Homberg, J. Berje, J. Burger and H. Hasse, *Ind. Eng. Chem. Res.*, 2015, **54**(25), 6409–6417.

31 N. Schmitz, J. Burger and H. Hasse, *Ind. Eng. Chem. Res.*, 2015, **54**(50), 12553–12560.

32 F. Wang, G. Zhu, Z. Li, F. Zhao, C. Xia and J. Chen, *J. Mol. Catal. A: Chem.*, 2015, **408**, 228–236.

33 G. Reuss, W. Disteldorf, A. O. Gamer and A. Hilt, in *Ullmann's Encyclopedia of Industrial Chemistry*, Wiley-VCH Verlag GmbH & Co. KGaA, Weinheim, Germany, 2000, ch. Formaldehyde, p. 744.

34 T. Grützner, H. Hasse, N. Lang, M. Siegert and E. Ströfer, *Chem. Eng. Sci.*, 2007, **62**(18–20), 5613–5620.

35 J. P. O'Connell and J. M. Haile, *Thermodynamics: Fundamentals for applications*, Cambridge University Press, New York, USA, 2005.

36 B. E. Poling, J. M. Prausnitz and J. P. O'Connell, *The properties of gases and liquids*, 5th edn, McGraw-Hill, New York, USA, 2001, ch. 4, p. 3.4.

37 C. Kuhnert, *Vapour-Liquid-Equilibrium in multicomponent Formaldehyde Containing Systems (*"*Dampf-Flüssigkeits-Gleichgewichte in mehrkomponentigen formaldhydhaltigen Systemen*"*)*, Shaker, Aachen, Germany, 2004, ISBN-3-8322-2689-3.

38 A. Jakob, H. Grensemann, J. Lohmann and J. Gmehling, *Ind. Eng. Chem. Res.*, 2006, **45**(23), 7924–7933.

39 (*a*) C. Kuhnert, M. Albert, S. Breyer, I. Hahnenstein, H. Hasse and G. Maurer, *Ind. Eng. Chem. Res.*, 2006, **45**(14), 5155–5164; (*b*) N. Schmitz, A. Friebel, E. von Harbou, J. Burger and H. Hasse, *Fluid Phase Equilib.*, 2016, **425**, 127–132.

40 U. Arnold, L. Lautenschütz, D. Oestreich and J. Sauer, *Production of Oxygenate Fuels from Biomass-derived Synthesis Gas*, Reprints 2015-2 of the DGMK-Conference "Synthesis Gas Chemistry", October 7–9, 2015, Dresden, Germany, p. 127.

41 J. F. Walker, *Formaldehyde*, American Chemical Society Monograph Series, Reinhold Publ. Corp., New York, 1944.

42 http://www.leistungszentrum-nachhaltigkeit.de/ (last accessed November 2016).

This journal is © The Royal Society of Chemistry 2017

React. Chem. Eng., 2017, **2**, 50–59 | 59

Supporting Information On: Poly(Oxymethylene) Dimethyl Ethers - A combined chemical equilibrium investigation towards increasingly efficient and a potentially sustainable synthetic route

M. Ouda,[a,b] G. Yarce,[a] R. J. White,[a,]* M. Hadrich,[a] D. Himmel,[c] A. Schaadt,[a] H. Klein,[b] E. Jacob[d] and I. Krossing,[c,e]

[a] Fraunhofer Institute for Solar Energy Systems ISE, Heidenhofstraße 2, 79110 Freiburg, Germany; Email: robin.white@ise.fraunhofer.de, Tel.: +497614588519

[b] Institute of Process and Plant Technology, Technical University Munich, Boltzmannstraße 15, 85748 Garching, Germany

[c] Institute for Inorganic and Analytical Chemistry, Albert-Ludwigs-University Freiburg, Albertstraße 21, 79104 Freiburg, Germany

[d] Motors Emissions Concepts UG, Karwendelstraße 25, 82152 Krailling, Germany

[e] FMF - Freiburger Materialforschungszentrum, Stefan-Meier-Straße 21, D-79104 Freiburg, Germany

Sources for Thermodynamic Standard Properties in Literature

Table S1 Sources for standard Gibbs energy of formation $\Delta g°_{if}$

Literature sources	Estimation methods
• DIPPR 801 project, Design institute for physical properties • NIST, the National Institute for Standards and Technology • NBS Technical Note 270 • JANAF (Joint Army-Navy-Air Force) tables	• Method of Joback (1984; 1987) • Method of Constantinou and Gani (1994) • Method of Benson (1968; 1969) • CHETAH-software from ASTM (1998)

Thermodynamic Chemical and Phase Equilibrium Model parameters

Table S2 Parameters A, B for chemical equilibrium constants (Kj) fitted to experimental data [1,2]

$\ln K(T) = A + \dfrac{B}{T}$	A	B
$FA + H_2O \leftrightharpoons MG_1$	-2.3250	2579.0
$FA + MG_{n-1} \leftrightharpoons MG_n; \quad n \geq 2$	-2.4334	3039.4
$FA + MeOH \leftrightharpoons HF_1$	-1.9020	3512.0
$FA + HF_{n-1} \leftrightharpoons HF_n; \quad n \geq 2$	-2.2496	3008.8
$HF_1 + MeOH \overset{H^+}{\leftrightarrow} OME_1 + H_2O$	0.8147	340.25
$FA + OME_{n-1} \overset{H^+}{\leftrightarrow} OME_n; \quad n \geq 2$	-2.4154	3029.6
$3FA \overset{H^+}{\leftrightarrow} TRI$	-4.3253	7347.3

Table S3 UNIFAC group assignment for all components

Group / Substance	CH_2O (FA)	H_2O	$C_3H_8O_2$ (OME1)	$OH(CH_2O)H$ (MG1)	OH	CH_2	CH_3O	CH_2OH	CH_3OH	CH_2O (OME)
Formaldehyde	1									
Water		1								
Methanol									1	
Methylal (OME1)			1							
MG1				1						
HF1							1	1		
MGn>2	n-1				2	1				
HFn>2	n-1						1	1		
OMEn>2			1							n-1
Trioxane	3									

Table S4 UNIFAC Interaction parameters aij (K) [3,4]

Group i / Group j	CH_2O (FA)	H_2O	OME1	MG1	OH	CH_2	CH_3O	CH_2OH	CH_3OH	CH_2O (OME)
CH_2O FA	-	867.8	0.0	189.2	237.7	83.36	0.0	238.4	238.4	0.0
H_2O	-254.5	-	$a_{2,3}(T)$	189.5	-229.1	300.0	-219.3	$a_{2,8}(T)$	289.6	$a_{2,10}(T)$
OME1	0.0	$a_{3,2}(T)$	-	$a_{3,2}(T)$	237.7	83.36	0.0	0.0	410.0	26,0
MG1	59.2	-191.8	$a_{2,3}(T)$	-	-229.1	300.0	-142.4	289.6	289.6	59.2
OH	28.06	353.5	28.06	353.5	-	156.4	112.8	-137.1	-137.1	28.06
CH_2	251.5	1318	251.5	1318	986.5	-	447.8	697.2	697.2	251.5
CH_3O	0.0	423.8	0.0	774.8	1164.8	273.0	-	238.4	238.4	0.0
CH_2OH	-128.6	$a_{8,2}(T)$	0.0	-181.0	249.1	16.5	-128.6	-	0.0	-128.6
CH_3OH	-128.6	-181.0	-71.21	-181.0	249.1	16.5	-128.6	0.0	-	-128.6
CH_2O (OME)	0.0	670.7	141.5	189.2	237.7	83.36	0.0	238.4	238.4	-

Here, $a_{2,3}(T) = -225.5 + 0.705(T/K)$; $a_{3,2}(T) = 1031.0 - 1.749(T/K)$; $a_{8,2}(T) = -1018.57 + 329.9(T/K)$; $a_{2,8}(T) = 451.64 - 114100(T/K)$; $a_{2,10}(T) = 168.9 - 0.8776(T/K)$

Experimental data T1 and T2

Table S5 Experimental data of OME-synthesis on T1

Test 13 – Autoclave – D50WX2 – Experimental data						
p-FA = 119.94 g MeOH = 80.20 g			Catalyst Mass = 1.0048 g MeOH for cat. loading = 7.41 g			
sample Time (min)	MeOH (%wt.)	OME1 (%wt.)	OME2 (%wt.)	OME3 (%wt.)	OME4 (%wt.)	OME5 (%wt.)
0	25.83	0.00	0.000	0.000	0.000	0.000
10	12.38	12.37	9.27	4.97	2.63	1.30
30	12.02	15.23	11.41	5.45	4.12	2.42
60	11.58	14.88	10.89	4.84	3.81	2.26
90	11.13	13.64	9.63	5.99	3.89	2.39
120	11.01	14.15	9.97	5.59	4.07	2.55
180	10.63	13.30	9.31	5.73	3.90	2.49
240	12.45	16.91	11.59	6.79	4.84	3.22
AV	**11.48**	**14.69**	**10.47**	**5.74**	**4.11**	**2.56**
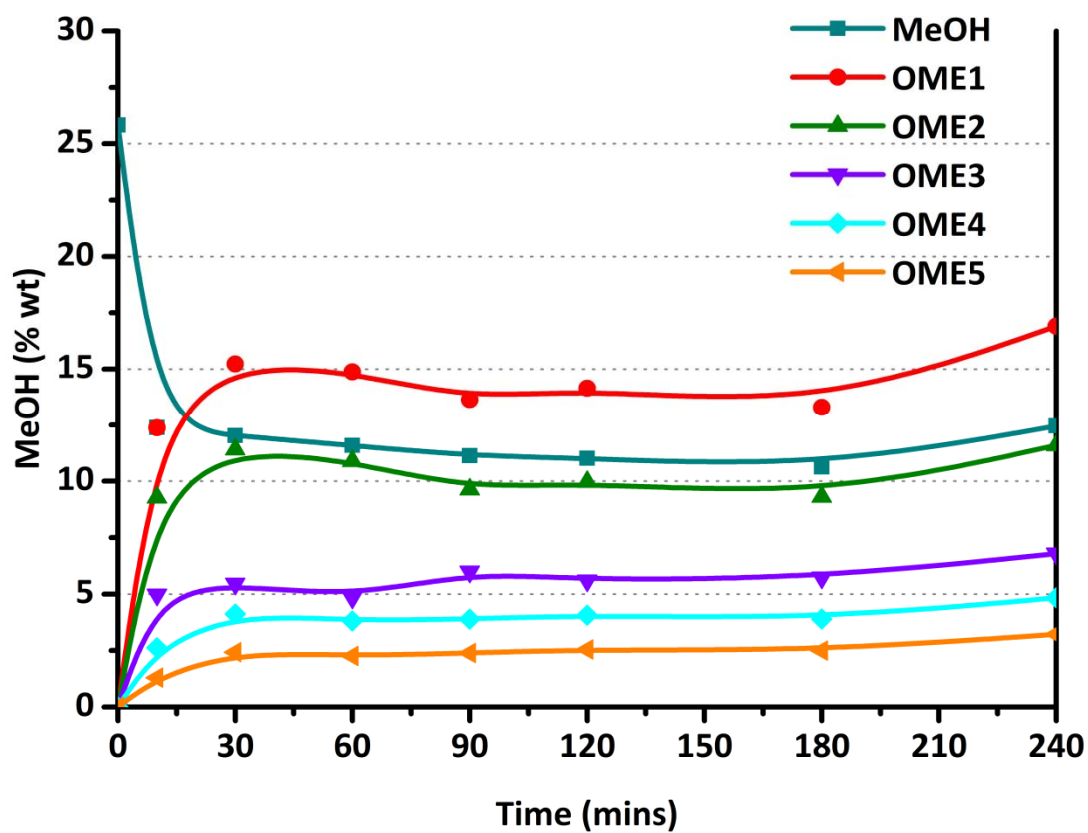
Figure S1 Graphic progress of OME-synthesis on T1

Table S6 Experimental data of OME-synthesis on T2

	Test 14 – Autoclave – A36 – Experimental data						
	p-FA = 120.05 g MeOH = 80.25 g			Catalyst Mass = 1.0038 g MeOH for cat. loading = 6.41 g			
sample Time (min)	MeOH (%wt.)	FA (%wt.)	OME1 (%wt.)	OME2 (%wt.)	OME3 (%wt.)	OME4 (%wt.)	OME5 (%wt.)
0	29.37	57.21	0.00	0.00	0.000	0.00	0.00
6	23.98	--	4.55	2.81	1.20	0.60	0.25
12	18.71	43.81	8.15	5.67	2.30	1.29	0.60
21	16.49	--	10.55	7.45	2.68	1.67	0.79
31	14.68	36.35	12.73	9.32	4.56	2.19	1.00
61	12.07	33.47	13.67	10.04	5.23	2.97	1.47
102	11.63	32.33	14.00	10.14	5.40	3.20	1.77
184	11.20	32.04	13.69	9.72	5.65	3.69	2.27
270	11.86	31.96	15.01	10.39	5.71	3.93	2.44
441	11.17	31.74	15.77	11.05	6.24	4.46	2.60
AV	**11.41**	**31.91**	**14.83**	**10.39**	**5.87**	**4.03**	**2.44**
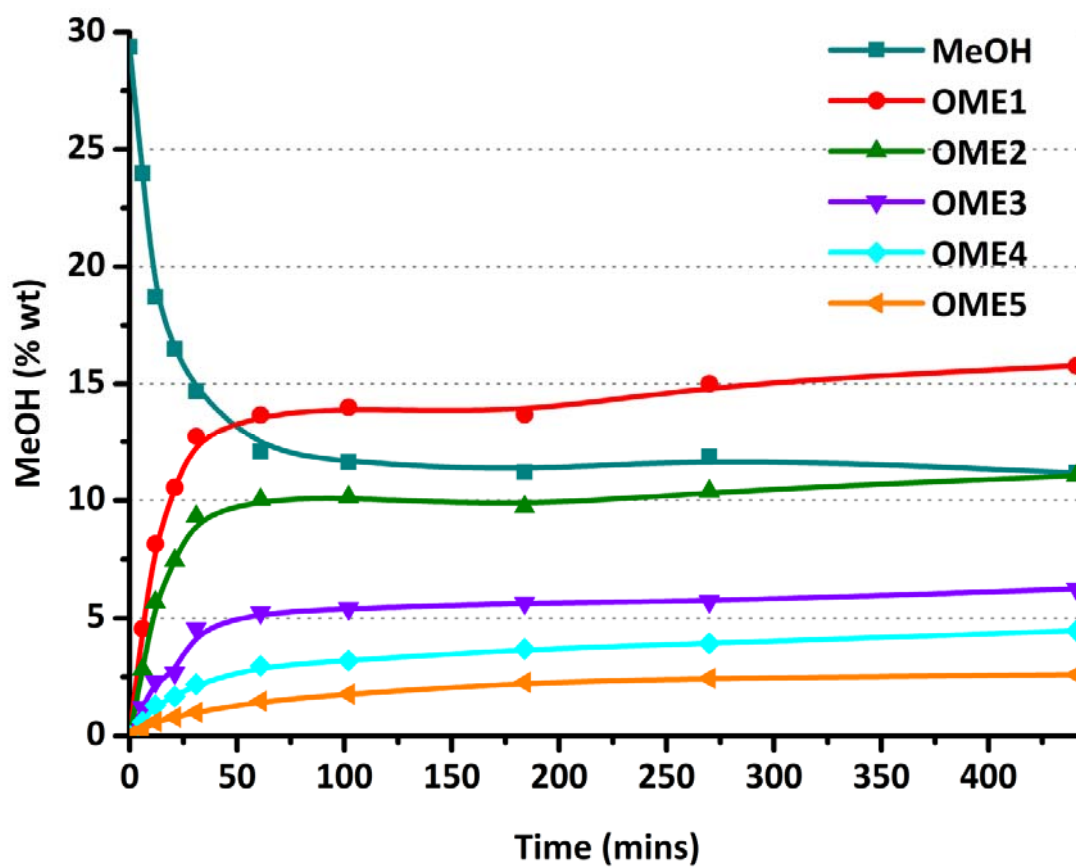
Figure S2 Graphic progress of OME-synthesis on T2

References

1. C. Kuhnert, *Dampf-Flüssigkeits-Gleichgewichte in mehrkomponentigen formaldhydhaltigen [formaldehydhaltigen] Systemen*, Shaker, Aachen, 2004.
2. N. Schmitz, F. Homberg, J. Berje, J. Burger and H. Hasse, *Ind. Eng. Chem. Res.*, 2015, **54**(25), 6409.
3. C. Kuhnert, M. Albert, S. Breyer, I. Hahnenstein, H. Hasse and G. Maurer, *Ind. Eng. Chem. Res.*, 2006, **45**(14), 5155.
4. N. Schmitz, A. Friebel, E. von Harbou, J. Burger and H. Hasse, *Fluid Phase Equilib.*, 2016, **425**, 127-135

7.6 Paper 2: Describing Oxymethylene Ether Synthesis based on the application of Non-Stoichiometric Gibbs Minimisation

Mohamed Ouda, Franz Mantei, Mahmoud Elmehlawy, Robin J. White, Harald Klein, and

Seif-Eddeen K. Fateen

7.6.1 Summary of the paper

The extension of the model developed in the previous work to consider the recycling of the non-reacted components and the stoichiometric reactor for methanol (MeOH) endothermic dehydrogenation to formaldehyde (FA) was described in this work. The conversion of MeOH and FA to oxymethylene dimethyl ethers (OME) is not complete and the per-path yield of the desired OME_{3-5} product is limited to ~0.14 g g^{-1}. Therefore, the model should consider the recycling of the non-reacted components and other OME fractions than the desired ones to increase this yield in a technical process. This leads to a sophisticated equilibrium problem for a system comprising 32 reactants undergoing 29 simultaneous equilibrium reactions. The unconstrained Gibbs minimisation approach using stochastic global optimiser algorithm was applied to achieve convergence of the equilibrium problem. A complimentary experimental validation is provided for the OME reaction equilibrium model based on the use of different feeds, namely 1) methanol (CH_3OH)/FA (CH_2O) and 2) methylal ($H_3C-O-(CH_2O)_1-CH_3$)/ Trioxane ($CH_2O)_3$. The results demonstrate the robustness and reliability of the applied SGO for this multi-reaction system. The MeOH endothermic dehydrogenation reactor was modelled as stoichiometric reactor with performance parameters defined from available literature.

With the two-step process main components modelled in Matlab®, a material and energy balance was carried out. The main process key performance indicators were evaluated based on the model results. The OME_{3-5} yield was the highest relative to literature evaluated processes. Furthermore, the study was complemented with a techno-economic evaluation considering several assumptions for the missing data. The annual production cost of OME_{3-5} based on the described process was calculated as 772.5 US\$ per t at small production capacity of *ca.* 30 kt per annum and at 571 US\$ per t at large scale production of 1 Mt per annum. The findings of this work elaborated the competitiveness of the investigated process against literature discussed process when a technical realization is demonstrated.

7.6.2 Overview of the contributions in this work

I was significantly involved in the essential phases of brainstorming and in the elaboration of all parts of the work. From (1) the conception phase, (2) initiating the collaboration with Prof. Fateen group with whom I studied physical chemistry and thermodynamic in my under- and postgraduate studies, (3) defining paper outline, (4) literature research and definition of the thermo-physical properties of the considered components, (5) discussing algorithms and how to apply the NSGM approach to our system, (6) discussing recycle consideration algorithm, (7) designing experimental validation plan, (8) modification of the batch autoclave, (9) calibration of analytical equipment, (10) running the validation experimental set together with my master student and co-author Franz K. Mantei, (11) implementing the discussed modifications with Prof. Fateen in the NSGM-SGO model in our Matlab® program, (12) implementing the stoichiometric reactor for MeOH endothermic dehydrogenation in the Matlab®

program, (13) material and energy balance evaluation based on the model results, (14) techno-economic evaluation based on technical process economics from Baerns[143]. (15) Finally, writing the whole paper except the parts describing the unconstrained Gibbs minimisation based on a stochastic global optimiser and part of the recycle process results which were done by Prof. Fateen group. Carrying out the corresponding adjustments after the review process was explicitly my task. The rest of the co-authors contributed in the initial concept discussion phase and did correction reading.

7.6.3 Paper as published in Peer-Reviewed journal

Describing oxymethylene ether synthesis based on the application of non-stoichiomsetric Gibbs minimisation†

M. Ouda,*[ab] F. K. Mantei,[a] M. Elmehlawy,[c] R. J. White, (iD) *[a] H. Klein[b] and S.-E. K. Fateen*[de]

The synthesis of short chain poly oxymethylene dimethyl ethers, also known as oxymethylene ethers (OME; molecular formula: $H_3CO–(CH_2O)_n–CH_3$ where n = 1–8) is described through the application of non-stoichiometric Gibbs minimisation (NSGM) to a synthesis based on methanol and anhydrous formaldehyde. The presented approach shows several synthesis efficiency and economic advantages as demonstrated through a simulation platform based on MATLAB® (where the two main reactors models are implemented) and the NSGM, which utilises stochastic global optimisation (SGO) to perform an unconstrained minimisation and convergence of the complex OME reaction system (comprising >31 reactants and also recycling of non-reacted components). A complimentary experimental validation is provided for the OME reaction equilibrium model based on the use of different feeds, namely 1) CH_3OH/CH_2O and 2) $H_3C–O–(CH_2O)_1–CH_3/(CH_2O)_3$. The presented results demonstrate the robustness of the applied NSGM for this multi-reaction system. With regard to the overall evaluation of the presented process, key performance indicators (KPIs) are discussed based on the material balance results of the simulation platform. A cost model for the OME synthesis process based on different feeds is also presented based on an annual production of one million metric tonnes of OME$_{3–5}$. The cost of 571 € per tonne demonstrates the economic potential of the presented OME production process.

Introduction

It is now well established that society must face the challenges of establishing more sustainable energy and chemical cycles (akin to natural processes), if the targets of various national and international frameworks (*e.g.* COP21) regarding greenhouse gas emissions (GHGE) are to be met.[1–3] One of the most challenging sectors in this context is (*e.g.* urban) mobility, which represents an ever growing share of global energy-related GHGE (*i.e. ca.* 23% or 6.7 Gt(CO_2) per annum).[4]

[a] *Sustainable Catalytic Materials Group, Division Hydrogen Technologies, Fraunhofer Institute for Solar Energy Systems, Heidenhofstr. 2, 79110 Freiburg, Germany. E-mail: mohamed.ouda@ise.fraunhofer.de, robin.white@ise.fraunhofer.de*
[b] *Institute of Process and Plant Technology, Technical University Munich, Boltzmannstr. 15, 85748 Garching, Germany*
[c] *Energy and Bioprocess Engineering Program, Zewail City of Science and Technology, Giza, Egypt*
[d] *Department of Chemical Engineering, Cairo University, Giza, Egypt*
[e] *Environmental Engineering Program, Zewail City of Science and Technology, Giza, Egypt. E-mail: sfateen@zewailcity.edu.eg*

† Electronic supplementary information (ESI) available: Algorithm for Gibbs energy minimisation technique, Algorithm for recycle calculation, tables for standard thermodynamic properties, tables for UNIFAC parameters, experimental setup schematic, model validation against experimental and literature simulation data. See DOI: 10.1039/c8re00006a

Furthermore, there is also an increasing awareness of health hazards associated with fuel (*e.g.* diesel) combustion and the release of particulate matter (PM) and nitrous oxides (NO$_x$) to the urban environment, with legislation and emission standards (*e.g.* Euro VI) reflecting this.[5] According to the U.S. Energy Information Administration (EIA), global fossil fuel consumption is predicted to decrease over the coming decades, although the consumption of diesel fuel is expected to increase till the middle of the current century.[6] Therefore, alternative mobility fuels that demonstrate benefits (*e.g.* reduced emissions) in both an urban health and global context,[7–9] that perform in a superior manner to conventional exhaust gas treatment systems, whilst supporting the expected demand in mobility (*e.g.* with population growth),[10] are of serious interest. With regard to emissions, another important concern relates to the continued use of volatile organic compound (VOC) solvents (*e.g.* in industrial sectors such as paints and coatings). Here it would be desirable to replace these potential mutagens, carcinogens or ozone depleters with greener, more environmentally friendly alternatives (*e.g.* as a consequence of associated legislation).[11–13]

One solution in this context is potentially the design and synthesis of fuels and solvents, with recent reports highlighting interest in synthetic oxygenates such as ethers,

This journal is © The Royal Society of Chemistry 2018

React. Chem. Eng., 2018, **3**, 277–292 | 277

carbonates and formates. In this regard poly acetals such as "*Poly-Oxymethylene Dimethyl Ethers*" (POMDE), or for short chain oligomers "*Oxymethylene Ethers*" (OME), are receiving interest as diesel substitutes or additives (*e.g.* due to reduced PM emissions upon combustion).[10,14–17] OMEs are known to be miscible[18] with diesel at any ratio,[19] are non-hazardous to human health or the environment, are weakly corrosive, have a high cetane number[20] (relative to conventional diesel), whilst, due to their chemical structure, have promising interesting intrinsic combustion properties.[21] Short chain OME (chemical formula $H_3CO–(CH_2O)_n–CH_3$ where n = 3–5) have successfully been applied as additives in diesel at 5–30 vol%, with the resulting fuel used without engine modification.[10,21–24] OME are also being considered with regard to solvent applications as a consequence of chain length dependent solvation properties (*e.g.* in CO_2 sorption) and appropriate vapour pressures.[25–27]

Regarding the theoretical and experimental synthesis of OME (where $n \leq 8$), reports from Burger *et al.* and Arnold, Sauer *et al.* are to be noted.[21,24,25,27–31] OME synthesis is typically based upon CH_3OH (denoted hereon as MeOH), which traditionally is produced based from syngas (*e.g.* from methane reforming) but can also be produced from direct hydrogenation of CO_2.[32] A recent report highlights the production of OME_1 ($H_3CO–(CH_2O)_1–CH_3$; also referred to as methylal or dimethoxymethane) *via* a multistep homogeneously catalysed reaction of MeOH, CO_2 and H_2.[33] Therefore, there is the longer term potential to produce OME sustainably if processing is achieved in an efficient manner (*e.g.* whereby CO_2 is captured initially at point sources and H_2 is supplied *via* renewable energy driven H_2O splitting).

OME synthesis is also possible *via* a number of other MeOH-based pathways, for example *via* oligomerisation with CH_2O (formaldehyde (FA)), whereby the MeOH acts as a methyl end capping agent.[27] Different FA sources and end capping agents including the reaction of trioxane (TRI; $(CH_2O)_3$) or *para*-formaldehyde (as FA sources) and OME_1 (as the end capping agent) have also been reported.[27] The choice of the FA source and methyl end capping agent is important as it influences the reaction mechanism and in turn dictates OME chain length distribution. OME synthesis where $n \geq 2$ can be achieved based on formalin (*i.e.* 37 wt% FA (aq)) or *para*-formaldehyde and OME_1.[34,35] Educts that selectively yield OME whilst avoiding H_2O and acetal formation (*e.g.* an anhydrous route), require energy intensive feed preparation steps. On the other hand, a direct synthesis based on MeOH and FA (*e.g.* an aqueous route) generates H_2O and further side products. These have to be separated downstream and ultimately reduce the feed to product final yield.[36] In the context of synthetic fuels and solvents, the selection of the most efficient synthesis route is clearly of significant importance (*e.g.* with regard to net energy content of the product relative to the feed energy content and the process energy consumption). When anhydrous monomeric FA is fed together with MeOH, a higher yield per reaction path can be achieved (relative to the aqueous route based on formalin) resulting in

lower recycle ratios for the OME synthesis step and overall higher process efficiency and carbon yield. This anhydrous FA feed can be synthesised *via* the endothermic thermal catalytic dissociation of MeOH, with H_2 as the main side product. This synthesis step has been discussed in the literature over a variety of different catalysts and in several reactor arrangements with FA yields <70 wt% reported with significant non-converted MeOH still available in the final product stream.[37–39] Regarding OME synthesis, this product stream is of interest as it can be directly fed to the OME synthesis reactor where a higher target product yield per path and overall process energy efficiency (relative to conventional synthesis processes) can be achieved. Therefore, an optimised process based on a direct synthesis would allow the comparison between both approaches and define the optimum synthesis route.

To synthesised OMEs, a number of catalytic and associated kinetic investigations have been reported, typically based on solid acids (*e.g.* Dowex®, Amberlyst®, and ZSM-5) and more recently graphene oxide.[23,40,41] Other reports have described the chemical equilibrium of OME synthesis from a thermodynamic viewpoint. The reports of Burger *et al.* are duly acknowledged regarding the development of a vapour–liquid–liquid equilibrium (VLLE), kinetic and equilibrium model for OME synthesis based on MeOH and FA (with *para*-FA as FA source), as well as a chemical equilibrium and kinetic model for the TRI and OME_1 system.[29,31,42,43] Elaborating on this previous work and other previously reported thermodynamic data sets, we have also recently reported on a combined reaction equilibrium and vapour–liquid equilibrium (VLE) model for OME synthesis based on MeOH and FA.[36] Applying *ab initio* computational calculations, Krossing *et al.* have also recently reported on the principal thermodynamic functions of gaseous and liquid phase OME formation and the combustion energies of different OMEs.[44]

Regarding the economics for OME production, Burger *et al.*[45] and Sauer *et al.*[46] have both considered syntheses based on MeOH. Burger *et al.* focused on OME synthesis through an anhydrous route (based on TRI and OME_1 with several energy intensive synthesis and separation steps prior to OME synthesis) while Sauer *et al.* focused on the synthesis based on MeOH and FA (aq). The former considered natural gas steam reforming for syngas (and in turn to MeOH) production and a cost of 614.8 US$ per $t_{OME_{3–6}}$ (based on a MeOH feed cost of 300 US$ per t, 1 Mt($OME_{3–6}$) plant capacity and Diesel cost between 460–870 US$ per t). In the latter report, syngas was sourced from biomass gasification, with the yield of $OME_{3–5}$ defined based on woody biomass (3.25 $t_{OME_{3–5}}/t_{Biomass}$).

Current industrial OME synthesis (*e.g.* in China) is at capacities of *ca.* 30–40 kt per annum but suffers from low overall process energy efficiency and based on fossil MeOH as feedstock.[10] In Germany, another process is being developed which enhances the synthesis efficiency (relative to the Chinese process) but as yet does not show economic feasibility (relative to fossil-based diesel) due to the expensive feedstock and several energy intensive synthesis steps.[47] Therefore,
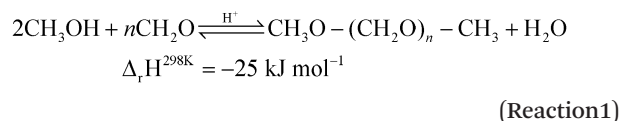
efforts and investigations are required to optimise OME synthesis further from both a process/thermodynamic basis but also with regard to reducing productions costs, particularly if these potential energy carriers or solvents are to find market entrance. In this context, this paper addresses the direct synthesis of OME with regard to the development of a simulation platform in order to evaluate the material and energy balance and consequently define key performance indicators (KPIs) for the process. The investigated synthesis is based on the development and implementation of a stoichiometric reactor for anhydrous FA synthesis (*i.e.* through MeOH dehydrogenation), whereby H_2 is the main side product (*e.g.* as based on existing literature data).[37–39] This is complimented by a non-stoichiometric Gibbs minimisation (NSGM) algorithm that uses a stochastic global optimiser (SGO) designed to allow an unconstrained Gibbs free energy minimisation, such that the chemical equilibrium of the OME synthesis process can be successfully converged. The product stream is separated in an ideal separator unit; an approach called ∞–∞ analysis[48] allowing early stage reactor optimisation (single parameter optimisation) prior to rigorous separation model development; this in turn allows the identification of maximum theoretical process technical and economic metrics. The process model is developed using the commercial software MATLAB®. The developed code for the OME synthesis unit (SGO) is in turn validated based on the use of two different feeds, namely MeOH/FA and the comparison TRI/OME$_1$. The presented findings highlight the merits of the developed SGO with regard to OME synthesis and its potential extrapolation to a wide range of other complex equilibrium calculations. The presented results and associated KPIs indicate the potential to go to higher overall synthesis efficiency and target product OME$_{3–5}$ yield (relative to the conventional OME synthesis). Additionally, the preliminary economic evaluation in this report indicates a potentially market acceptable OME production cost, whilst the integration of the developed algorithms in a commercial process simulation (*i.e.* CHEMCAD®), the rigorous product separation units and the auxiliary units (heat exchangers, pumps...*etc.*) provides a solid basis and robust tool for a detailed OME synthesis process evaluation, which can be extended to other complex equilibrium systems.

Theory and background

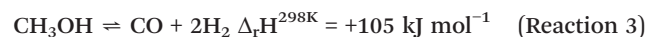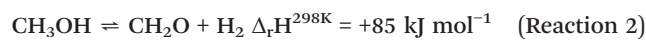### Process description based on methanol and anhydrous formaldehyde

As aforementioned, a key component in OME synthesis is FA (*e.g.* as supplied from the partial oxidation of MeOH). However, OME synthesis in the presence of H_2O is thermodynamically unfavoured and reduces the final product yield (Reaction 1).[29] Furthermore, a "*direct*" OME synthesis from MeOH and anhydrous FA requires two reaction steps followed by product separation with H_2 as the main by-product, in turn providing scope to reduce both CAPEX and OPEX in comparison with other reported processes. For example, other OME synthesis

processes require four reaction steps and reactive distillation/rectification in order to reach the target product.[45] In our recently reported work, the potential of the "*direct*" route based on an anhydrous FA feed with a molar ratio of FA/MeOH of *ca.* 1.8–2 can potentially generate a high per path yield of OME with chain length n = 3–5 (a target range for both solvents and fuel applications), a high theoretical overall process energy efficiency and indeed favourable process economics.[36]

$$2CH_3OH + nCH_2O \underset{}{\overset{H^+}{\rightleftharpoons}} CH_3O-(CH_2O)_n-CH_3 + H_2O$$
$$\Delta_r H^{298K} = -25 \text{ kJ mol}^{-1}$$

(Reaction 1)

This "*direct*" OME synthesis starts with the introduction of MeOH diluted in an inert carrier gas (stream (S)1) to the quasi-isothermal fixed bed reactor (reactor (R)1; Scheme 1).

Within this stoichiometric FA reactor, the anhydrous production of FA *via* the catalytic dehydrogenation of MeOH takes place with H_2 as the main side product (Reaction 2).[38] Simultaneously the competing thermodynamically favourable MeOH dissociation to CO can occur (Reaction 3).[39] Therefore the anhydrous FA synthesis is kinetic controlled and short residence times ($t < 0.01$ s) and fast product cooling[49] are required for such a reaction system.

$$CH_3OH \rightleftharpoons CH_2O + H_2 \quad \Delta_r H^{298K} = +85 \text{ kJ mol}^{-1} \quad (\text{Reaction 2})$$

$$CH_3OH \rightleftharpoons CO + 2H_2 \quad \Delta_r H^{298K} = +105 \text{ kJ mol}^{-1} \quad (\text{Reaction 3})$$

The performance of this reaction step is dictated by the optimum molar ratio of FA/MeOH required by the OME synthesis step; which is identified at FA/MeOH = 1.8–2 [mol/mol] to have a maximum overall yield considering recycling of non-converted reactants and other OME fractions than the target product OME$_{3–5}$. To achieve this desired ratio, MeOH conversion $\left(U_{MeOH} = 1 - \dfrac{N_{MeOH.out}}{N_{MeOH.in}}\right)$ of at least 69% and FA selectivity ($\left(S_{FA} = \dfrac{N_{FA.out} \times v_{FA}}{N_{MeOH.in} - N_{MeOH.out}}\right)$, where v_{FA} is the stoichiometric coefficient of FA), more than 90% are required. Sauer *et al.* synthesised anhydrous FA over Na–Al based catalyst and achieved $U_{MeOH} = 100\%$ and $S_{FA} = 70\%$ at temperature of *ca.* 840–920 °C. Su *et al.*[50] could successfully synthesise anhydrous FA over Na_2CO_3 catalyst at lower temperature of *ca.* 690 °C with $U_{MeOH} = 53\%$ and $S_{FA} = 84\%$. The product of R1 (S2) is then absorbed in the recycle stream (S6) of the OME synthesis reactor R2 which consists mainly of non-converted MeOH and FA, OME$_{1–2}$ and OME$_{n<5}$. In this step the inert gas and by-products H_2 and CO (S7) are separated from the anhydrous FA (from R1) and non-converted MeOH, before being absorbed. The mixed stream (S3) is then introduced to the OME synthesis reactor where oligomerization, condensation and acetalisation reactions
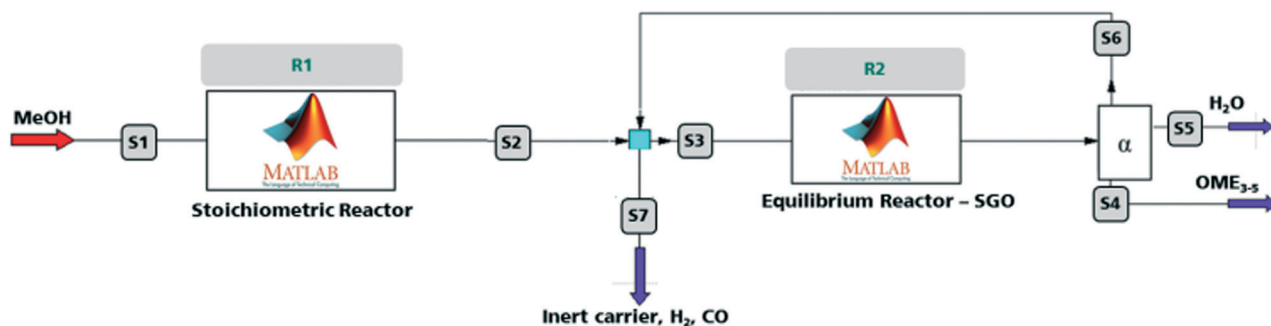
Scheme 1 Novel OME synthesis process simplified block diagram based on MeOH and anhydrous FA. R1: anhydrous FA synthesis reactor; R2: OME synthesis reactor; α-separator: ideal product separator.

(Table 1; reactions 4–11) take place simultaneously at mild T (50–80 °C) and ambient p. The product from R2 is then introduced to the rectifier and the target product OME_{3-5} (S4) is separated from non-reactants, side product H_2O (S5), $OME_{n<3}$ and $OME_{n>5}$. This step is presented in this investigation *via* the α-separator.

Chemical reaction equilibrium and mechanism of OME synthesis

The synthesis of OME represents a complex, multicomponent reactive system starting initially by two main compounds – FA and MeOH. In turn different reactions lead to the formation of *ca.* 32 compounds at equilibrium. The reaction cascade leads to chain elongation of the three main products, namely poly(oxymethylene) hemiformals (HF, $HO–(CH_2O)_n–CH_3$), poly(oxymethylene) glycols (MG, $HO–(CH_2O)_n–H$) and OME ($H_3CO–(CH_2O)_n–CH_3$). The system has been studied previously by Schmitz *et al.*[29] and the formation of glycols and hemiformals was observed at all pHs, even without the addition of a catalyst (Table 1; reactions 4 to 7). However, the formation of OME takes place only in the presence of an acid catalyst (Table 1; reactions 8 to 9). Unlike OME, HF and MG are known to be unstable and are expected to easily decompose to the reactants. Two side products are also known in

the cascade, namely TRI and methyl formate (MEFO) (Table 1; reactions 10 to 11).

Model of the chemical equilibrium – the unconstrained Gibbs minimisation based on a stochastic global optimiser (SGO)

Unconstrained Gibbs energy minimisation using an SGO approach represents an efficient method for solving multi-reaction chemical equilibrium problems.[51] In this investigation, a general and scalable method of performing chemical equilibrium calculations using the unconstrained Gibbs energy minimisation approach is developed and applied. Promisingly, this method is suitable for the calculation of the chemical equilibrium in the system under discussion as it does not require a good initial guess for the equilibrium composition and it does not need information about the reactions involved. Further particulars concerning the finer details behind this method can be found in previous literature reports,[51] but a brief introduction is given below for clarity.

A mixture of reacting species at a certain T and p moves spontaneously toward a state that minimises its total Gibbs free energy, G^t. Thus, as the reactions proceed, the number of moles of reactants and products changes until a minimum G^t is attained, at which point further change in G^t is not possible. G^t can thus be calculated from the summation of the chemical potential of each species, μ_i, multiplied by its number of moles, n_i (where N is the number of species present in the reacting mixture; eqn (1)):

$$G^t = \sum_i^N n_i \mu_i \qquad (1)$$

The chemical potential can be obtained from the Gibbs free energy of formation at the standard state, the fugacity of the pure components at the standard state, and the fugacity of the species in the reacting mixture. Thus, for a reaction occurring in the liquid phase, the G^t can be written as (eqn (2)):

$$G^t = \sum_i^N n_i G_i^o + RT \sum_i^N n_i \ln \gamma_i \chi_i \qquad (2)$$

where R = gas constant (value/units), T = temperature (K), x_i = molar fraction in the liquid phase, and γ_i = activity coefficient of component i in the liquid phase.

Table 1 List of key equilibrium reactions to be found in the OME synthesis reaction cascade

Reaction no.	Equation
4	$FA + H_2O \rightleftharpoons MG$
5	$FA + MG_{n-1} \rightleftharpoons MG_n$, $n \geq 2$
6	$FA + MeOH \rightleftharpoons HF_1$
7	$FA + HF_{n-1} \rightleftharpoons HF_n$, $n \geq 2$
8	$MeOH + HF_1 \overset{H^+}{\rightleftharpoons} OME_1 + H_2O$
9	$FA + OME_{n-1} \overset{H^+}{\rightleftharpoons} OME_n$, $n \geq 2$
10	$3\,FA \overset{H^+}{\rightleftharpoons} TRI$
11	$2\,FA \overset{H^+}{\rightleftharpoons} MEFO$

*Enthalpy of reactions 8–9 is −25.2 kJ mol^{-1} and is equal for all OME formation reactions.[29]

280 | *React. Chem. Eng.*, 2018, **3**, 277–292

This journal is © The Royal Society of Chemistry 2018

As the total number of moles of each atom is conserved during the chemical reactions, for a system that contains M atomic elements, there exist M mass balance relations equating the summation of the number of moles of species i by the number of atoms of the kth element present in species i, $a_{i,k}$, with the initial number of moles of element k, A_k as follows:

$$\sum_i^N n_i a_{i,k} = A_k \qquad (3)$$

The equilibrium problem is now simplified to the task of finding the set of n_i that minimizes G^t (eqn (2)), within the identified constraints (eqn (3)). In the language of optimization, the decision variables for the minimisation problem are the number of moles of each species, while the objective function is the G^t of the mixture and the constraints are the material balance equations. The number of decision variables can be reduced by converting the constrained minimisation problem into an unconstrained problem. Since eqn (14) relates the number of moles of species to one another, they are not all independent. The number of independent variables is the number of species subtracted from the number of independent material balance equations. The decision variables are in turn reduced to $V = N - M$ (where M is the number of independent material balance equations for the system). The rest of n_i ($i = V + 1$ to N) can be calculated from the mass balance constraints. The details of this conversion with respect to an unconstrained minimisation and the limits set on the number of moles of each species have been discussed in a previous report.[51]

This method can be classified as a non-stoichiometric method, and as such does not require knowledge of the chemical reactions that the initial components undergo to reach the equilibrium state. Since the Gibbs energy is a state function, knowledge of the path leading to the equilibrium state is not needed. The above non-stoichiometric approach needs only the values of the Gibbs energy of formation for every component at the reaction T. The lack of the need of knowledge of the chemical reactions is an important advantage, especially for systems whose reaction mechanisms are complicated (or indeed not well known). The synthesis of OME represents such a complex, multi-component system.

Another important advantage of this Gibbs energy minimisation approach is the lack of a dependence of the problem solution on a good starting point for iterations. The alternative methodology which would rely on the solution of a set of non-linear equations resulting from the condition of $dG = 0$ by using a Newton–Raphson (NRS) approach or a similar numerical method, has an inherent initialization difficulty. The set of non-linear equations derived *via* the use of UNIFAC activity coefficient model has multiple solutions, each of which represents a local Gibbs energy minimum. Starting from a different initial point can simply lead to a different solution. Establishing which of these solutions is the most appropriate can be achieved by comparing the value of the G^t at that point.

With this Gibbs energy minimisation approach, the solution domain is scoped by randomly generated initial points.

With an effective SGO that possesses a good balance between exploitation and exploration steps to avoid the entrapment in local minima, the global minimum can be obtained without the need of having a good initial point. For a system of tens of components such as the OME synthesis, this is a great advantage as it is extremely difficult to obtain a good initial value for the equilibrium composition of each component.

While there is no need for an accurate initial guess, there still exits a need to initialize the location of the population in such a way that does not violate the mass balance equation, which is an easier task. The initialisation approach used in this investigation is explained as follows. For a SGO, a population of agents moves from one position to the next. The position is defined as a certain set of values for the decision variables.

1. The initial values of the population are determined randomly within the limits of zero and maximum mole numbers for each component.

2. The rest of the number of moles is calculated using the mass balance equations (eqn (3)).

3. If any of the number of moles (as calculated *via* eqn (3)) is negative, this initial position of the agent is rejected and another position is randomly selected.

4. The process is repeated until the initial positions of all agents, which satisfy the mass balance equations, are positive.

To reduce the iterations needed to find the initial positions of the population, it was deemed important to determine (as calculated by step 2 above) the components whose numbers of moles have a high mole fraction in the final equilibrium composition. Achieving this provides the opportunity to calculate and reduce the negative numbers in step 2 and the number of iterations needed for setting values of the initial population. This unconstrained Gibbs energy minimisation approach has been summarised (Fig. S1†).

Model of the chemical equilibrium – implementation of a liquid-phase reaction for OME synthesis

Our model was developed to describe the system in the liquid phase. Activity based chemical equilibrium constants correlations were adapted from Drunsel *et al.*[52] and Schmitz *et al.*[29] The equilibrium constant for a specific reaction can be evaluated (eqn (4)) and the corresponding parameters (Table 2).

$$\ln K_a(T) = A + \frac{B}{T} + C \ln(T) + DT \qquad (4)$$

MEFO was not considered in our model as it was found at extremely low trace amounts at equilibrium and therefore is expected to have little impact on the equilibrium compositions. In addition, there is no reliable equilibrium constant data available for MEFO.

The Gibbs free energy of formation for each component in the system is needed at the reaction T and p. These data were obtained from various sources. For H_2O, FA and MeOH, the Gibbs free energy of formation and the enthalpy of formation

This journal is © The Royal Society of Chemistry 2018

React. Chem. Eng., 2018, **3**, 277–292 | 281

Table 2 Parameters for calculating activity based chemical equilibrium constants[29,52]

Reaction	A	B	C	D
(1)	−30.946	4819	3.741	−0.0045
(2) ($n = 2$)	−30.941	5653	3.741	−0.0045
(2) ($n \geq 3$)	−30.933	5361	3.741	−0.0045
(3)	1130	−25 100	−198.4	0.316
(4) ($n = 2$)	1129	−25 510	−198.4	0.316
(4) ($n \geq 3$)	1129	−25 630	−198.4	0.316
(5)	1.8244	202.39	0	0
(6)	−8.7322	4696.7	0	0

were obtained from literature at T = 298.15 K.[53] In turn these values are used to obtain the Gibbs free energy of formation at the given reaction T (eqn (5)).

$$\frac{\Delta G_f^0(T)}{RT} = \frac{\Delta G_f^0(298.15)}{298.15R} - \frac{\Delta H_f^0(298.15)}{R}\left(\frac{1}{298.15} - \frac{1}{T}\right) \quad (5)$$

Next, eqn (6) below was used to obtain the Gibbs free energy change for Reaction 4–10, based on the activity-based equilibrium constants available in the literature.[29]

$$\ln K_i = -\frac{\Delta G_{rxn}^0}{RT} \quad (6)$$

Starting from the values obtained for H_2O, FA and MeOH and from the Gibbs free energy change of each reaction, the Gibbs free energy of formation of the missing components can be obtained using eqn (7) (Table S1† provides the standard Gibbs energy of formation for all species at T = 333.15 K based on this calculation procedure).

$$\Delta G_{rxn}^0 = \sum_i \upsilon_i G_{f,i}^0 \quad (7)$$

The UNIFAC method was used to calculate the activity coefficients needed in the calculation of the OME system's total Gibbs energy (*i.e.* according to eqn (2)). UNIFAC structural groups with size, surface parameters and interaction parameters were obtained from previously published reports,[30,54] (Tables S2–S4†). This data constitutes the needed information for the non-constrained Gibbs energy minimisation model in the calculation of the equilibrium composition. The equilibrium model was then implemented using the MATLAB® software platform. The SGO uses a Cuckoo Search solver approach, which has been shown to be successful for chemical and phase equilibrium calculations.[55] Note that our choice is based on familiarity only and other global optimisers could be just as effective.

Model of the chemical equilibrium – implementation of the recycle loop with ideal separator

From the experimental and simulation parametric study results previously published, the single-pass equilibrium yield of the desired OME_{3-5} did not exceed 0.14 (g/g_product).[36,56] The best feed composition experimentally tested by Schmitz *et al.*, (Educt 9 from Schmitz *et al.*[29] (FA = 0.57 g/g, MeOH =

0.41 g/g, H_2O = 0.02 g/g); denoted hereon as E9) has a very low H_2O content and high FA/MeOH ratio ~1.5 (mol/mol). This composition yielded 0.13 (g/g_product) of OME_{3-5} over a commercial A-46 polymeric acid catalyst.[29] The highest published theoretical OME_{3-5} yield, as obtained under completely dry feed conditions at an FA/MeOH ~1.8–2 (mol/mol), was 0.14,[36] while a value of 0.176 (g/g_product) was obtained in this work (using the SGO). This yield when translated into efficiency and feed to product yields gives a poor process performance. However, the product of this reaction step is still rich in unreacted FA and MeOH (~0.5 g/g_product), short chain OME_{1-2} (~0.247 g/g_product) and long chains OME_{6-8} (~0.024 g/g_product) when E9 is considered.[29] The recycling of these educts and mixing with the fresh feed therefore can significantly increase the target OME_{3-5} yield.

In this context, the single parameter optimization of the recycling of unreacted components with the fresh feed considers that the separation task of the reactor downstream is achieved completely (α-separator; Fig. 1). As a consequence separation calculations were conducted using separation factors without performing rigorous column calculations for the distillation train. The simple separation model is considered a sufficient analysis tool for this early stage of process optimisation.

As described earlier, an efficient OME synthesis process would include recycling unreacted educts and undesired side products to overcome the thermodynamic equilibrium conversion limitation. With the OME reaction system including 32 components contributing simultaneously in *ca.* 29 equilibrium reactions, converging a recycle calculation to predict the equilibrium composition while conserving the atomic balance constraint is cumbersome. Therefore, an iterative method was developed for this purpose. The aim is to define the equilibrium composition not only when the feed consists of the starting components FA/MeOH, but also with all the recycled components entering the reactor unit (Fig. 1). The steady-state flow rate and composition of each stream in the reactor/separation module is defined when the model convergence is achieved. A separation factor (a_i) is defined at the separator unit (D) to determine the separation ratio of each component i between the recycle and final product stream.

The following steps explain the methodology for performing the recycle calculations:

1. The provided feed is combined with a guessed value of the recycle stream. Then vector [A] representing the elemental molar value of the combined feeds is used as an input for the unconstrained Gibbs energy minimisation algorithm as discussed earlier.

2. The algorithm determines the equilibrium composition of the 32 reacting species (OME, MG, HF, FA, H_2O, MeOH, and TRI).

3. Then, unstable components are decomposed to their reactants as reported in Schmitz *et al.*,[29] to reduce the number of components in the system to 12 stable compounds only (OME, FA, H_2O, MeOH, and TRI).

4. At this stage, the separation ratios a_i are applied to determine the composition of the product and recycle streams.
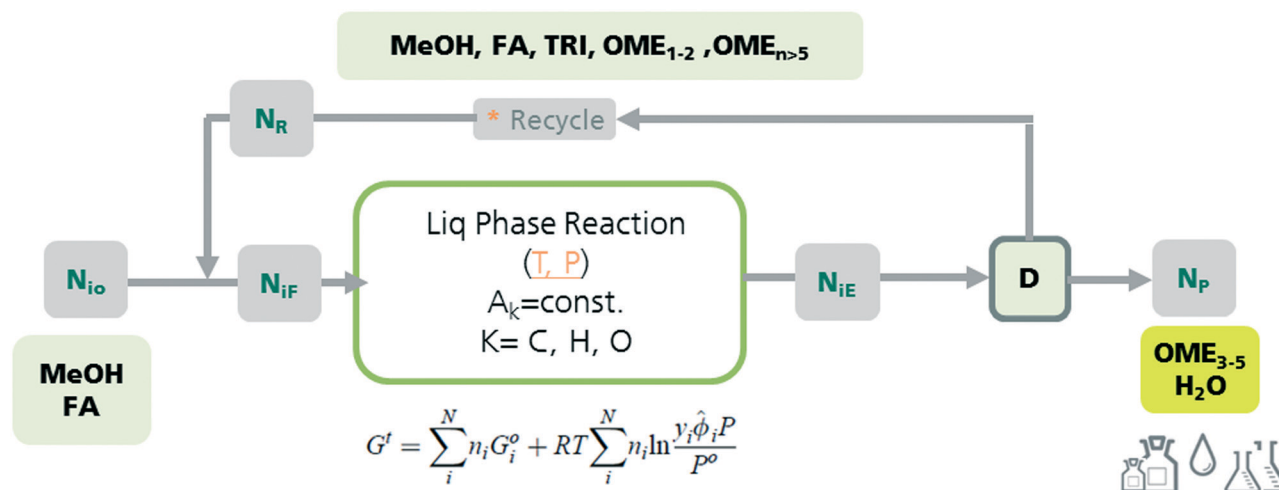
Fig. 1 Block diagram for the chemical equilibrium component system for OME liquid phase synthesis with recycle of unreacted components and side products. N_{io}: fresh feed, N_{iF}: reactor combined feed, N_R: recycle, N_{iE}: reactor outlet, N_p: product, D: separation unit, A_k: elementary vector.

5. The new recycle stream calculated is combined with the fresh feed and a new vector [A] is calculated.

The steps are repeated until the steady state is reached where the elemental molar flow of the product stream equals to that of the feed stream and the compositions of the different streams become constant. Fig. S5† provides a flowchart of the recycle calculation algorithm.

The separation factors used in the algorithm were based on complete separation of H_2O as side stream and OME_{3-5} as a product stream, while the rest of the components were recycled. Defining the optimum feed ratio of FA/MeOH, and reaction T with the consideration of component recycling is imperative for this novel process evaluation and KPIs definition. The use of this simulation tool together with the kinetic models reported by Oestreich et al.[41] and Schmitz et al.[56] represent a good basis for a complete process optimisation.

Experimental

Chemicals

Trioxane (purity $\geq$ 99%), OME_1 (purity $\geq$ 99.9%), dodecane (anhydrous, purity $\geq$ 99%) and Amberlyst®-36 (55% H_2O, D_p = 600–850 μm) were purchased from Sigma-Aldrich. OME_3 (purity = 98.6%), OME_4 (purity > 99%) and OME_5 (purity = 97%) were supplied by ASG Analytik Service GmbH. MEFO (purity = 97%, containing 3% of MeOH) was purchased from Alfa Aesar. MeOH (purity $\geq$ 99.5%) was purchased from Carl Roth GmbH and Co. KG. No further purifications have been applied to the chemicals before use. Prior to application catalyst A-36 which was dried overnight under vacuum (100 mbar) at T = 373.15 K. Reaction mixtures were prepared by dissolving TRI in OME_1 in a closed three-neck flask equipped with an overhead condenser, with in situ T and p monitoring. Feed mixtures were prepared at T = 298 K at OME_1/TRI ratios of 3:1, 2.5:1, 2:1 [g/g]. A clear solution was obtained for all ratios after ca. 30 minutes.

Analytics

An Agilent 7890A gas chromatograph (GC), equipped with a flame ionisation detector (GC-FID) and auto-sampler, and was used for the quantitative analysis of the obtained product mixtures (1 μL sample volume). Samples were injected on to a DB-5 ms column (dimensions: 30 m × 250 μm × 0.5 μm) using He (g) as the carrier gas (flow = 4.1 mL min⁻¹ at ca. 2 bar) with GC inlet T = 543.15 K with a split ratio of 20:1. The oven T was set at 308.15 K for 6 min with a following ramp of 50 K min⁻¹ to 543.15 K and hold for 5 min at 543.15 K. Dodecane was used as an internal standard. The weight fractions for the calibration of the components have been taken as average values of the results from Burger et al.[31] OME_1 was used as solvent for most of the components, while benzene was used as solvent for OME_1. Dodecane has been added to the calibrating samples thus the number of C-atoms from dodecane equals the average number of C-atoms from the calibrated components. The components have been calibrated in five different sample compositions (i.e. OME_1 + TRI for the feed composition and MEFO + MeOH, OME_{2-4}, OME_1 and TRI for the final concentration respectively). OME_{1-5}, MeOH, MEFO and TRI were available as pure components, while OME_{5-8} were calibrated via extrapolation of the average areas and factors to the internal standard from OME_{1-4}, in accordance with the previous report of Burger et al.[31]

Experimental set-up

The acid catalysed synthesis of OME was performed in a 500 mL volume autoclave, equipped with a stainless steel reactor (P_{max} = 100 bar; Fig. 2). The reaction T was set up using a fixed electrical heating jacket and controlled with an integrated thermocouple (i.e. K-type thermocouple; accuracy ± 1.5 K). Mixing of the reaction mixture was performed using an magnetic stirrer. A diaphragm pressure indicator (accuracy ± 0.24 bar) was used to measure the reaction P. To ensure

sample withdrawal without catalyst particles, a cylindrical sintered stainless steel (AISI 316TI) filter (F1) with 10 μm pore size was mounted on the sampling line and positioned near to the reactor base. For feed and catalyst loading, sample withdrawal and pressure regulation in the batch reactor a set of ball valves (HR) and needle valves (VN) were installed. Fig. 3 shows the experimental setup used for the SGO model validation tests.

Feed – FA and MeOH

Equilibrium data for the OME system were reported previously by Schmitz *et al.*[29] 11 different educts were tested for thermodynamic equilibrium at four different T. Mass fractions of the equilibrium compositions were reported for the different species. The reported mass fraction values represent the overall concentrations, which are the concentrations of FA, MeOH, H_2O and OME found when the unstable MG and HF completely decompose into FA, MeOH and H_2O. Other required experimental data were sourced from previous reports (*i.e.* White *et al.*[36] and references therein). Thermodynamic equilibrium was established over two different commercial catalysts in two separate tests; D50WX2 as a catalyst for Test 1 and A-36 for Test 2. Furthermore, the initial number of moles for the different components needs to be calculated which will be constant in the system due to mass conservation. Based on the educt mass and composition (Table S5†), the number of moles for the different components was calculated using eqn (3).
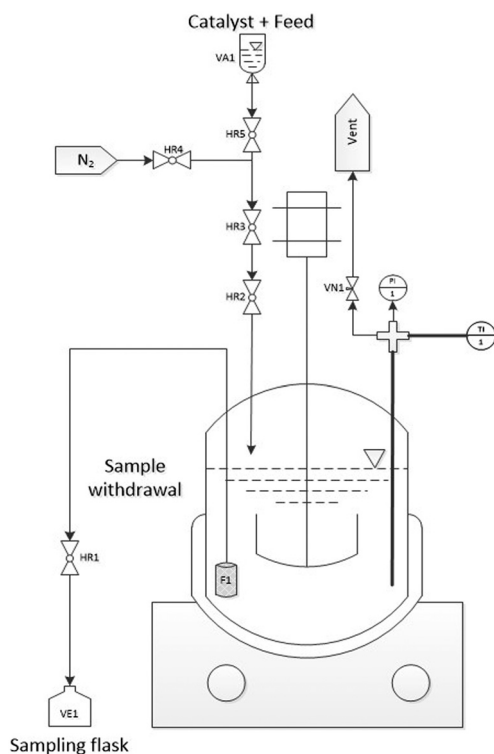

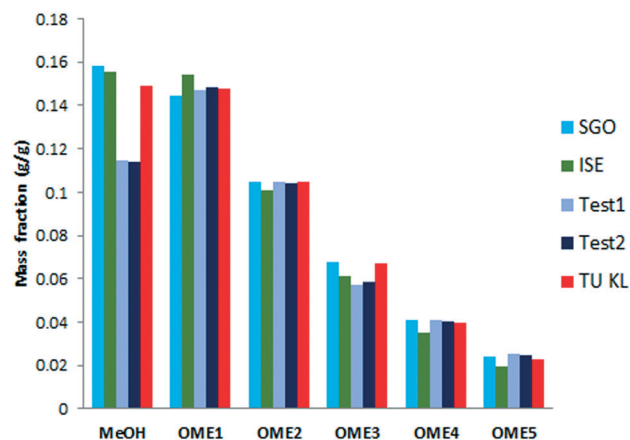Fig. 2 Experimental setup for the OME equilibrium synthesis (*i.e.* HR = ball valve, VN = needle valve).

Fig. 3 Comparison of chemical equilibrium composition of experimental results of Test1, Test2 and Fraunhofer ISE NRS model[36] at T = 353 K and FA/MeOH = 1.5 and results from TU KL - LTD[29] at T = 348 K and FA/MeOH = 1.42 and the unconstrained Gibbs energy minimisation equilibrium results.

Feed – TRI and OME1

Applying the unconstrained Gibbs energy minimisation approach is advantageous due to the flexibility and robustness when applied to different systems. Changing the feed and the system components does not correspond to major changes in the algorithm rather changing the three input matrices $[A]$, $[F]$ and $[GRT]$. The three inputs represent the initial amounts of each atom, the atomic distribution in each component, and the Gibbs energy of formation at reaction T respectively. With this input, the system is defined and capable of evaluating the equilibrium composition for complex systems. Experimental runs using TRI/OME$_1$ feed were performed to validate and qualify the unconstrained Gibbs energy minimisation algorithm. Literature reported feed compositions were adopted for validation and also new feed compositions were used to extend the level of confidence. Feed and reactions conditions are listed in Table S6.†[31]

Synthesis procedure

The preparation of the feed mixture was performed in an externally-closed three-neck flask containing a magnetic stirrer. After TRI was dissolved in OME, the commercial catalyst A-36 was added to the mixture and the content of the flask was poured in the autoclave reactor. A N_2 (g) line was connected, the system sealed and the reaction P set. The reaction T was set and the stirring started. Before the sample withdrawal a flush of at least 3 mL of product was dispensed to rinse the sample line. The reaction T, P and stirring rate were kept constant during the reaction. With one feed composition, three conditions were analysed, (*i.e.* at T = 323.15, 338.15, and 353.15 K) with increasing reaction P to keep the reaction mixture in the liquid phase. The reactions were run overnight and the first sample was taken at t = 15 h. Two more samples were taken at a time interval of at least 1 h to determine if equilibrium had been reached.

284 | *React. Chem. Eng.*, 2018, **3**, 277–292

This journal is © The Royal Society of Chemistry 2018

Results and discussion

The presented model herein produces the number of moles that have the minimum Gibbs energy, which represent the thermodynamic equilibrium. This can be achieved by defining the different compounds in the system and their standard Gibbs energy of formation. Experiments were conducted to study the equilibrium of such complex reaction system. The model was validated using two different groups of experimental data. Furthermore a parametric study is carried out to define the operational conditions to have the maximum yield of the target product. At these operating parameters, the process material balance is then evaluated and KPIs are identified and discussed.

Model validation – formaldehyde and methanol feed

The equilibrium was studied for the 11 different educts where T = 333.15, 348.15, 363.15, and 378.15 K (Table S5†). The overall composition was calculated using the presented platform. A parity plot was created between the overall mass fraction at equilibrium of FA, MeOH, H_2O and OME of the experimental values and the calculated values using the presented model platform. The generated parity plot shows a good agreement between the model predictions and the experimental results (Fig. S2†). The model also shows good agreement with previously reported experimental tests.[36] Fig. 3 shows the comparison between our model using the unconstrained Gibbs energy minimisation algorithm (SGO), our model using a Newton–Raphson based solver (ISE), the two tests previously reported by White et al.[36] using two different catalyst systems (Test1, Test2) and the results obtained at TU Kaiserslautern (TU KL) (E9 from Schmitz et al.[29] at T = 348 K and a feed composition FA/MeOH = 1.42).

Model validation – trioxane and OME1 feed

The equilibrium composition for the feed stream containing TRI and OME_1 was studied for three different educts (Test 3, Test 4, Test 5) at T = 323.15, 338.15, and 353.15 K (Table 3), the overall composition was calculated using the presented model.

A parity plot was established for the overall mass fraction at equilibrium of TRI, MeOH and OME of the experimental values and the calculated values using the unconstrained Gibbs energy minimisation equilibrium model (Fig. S3†), showing good agreement. Fig. 4 shows the comparison between our model using the unconstrained Gibbs energy minimisation algorithm (SGO), the results obtained at TU KL,[31] and our own results at T = 353 K and feed composition OME_1/TRI = 3.

Parametric study

The equilibrium model was used to describe the OME complex reaction equilibrium system at various operating conditions. Different educts with different FA/MeOH molar feed ratios were studied at different T to examine how the

equilibrium composition of the desired species (OME_3, OME_4 and OME_5) is influenced by a ΔT. The change in the total equilibrium mass fractions of the three desired species with respect to T is shown (Fig. 5). The model shows good agreement with the experimental values and suggests that the effect of T on the equilibrium composition is relatively small.

The different educts molar compositions studied by Schmitz et al.[29] show that the equilibrium composition of OME_{3-5} depends strongly on feed composition. Our model was used to study the effect of anhydrous FA/MeOH molar ratio in the feed on the OME_{3-5} equilibrium composition. Information regarding the equilibrium composition of OME_{3-5} with FA/MeOH molar ratio in anhydrous feeds at different T is provided (Fig. S4†). This demonstrates that the equilibrium composition can be increased by increasing the FA/MeOH ratio; after reaching an optimum value, the composition starts to slightly decrease with increasing FA/MeOH molar ratio. The effect of T is relatively small: feeds at higher T would be expected to yield slightly higher OME_{3-5} equilibrium mass fractions. This trend was confirmed using the activity-based model described in previous reports.[30,36]

Recycle process with ideal separator

Table 4 shows the material flow rates of different streams after converging the recycle algorithm for FA/MeOH = 1.9 anhydrous feed at T = 335 K.

The effect of ΔT on the final product yield using the recycle algorithm was also investigated (Table 5). It is clear that reaction T does not influence significantly the final product OME_{3-5} yield. The same behaviour was noticed in the single reaction pass simulation and experimental results.

The FA/MeOH feed ratio has a stronger influence on the equilibrium composition when a single pass reaction is applied. This effect is more pronounced in the recycle calculations since the reactor outlet composition significantly influences the whole recycle calculations. The final product molar distribution shows that increasing the molar ratio of FA to MeOH in the feed stream from 1.6 to 2 favours the production of OME_5 over OME_3 at 350 K (Fig. 6).

It is interesting to note that the recycle convergence is limited to a small band of FA/MeOH molar feed ratio (Fig. 7). The steady-state recycle ratio varies from less than 3 to about 8 in this band. Due to the complexity of the equilibrium calculation, the change in the combined feed composition at each iteration results in shifting the equilibrium to a new

Table 3 Parameters of the experimental runs for the OME synthesis starting from TRI and OME_1

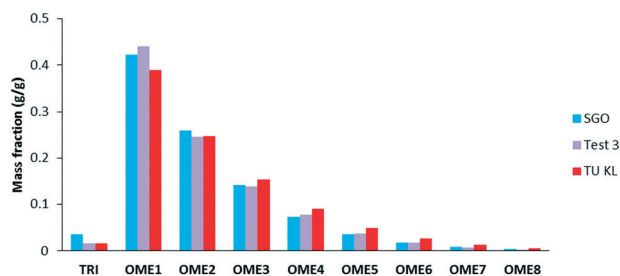| Test	Test 3	Test 4	Test 5
OME_1 : TRI [g/g]	2.91 : 1	2.06 : 1	2.49 : 1
T [K]	323, 338, 353	323, 338, 353	323, 338, 353
P [bar]	3, 4, 6.3	4, 5, 8	4, 5.5, 9.5
Catalyst name	A-36	A-36	A-36
Cat. Load [g/g_{mix}]	1%	1%	1%
Reactant mix. load [g]	175	230	220

Fig. 4 Comparison of chemical equilibrium composition of experimental results of Test 3 and results from TU KL[31] at T = 353 K and OME_1/TRI = 3 and the unconstrained Gibbs energy minimisation equilibrium results.

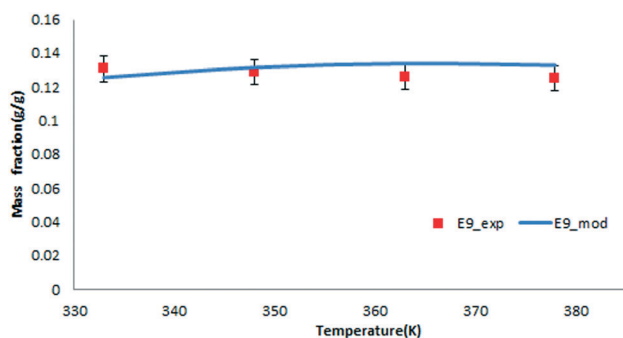**Fig. 5** E9 (ref. 29) equilibrium composition (OME_{3-5}) as function of T.

state. This new equilibrium state in turn results in a change in the recycle stream. If the conversions and extents of the different reactions are constant, the recycle could converge and the system can reach a steady state. However, for this complex system, the conversions and extents of the different reactions are sensitive to the variations in the combined feed composition. The divergence prediction of the model is yet to be confirmed by experiment. The model provides a word of caution for the experimentalists to recognize conditions whereby achieving a steady-state recycle process may not be feasible.

Table 4 The material composition of the process streams using an anhydrous feed (FA/MeOH = 1.9) at T = 335 K

	[g]				
Component	Fresh feed	Combined feed	Reactor outlet	Recycle	Product
FA	10.67	32.68	22.01	22.01	0
H_2O	0	0	2.51	0	2.51
MeOH	5	7.45	2.40	2.40	0
OME_1	0	0.46	0.46	0.46	0
OME_2	0	0.57	0.57	0.57	0
OME_3	0	0	0.70	0	0.70
OME_4	0	0	0.84	0	0.84
OME_5	0	0	1.00	0	1.00
OME_6	0	1.20	1.20	1.20	0
OME_7	0	1.43	1.43	1.43	0
OME_8	0	1.71	1.71	1.71	0
TRI	0	17.28	17.28	17.28	0

Process evaluation – material balance and process energy efficiency

With the defined operational parameters for both synthesis steps and convergence of the reactor algorithms, the material balance of the synthesis process is evaluated. The following are the basis (assumptions and considerations) for the direct OME synthesis evaluation:

1. OME of chain length n = 3–5 are produced with a plant capacity of 30 kt per annum.

2. Plant is operated for 8000 hours per annum (*ca.* 100 t per day production capacity)

3. Anhydrous FA synthesis is operated at steady state and implemented in the simulation as stoichiometric reactor with U_{MeOH} = 68% and S_{FA} = 90%.

4. OME synthesis step proceeds to equilibrium and side products HF and MG dissociate thermally after the reaction step to FA, MeOH and H_2O.

5. A complete separation of non-reactants, side product H_2O and $OME_{n \neq 3-5}$ is achieved *via* ideal α-separator.

6. The process energy consumption (heating and cooling) corresponds to 30% of the LHV of the final product OME_{3-5} (conservative assumption and being investigated in details while developing rigorous product separation columns models).

7. For the preliminary production cost evaluation, a capital investment of 1 Mt per annual capacity plant of a refinery which was used by Schmitz *et al.*[45] was adopted in this work. To adjust the CAPEX to the considered capacity in this work, a power law with a capacity factor, also called six-tenths rule due to the regression coefficient of 0.6 was used. The operational expenditures are considered here as factors of the CAPEX.

As discussed earlier, the process starts with a MeOH feed stream entering the endothermic anhydrous FA synthesis step in R1 and proceeding towards OME synthesis in R2. The feed for R1 is diluted thus the MeOH concentration between 5–15 vol% carried in an inert gas which is N_2 for this evaluation. For conservative evaluation, a MeOH feed concentration of 5 vol% is considered. In the mixing step after R1, it is assumed that N_2 and side products H_2 and CO are separated (S7). Table 6 summarises the material balance of the process.

The energy efficiency can be evaluated through eqn (8):

$$\eta_{eff} = \frac{(w_i \times LHV_i)_{product}}{(w_i \times LHV_i)\,feed + E_{process}} \quad (8)$$

where η_{eff} is the overall process efficiency, w_i is the mass of component i, LHV_i is the lower heating value of component i and $E_{process}$ is the net energy consumption in the process. Table S7† summarises the thermochemical properties required for process energy evaluation.

For production cost evaluation, in literature, a first CAPEX estimate of an OME_{3-6} plant with the synthesis path starting from TRI and OME_1 is carried out for a capacity of 1 Mt per annum. It compares the OME synthesis plant to a

Table 5 Simulation results based on the developed recycle algorithm

Feed composition	T [K]	Recycle/feed (g/g)	OME_{3-5} (g/g) product stream
Anhydrous feed	335	7.33	0.901
Only FA, MeOH	350	7.29	0.902
FA/MeOH = 1.9 $[N_{io}]$	365	7.17	0.903

refinery, also dominated by distillation-based units and the corresponding investment is 274m US$.[45] Using these values to downscale according to the base case scenario, the CAPEX is evaluated as follows:

$$C_{OME\ Plant} = 274 \times \left(\frac{C2}{C1}\right)^{0.6} \qquad (9)$$

where C1 and C2 are the capacities of the literature process and the evaluated process respectively. The operational expenditures OPEX are additional costs that are incurred for ongoing operations. OPEX is divided into Variable Costs of Production (VCP) and Fixed Costs of Production (FCP). VCP are proportional to the plant production; they comprise the material costs, *i.e.* the raw and auxiliary materials, together with the energy costs. While FCP are spent independently of the performance of the plant, such as salaries and overheads, maintenance or capital charges. In this basic evaluation, VCP are basically MeOH raw material cost (354 US$ per t, Methanex.org, 01/10/2017 until 31/12/2017) and the process energy cost. The former is provided by the material balance while the latter is calculated from assumption 6 and considering the process energy demand is supplied by high pressure steam (1441 kJ kg^{-1}, 23 US$ per t). The FCP are evaluated using a factorial method as discussed by Baerns.[57]
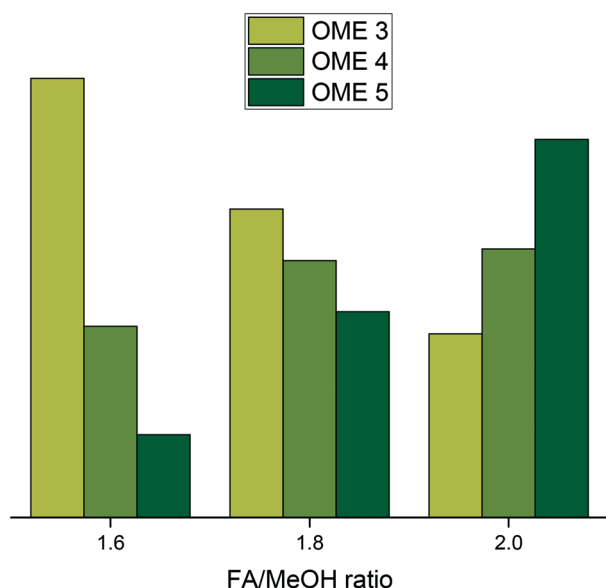
Key performance indicators and discussion

Based on the material balance results, the synthesis characteristic figures can be identified. Table 7 summarises the direct OME synthesis based on MeOH and anhydrous FA KPIs.

From the economic indicators it is clear that the major production cost component is the MeOH feed cost (84% of the VCP). Therefore the overall target product yield is significantly influencing the process economics. In this level of this innovated process evaluation with ideal product separation, the overall yield is at 1.23 $[t_{MeOH}/t_{OME_{3-5}}]$ which is higher than the yield of the conventional processes (Burger *et al.*[45] process based on TRI/OME_1 feed with 1.26 $[t_{MeOH}/t_{OME_{3-6}}]$ and Jiangsau Kaimao Ltd. Co. with 1.39 $[t_{MeOH}/t_{OME_{3-5}}]$).[10] With detailed process investigation and rigorous distillation unit implementation with certain separation efficiencies (under development), the total product yield could slightly decrease but projected to be still much lower than the compared processes.

Another important parameter is the process overall efficiency. With conservative assumption that the process consumes 30% of the final product LHV, the overall process energy efficiency (eqn (8)) is calculated at 86.4% (starting from MeOH feed till OME_{3-5} product) while the highest conventional process energy efficiency evaluated is at *ca.* 53% (Burger *et al.*[45] process based on TRI/OME_1 feed with overall efficiency 52.6% and Jiangsau Kaimao Ltd. Co. with efficiency of 45.1% evaluated from published data).[10] This is clear since in the aforementioned processes; several energy intensive reaction, extraction, reactive distillation and rectification steps are required to reach the final OME desired fraction. With a detailed process simulation and validation with all auxiliary and rectification units (under development in our group), the process energy consumption is projected to be less than the value considered in our assumption 6. This will even enhance the overall process efficiency which is far higher than the state-of the-art processes.
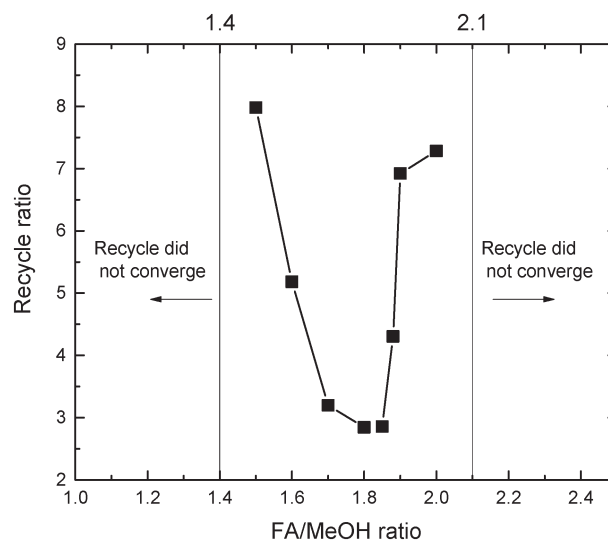

Fig. 6 The relative molar distribution (OME_{3-5}) in the product stream exiting the recycle process when reaction equilibrium was attained at 350 K *vs.* the FA/MeOH molar ratio of the feed.

Fig. 7 The steady-state recycle ratio *versus* the FA/MeOH [mol/mol] ratio and the regions of non-convergence.

This journal is © The Royal Society of Chemistry 2018

React. Chem. Eng., 2018, **3**, 277–292 | 287

Table 6 Material balance of the direct OME synthesis process (stream number according to Scheme 1)

Component i	Stream [tonne per day]						
	S1	S2	S3	S4	S5	S6	S7
N_2	2145	2145	—	—	—	—	2145
H_2	—	6.1	—	—	—	—	6.1
CO	—	7.7	—	—	—	—	7.7
MeOH	130	41.7	90	—	—	48.3	—
FA	—	74.2	225.8	—	—	151.6	—
OME_1	—	—	34.5	—	—	34.5	—
OME_2	—	—	39.2	—	—	39.2	—
OME_{3-5}	—	—	—	104.1	—	—	—
$OME_{n>5}$	—	—	61.5	—	—	61.5	—
H_2O	—	—	—	—	11.7	—	—

For the CAPEX evaluation and as mentioned earlier, a correlation was adopted to evaluate the CAPEX from the process described in literature with four synthesis steps including reactive distillation and extraction steps.[45] This is obviously a conservative figure since the novel process described in this work proceeds through two main synthesis steps followed by product rectification which will not yield to the same CAPEX when the synthesis capacity is reduced. Two reasons were considered; first the synthesis technology discussed here has a high temperature reaction step for anhydrous FA synthesis which lead to a higher CAPEX. Second that the product rectification of the OME synthesis reactor in this case will require relatively larger rectification units (due to the side products abundance and also H_2O) with considerable reboiler duties.

For these reasons the CAPEX was adopted directly from literature without adaption factor. However with detailed process evaluation, this figure can be enhanced reflecting on even better economics. It is important to notice that the process evaluated at production capacity of 30 kt per annum while state-of-the-art technology in Germany and EU is economically evaluated at refineries capacities of 1 Mt per annum. This parameter significantly influences the production cost. When the CAPEX for the same production capacity of 1 Mt per annum is considered with the rest of the cost calculation parameters not changed (except steam consumption adjusted to the corresponding new capacity), the production cost of OME_{3-5} from this novel process is at 571 US\$/$t_{OME_{3-5}}$; which is 13.45% cheaper than the only OME process evaluated economically so far in EU and 14% cheaper than diesel fuel when crude oil barrel price is between 50–110 US\$ (cost of production without taxes).[45] A comparison of the production cost of different technologies with the share of the MeOH feed cost and the OME synthesis process cost is depicted (Fig. 8).
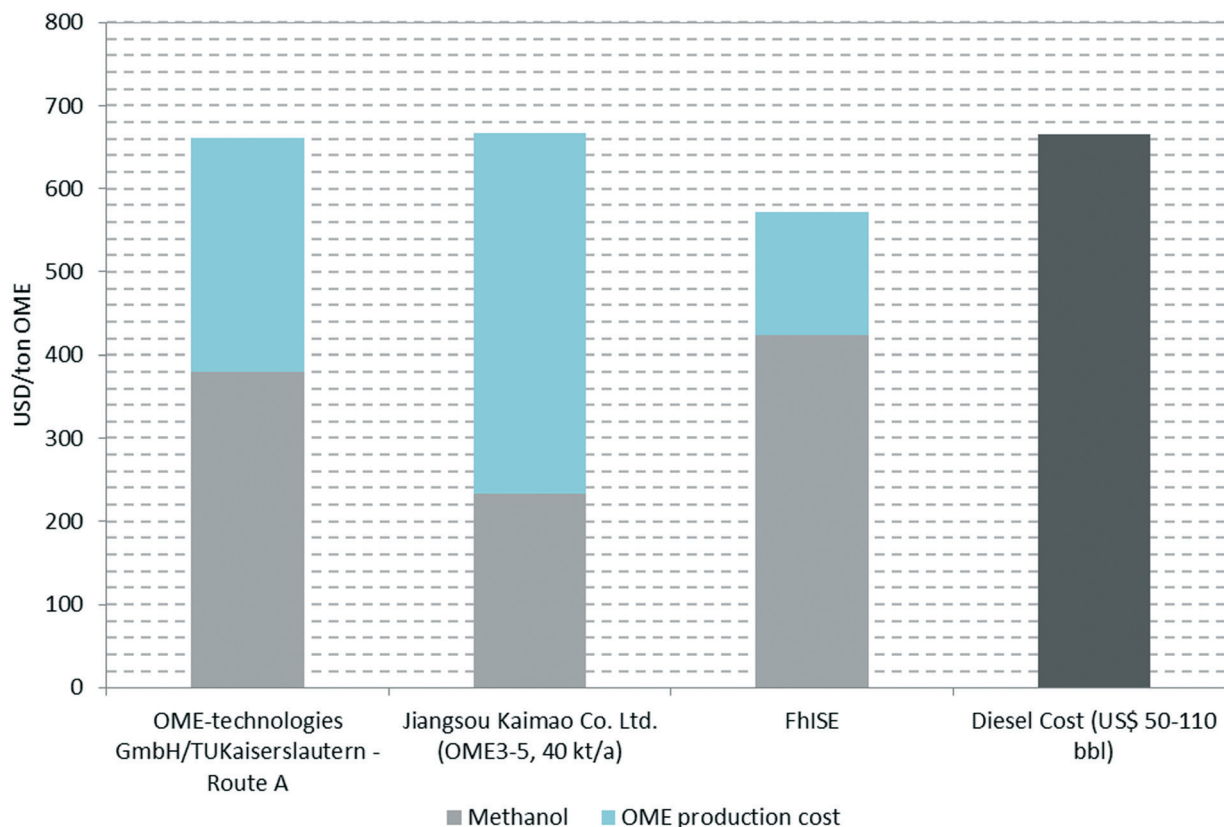
However an OME_{3-5} mixture with this composition (Table 7) has a LHV of 18.5 MJ kg^{-1} (ca. 42% of Paraffinic Diesel (PD) EN 15940 LHV). On the other hand, OME_{3-5} are 37% denser than diesel (relative to PD EN 15940 on a kg L^{-1} basis), which means that for the same tank volume, OME_{3-5} will have 45% energy content less than when the tank is filled with diesel.[17] These factors together with mobility emission legislations should be further considered for a fair comparison with diesel.

Table 7 Technical and economic KPIs for the direct OME synthesis processTechnical and economic KPIs for the direct OME synthesis process

Technological indicators		
Material balance	[t per annum]	[t/t(OME_{3-5})]
Inlet MeOH	43211.5	1.245
Outlet CO	2563.2	0.074
Outlet H_2	2029.2	0.058
Outlet H_2O	3901.3	0.112
Outlet OME_{3-5}	34714.6	OME_3: 0.372
		OME_4: 0.338
		OME_5: 0.291
Overall yield [g/g]	[OME_{3-5}/MeOH]	80.3%
R1 yield [g/g]	[FA/MeOH]	57.2%
R1 feed ratio [mol/mol]	[FA/MeOH]	1.9
R2 yield [g/g]	[MeOH/OME_{3-5}]	0.4
Recycle ratio R2	[mol product/mol recycle]	0.17
Energy balance	[kt per annum]	MW h/t(OME_{3-5})
Steam consumption	119.9	1.6
η_{eff}^1		86.4%
η_{eff}^2		61.03%
Economic indicators		
CAPEX	33 424 298.22 US\$	
OPEX	[US\$ per annum]	[US\$ per t(OME_{3-5})]
VCP	17 460 384.57	504.67 (65%)
FCP	9 239 031.63	307.97 (35%)
Total	26 699 416.2	772.51

*η_{eff}^1 is the process energy efficiency when H_2 and CO side products are considered in the frame of the process, *η_{eff}^2 is the process energy efficiency when H_2 and CO are not considered.

288 | React. Chem. Eng., 2018, **3**, 277–292

This journal is © The Royal Society of Chemistry 2018

Fig. 8 Production costs of OME and proportion of MeOH costs, OME-technology GmbH/TU Kaiserslautern route A: with Methylal (OME$_1$) and tri-oxane feed, production capacities 1 Mt per annum; FhISE: MeOH and anhydrous formaldehyde, production capacities 1 Mt per annum; Jiangsou Kaimao Co. Ltd.: MeOH and aqueous formaldehyde feed, production capacity 40 kt per annum.

These results demonstrate the potential of the described process to produce OME economically and in an energy efficient manner which facilitates the market entry in the applications mentioned before.

The anhydrous FA synthesis as a key step for the process chain discussed in this work is in R&D phase. Realising stable long term operation under the harsh reaction conditions in H$_2$ reducing environment is challenging. To support this endeavour, several catalyst systems and reactor technologies are being investigated in our group with promising performance in the vicinity of the target performance discussed in this report. Realistically, a technically feasible process to produce OME based on the innovated technology is most likely to be realized initially in smaller scales (<50 kt per annum) as market entry strategy which can be scaled-up with enhanced economics and extended markets.

Conclusions

A two-step direct OME synthesis with only MeOH as the starting material showed a significant synthesis efficiency and economic advantages over conventional synthesis processes discussed in literature. The synthesis starts by endothermic dehydrogenation of MeOH to yield anhydrous FA and H$_2$ – key steps for the innovative process – followed by

reacting the produced H$_2$O free FA and non-converted MeOH directly to OME. The molar ratio of FA/MeOH in the first step significantly influences the OME reaction equilibrium and at FA/MeOH = 1.8–2 [mol/mol], the highest yield per path for such educts system is achieved reflecting on enhanced KPIs. A simulation platform was developed using Matlab® for evaluating this novel process concept. The anhydrous FA synthesis was modelled as a stoichiometric reactor which is operating at steady state with conversion and selectivity of products that yield the desired FA/MeOH ratio in this step; performance parameters were approved from literature. For the OME reaction step, unconstrained non-stoichiometric Gibbs energy minimisation was applied with and SGO algorithm to converge this complex equilibrium system. The downstream of OME reactor separation was done at this stage using an ideal separator – a step required for early stage reactors single parameter optimisation – where the non-reacted educts and OME fractions other than the target fraction OME$_{3-5}$ are separated and recycled to the OME reactor. The SGO approach is advantageous for reaction with recycle equilibrium convergence, as a requirement for an implicit good initial guess could be avoided for this complex synthetic system (32 components contributing simultaneously in *ca.* 29 equilibrium reactions). A complimentary experimental validation is provided for the OME reaction equilibrium model based on

the use of different feeds, namely 1) CH_3OH/CH_2O and 2) $H_3C–O–(CH_2O)_1–CH_3/(CH_2O)_3$, demonstrates the robustness and reliability of the applied SGO for this multi-reaction system.

With the simulation main components modelled and interlinked, a material balance was carried out to define the main process KPIs. The described process yield is the highest yield so far reported (relative to OME processes described in literature) with yield up to 0.84 [g/g] $OME_{3–5}$/MeOH. The process overall efficiency was also evaluated from the simulation material balance results and conservative assumption that the process energy requirement accounts 30% of the final product heating value and will be supplied with super-heated steam. The calculated efficiency at 86.4% (since the by-product H_2 has high energy content and the few synthesis steps towards target product) is almost twice the synthesis efficiency of the Chinese state-of-the-art process. A cost model was then applied adopting the CAPEX for the synthesis from an OME plant with different educts that was presented in literature. The OPEX was evaluated based on MeOH and process steam market values (VCP) and the fixed operational cost (FCP) was evaluated as factors from CAPEX according to literature methodology. The production cost of $OME_{3–5}$ with this described novel process and production capacity of 30 kt per annum was evaluated at 772.5 US$ per t; a rather high cost relative to the OME target market candidates. However the process yield and energy efficiency are quite high, the cost of production is still not that competitive; a direct example of the economy of scale. Therefore the process was evaluated at production capacity of 1 Mt per annum and showed the lowest cost of production for $OME_{3–5}$ (571 US$ per t) in comparison with all OME synthesis processes were economic metrics were discussed in literature. The simulation platform with SGO algorithm and the implementation of a simple cost model for the KPIs evaluation represents a basic building block for the further development of OME synthesis.

Nomenclature

Abbreviations

Abbreviation	Full name
A-36	Amberlyst®-36
A-46	Amberlyst®- 46
MeOH	Methanol
FA	Formaldehyde
GHGE	Green house gas emissions
HF	Polyoxymethylene hemiformals
LHV	Lower heating value
MEFO	Methyl formate
MG	Polyoxymethylene glycols
NO_x	Nitrous oxides
NRS	Newton Raphson Solver
OME	Oxymethylene ethers
OME_n	Oligomer of OME of chain length n
PM	Particulate matter

POMDE	Poly-oxymethylene dimethyl ethers
SGO	Stochastic global optimizer
TRI	Trioxane
VBA	Visual basics for applications
VLLE	Vapor–liquid–liquid-equilibrium
VOC	Volatile organic compound

Symbols and indices

Symbol or index	Name
γ_i	Activity coefficient (−)
f_i^l	Fugacity of component i in liquid phase (bar)
f_i^v	Fugacity of component i in vapor phase (bar)
G^t	Gibbs free energy (J mol^{-1})
G_i^0	Gibbs free energy at standard conditions (J mol^{-1})
K	Equilibrium constant (−)
μ_i	chemical potential of species i (J mol^{-1})
v_i	Stoichiometric coefficient (−)
n_i	Molar amount (mol)
P	Pressure (bar)
P_i^{sat}	Saturation pressure (bar)
R	Gas constant (J mol^{-1} K^{-1})
T	Temperature (K)
t	Metric tonnes (t)
x_i	Molar fraction liquid phase (−)
y_i	Molar fraction gas phase (−)
N_{io}	Initial feed (mol)

Conflicts of interest

There are no conflicts to declare.

Acknowledgements

References

1 J. Rogelj, M. Den Elzen, N. Höhne, T. Fransen, H. Fekete, H. Winkler, R. Schaeffer, F. Sha, K. Riahi and M. Meinshausen, *Nature*, 2016, **534**(7609), 631.

2 M. Meinshausen, N. Meinshausen, W. Hare, S. C. B. Raper, K. Frieler, R. Knutti, D. J. Frame and M. R. Allen, *Nature*, 2009, **458**(7242), 1158.

3 L. Mennicken, A. Janz and S. Roth, *Environ. Sci. Pollut. Res.*, 2016, **23**(11), 11386.

4 International Panel on Climate Change, *2014: Mitigation of Climate Change*, Cambridge University Press, 2015, vol. 3.

5 European Union, Regulation (EC) No 715/2007 on Type Approval of Motor Vehicles with Respect to Emissions from Light Passenger and Commercial Vehicles (Euro 5 and Euro 6) and on Access to Vehicle Repair and Maintenance, Off. J. Eur. Union L. Ser., 2007, p. 171.

6 A. Sieminski, *International Energy Outlook. Energy Inf. Adm.*, 2014.

7 B. L. Salvi, K. A. Subramanian and N. L. Panwar, *Renewable Sustainable Energy Rev.*, 2013, **25**, 404.

8 B. S. Chauhan, R. K. Singh, H. M. Cho and H. C. Lim, *Renewable Sustainable Energy Rev.*, 2016, **59**, 1358.

9 M. Tuner, Review and Benchmarking of Alternative Fuels in Conventional and Advanced Engine Concepts with Emphasis on Efficiency, CO2, and Regulated Emissions, *SAE Technical Paper*, 2016.

10 E. Jacob and W. Maus, *MTZ Worldwide*, 2017, vol. 78(3), p. 52.

11 F. M. Kerton and R. Marriott, Alternative Solvents for Green Chemistry, *RSC Green Chemistry Book Series*, Royal Society of Chemistry, 2013.

12 S. N. Shah, S. K. Mendon and S. F. Thames, Utilisation of Green Materials for Coating Applications, in *Green Materials from Plant Oils, RSC Green Chemistry Book Series*, Royal Society of Chemistry, 2014, vol. 29, p. 293.

13 C. M. Alder, J. D. Hayler, R. K. Henderson, A. M. Redman, L. Shukla, L. E. Shuster and H. F. Sneddon, *Green Chem.*, 2016, **18**(13), 3879.

14 A. Feiling and M. Münz, *ATZextra Worldwide*, 2016, vol. 21(11), p. 16.

15 W. Maus, E. Jacob, M. Härtl, P. Seidenspinner and G. Wachtmeister, *35th Internat. Wiener Motorensymposium, Fortschritt-Berichte*, VDI Reihe 12, 2014, vol. 777(1), p. 325.

16 M. Härtl, P. Seidenspinner, E. Jacob and G. Wachtmeister, *Fuel*, 2015, **153**, 328.

17 M. Härtl, K. Gaukel, D. Pélerin and G. Wachtmeister, *MTZ Worldwide*, 2017, vol. 78(2), p. 52.

18 W. Ying, L. Genbao, Z. Wei and Z. Longbao, *Fuel Process. Technol.*, 2008, **89**(12), 1272.

19 B. Lumpp, D. Rothe, C. Pastötter, R. Lämmermann and E. Jacob, *MTZ Worldwide*, 2011, vol. 72(3), p. 34.

20 L. Lautenschütz, D. Oestreich, P. Seidenspinner, U. Arnold, E. Dinjus and J. Sauer, *Fuel*, 2016, **173**, 129.

21 K. Gaukel, D. Pélerin, M. Härtl, G. Wachtmeister, J. Burger, W. Maus and E. Jacob, *37th Internat. Wiener Motorensymposium, Fortschritt-Berichte*, VDI Reihe 12, 2016, vol. 777(1), p. 325.

22 J. Wang, Y. Zheng, S. Wang, T. Wang, S. Chen and C. Zhu, Method for Producing Polyoxymethylene Dimethyl Ethers, WO2015154626A1, US9266990, US20150291722, CN104974025A, 2017.

23 R. Wang, Z. Wu, Z. Qin, C. Chen, H. Zhu, J. Wu, G. Chen, W. Fan and J. Wang, *Catal. Sci. Technol.*, 2016, **6**(4), 993.

24 D. Deutsch, D. Oestreich, L. Lautenschütz, P. Haltenort, U. Arnold and J. Sauer, *Chem. Ing. Tech.*, 2017, **89**(4), 486.

25 J. Burger, V. Papaioannou, S. Gopinath, G. Jackson, A. Galindo and C. S. Adjiman, *AIChE J.*, 2015, **61**(10), 3249.

26 M. Schappals, T. Breug-Nissen, K. Langenbach, J. Burger and H. Hasse, *J. Chem. Eng. Data*, 2017, **62**(11), 4027.

27 J. Burger, M. Siegert, E. Ströfer and H. Hasse, *Fuel*, 2010, **89**(11), 3315.

28 J. Burger, E. Ströfer and H. Hasse, *Chem. Eng. Res. Des.*, 2013, **91**(12), 2648.

29 N. Schmitz, F. Homberg, J. Berje, J. Burger and H. Hasse, *Ind. Eng. Chem. Res.*, 2015, **54**(25), 6409.

30 N. Schmitz, A. Friebel, E. von Harbou, J. Burger and H. Hasse, *Fluid Phase Equilib.*, 2016, **425**, 127.

31 J. Burger, E. Ströfer and H. Hasse, *Ind. Eng. Chem. Res.*, 2012, **51**(39), 12751.

32 S. Schemme, R. C. Samsun, R. Peters and D. Stolten, *Fuel*, 2017, **205**, 198.

33 K. Thenert, K. Beydoun, J. Wiesenthal, W. Leitner and J. Klankermayer, *Angew. Chem., Int. Ed.*, 2016, **55**(40), 12266.

34 Y. Zheng, Q. Tang, T. Wang, Y. Liao and J. Wang, *Chem. Eng. Technol.*, 2013, **36**(11), 1951.

35 Y. Zheng, Q. Tang, T. Wang, Y. Liao and J. Wang, *Chem. Eng. Sci.*, 2015, **134**, 758.

36 M. Ouda, G. Yarce, R. J. White, M. Hadrich, D. Himmel, A. Schaadt, H. Klein, E. Jacob and I. Krossing, *React. Chem. Eng.*, 2017, **2**(1), 50.

37 E. Schweers, T. Kaiser, C. Meister, M. Rosenberg and R. Schulz, Method for Producing Formaldehyde from Methanol, US6362305B1, 2002.

38 S. Su, P. Zaza and A. Renken, *Chem. Eng. Technol.*, 1994, **17**(1), 34.

39 J. Sauer and G. Eming, *Chem. Eng. Technol.*, 1995, **18**, 284.

40 J. Wu, H. Zhu, Z. Wu, Z. Qin, L. Yan, B. Du, W. Fan and J. Wang, *Green Chem.*, 2015, **17**(4), 2353.

41 D. Oestreich, L. Lautenschütz, U. Arnold and J. Sauer, *Chem. Eng. Sci.*, 2017, **163**, 92.

42 I. Hahnenstein, H. Hasse, C. G. Kreiter and G. Maurer, *Ind. Eng. Chem. Res.*, 1994, **33**(4), 1022.

43 I. Hahnenstein, M. Albert, H. Hasse, C. G. Kreiter and G. Maurer, *Ind. Eng. Chem. Res.*, 1995, **34**(2), 440.

44 D. Himmel, R. J. White, E. Jacob and I. Krossing, *Sustainable Energy Fuels*, 2017, **1**, 1177.

45 A. Schmitz, J. Burger, E. Ströfer and H. Hasse, *Fuel*, 2016, **185**, 67.

46 X. Zhang, A. O. Oyedun, A. Kumar, D. Oestreich, U. Arnold and J. Sauer, *Biomass Bioenergy*, 2016, **90**, 7.

47 Z. Ye and J. Xiang, Formaldehyde Absorption Process Device and Method in Polyoxymethylene Dimethyl Ether Synthesis, WO2016180085A1, CN104817440A, CN104817440B, 2016.

48 J. Burger, *A Novel Process for the Production of Diesel Fuel Additives by Hierarchical Design, Scientific report series*, Techn. Univ: Kaiserslautern, vol. 3, 2012.

49 *Ullmann's Encyclopedia of Industrial Chemistry: Formaldehyde*, ed. A. W. Franz, H. Kronemayer, D. Pfeiffer, R. D. Pilz, G. Reuss, W. Disteldorf and A. O. Gamer, Wiley-VCH, Weinheim, Germany, 2016.

50 S. Su, M. R. Prairie and A. Renken, *Appl. Catal., A*, 1992, **91**, 131.

51 S. K. Fateen, *Comput. Appl. Eng. Educ.*, 2016, **24**(6), 899.

52 J. O. Drunsel, M. Renner and H. Hasse, *Chem. Eng. Res. Des.*, 2012, **90**(5), 696.

53 W. M. Haynes, *CRC Handbook of Chemistry and Physics*, 98th edn., CRC press, 2017, ISBN 9781498784542.

54 C. Kuhnert, M. Albert, S. Breyer, I. Hahnenstein, H. Hasse and G. Maurer, *Ind. Eng. Chem. Res.*, 2006, **45**(14), 5155.

55 V. Bhargava, S.-E. K. Fateen and A. Bonilla-Petriciolet, *Fluid Phase Equilib.*, 2013, **337**, 191.

56 N. Schmitz, J. Burger and H. Hasse, *Ind. Eng. Chem. Res.*, 2015, **54**(50), 12553.

57 M. Baerns, A. Behr, A. Brehm, J. Gmehling, H. Hofmann, U. Onken, A. Renken, K. O. Hinrichsen and R. Palkovits, *Technische Chemie*, 2nd edn., Wiley-VCH, Weinheim, Germany, 2013, ISBN: 978-3-527-33072-0.

Electronic Supporting Information

Describing Oxymethylene Ether Synthesis based on the application of Non-Stoichiometric Gibbs Minimisation

M. Ouda,[a,b]* F. Mantei,[a] M. Elmehlawy,[c] R. J. White,[a,]* H. Klein,[b] and S.-E. K. Fateen[d,e]*

[a] *Sustainable Catalytic Materials Group, Division Hydrogen Technologies, Fraunhofer Institute for Solar Energy Systems, Heidenhofstraße 2, 79110 Freiburg, Germany;* *mohamed.ouda@ise.fraunhofer.de* / *robin.white@ise.fraunhofer.de*

[b] *Institute of Process and Plant Technology, Technical University Munich, Boltzmannstraße 15, 85748 Garching, Germany*

[c] *Energy and Bioprocess Engineering Program, Zewail City of Science and Technology, Giza, Egypt*

[d] *Department of Chemical Engineering, Cairo University, Giza, Egypt*

[e] *Environmental Engineering Program, Zewail City of Science and Technology, Giza, Egypt;* *sfateen@zewailcity.edu.eg*

UNCONSTRAINTED GIBBS MINIMIZATION TECHNIQUE
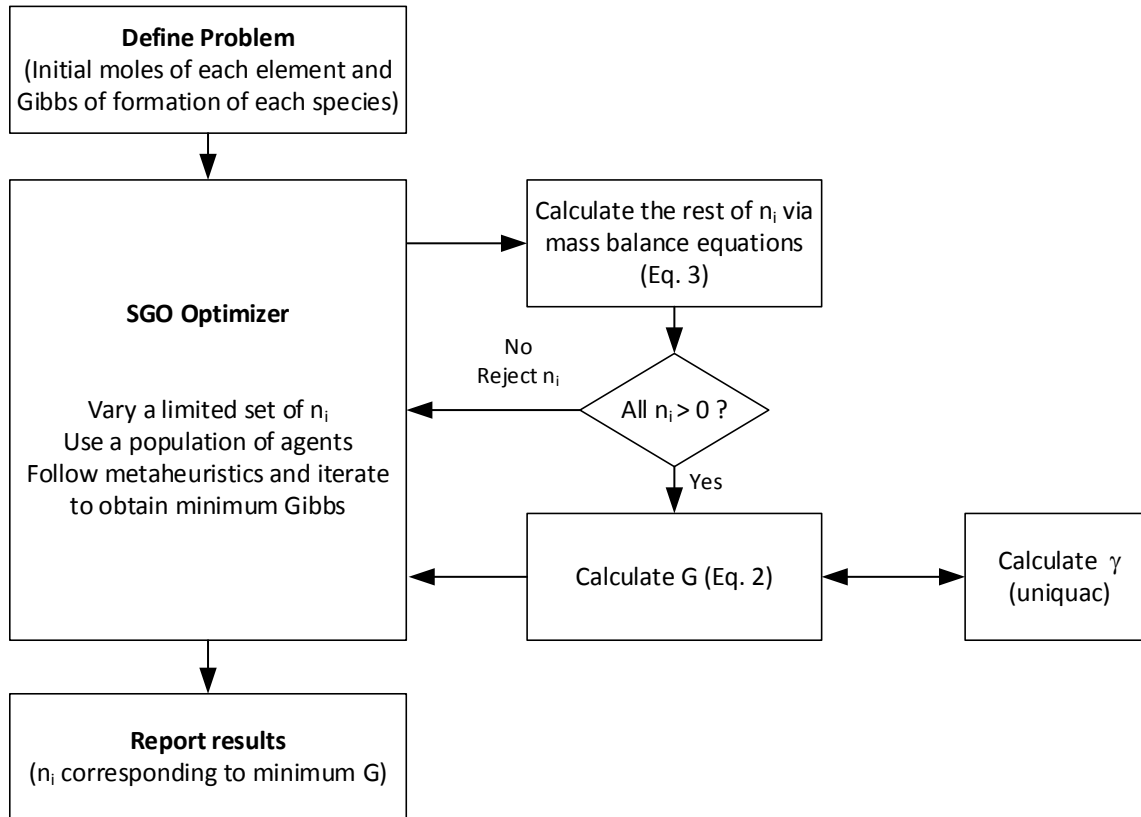
Figure S1 Scheme of the unconstrained Gibbs minimisation approach

IMPLEMENTATION ON OME LIQUID-PHASE REACTION

Table S1 Standard Gibbs of formation values at T = 333.15 K for different species in the system calculated using data extraction method

Species	Std. Gibbs Energy of formation (Liquid) at 333.15 K (kJ/mol)
OME_1	-207.12
OME_2	-316.79
OME_3	-426.46
OME_4	-536.13
OME_5	-645.80
OME_6	-755.48
OME_7	-865.15
OME_8	-974.82
MG_1	-336.55
MG_2	-448.66
MG_3	-558.37
MG_4	-668.07
MG_5	-777.78
MG_6	-887.49
MG_7	-997.20
MG_8	-1106.90
HF_1	-273.69
HF_2	-383.12
HF_3	-491.55
HF_4	-599.98
HF_5	-708.42

HF$_6$	-816.85
HF$_7$	-925.28
HF$_8$	-1033.71
FA	-94.81
MeOH	-158.01
H$_2$O	-231.38

Table S2. UNIFAC structural groups with size- and surface parameters (Adapted from Schmitz *et al.* (Ref. 1) and (Kuhnert et al. (Ref. 2))

Structural group	Number	*R*	*Q*
CH$_2$O	1	0.9183	0.78
H$_2$O	2	0.92	1.4
H$_3$C-O-CH$_2$O-CH$_3$	3	2.9644	2.716
HO-CH$_2$O-H	4	2.6744	2.94
OH	5	1	1.2
CH$_2$	6	0.6744	0.54
CH$_3$O	7	1.1459	1.088
CH$_2$OH	8	1.2044	1.124
CH$_3$OH	9	1.4311	1.432
(CH$_2$O)OME	10	0.9183	0.78

Table S3. UNIFAC interaction parameters a_{km}/K (Adapted from Schmitz *et al.* (Ref. 1) and (Kuhnert et al. (Ref. 2))

k	*m*									
	1	2	3	4	5	6	7	8	9	10

1	-	867.8	0	189.2	237.7	83.36	0	238.4	238.4	0
2	-254.5	-	$a_{2,3}(T)$	189.5	-229.1	300	-219.3	$a_{2,8}(T)$	289.6	$a_{2,10}(T)$
3	0	$a_{3,2}(T)$	-	$a_{3,2}(T)$	237.7	83.36	0	0	410	26
4	59.2	-191.8	$a_{2,3}(T)$	-	-229.1	300	-142.4	289.6	289.6	59.2
5	28.06	353.5	28.06	353.5	-	156.4	112.8	-137.1	-137.1	28.06
6	251.5	1318	251.5	1318	986.5	-	447.8	697.2	697.2	251.5
7	0	423.8	0	774.8	1164.8	273	-	238.4	238.4	0
8	-128.6	$a_{8,2}(T)$	0	-181	249.1	16.5	-128.6	-	0	-128.6
9	-128.6	-181	-71.21	-181	249.1	16.5	-128.6	0	-	-128.6
10	0	670.7	141.5	189.2	237.7	83.36	0	238.4	238.4	-

$a_{2,3}(T)=-225.5+0.7205(T/K)$; $a_{3,2}(T)=1031.0-1.749(T/K)$; $a_{8,2}(T)=-1018.57+329900/(T/K)$; $a_{2,8}(T)=451.64-114100/(T/K)$; $a_{2,10}(T)=168.9-0.8776(T/K)$

Table S4 UNIFAC group assignment for all components adapted from K (Adapted from Schmitz *et al.* (Ref. 1) and (Kuhnert et al. (Ref. 2))

| Substance/Group	CH_2O (FA)	H_2O	$C_3H_8O_2$ (OME_1)	$OH(CH_2O)H$ (MG_1)	OH	CH_2	CH_3O	CH_2OH	CH_3OH	CH_2O (OME)
FA	1									
Water		1								
Methanol									1	
Methylal (OME_1)			1							
MG_1				1						
HF_1							1	1		
$MG_{n>2}$	n-1				2	1				
$HF_{n>2}$	n-1						1	1		
$OME_{n>2}$			1							n-1

EXPERIMENTAL VALIDATION

Table S5 Different educts used for chemical equilibrium of the OME system Adapted from the supporting information of Schmitz et al. (Ref. 2)

| Educt	Total Mass of Educt (g)	FA (mass fraction)	Water (mass fraction)	MeOH (mass fraction)
1	820	0.4841	0.0226	0.4933
2	790	0.3669	0.2225	0.4106
3	798	0.4743	0.1866	0.3391
4	776	0.3682	0.3454	0.2865
5	779	0.3447	0.0227	0.6315
6	763	0.2824	0.2181	0.4992
7	763	0.4713	0.0288	0.4996
8	801	0.3970	0.0152	0.5879
9	813	0.5697	0.0235	0.4014
10	791	0.4289	0.113	0.4580
11	799	0.5140	0.1209	0.3651

Table S6 Equilibrium composition of the OME synthesis for different reaction conditions and different feed compositions in comparison to the literature values (Ref. 1 and 2).

EQ (OME 1:TRI)	T [°C]	Exp.	p [bar]	[wt.%]										
				TRI	OME_1	OME_2	OME_3	OME_4	OME_5	OME_6	OME_7	OME_8	MEFO	MeOH
3:1	50	B	1.5	1.28	39.12	24.76	15.57	9.17	5.02	2.70	1.39	0.65	0.00	0.13
	50	Own	3	1.22	44.08	24.59	13.99	8.03	3.89	1.79	0.81	0.34	0.01	1.25
	65	B	1.9	1.45	39	24.72	15.53	9.16	5.00	2.71	1.39	0.65	0.00	0.16

|													
	65	Own	4	1.44	44.20	24.33	13.77	8.02	3.91	1.87	0.81	0.34	0.05	1.26
	80	B	2.6	1.62	38.96	24.69	15.43	9.10	4.96	2.67	1.37	0.65	0.09	0.17
	80	Own	6.3	1.61	44.07	24.67	13.84	7.85	3.81	1.82	0.82	0.36	0.40	0.75
2:1	50	B	1.5	1.69	33.83	23.59	16.32	10.64	6.45	3.84	2.21	1.24	0.00	0.03
	50	Own	4	2.07	35.50	22.71	15.32	10.66	6.23	3.63	1.95	1.05	0.02	0.86
	65	B	1.9	1.91	33.85	23.52	16.21	10.57	6.41	3.83	2.19	1.27	0.00	0.03
	65	Own	5	2.26	35.91	22.64	15.19	10.47	6.07	3.44	1.93	1.07	0.15	0.87
	80	B	2.6	2.14	33.67	23.52	16.18	10.55	6.40	3.82	2.17	1.24	0.00	0.05
	80	Own	8	2.62	37.80	22.46	14.50	9.67	5.44	3.08	1.67	0.87	1.21	0.67
2.5:1	50	Own	4	1.56	40.34	23.59	14.67	9.29	4.93	2.59	1.27	0.61	0.00	1.16
	65	Own	5.5	1.84	40.76	23.04	14.40	9.12	4.89	2.60	1.34	0.66	0.13	1.22
	80	Own	9.5	2.15	40.99	23.48	14.22	8.68	4.48	2.29	1.09	0.50	1.31	0.80
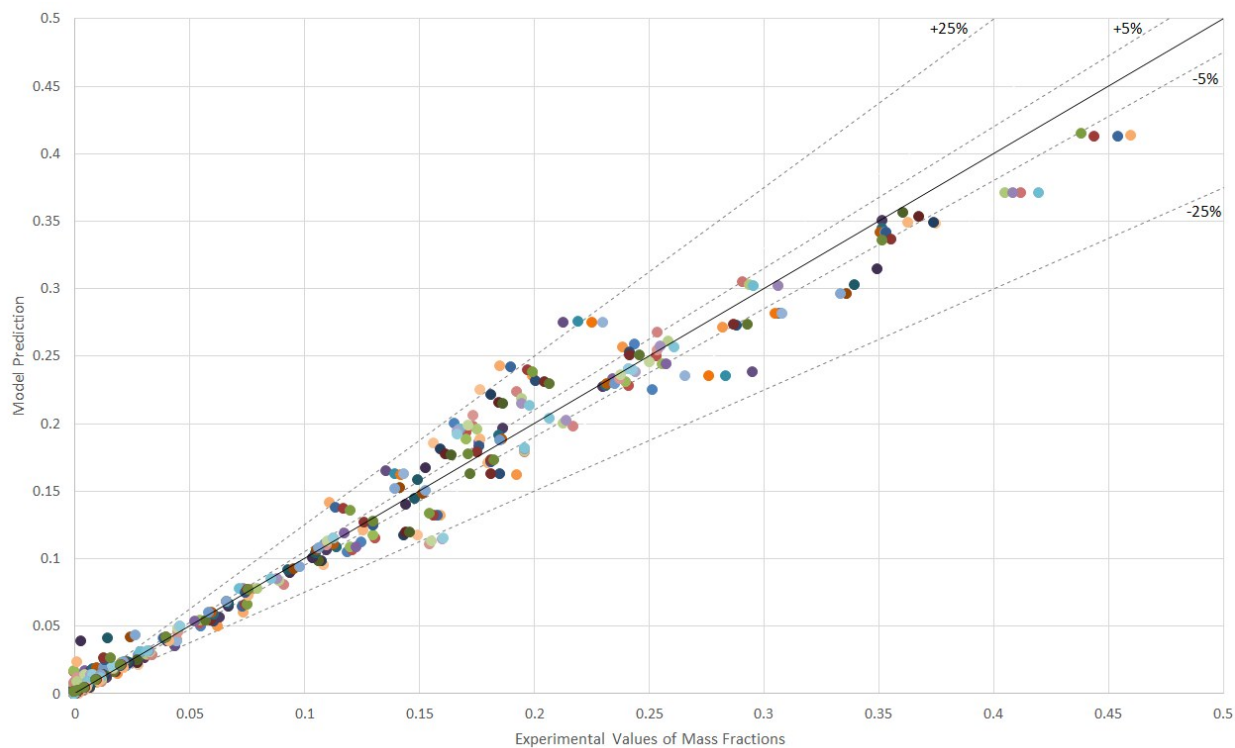
Figure S2 A parity plot of overall mass fractions of FA, MeOH, water and OME of the different educts at equilibrium calculated by the model to the literature experimental values from Schmitz et al. (Ref. 1)
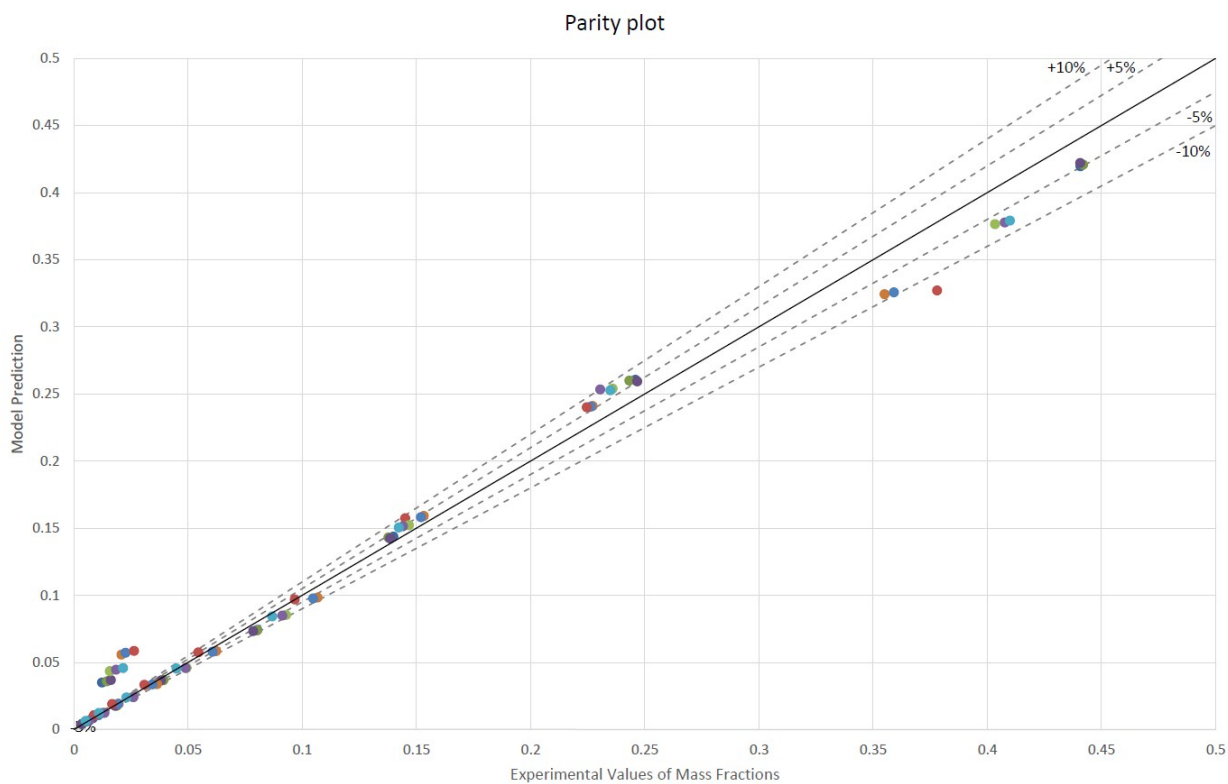
Figure S3 Parity plot between the equilibrium overall mass fractions of FA, MeOH, water and OME of different educts and reaction conditions calculated by the unconstrained Gibbs energy minimisation equilibrium model to the experimental values reported in Table S6
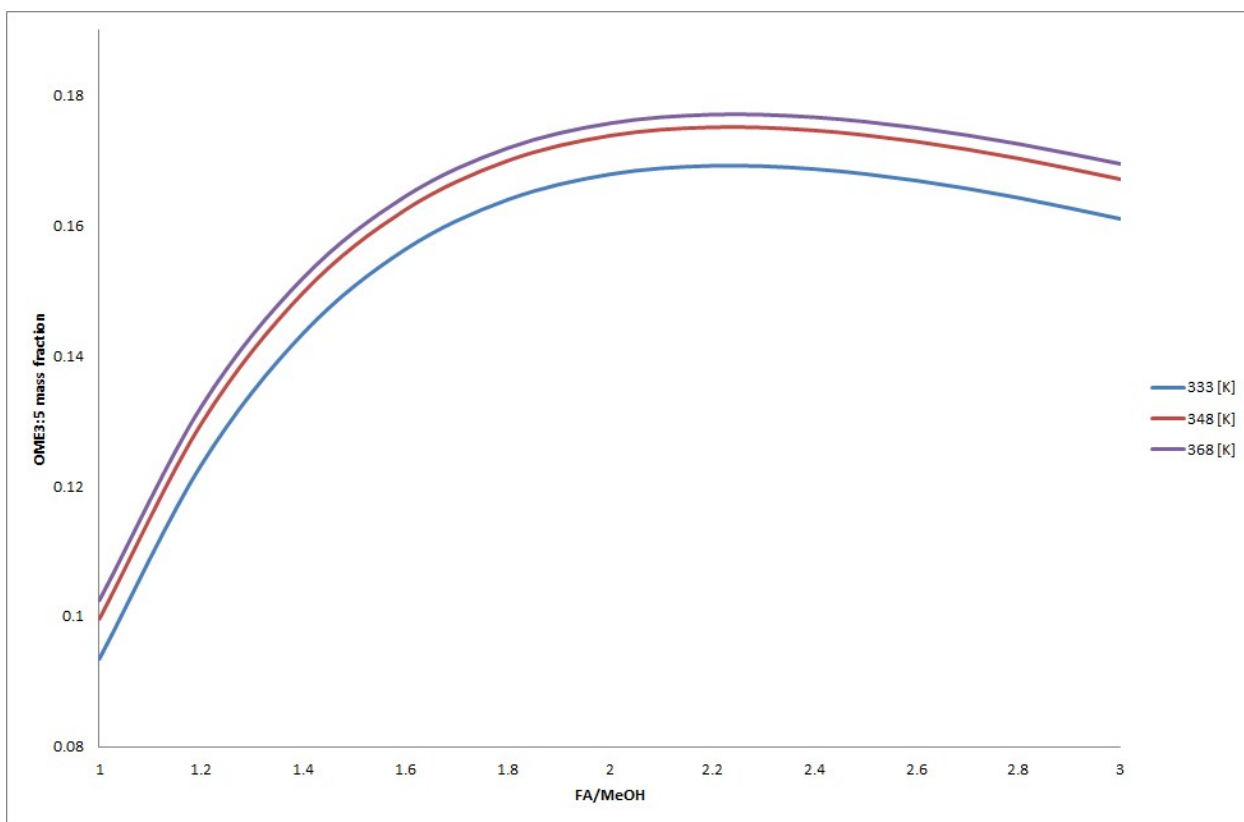
Figure S4 Effect of FA and MeOH ratio for anhydrous feeds on the OME$_{3-5}$ equilibrium composition
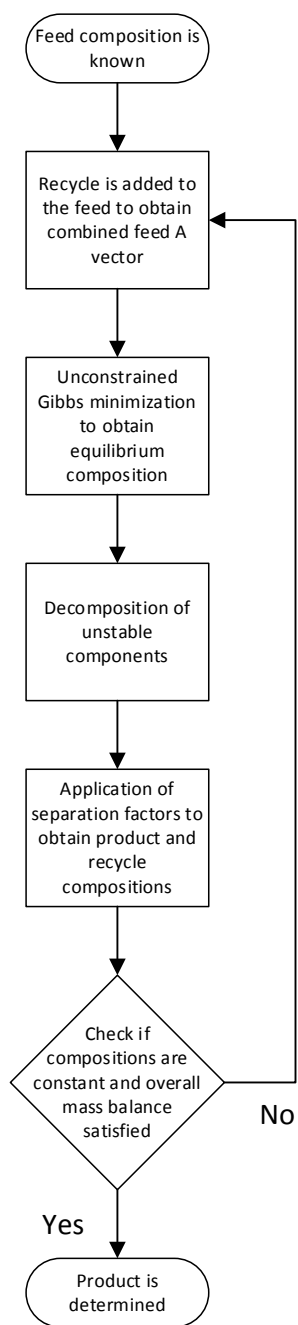
Figure S5 The recycle calculation algorithm

Table S7 Fuel properties of DME, OME and diesel (EN 590) as sourced from Refs. 3, 4, and 5.

Component	M [g/mol]	Oxygen-content [wt. %]	Cetane number	Density at 15°C [kg/m³]	Melting point [°C]	Boiling point [°C]	v at 40°C [mm²/s]	LHV [kWh/kg]	Equivalent to diesel [m³/m³]
DME	46.1	34.7	55	668	-141	-25	<0,1	7.5	1.96
OME$_1$	76.1	42.1	29	866.8	-105	42.3	0.58$_{(20°C)}$	6.5	1.75
OME$_2$	106.1	45.2	63	970	-69.7	105	0.66$_{(20°C)}$	5.4	1.75
OME$_3$	136.1	47	67	1,031	-42.5	155.9	1.08	5.4	1.75
OME$_4$	166.2	48.1	76	1,075	-9.8	201.8	1.72	5.3	1.73
OME$_5$	196.2	48.9	90	1,106	18.3	242.3	2.63	5.1	1.72
OME$_6$	226.2	49.5	-	1,135	45.8	273	-	-	-
OME$_7$	256.3	49.9	-	1,157	72.4	297	-	-	-
OME$_8$	286.3	50.3	-	-	-	-	-	-	-
OME$_{3-5}$	166.2	48.8	70-100	1,070	-19	155-242	1.89	5.4	1.8
Diesel	-	-	>51	820-840	-20$_{winter}$ / 0$_{summer}$	170-390	2-4.5	11.833	1

References

1. (a) N. Schmitz, F. Homberg, J. Berje, J. Burger, and H. Hasse, H, *Ind. Eng. Chem. Res.*, 2015, **54**, 25, 6409; (b) N. Schmitz, J. Burger, and H. Hasse, *Ind. Eng. Chem. Res.* 2015, **54**, 50, 12553; (c) N. Schmitz, A. Friebel, E. von Harbou, J. Burger, and H. Hasse, Fluid Phase Equilib., 2016, 425, 127; (d) N. Schmitz, J. Burger, E. Ströfer, and H. Hasse, *Fuel*, 2016, **185**, 67.

2. (a) C. Kuhnert, M. Albert, S. Breyer, I. Hahnenstein, H. Hasse, and G. Maurer, *Ind. Eng. Chem. Res.,* 2006, **45**, 14, 5155; (b) C. Kuhnert, M. Albert, S. Breyer, I. Hahnenstein, H. Hasse and G. Maurer, *Ind. Eng. Chem. Res.*, 2006, **45**, 14, 5155.

3. L. P. Lautenschütz, "New findings in the optimisation of oxymethylene diethylether oligomer synthesis from dimethoxymethane and trioxane" / ("Neue Erkenntnisse in der Syntheseoptimierung oligomerer Oxymethylen-dimethylether aus Dimethoxymethan und Trioxan"), Dissertation, University of Heidelberg, URN:nbn:de:bsz:16-heidok-192102, 2015.

4. L. Lautenschütz, D. Oestreich, P. Seidenspinner, U. Arnold, E. Dinjus and J. Sauer, *Fuel*, 2016, **173**, 129.

5. B. Lumpp, D. Rothe, C. Pastötter, R. Lämmermann, and E. Jacob, *MTZ Worldwide,* 2011, **72**, 3, 34.

7.7 Paper 3: A Hybrid Description and Evaluation of Oxymethylene Dimethyl Ethers Synthesis based on the Endothermic Dehydrogenation of Methanol

Mohamed Ouda, Franz Mantei, Kai Hesterwerth, Eleonora Bargiacchi, Harald Klein, and Robin J. White

7.7.1 Summary of the paper

The process models of the two-step OME synthesis process described in the previous papers are integrated in this work in a hybrid model. The Matlab® based self-developed reactor models are integrated in the flowsheet simulation CHEMCAD® platform. The coupling of the two platforms was done using a Visual Basic for Applications (VBA) node. The simulation was extended to consider the whole process components as heat exchangers, pumps and rigorous separation units. This was followed by process heat integration using PinCH 2.0 software. Using this platform a technical process evaluation for the considered process can be done.

The key step in the considered OME synthesis process is the methanol (MeOH) endothermic dissociation to formaldehyde (FA) and hydrogen. An experimental setup for the heterogeneous high temperature catalytic reaction investigated was designed and constructed in this work. This reaction is kinetically controlled and special reactor design is required. The reaction is characterized by very short residence time and requires direct quenching of the produced FA to avoid the further dissociation to the thermodynamically preferred formation of carbon monoxide (CO). For this purpose, an annular counter current reactor ACCR was specially designed and integrated in the setup. Na_2CO_3 catalyst was selected based on literature investigations. A global kinetic reactor model was developed based on experimental and literature data. The designed reactor allowed advantageous temperature profile relative to reactors discussed in literature. However, change of activity of Na_2CO_3 was observed with increasing time on stream. Also catalyst performance changed significantly with shutdown and startup events. Preliminary characterization using SEM showed significant structural changes of the catalyst material after time on stream. This aspect should be further investigated from material development point of view for technical realization of this process.

With the convergence of the energy integrated process flowsheet hybrid simulation, all streams material and energy data were extracted using VBA node for techno-economic evaluation. Equipment sizing for CAPEX evaluation was then carried out. The techno-economic evaluation model was implemented in the VBA/Excel environment. Each main component performance could be evaluated separately. Furthermore, the whole utilities required externally were defined and the process overall energy efficiency was evaluated. The main energy consuming equipment and main production cost contributing sub-processes where improvement potential is possible were identified. The production cost of OME_{3-5} for a base case scenario was evaluated as 951 US$ per t at *ca.* 35 kt per annum productivity. Several scenarios and synergies were considered in a sensitivity analysis. This identified the importance of research and development on the MeOH endothermic dehydrogenation catalyst aspect to improve this process chain and allow a technical realization. The hybrid process model developed in the frame of this work presents for the first time an integrated platform where OME synthesis technologies can be robustly evaluated.

7.7.2 Overview of the contributions in this work

I was significantly involved in the essential phases of brainstorming and in the elaboration of all parts of the work. (1) The development of the test setup for endothermic MeOH dehydrogenation accompanied the whole PhD journey. This included conception, design of the setup components (specially ACCR reactor), mechanical drawings, construction, safety concept, operational strategy for setup monitoring and control (programming is done by specialized colleagues), commissioning and running tests. On the other hand, analysis for anhydrous FA is quite challenging, (2) the development of analytical concept and identifying the right gas chromatographs columns were also my tasks. Kai Hesterwerth and Eleonora Bargiacchi assisted in the development of the test setup and running the experiments. (3) Developing the paper outline and coordinating with the co-authors were explicitly my tasks. (4) Implementing the reactors models in CHEMCAD and implementing the physical property models, (5) coupling software platforms using VBA node, (6) implementing the rigorous distillation units, (7) whole process flow sheet energy integration were done with assistance of my master student Franz K. Mantei. (8) Process techno-economic evaluation and considering different scenarios were explicitly done by me. (9) Finally, writing the whole paper and doing the corresponding adjustments after the review process was explicitly my task. The rest of the co-authors contributed in the initial concept discussion phase and correction reading.

7.7.3 Paper as published in Peer-Reviewed journal

PAPER

A hybrid description and evaluation of oxymethylene dimethyl ethers synthesis based on the endothermic dehydrogenation of methanol†

Mohamed Ouda, [*ab] Franz Mantei,[a] Kai Hesterwerth,[a] Eleonora Bargiacchi, [a] Harald Klein[a] and Robin J. White [*a]

Concerning oxymethylene dimethyl ethers (*e.g.* a class of potential oxygenated diesel substitutes; denoted as OME), this work utilises a hybrid process model based on methanol (MeOH) and its partially selective conversion to anhydrous formaldehyde (FA, target MeOH conversion ≥67% and target FA selectivity ≥93%), which in turn is used as the feed for OME synthesis. The model couples the merits of algorithms available in the commercial software CHEMCAD® together with self-developed reactor models as implemented through Matlab® and the coupling node implemented in Visual Basic for Applications (VBA) software. This is followed by process heat integration using PinCH 2.0 software. This modelling is complemented by experimental investigations and results concerning the synthesis of the anhydrous FA/MeOH feed through a designed and developed annular counter current reactor, with the use of Na_2CO_3 as an inexpensive and sustainable dehydrogenation catalyst. The process material and energy balance of the proposed process have also been used to evaluate the key performance indicators (KPIs). An overall process yield of 80.3% at 71.7% process energy efficiency and production cost of 951 US$ per ton of OME_{3-5} at small production capacity (35 kt per annum) demonstrates the technical and the economic potential of the described process.

[a] *Sustainable Catalytic Materials Group, Division Hydrogen Technologies, Fraunhofer Institute for Solar Energy Systems, Heidenhofstr. 2, 79110 Freiburg, Germany. E-mail: mohamed.ouda@ise.fraunhofer.de, robin.white@ise.fraunhofer.de*

[b] *Institute of Process and Plant Technology, Technical University Munich, Boltzmannstr. 15, 85748 Garching, Germany*

† Electronic supplementary information (ESI) available: Experimental results for equilibrium constant evaluation for Na_2CO_3 catalyst; kinetic model results for endothermic selective MeOH dehydrogenation to FA reaction over Na_2CO_3 catalyst; chemical equilibrium composition using different reaction models; results and HEN from PinCH 2.0; process flow diagram of the test stand for endothermic MeOH catalytic dehydrogenation to FA; Ergun's equation for pressure drop evaluation in ACCR; photographs of the ACCR with relative dimensions; Na_2CO_3 catalyst characterization. See DOI: 10.1039/c8re00100f

Introduction

Global CO_2 emissions contributing to Green House Gases (GHG) and local emissions (NO_x, PM) regarding urban mobility are an increasingly part of the political and indeed public debate.[1–3] The European Commission has set out in a white paper for the transport sector, a reduction in CO_2 emissions of 60% by 2050, relative to 1990.[4] Euro 6 regulations set sharp NO_x and PM emissions limits (*i.e.* for diesel private vehicles 80 mg km^{-1} for the former and 5 mg km^{-1} for the latter with almost a hundred fold reduction relative to Euro 1 limits).[5,6]

Taking Germany as an example, road passengers and road freight transport represents >82% of the net transport sector primary energy consumption and *ca.* 90% of corresponding CO_2 emissions.[5,7] To meet these targets, several solutions are being considered. One option is the large scale production of synthetic (also called electro or designer) fuels,[8] which could potentially be "dropped in" to existing fuel delivery infrastructure and be used with minimal modifications to existing fleet engines. Systematically evaluating this and other proposed solutions (*e.g.* battery vehicles, biodiesel *etc.*) reveals the magnitude of the challenge. For example, in Germany 295 TWh electricity would be needed to cover (private) electro mobility,[2] whilst enormous amounts of biomass (and land) would be needed to establish suitable bio-diesel capacities to cover the same sector,[1] or indeed >300 Mt of MeOH would be the annual demand to provide a suitable sized synthetic (diesel) fuel production (*e.g.* at a very optimistic yield of 1.1 t_{MeOH} $t_{syntheticfuel}{}^{-1}$; current global annual MeOH production is *ca.* 80 Mt (ref. 9)) – therefore a combination of all these fuel provision options should provide a contribution to a sustainable mobility sector. In this context, polyoxymethylene dimethyl ethers (molecular formula: $H_3CO–(CH_2O)_n–CH_3$, OME for short chains with n = 3–5) are a class of synthetic oxygenates that can make a potential contribution to the mobility sector and in particular as a diesel substitute.

676 | *React. Chem. Eng.*, 2018, **3**, 676–695

This journal is © The Royal Society of Chemistry 2018

OME are known to have very attractive combustion properties.[6,10,11] They are known to have good miscibility with diesel and a high cetane number,[10,12] and can be used in existing infrastructure.[3,13] Several contributions regarding the direct use of OME or blends in diesel engines, in particular the work of Wachtmeister et al.,[10] Richter et al.[14] and Liu et al.,[15,16] – have demonstrated the potential for drastic reduction in the PM emissions and an override of the NO_x-soot trade-off allowing measures to reduce the NO_x emissions (i.e. exhaust gas recycle EGR).[17–28] With regards to other applications, OME are also sparking interest as potential CO_2 sorption media, as fuel for direct oxidation fuel cells, and in the production of perfume, resins, and protective coatings.[12,29–31]

Although currently produced based on "grey" MeOH (e.g. fossil based), the synthesis of OME can be logically also performed based on MeOH as sourced from the hydrogenation of (e.g. captured) CO_2 using renewable H_2 (e.g. as sourced from H_2O electrolysis or photolysis). These drop-in liquid synthetic oxygenates can thus be produced with potentially net CO_2 emission reductions. An overview of different OME synthesis routes has been reported recently by Barnowski et al. and Niethammer et al.[6,30] As a general basis, OME synthesis requires an FA source – which can be formalin, para-formaldehyde, or trioxane – and also a methyl capping group supplier, as provided by MeOH, methylal (OME_1) or DME. Subsequent oligomer extension reactions (e.g. acetalisation, condensation, addition, etc.) then take place according to the feed components as explained in detail previously by Burger et al.[32] and Zhao et al.[33] Known (e.g. industrial) processes for OME synthesis are relatively complex, composed of a variety of process synthesis steps, for example involving reactive distillation, extraction, etc., often leading to relatively low synthesis efficiency, whilst being based on expensive feedstocks (e.g. trioxane).[3,34,35]

A so-called "Direct OME synthesis" based on MeOH and aqueous formaldehyde ($FA_{aq.}$) has been investigated previously due to the theoretical potential to increase process energy efficiency and reduce capital investment (CAPEX).[34–40] This two-step synthesis represents in principle a simpler route in comparison with other known processes featuring several intermediate synthesis steps.[30,34,35] In the first synthesis step MeOH undergoes selective oxidative dehydrogenation to yield $FA_{aq.}$ (formalin, FA = 37–50 wt%). $FA_{aq.}$ reacts in a second step with MeOH to produce OME and H_2O followed by working up of the product to produce the target $OME_{3–5}$ fraction. It is important to note that using $FA_{aq.}$ feed is not thermodynamically favoured for the OME synthesis step since it limits the $OME_{3–5}$ yield (maximum of 8 wt% per path yield [$g_{OME_{3–5}}$ $g_{product}^{-1}$] and enhances side product formation.[38,41] Therefore H_2O management in this direct synthesis path is essential (as discussed in previous report by Schmitz et al.,[35] and Arnold et al.[42]). Other reports have also focused on defining system kinetics for example over different catalysts or describing the OME synthesis equilibrium.[36]

In this report a process for a direct synthesis of OME based on MeOH and an anhydrous FA is evaluated. This ap-

proach has the potential to double the $OME_{3–5}$ per path yield, in turn improving the whole process energy and economic efficiency as discussed in our recently reported work.[34] Instead of oxidative dehydrogenation, anhydrous FA is generated in the evaluated process through the catalytic endothermic dehydrogenation of MeOH to yield anhydrous FA and H_2 as the main side product. The reaction takes place at temperatures ≥700 °C to generate appropriate MeOH conversions. Different catalyst systems have been investigated for the this step as reported previously by Su et al.[43] As discussed below, thermodynamically favoured side reactions compete during this endothermic dehydrogenation and therefore a selective catalyst is required, alongside consideration of appropriate reactor design, to achieve selective FA production.[44] However FA yields of ≥70% have been reported with high synthesis efficiency, but the anhydrous FA needs to be handled carefully due to its reactivity and converted directly to the desired end product in a continuous manner, e.g. if a financially attractive process vs. conventional $FA_{aq.}$ production is to be established.[44,45] In the context of OME synthesis where MeOH is a co-reactant with FA, the endothermic MeOH dehydrogenation synthesis path becomes very attractive, as selective anhydrous FA synthesis at partial MeOH conversion is a significant process advantage, e.g. at 50% MeOH conversion and with 95% FA selectivity, the overall process yield is 47.5% which is negative when FA is the end product. Operation of conversion and selectivity to generate a FA/MeOH ratio of ca. 1.9 [mol mol^{-1}] can be considered an optimal feed for the subsequent OME synthesis, and thus control of MeOH dehydrogenation opens the possibility alongside reactor optimisation, of producing an optimal OME synthesis with enhanced overall process efficiency.

In this context, the described process in this report has been simulated using a hybrid model, where all process components are described along with process material and energy demands can be observed and extracted for process evaluation. To the best of our knowledge, synthesis models as reported in the literature have thus predominantly focused on the OME synthesis step from a kinetic or reaction equilibrium perspective.[36,37,40] In this context, the work from Burger et al.[46] and Schmitz et al.[35] regarding process modelling are duly acknowledged regarding steps forward concerning OME synthesis reactors and separation equipment.

Previously we reported on the basic material balance evaluation of the direct OME synthesis based on MeOH and anhydrous FA. Based on these preliminary results and assumptions regarding process energy consumption and ideal product separation, we have been able to define so-called "Key Performance Indicators" (KPIs) for the process (e.g. regarding MeOH demand, cost per tonne $OME_{3–5}$ etc.). On this basis, an approach to OME synthesis is defined, with the main process reaction and separation steps are implemented through a hybrid simulation platform. The hybrid model couples the merits of algorithms available in the commercial software CHEMCAD® together with our own "in-house" developed reactor models as implemented in

This journal is © The Royal Society of Chemistry 2018

React. Chem. Eng., 2018, 3, 676–695 | 677

Matlab®. The model components are described and the methodology of model implementation by developing the interface between the two software programs using "Visual Basic for Applications" (VBA) is also reported. Furthermore, the convergence criteria and methodology of implementation of each simulation component is described. After the process simulation is converged, the process energy integration task is performed using the software PinCH 2.0, where a heat exchange network (HEN) is designed to allow maximum process heat recovery.

As it has been highlighted as a key synthesis step in the described process, the anhydrous FA synthesis is also experimentally investigated using an "in-house" designed and applied annular counter current reactor (ACCR), to validate the endothermic MeOH dehydrogenation reaction. With the model converged for a base case scenario, the process technical and economic metrics are defined. These metrics are presented as KPIs allowing the process evaluation and comparison with other literature processes, highlighting the potential of the presented process. Furthermore, the introduction here and use of our integrated tool which is capable of a robust evaluation of both FA and indeed OME production, represents an innovative approach (as complimented by experimental investigations) and lays the basis for further OME (or indeed anhydrous FA) synthesis progress.

Hybrid process model

Model basis

The process is simulated using the simulation software CHEMCAD® (version 5.2.0) which contains a variety of models for various process units, the possibility to implement user generated models and cost functions for most of the units. For the simulation, the chemical components are selected from the built-in library containing the physiochemical and thermodynamic properties of >1900 components. Additionally, the user can implement self-defined components and property models. As yet, reflecting the novelty of the topic, $OME_{n>1}$, poly(oxymethylene) hemiformals (HF_n) and poly(oxymethylene) glycols (MG_n) are not included in the built-in component library and have thus been added manually based on available literature.[47] Furthermore, a UNIFAC model has been adopted as reported in the literature and implemented to take into account the non-ideal behaviour of the liquid phase of this reaction system.[48–50] For HF_n and MG_n, there are very few properties available in the literature. Therefore, to still use the CHEMCAD® to solve the separation task after the reaction unit, some assumptions had to be made. First, as described by Schmitz et al.,[37] the OME reactions reach equilibrium for MeOH, FA, H_2O, $OME_{1–8}$, $HF_{1–10}$ and $MG_{1–10}$. Second as stated by Hahnenstein et al.,[51] the degradation reactions of HF and MG are slow in comparison to typical residence times in separation equipment. Third, $HF_{n>1}$ and $MG_{n>1}$ stay in the liquid phase. According to Albert et al.[52] there is no experimental evidence for the presence of substantial amounts of MG_n or HF_n in the gas phase.

Therefore, the process considers the equilibrium composition to be achieved in the reactor and further changes so slowly in comparison to the separation residence time that this change can be neglected. Furthermore, $HF_{n>1}$ and $MG_{n>1}$ completely split to the bottom stream. The minimum required properties for the distillation calculation comprise the dependency of vapor pressure on temperature, the dependency of the heat capacity on temperature and for HF_1 and MG_1 the enthalpy of vaporization. Liu et al.[53] published a physicochemical model for VLE in mixtures of FA with MeOH and FA with H_2O. From this model heat capacities for $HF_{1–10}$ and $MG_{1–10}$ could be extracted. However, since the considered temperature range of 323 to 363 K for FA aqueous solution and 312 to 347 K for FA methanolic solution is comparatively small to the temperatures reached in the distillation unit, the extrapolation of these relations led partially to negative heat capacities. Therefore, the heat capacities of $HF_{n>1}$ and $MG_{n>1}$ have been assumed to be equal to the heat capacity of the corresponding OME, whereby the heat capacity of $HF_{9–10}$ and $MG_{9–10}$ has been assumed to be equal to OME_8. The extracted relations for HF_1 and MG_1 were used, since they will mainly stay in the vapor phase and therefore exposed much smaller temperatures in the distillation separation units. Albert et al.[52] furthermore published relations for the vapor pressure depending on temperature for HF_1 and MG_1 for the temperature range of 293 to 413 K. Nonetheless, for $HF_{n>1}$ and $MG_{n>1}$ no vapor pressure relations could be found. But since they are assumed to stay in the liquid phase their vapor pressure has been assumed to be equal to the vapor pressure of OME_8.

Together with the component properties, global thermodynamic packages should be specified to define and unify the model basis for the simulation. For the definition of the K-value estimation the UNIFAC package was selected, since it was specifically implemented in the component properties, while the enthalpy is defined using the latent heat package, which was recommended by CHEMCAD® in combination with UNIFAC. Additionally, single unit operations thermodynamic packages could be assigned when it is more convenient.

Several assumptions and basis were selected on the global model level for a successful model convergence. The following points summarise the most prominent of these considerations:

1. Model basis of a production capacity of ca. 35 kt per annum $OME_{3–5}$.

2. N_2 is used as a carrier gas for the MeOH feed stream. After the MeOH endothermic dehydrogenation reaction, the product stream (Fig. 1 – Stream 207) containing FA, MeOH, CO, H_2 and N_2 is absorbed in the recycle stream (Fig. 1 – Stream 321) where FA and MeOH are separated. The gaseous components N_2, H_2 and traces of CO (<0.3 vol% of stream 209) are separated conceptually as follows: H_2 and N_2 are separated using membrane technology[54] and N_2 and CO are recycled. A portion of this recycle stream (Fig. 1 – Stream 211) is purged and new make-up N_2 is introduced (0.5 vol% volume is assumed and considered in the production cost
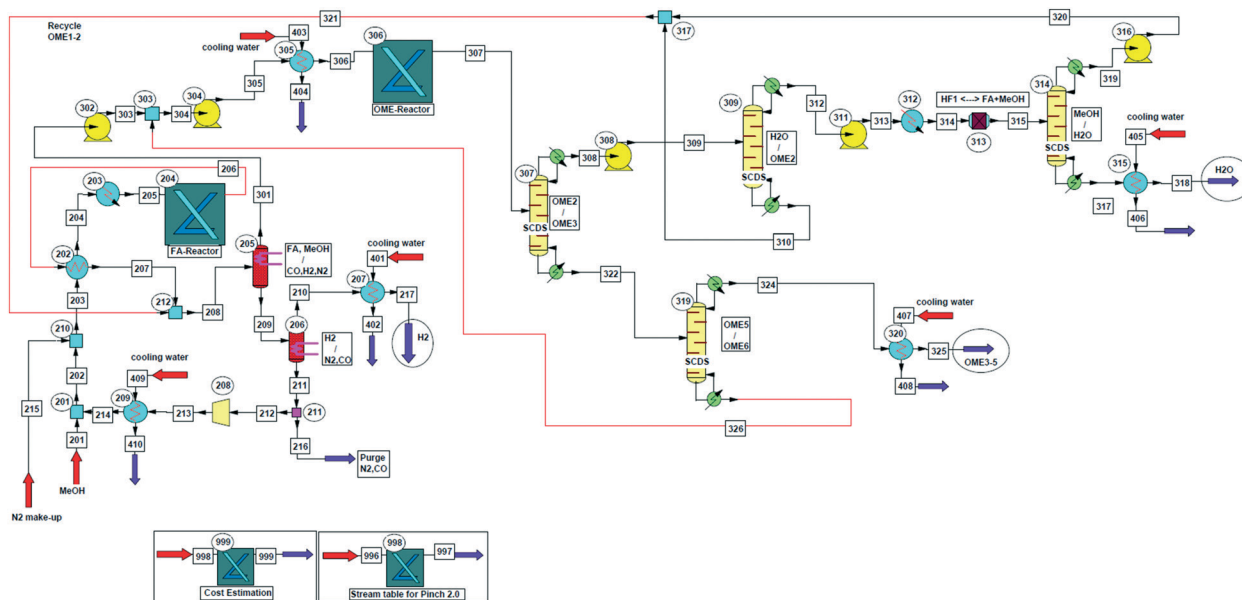
Fig. 1 Hybrid process model flow diagram as implemented in CHEMCAD®.

assessment). These steps are considered using the mixer unit (Fig. 1 – Unit 212) and the ideal separation equipment (Fig. 1 – Units 205 and 206). The energy required for performing these tasks is not considered in the evaluated KPIs.

3. The endothermic dehydrogenation of MeOH is performed through a kinetic reactor (Fig. 1 – Unit 204) operating at a certain residence time to yield the desired FA/MeOH molar ratio.

4. The OME synthesis reaction proceeds to equilibrium and occurs only in the liquid phase (Fig. 1 – Unit 306).

5. Concerning distillation equipment, the gas phase is considered as ideal gas while non-ideal behaviour in the liquid phase is considered using a UNIFAC model to calculate activity coefficients.

6. Distillation units are assumed to reach phase equilibrium on every stage.

7. Since no satisfying vapour pressures for $MG_{n>1}$ and $HF_{n>1}$ are available in the literature, low vapour pressure values (from OME_8) are assigned for these components. The heat capacities of $HF_{n>1}$ and $MG_{n>1}$ have been assumed to be equal to the heat capacity of the corresponding OME, whereby the heat capacity of HF_{9-10} and MG_{9-10} has been assumed to be equal to OME_8. Generally physical property model for these unstable intermediates is lacking.

8. A pressure drop of 340 mbar (ref. 55) is considered for a heat exchanger, 6.9 mbar (ref. 55) per distillation stage, 345 mbar (ref. 56) for the condenser and 100 mbar for reactor units.[57] Pumps and compressors are included in the process design to account for this pressure drop.

Process description

The OME synthesis described here based on MeOH as a single educt has been divided for clarity into two main sub-

process steps (Fig. 1), namely: FA synthesis (Fig. 1 – No. 200) and OME synthesis (Fig. 1 – No. 300). The FA synthesis sub-process starts with the saturation of MeOH in N_2 as carrier gas (Fig. 1 – Mixer, Unit 201) where the feed concentration is defined. This feed (Fig. 1 – Stream 203) is preheated *via* a heat exchanger (Fig. 1 – Unit 202) which recovers the heat from the product (Fig. 1 – Stream 206) to the feed ($T = 670$ °C) of the FA reactor (Fig. 1 – Unit 204). The feed is then heated up to the reaction temperature of 690 °C in a high temperature trim heater (supplied by natural gas; Fig. 1 – Unit 203) before being introduced to the FA reactor. In the reactor the endothermic catalytic dehydrogenation of MeOH takes place (reactions (1)–(3)).[44]
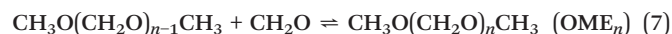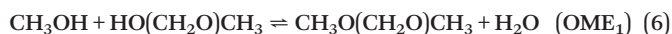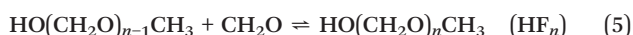
$$CH_3OH \rightleftharpoons CH_2O + H_2 \quad \Delta H_R^{298} = +85 \text{ kJ mol}^{-1} \quad (1)$$

In addition secondary competing reactions occur:[43]

$$CH_3OH \rightleftharpoons CO + 2H_2 \quad \Delta H_R^{298} = +105 \text{ kJ mol}^{-1} \quad (2)$$

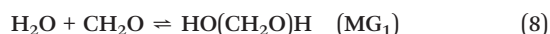$$CH_3OH \rightleftharpoons C + H_2O + H_2 \quad \Delta H_R^{298} = -31 \text{ kJ mol}^{-1} \quad (3)$$

Next to the competing reactions, FA is thermodynamically unstable and can react further to more thermodynamically favoured products including HCOOH, CH_4, CO and CO_2.[43] Therefore, the reaction temperature should be sufficiently high, an effective, selective and active catalyst should be used, the residence time in the reactor should be as short as possible to minimize further conversion of FA and the product (Fig. 1 – Stream 206) needs to be quenched as fast as possible to limit FA decomposition.[43] This reaction step is simulated using a kinetic reactor model which is implemented in Matlab® and coupled *via* an Excel® unit using VBA (as elaborated in more detail later in this article).

After the first reaction step, the product stream (Fig. 1 – Stream 207) is mixed with the recycle stream (Fig. 1 – Stream 321) and separated using a component separator (Fig. 1 – Unit 205) from CHEMCAD®, where FA, MeOH and recycled components in stream 321 are directed towards the OME synthesis sub-process (Fig. 1 – Stream 301), the side products H_2 is exiting the process (Fig. 1 – Stream 217) and the carrier gas N_2 with the side product CO (Fig. 1 – Stream 211) are separated as explained in the model basis and recycled using an isotropic compressor with an efficiency of 75% to close the loop and be saturated again with MeOH (Fig. 1).

OME synthesis starts with mixing the MeOH dehydrogenation production stream with the recycle stream (Fig. 1 – Stream 326) – constituting of $OME_{n>5}$, HF_n and MG_n – before being cooled to the reaction temperature of 50 °C (Fig. 1 – Unit 305) and entering the OME reactor (Fig. 1 – Unit 306). In this reactor FA and MeOH are converted to OME through simultaneous oligomerisation, addition and condensation reactions as reported previously.[38] The major contributing reactions are summarised here:[36,38]

$$CH_3OH + CH_2O \rightleftharpoons HO(CH_2O)CH_3 \quad (HF_1) \tag{4}$$

$$HO(CH_2O)_{n-1}CH_3 + CH_2O \rightleftharpoons HO(CH_2O)_nCH_3 \quad (HF_n) \tag{5}$$

$$CH_3OH + HO(CH_2O)CH_3 \rightleftharpoons CH_3O(CH_2O)CH_3 + H_2O \quad (OME_1) \tag{6}$$

$$CH_3O(CH_2O)_{n-1}CH_3 + CH_2O \rightleftharpoons CH_3O(CH_2O)_nCH_3 \quad (OME_n) \tag{7}$$

These are equilibrium reactions strongly depending on the concentration of FA, with higher concentrations promoting longer chain oligomer formation.[32] The OME formation reactions are slightly exothermic reactions (ΔH_R^{298} = −25.2 kJ mol^{-1}) and take place at mild conditions (T = 50–90 °C), the temperature is not significantly influencing the reaction system.[38] The presence of FA and H_2O leads to further competing reactions:[34]

$$H_2O + CH_2O \rightleftharpoons HO(CH_2O)H \quad (MG_1) \tag{8}$$

$$HO(CH_2O)_{n-1}H + CH_2O \rightleftharpoons HO(CH_2O)_nH \quad (MG_n) \tag{9}$$

For the reaction model of the OME synthesis, MG_n and HF_n (reactions (5) and (9)) have been considered for chain lengths up to $n = 10$, while OME_n are considered until $n = 8$ as assumed previously by Schmitz et al.[38] The reaction steps have been simulated using an isothermal equilibrium reactor model, as implemented through Matlab® and interfaced to CHEMCAD® via an Excel® unit using VBA. Due to the presence of an acidic catalyst further side reactions are possible where CH_3OCH_3, $HCOOCH_3$ or $(CH_2O)_3$ can be formed. Therefore, the choice of the catalyst system and reaction conditions can significantly suppress secondary reactions and avoid side product formation in this equilibrium system, thus side products have not been considered in the OME reactor.

Following OME synthesis, the product stream (Fig. 1 – Stream 307) is separated as follows: the desired product $OME_{3–5}$ (Fig. 1 – Stream 325), a second by-product stream mainly containing H_2O (Fig. 1 – Stream 318) and the recycled streams (Fig. 1 – Streams 321 and 326) containing the rest of the components are brought back to the OME synthesis reactor. This separation is mainly performed through four distillation columns. The first column (Fig. 1 – Unit 307) splits the stream between OME_2 as light component and OME_3 as heavy component on 22 stages and a reflux ratio of 1. Therefore, $OME_{1–2}$, unreacted MeOH and FA, H_2O, HF_1 and MG_1 are leaving the column in the distillate (Fig. 1 – Stream 308) at ca. 79 °C while $OME_{n>2}$, $HF_{n>1}$ and $MG_{n>1}$ are withdrawn from the bottom (Fig. 1 – Stream 322) at ca. 264 °C. As a result about 99.99% of OME_2 of the feed and 0.02% of OME_3 of the feed are leaving the column in the distillate which is purified from H_2O in two additional columns. For this purification other process units like adsorption or membrane could lead to significant production cost reductions, however, this is still under investigation.[35] The second column (Fig. 1 – Unit 309) splits the stream between H_2O as the light component and OME_2 as the heavy component on 80 stages and a reflux ratio of 4. Due to the small difference in vapour pressure between H_2O, HF_1 and OME_2 a thermal separation is CAPEX and energy intensive. H_2O, MeOH, FA, OME_1, and HF_1 are leaving as distillate at ca. 53 °C while OME_2 and HF_1 are leaving the column in the bottom at ca. 126 °C. As a result ca. 99.99% of H_2O, 50.89% HF_1 and 1.02% of OME_2 of the feed are leaving the column in the distillate. Before the MeOH and H_2O separation column (Fig. 1 – Unit 314), the rest of the unstable HF_1 in stream 314 is heated (Fig. 1 – Unit 312) and thermally dissociated in equilibrium reactor (Fig. 1 – Unit 313) to its forming components MeOH and FA (reaction (4)). This takes place at long residence time without a catalyst according to equilibrium relations as described by Hahnsteinet al.[51,58] This decomposition at this stage is essential to allow the separation of water. Stream 315 composed mainly of OME_1, MeOH, FA and H_2O is directed to the third column (Fig. 1 – Unit 314) splitting the stream between MeOH as the light component and H_2O as the heavy component on 21 stages and a reflux ratio of 1. MeOH, FA and OME_1 are leaving as distillate at ca. 12.9 °C and are mixed with the separated OME_2 (Fig. 1 – Unit 317) while H_2O is leaving the column in the bottom at ca. 107 °C. As a result ca. 98.93% of MeOH of the feed is leaving the column in the distillate.

The fourth column (Fig. 1 – Unit 319) splits the stream between OME_5 as the light component and OME_6 as the heavy component on 40 stages and a reflux ratio of 7. $OME_{3–5}$ are leaving as distillate at ca. 173 °C while $OME_{n>6}$, $HF_{n>1}$ and $MG_{n>1}$ are leaving the column in the bottom at ca. 352.5 °C. As a result ca. 95% of OME_5 of the feed is leaving the column in the distillate. After the separation all components (Fig. 1 – Streams 321 and 326) other than $OME_{3–5}$ and H_2O are recycled back to the OME reactor to be converted to the desired $OME_{3–5}$.

Description of the process model components

The description of each model component and convergence methodology is specified in the following:

Endothermic FA synthesis reactor. From our previous reported works, which have focused on modelling of the OME reaction equilibria, the composition ratio of FA/MeOH was optimised to obtain the highest OME_{3-5} product yield possible. This was narrowed and established to lie between 1.8–2 [mol mol^{-1}].[34] This was defined as the target performance for the anhydrous FA synthesis reactor. As discussed earlier, the mechanism of endothermic MeOH dehydrogenation, secondary side reactions are thermodynamically favoured, thus making overall reaction modelling a kinetic challenge. Kinetic reactor models in CHEMCAD® require the definition of the reaction rate constant k_j of each reaction j as a function of temperature. In this work, a Na_2CO_3 catalyst was used, whilst the kinetic data for this reaction was not available in literature. To establish kinetic data, three main reactions are considered. k_j values for the main contributing reactions (reaction (1) and (2)) were evaluated experimentally at T = 690 °C using an annular counter current reactor as explained in Catalyst choice and reactor design. k_j for the MeOH pyrolysis to carbon (reaction (3)) was evaluated from previously published experimental results over a similar catalyst system.[59] In this report and based on experimental and available literature data, a global kinetic model was implemented to describe this synthesis step. An ideal plug flow reactor model was adopted with the following assumptions:

1. Irreversibility of the considered reactions.
2. Constant gas density.
3. Quasi-isothermal operation.

The generic equation for the reaction rate r_j for the consumption of a reactant A (here MeOH) in a reaction j is:[60]

$$-r_j = \frac{-\mathrm{d}C_A}{\mathrm{d}t} = k_j C_{A_j}^{n_i} \tag{10}$$

Thereby C_A is the concentration in [mol m^{-3}], t the time in [s], n_i the order of the reaction and i the component counter. For parallel simultaneous reactions based on the same feed A, the concentration of a component i at certain time can thus be evaluated as follows:

$$C_i = \frac{r_j}{\sum r_j}\left(C_{A_0} - C_A\right) \tag{11}$$

Assuming constant gas density, the following equation applies for plug flow reactors:[60]

$$\tau = \frac{V}{\dot{V}} = C_{A_0}\int_0^{X_A}\frac{\mathrm{d}X_A}{-r_A} = \int_{C_{A_0}}^{C_A}\frac{\mathrm{d}C_A}{-r_A} \tag{12}$$

Thereby τ is the residence time in [s], V the volume of the reactor in [m^3], $\dot{V}$ the volume flow in [m^3 s^{-1}], X the mol fraction in and the index 0 represents the initial time. MeOH dehydrogenation tests were carried out at same test parameters

with varying the residence time. By plotting the concentration of MeOH corresponding to each product in the considered reactions (FA and CO) against the residence time, the reaction orders could be defined and k_j values are evaluated (Fig. S1 and S2†).

Table 1 summarises the reaction order and k_j values for reaction (1)–(3) at T = 690 °C.

With defined reaction orders, the total rate equation results in:

$$-\sum r_j = k_1 C_A + k_2 + k_3 C_A \tag{13}$$

Substituting in eqn (12) followed by integration, the kinetic equation results as:

$$\tau = \frac{\ln\left(\frac{(k_1 + k_3)C_{A_0} + k_2}{(k_1 + k_3)C_A + k_2}\right)}{k_1 + k_3} \tag{14}$$

The equation system is implemented through Matlab® whereby at a certain feed concentration C_{A_0} and given residence time, the concentration of each component C_i in the product stream can be evaluated. An exemplary result at a given initial [MeOH] feed has been provided (Fig. S3†). The conversion of MeOH and the corresponding selectivity to FA have also been evaluated at each τ (Fig. S4†). For the convergence of the whole process model, τ was selected to achieve the desired FA/MeOH mole ratio. The results were in turn added to CHEMCAD® using an Excel® unit interface.

Equilibrium OME synthesis reactor. The routine for chemical reaction equilibrium calculations using the available reactor modules in CHEMCAD® requires currently unavailable information *i.e.* for the OME components and side products. In addition, to the standard G_f (Gibbs reactor) or equilibrium constant K_{eq} as a function of T for pre-defined reactions (equilibrium reactor module), UNIFAC parameters to consider the non-ideal nature of the liquid phase, reaction conditions (P,T), the reactor operating mode isothermal or adiabatic and the saturation pressure of each component, the routine also requires the standard enthalpy and entropy of formation for each component in order to solve simultaneously the energy balance and the phase equilibria of each stream. The equilibrium reactor model of CHEMCAD® only considers up to 20 simultaneous reactions which is not sufficient for the previously mentioned reaction system, while the Gibbs reactor model requires the heat capacity of the components in addition to standard enthalpies and entropies of

Table 1 Reaction orders and k_j values for the considered reactions in the kinetic FA reactor model

Reaction	Reaction order	k_j	Rate equation
1	1	6.94	$C_A = C_{A_0}e^{-k\tau}C_A$
2	0	0.291	$C_A = K\tau + C_{A_0}$
3	1	0.000066	$C_A = C_{A_0}e^{-k\tau}$

This journal is © The Royal Society of Chemistry 2018

React. Chem. Eng., 2018, **3**, 676–695 | **681**

formation to evaluate the standard Gibbs energy of the components at given P and T. These are unfortunately currently not available. Estimations of the missing properties using UNIFAC, Joback or CHETAH 9.0 ASTM thermodynamic calculator software did not yield satisfactory results relative to experimental values (Fig. S5†). This comparison shows the chemical equilibrium compositions of experimental results from Schmitz et al.[38] against the simulation results obtained from our previous report regarding the convergence of an OME reaction equilibrium, based on a Gibbs energy minimisation approach with the aid of an stochastic global optimizer (SGO) reactor model and the CHEMCAD® Gibbs and equilibrium reactors modules at $T = 348$ K, $P = 2$ bar and a feed molar composition of FA/MeOH = 0.89 and H2O/MeOH = 0.54.[34]

The SGO shows good agreement with the equilibrium compositions from the experimental results with a mean error of 0.01, while the results from the CHEMCAD® Gibbs and equilibrium reactors reach mean errors of 0.07 and 0.08 in mass fraction, respectively and with quite different components equilibrium composition distribution. However, the known reaction equilibrium constants as a function of T are defined experimentally and accordingly the Gibbs energy can be evaluated. The calculation method described in our previous report can therefore shortcut the equilibrium evaluation importantly whilst providing good accuracy, based on experimental values and consideration of activity-based relations.[34] Accordingly, integrating our reactor equilibrium calculation module in the CHEMCAD® platform was imperative.

In our previous work we discussed the OME synthesis reaction equilibrium system in single and multiphase.[34,41] The equilibrium model applied a non-stoichiometric Gibbs minimisation (NSGM) approach with a SGO solver to converge the complex OME multicomponent reaction equilibrium. The merits of this algorithm for the complex reaction system was further validated against literature and own experimental results for different feed systems:[34]

$$G^{\mathrm{t}} = \sum_i^N n_i G_i^0 + RT \sum_i^N n_i \ln X_i \gamma_i \qquad (15)$$

Where G^{t} = total Gibbs free energy, N = number of species present in the reacting mixture, n_i = number of moles of component i, R = gas constant, T = temperature, X_i = molar fraction in the liquid phase, γ_i = activity coefficient of component i in the liquid phase and the index 0 refers to the standard state. The non-ideality in the liquid phase is accounted by considering activity based chemical equilibrium constants and using the UNIFAC method for evaluating the activity coefficients.[34]

A Microsoft Excel®-based unit was developed to include the reaction code developed in Matlab® using the NSGM reaction model.[34] In this context, Microsoft Excel® offers the possibility to open and run a Matlab® code *via* the use of a VBA add-on, as well as exchanging matrices and single values, as long as both programs are installed within the same operating system. The extracted results from Matlab® using VBA can be translated and introduced in the CHEMCAD® platform. The development of the VBA unit is significant as it enables a "hybrid" combination of CHEMCAD® functionality and the flexibility and calculation speed of Matlab®. Running the Matlab® code through the VBA node does not alter the results as long as the input/output variables (as defined in each platform) are translated correctly *via* VBA. Calculations using the VBA node as interfaced between the two software platforms require additional computational time (*i.e. vs.* those performed with Matlab® directly).

Rigorous distillation units. For the simulation of the distillation columns the SCDS distillation column unit – following the MESH equations – was selected with the assumption of reaching equilibrium on every tray. The simultaneous (SC) method, (*i.e.* the Naphtali–Sandholm method),[61] was applied for the final simulation. This method is used by a range of simulation software and is better suited for non-ideal mixtures than other global Newton methods.[55] To define the initial parameters for the SCDS algorithm, the shortcut column (SHOR) unit using Fenske–Underwood–Gilliland method was applied. The algorithm generally simplifies the separation problem to a binary system of the light and heavy key component. The light key component was specified as the more volatile component of the two components between whom the column splits the stream with the assumption that *ca.* 99.9% of the amount in the feed stream are leaving the column in the distillate. The heavy key component was specified as the less volatile component with the assumption that *ca.* 0.1% is leaving the column in distillate. The distribution of the non-key components is determined according to this specification.[62] Furthermore, to determine the number of stages and the reflux ratio a minimum reflux $R/R_{\mathrm{min}} = 1.3$ was selected.[56] For the SHOR algorithm no pressure drop was assumed. The estimated column properties have been used as an initial definition of the SCDS parameters. Additionally the specification of the condenser and reboiler mode is required. To find a point of convergence those modes have been specified with the definition of the condenser and reboiler duty, respectively. The parameters to reach the separation target of the columns were narrowed and defined by varying the reflux ratio at the condenser mode and the bottom temperature for the reboiler mode. In every convergence step, the energy and mass balances were checked to monitor the state of convergence.

The SCDS columns have been defined and specified in order of their position in the flow sheet (Fig. 1). Therefore, the exit stream of the OME reactor, defined by the Matlab® simulation considering a perfectly sharp separation and recycle, was used as the first feed stream for the first column (Fig. 1 – Unit 307). The required parameters of this column to fulfil the separation task have been pre-estimated using the SHOR unit and adjusted in the SCDS unit until convergence and separation task were achieved. Distillate (Fig. 1 – Stream 308)

682 | *React. Chem. Eng.*, 2018, **3**, 676–695

This journal is © The Royal Society of Chemistry 2018

and bottom (Fig. 1 – Stream 322) were used as feed streams for the following columns and the same procedure was applied to reach convergence and achieve the separation task until the two product streams (Fig. 1 – Stream 318 and 325) containing mainly H_2O and OME_{3-5}, respectively were separated. The other components were recycled to the OME reactor and the loop of adjusting the parameters of the SCDS columns continued until the process converged and steady state was reached.

Auxillaries. Auxillary units where implemented to simulate heat exchange between streams and to compensate the pressure drop of reactors and separation units. Counter current heat exchangers were used with the *U*-value defined according to Towler *et al.* as computed by CHEMCAD®.[63] Pressure regulating units (pumps, compressors and throttles) are specified according the desired outlet stream pressure and for the centrifugal compressor an efficiency of 75% was assumed, while the centrifugal pumps have an efficiency of 60%. These efficiency figures were defined according to practical data and CHEMCAD® recommendations.[57,64]

Methodology for process model convergence

Through CHEMCAD® the physico-chemical and thermodynamic properties of the considered components were implemented based on the component library. The reactor models (FA synthesis and OME synthesis) were implemented through the Matlab®/CHEMCAD®/Excel®-VBA hybrid platform. The product purification is conducted using a series of distillation columns which are simulated using a rigorous SC distillation algorithm which is implemented in the SCDS unit in CHEMCAD®. Due to the consideration of pressure drop, the implementation of pumps, compressors and throttles was necessary and the according CHEMCAD® library units were used.

The process model considers recycle of non-product components, therefore the Matlab® reactor models and distillation units were solved interactively during the first loops to reach convergence for the whole process simulation. Since the FA synthesis sub-process does not contain recycles with changing composition or enthalpies, this process was specified according to the FA/MeOH ratio of 1.9 [mol mol^{-1}] as a first step of the model convergence. This stream was then introduced to the OME reactor model were equilibrium composition was calculated. The product stream of this model was implemented in Matlab® considering perfectly sharp separations of OME_{3-5} and H_2O and the recycle of non-product components. After this simulation had reached convergence and therefore a steady state, the OME reactor exit stream was used as the tear stream and implemented in the CHEMCAD® model. This stream was defined as the feed stream for the first column to split the stream between OME_2 as the light component and OME_3 as the heavy component. For the first estimation of necessary column parameters the SHOR unit from CHEMCAD® was used and the results implemented in the rigorous SCDS column. For the

first point of convergence using the SCDS model the condenser and reboiler duties, specified by the SHOR model, were set. Afterwards, the associated reflux ratio and bottom temperature were set and adjusted to fulfil the separation task and reach convergence. The same procedure was applied to the other three columns. At this stage, the product streams were separated and the recycle streams were brought back to the OME reactor model interfaced with the Excel® unit in CHEMCAD®. This model was set to a single reaction pass and the exit stream was again implemented in the first distillation column and its parameters adjusted to fulfil the separation task and obtain convergence. This loop was conducted manually until the parameters of the columns got stable. Afterwards the loop was set to run automatically until the convergence criteria of 10^{-3} for flow rates, *T*, *P*, vapour fraction and enthalpy of the tear stream was reached.

After completion of the process simulation/convergence, integration of the process heat was conducted using the software PinCH 2.0. The process flowsheet was updated accordingly and the convergence loop repeated.

Methodology for process heat integration

The PinCH 2.0 software platform was used to generate a HEN according to specified streams (*e.g.* based on specified initial and final temperatures which define the stream as a hot or a cold stream), duties, a constant heat capacity C_p or specific enthalpy of vaporisation, a heat transfer coefficient and the pressure level. If a phase change occurs during the heat exchange, the user can split the stream in various segments and define both – *e.g.* parts with temperature differences and parts for the phase change. In this study, these phase changes were computed using CHEMCAD® and an associated VBA code. A constant heat capacity can be extracted using the temperature difference, the corresponding enthalpy difference and the mass flow. However, if a phase change occurs during the heat exchange its consideration is beneficial regarding the pinch point temperature. Therefore, after defining the initial and final enthalpy of the stream according to the respective temperatures, the considered stream is checked regarding the occurrence of a phase change. Since most of the considered streams are mixtures of various components a phase change occurs over a temperature range. If the phase does not change, the heat capacity is calculated for various points over the considered temperature range, the average C_p of these points is estimated and the deviation of each point is checked.

If the phase changes, the vaporisation enthalpy is extracted based on a CHEMCAD® function, where an isothermal change is assumed. If the stream is cooled or heated beyond the phase change another segment is defined which contains the average heat capacity up till the final temperature. Therefore, a stream which changes its phase and is additionally heated or cooled beyond the phase change, is split into several segments whereby representing the latent and

This journal is © The Royal Society of Chemistry 2018

React. Chem. Eng., 2018, **3**, 676–695 | 683

sensible heat intervals. Heat transfer coefficients were computed according to Towler *et al.*[63] as calculated in CHEMCAD®. Mass flow and pressure level were extracted from CHEMCAD®.

After the definition of the process streams, the utility streams were also defined. Cooling water at 25 °C with an increase of an additional 10 °C was defined as the cold utility and steam at 80 bar was assumed as the hot utility. Since CHEMCAD® does not include the option to integrate the heat of a stream in the reboiler or condenser of a column, the integration of the condenser and reboiler duties with the process streams was done manually by considering the required heat duties and temperature levels at minimum pinch temperature difference of *ca.* 20 °C (*e.g.* Fig. 2 – units 324 and 327). Streams 205, 208, 211, 212, 307, 309, 310, 317, 322, 325 and 326 (Fig. 1) were considered for the heat integration, resulting in the issuing of a composite and grand composite curve (Fig. S6†). The Pinch temperature was defined as 88.6 °C and the recommended minimum temperature difference for the heat exchangers was 20.17 °C (please see the designed HEN in Fig. S7†). The HEN was implemented in the hybrid platform using nine heat exchangers (Fig. 2).

Experimental – anhydrous FA synthesis

Experimental fundamentals

Methanol (ROTISLOV®, purity >99.9 wt%) was purchased from Carl Roth GmBH. Anhydrous sodium sulphite (Na_2SO_3; Bioultra grade, purity ≥98 wt%) and 1.0M $HCl_{aq.}$ (Fluka standard grade solution) were purchased from Sigma Aldrich. All chemicals were used without further purification. CO, CO_2, H_2 and N_2 calibration mixtures, CH_4 in N_2 calibration mixtures and DME 3.0 (purity >99.9 vol%) gas cylinders were purchased from Linde AG. N_2 6.0 and Ar 5.0 were supplied from in-house supply lines. Sodium carbonate (Na_2CO_3, purity >99.9 wt%) from VWR Chemicals was used to produce the anhydrous formaldehyde synthesis catalyst. Na_2CO_3 (3 g) was pressed into a tablet (diameter 2.5 cm) with 15 tons of pressure. The tablet was then carefully crushed in a mortar and sieved into the desired fraction (630–800 μm). The particles obtained were placed in the formaldehyde synthesis reactor without further treatment.

Two Gas Chromatography (GC) devices equipped with thermal conductivity detectors (GC-TCD) were employed for the product analysis. An Agilent 6890A GC with a CP-SIL5CB (30 m × 8 μm) capillary column was employed for the quantitative analysis of FA and MeOH. Samples were analysed using He as the carrier gas, an oven temperature 100 °C, and a column pressure of 35 psi. Another Agilent 7890 A GC with a poraplot Q (30 m × 530 μm × 20 μm) capillary column was used for the analysis of the rest of the product mixture other than H_2. He was used as the carrier gas for the front detector. Carrier gas flow (flow: 4 mL min^{-1} at *ca.* 36 psi). A packed porapack Q column (0.91 m × 3 mm and Mesh 80/100) followed by a molsieve (30 × 530 μm × 25 μm) capillary column were used for the H_2 separation before being introduced to the back detector. N_2 was used as the carrier gas (flow: 26.6 mL min^{-1} at *ca.* 35 psi). The GC inlet temperature was set at 200 °C and operated in split mode (split ratio = 2). Chromatograms were obtained using a programmed oven temperature ramp (*i.e.* 70 to 150 then back to 70 °C, over 11 min). An ABB gas analyser (GA) with a Caldos 17 and Uras 14 modules was used for the online detection of H_2, CO, CO_2 and CH_4.

All mass flow controllers were calibrated using mass flow meter range check device setup (Bronkhorst). MeOH and

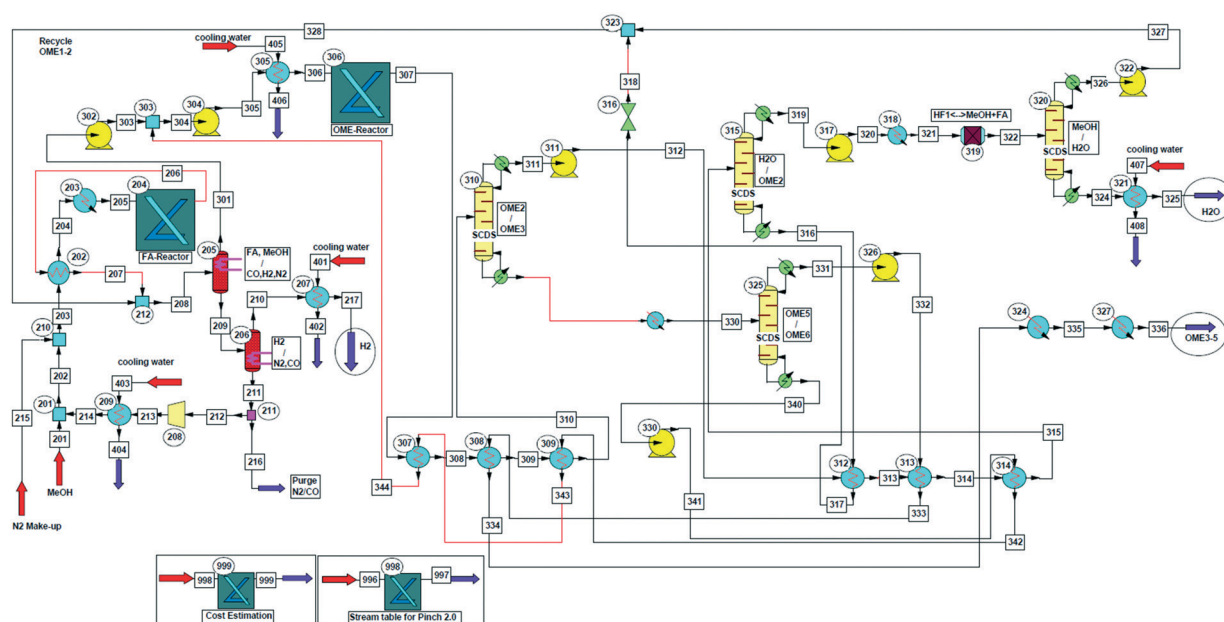**Fig. 2** Hybrid simulation platform for the production of OME$_{3-5}$ from MeOH *via* FA in CHEMCAD®, heat integrated using PinCH 2.0.

684 | *React. Chem. Eng.*, 2018, **3**, 676–695

This journal is © The Royal Society of Chemistry 2018

H_2O were calibrated *via* saturation in carrier gas at nominal operating volumetric flow rate and exact saturation T and P. CO, CO_2, CH_4 and H_2 were calibrated using standard calibration gas mixtures. DME was calibrated by mixing several concentrations with N_2 using MFCs. FA was calibrated based on a Na_2SO_3 volumetric titration method, using 1 M $HCl_{aq.}$ as titre and thymolphtalein as indicator.[65]

All T, P, flow rates and GA readings are monitored and controlled using a LabVIEW program. Extracted results and data from GCs, GA and Labview program are evaluated using a developed Excel® program with data extraction *via* VBA tool. The selectivity of FA and the conversion of MeOH are evaluated as follows:

$$U_{MeOH} = \frac{n_{MeOH_i} - n_{MeOH_0}}{n_{MeOH_i}} \qquad (16)$$

$$S_{FA} = \frac{n_{FA_0}}{n_{MeOH_i} - n_{MeOH_0}} \qquad (17)$$

where n_{MeOH_i} is the number of moles of MeOH in the feed gas, n_{MeOH_0} is the number of moles of MeOH in the product gas, n_{FA} is the number of FA moles in the product.

The gas hourly space velocity (GHSV) is calculated as follows:

$$GHSV = \dot{V}/V \qquad (18)$$

where V is the bulk volume of the catalyst in [L], $\dot{V}$ is the volume flow in [L STP h^{-1}].

Reaction conditions were based on the results from Su *et al.* over similar catalyst system.[43] Reaction temperature of 690 °C, MeOH feed concentration of 5–6 vol%, pressure of 1.05–1.15 bar and Na_2CO_3 with particle size of 830–600 µm were fixed as basis testing parameters. Parameters were selected after several pre-tests. GHSV could be varied by changing the carrier gas flow or varying the catalyst bed length.

Catalyst choice and reactor design

The endothermic MeOH dehydrogenation has been discussed in previous literature reports, for example over different catalysts and/or reactor types.[46,47,63] As discussed in these reports, the typical aim was to produce pure anhydrous FA or derivatives such as para formaldehyde (pFA) or trioxane in high yield (*e.g.* as precursors for polyacetal production).[44] Typically this dehydrogenation reaction occurs at elevated temperatures ≥700 °C to achieve reasonable conversion of MeOH.[45] However, such temperatures promote MeOH pyrolysis and thermodynamically favoured production of CO and H_2 (reaction (2)). Therefore this reaction is kinetically controlled whereby a selective catalyst and reactor design are required for a satisfactory anhydrous FA yield.[44] In this context, the following are identified as key prerequisites to achieve this, namely (a) a fast heating of

educts to avoid pyrolysis of MeOH, (b) a fast reaction over the catalytic species (*e.g.* residence times ≤0.01 s),[45] (c) a fast quenching of products to avoid further conversion of the thermodynamically unstable FA to CO and H_2 and (d) the maintenance of a stream containing the FA product in a stable temperature range (*e.g.* between 100–150 °C) to avoid FA from polymerisation.[44,45]

Regarding catalyst choice, Su *et al.* have investigated endothermic MeOH dehydrogenation over Na_2CO_3 through a packed bed reactor at T = 690 °C, resulting in an FA selectivity (S_{FA}) of 84% and MeOH conversion (U_{MeOH}) of 54%.[43] Zaza *et al.* have investigated the same catalyst but using a circulating fluidised bed reactor, leading to S_{FA} = 80% at less than 20% U_{MeOH}.[46,64] Sauer *et al.* investigated this reaction in a tube wall reactor using a $NaAlO_2$ catalyst and at T ≤900 °C. Almost 100% U_{MeOH} was achieved over this system with S_{FA} of *ca.* 70%.[44] Schweers *et al.* introduced a homogeneous reaction concept where the catalyst active species Na (from NaOH, or Na_2C_2) was evaporated in super-heated circulating gas (consists mainly of H_2 and CO or N_2) and introduced with MeOH vapour to a reaction zone where dehydrogenation reaction took place over the range T = 600–800 °C. FA yield was reported as ≥60%.[66] Based on this information, and indeed regarding cost, sustainability and ease of synthesis, Na_2CO_3 was selected as an exemplary catalyst in this investigation.

Regarding reactor design, from the reported literature and our first experimental investigations, selective anhydrous FA synthesis through tubular packed bed reactors has been identified as a challenge.[67] For example carbon formation in pre-catalytic zone due to pyrolysis of MeOH is typically observed, resulting in turn in low FA selectivity. Furthermore, with increasing reaction T, selectivity towards CO formation also increases. Therefore, to overcome these challenges, and in an attempt to fulfil the aforementioned key prerequisites, a new reactor design concept was developed (Fig. 3). This initial lab-scale design is defined as an "Annular Counter Current Reactor"(ACCR), constructed from quartz glass (*e.g.* to observe any decomposition/deposition processes) and was conceptualised with the aim of achieving a selective and stable anhydrous FA synthesis. The ACCR was designed to allow testing of different catalyst systems over a wide range of Gas Hourly Space Velocities GHSV (5000–35 000 h^{-1}) and T. The reactor was integrated in a continuous flow test stand (Fig. S8†). MeOH was fed to the reactor in a saturated inert carrier gas at the identified pre-catalytic zones (1, 2 and 3; Fig. 3b). These zones were designed to minimise the residence time of the feed gas before it reached the catalyst surface (*e.g.* to reduce/avoid undesired MeOH pyrolysis). A residence time of ≤0.05 s was identified as desirable in this zone *i.e.* based on preliminary testing in tubular reactor. The dehydrogenation reaction initiates and proceeds through the catalyst bed (zone 4), where short residence times over Na_2CO_3 have been reported as positive (0.001–0.03 s).[68] Catalyst particles are supported in the catalytic zone on a porous quartz glass frit (Porosity 2;

This journal is © The Royal Society of Chemistry 2018

React. Chem. Eng., 2018, **3**, 676–695 | **685**
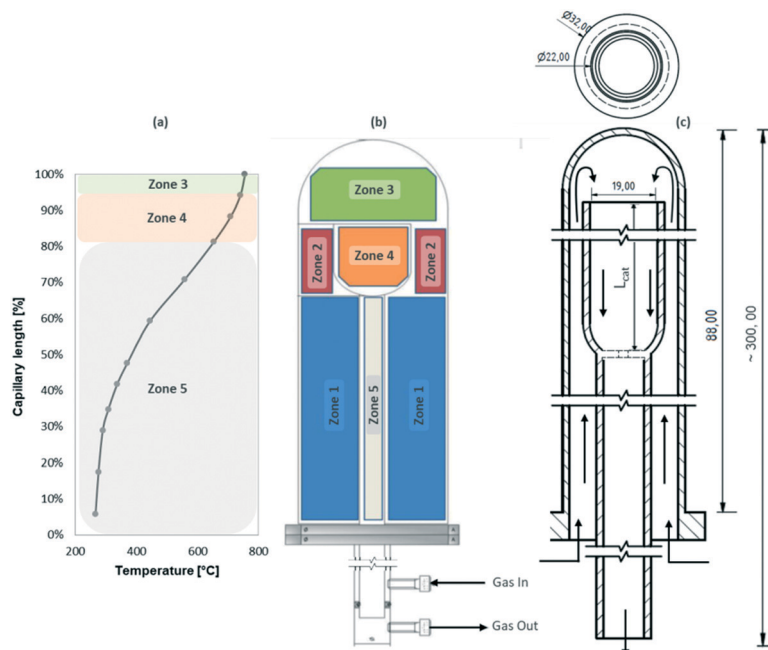
Fig. 3 The annular counter current reactor (ACCR) designed as applied in this investigation – (a) temperature profile of ACCR during test with Na_2CO_3 catalyst (along the whole reactor capillary length 88 mm as shown in Fig. S9†); T = 690 °C, Y_{MeOH} = 5–6 vol%, Q_{N_2} = 1.3 nL min^{-1}, GHSV = 15 000 h^{-1} (b) schematic of ACCR with illustration of different zones. Zone 1, 2 and 3: pre-catalytic zones, Zone 4: catalyst bed, Zone 5: post-catalytic zone. (c) Section of the ACCR with the main dimensions in [mm] and flow directions.

40–100 μm). In the post-catalytic zone (zone 5), a fast quenching of the reaction mixture is desired to suppress the secondary competing reactions of MeOH or the dissociation of FA to CO and H_2. The ACCR applied in this study is designed with a high volumetric ratio between zone 1 and zone 5 where "feed-to-product" heat exchange occurs. The diameter of the catalyst capillary tube was selected to achieve (a) a minimal temperature gradient in the catalyst bed and (b) to avoid a pressure rise >250 mbar (evaluated using Ergun's eqn (S1†)) considering the highest flow rate possible from the feed gas mass flow controller MFC. The quartz glass jacket and inner tube are assembled together with the gas inlet/outlet tube using a metallic screw made from a brass nut and a threaded piece made of aluminium allowing easy access and fast catalyst loading/removal (Fig. S9†).

Regarding the ACCR temperature profile, the calculated temperature drop in the post catalytic zone is *ca.* 7.75 K mm^{-1} (Fig. 3a). Reported results using packed bed reactor, the same catalyst system and similar operating conditions indicate that a maximum post-catalytic temperature drop of *ca.* 1.7 K mm^{-1} is reached. Fast cooling after the catalyst bed is required to avoid post-catalytic dissociation of FA. This was successfully achieved using the ACCR.[59]

Concerning the tests procedure, N_2 can be introduced to the saturator filled with MeOH using MFC. The desired MeOH concentration in the feed is controlled by setting the saturation temperature and by monitoring the total saturation pressure. The feed gas is introduced to the ACCR as heated by a programmable electrically heated oven (Fig. S9a†). The reaction product stream exits the reactor and is analysed online (*i.e.* through two GC and GA as previously discussed). Through a set of manual and magnetic valves feed and products can be analysed at different positions in the test stand.

Experimental results and discussion

As a control reaction, the endothermic dehydrogenation of MeOH was attempted through the ACCR without the use of the Na_2CO_3 catalyst. This was performed at GHSV = 15 000 h^{-1} and was used as a basis for further tests. This "blank" reaction showed a U_{MeOH} of 6–9% with no FA formation detected. Reference test was carried out over activated charcoal and showed activity towards MeOH conversion but rather selectivity towards CO than FA (U_{MeOH} of 74% with 24% S_{FA}). Under the same test conditions in the presence of the Na_2CO_3 catalyst showed selective MeOH conversion to FA (Fig. 4). An S_{FA} of over 90% at U_{MeOH} of 40% was achieved. During a single test the tendency of increasing selectivity with slight conversion reduction was observed (Fig. 4). This was also observed previously by Su *et al.*, who explained that this trend is due to carbon formation (*e.g.* on the catalyst surface), which poisons the CO selective sites and enhances the rate limiting H_2 spill-over reaction.[59] Due to the very narrow feed and product concentration ranges, the standard deviations of the measured U_{MeOH}, S_{FA} and MeOH concentration (in vol%, calculated using GC analysis) were found to be in the range of 4.2, 4.4 and 20.6% respectively.

To investigate the longer term behaviour of the system, the experiment was repeated for a test run length of 60 h
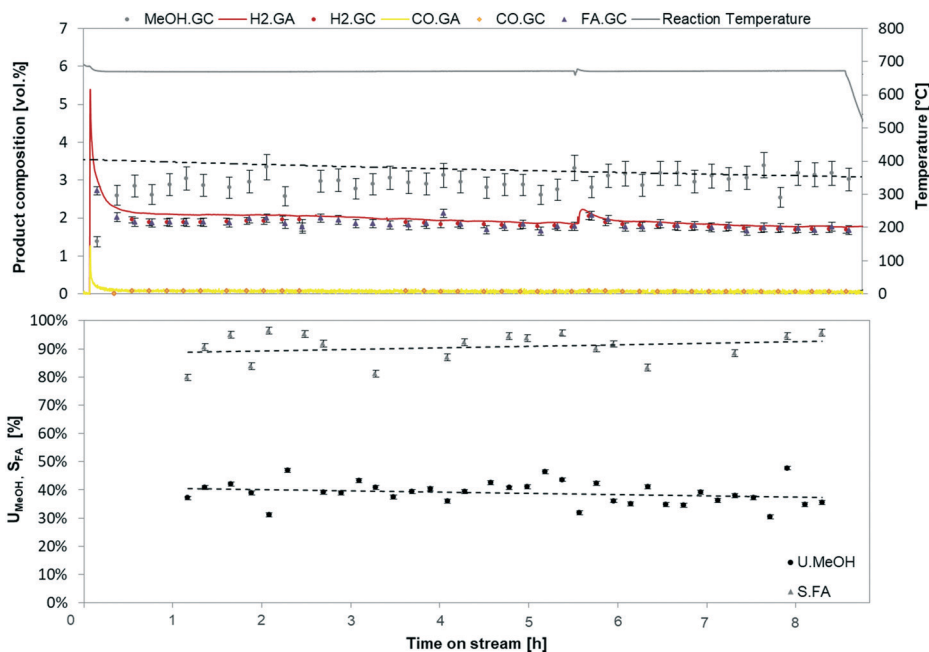
686 | *React. Chem. Eng.*, 2018, **3**, 676–695

This journal is © The Royal Society of Chemistry 2018

Fig. 4 Initial exemplary test results of endothermic MeOH dehydrogenation over Na_2CO_3 at T = 690 °C (D_p = 800–630 μm; Y_{MeOH} = 5–6 vol%; Q_{N_2} = 1.65 nL min^{-1}; GHSV = 15 000 h^{-1}).

(Fig. 5). It was observed that with increasing time online, S_{FA} continuously reduced while catalyst activity to MeOH conversion increased. Initial characterisation of the catalyst after a defined time "online" (e.g. 8 h), using scanning electron microscope (SEM) demonstrated that a significant catalyst structural change is observed (e.g. used vs. the original catalyst; Fig. S10†). The relationship between the changes in the catalyst physicochemical properties and its performance online are currently being evaluated and will be discussed further in a forthcoming article on this topic. What is clear at this point is that extended time online leads to the deposition of a "carbon" layer (e.g. as observed by a physical colour change), which may result in the blocking of catalytic sites favouring undesired side-reactions

and/or the generation of additional sites that promote the dehydrogenation mechanism.

Regarding the current work, the use of a Na_2CO_3 has shown selectivity for the endothermic dehydrogenation of MeOH to FA. The presented experimental results over this catalyst in a lab scale ACCR specially designed to meet this reaction system requirements, has demonstrated the potential to increase towards FA selectivity, e.g. with respect to other reactor types discussed in literature.[43,44,59] However, the behaviour of the catalyst and the potential scaling up of this innovative reactor concept remain open questions which are under investigation. These initial results are however very promising regarding achieving the desired FA/MeOH mole ratio for the subsequent OME synthesis.
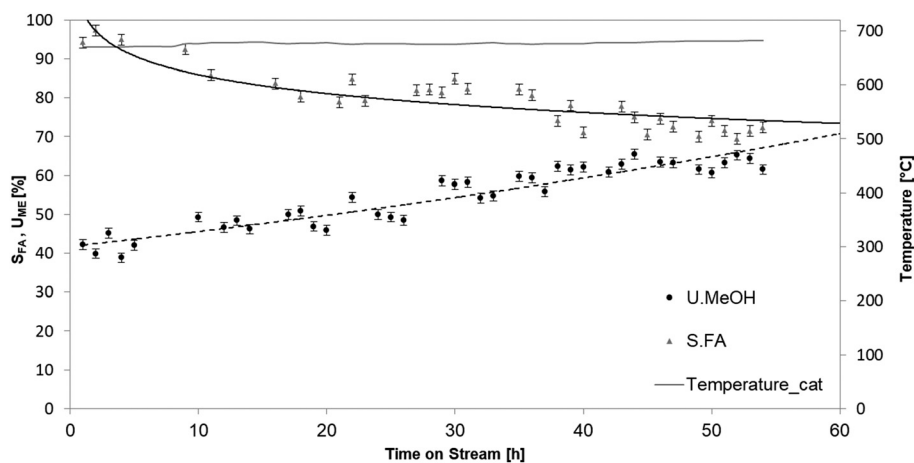

Fig. 5 Duration test with consecutive start-up and shutdowns over Na_2CO_3 catalyst at basis test parameter; D_p = 800–630 μm; T = 690 °C; Y_{MeOH} = 5–6 vol%; Q_{N_2} = 1.65 nL min^{-1}; GHSV = 15 000 h^{-1}. Test setup shutdown after single tests with duration of 6 to 8 h and start-up the next test day.

This journal is © The Royal Society of Chemistry 2018

React. Chem. Eng., 2018, **3**, 676–695 | 687

Hybrid model results and discussion

The presented process hybrid model allows the extraction, analysis and evaluation of all process streams and units. With the model results, different KPIs can be generated and evaluated extending understanding with regard to where further process improvements can be made. For the integrated process, the energy consumption in different process units was evaluated and the major process energy consumers were identified. Distillation equipment technical data were also generated. The overall process energy efficiency is evaluated and a summary of the major KPIs is given. Finally, with detailed energy consumption and utility requirements data provided by the hybrid process model, a simple production cost evaluation based on our previously reported simple cost evaluation method is provided.[34]

Material and energy balance

With the model implemented in CHEMCAD®, convergence of the whole flow sheet and performing the heat integration task, the material and energy balance for the described process are evaluated for the direct OME synthesis process based on endothermic MeOH dehydrogenation as illustrated in Table 2.

The total heating load is supplied either from other process hot streams or externally using high pressure steam (80 bar, up to 295 °C, with 1437 kJ kg^{-1}) or using natural gas (NG) for high temperature energy supply of the FA synthesis. The cooling load is supplied externally using cooling water at 25 °C (C_p = 4.2 kJ kg^{-1} K^{-1} and allowable T rise of 10 °C). Chilled water was used for cooling the condenser of distillation column (Unit – 314) and the electrical load required for this refrigeration task was evaluated using coefficient of performance with refrigeration cycle efficiency of 80%.[69] The

electricity supply resulting from pumping of process streams to account for process unit pressure drops or from the compression of the recycled N_2/CO carrier gas stream is supplied externally. The energy and utility consumption of the heat integrated process are shown in Table 3 with the corresponding shares.

The heating of the feed gas to such high temperature (690 °C) represents one of the major energy consumption in the process (Fig. 6). The highest energy share is allocated by the reboiler of the first distillation column (Fig. 2 – Unit 310) where the OME reactor product is initially separated; this is due to the high flow rate of the stream entering this column. Also the reboiler duty of the column for the separation of H_2O and OME_2 separation (Fig. 2 – Unit 315) is consuming much energy due to the complexity of the separation task. Regarding the electricity consumption, the compression of the N_2 carrier gas to recycle it is representing a significant process energy consumer. When the reaction can be operated at higher MeOH concentration in the feed, major energy savings can be achieved at the compressor side.

A comparison of the external utilities supply before and after heat integration showed a reduction of the steam consumption by 16.1%, cooling water consumption by 30.4% and increase in the electricity consumption by 5.07% due to the increased pressure drop by installing more heat exchangers.

The separation of the final product from H_2O and non-reactants or other OME fractions is cumbersome. The fact that H_2O is a main by-product of the condensation reactions, which take place in the OME synthesis, sophisticates the separation task due to the very small boiling point difference between H_2O, HF_1 and OME_2. Table 4 illustrates the operational conditions and summary of the distillation columns technical data.

Table 2 Material stream table of the described direct OME process with the main representative streams as depicted in Fig. 2

		Process feed	FA reactor feed	FA reactor product	OME reactor feed	Final product	SCDS 310		SCDS 315		SCDS 320		SCDS 325	
							Distil.	Bot.	Distil.	Bot.	Distil.	Bot.	Distil.	Bot.
Stream	Unit	201	205	206	306	336	311	330	319	316	326	324	331	340
$\dot{m}$	[t h^{-1}]	5.4	95.7	95.7	22.4	4.3	6.3	16.1	3.4	2.9	1.8	0.5	4.3	2.1
T	[°C]	25	690	690	50	32	79	264	53	126	13	109	167	353
P	[bar]	2.2	1.6	1.6	3.1	1.0	1.5	2.0	1.0	1.9	1.0	1.6	1.0	1.0
w_i	[wt%]													
N_2		0	25	25	0	0	0	0	0	0	0	0	0	0
H_2		0	0	0.26	0	0	0	0	0	0	0	0	0	0
CO		0	69.1	69.6	0	0	0	0	0	0	0	0	0	0
MeOH		100	5.8	1.8	8.5	0	2.7	0	4.9	0	24.6	1.5	0	0
FA		0	0	3.2	13.9	0	0.3	0	0.6	0	18.7	0	0	0
H_2O		0	0	0	0	0	7.3	0	13.5	0	0	91.8	0	0
OME_1		0	0	0	7.3	0	26.0	0	47.9	0	56.0	0	0	0
OME_2		0	0	0	7.8	0	28.1	0	0.9	60.2	0.5	3.2	0	0
OME_{3-5}		0	0	0	0.0	98.3	0	26.5	0	0	0	0	98.2	0.5
$OME_{n>5}$		0	0	0	9.6	0.1	0	13.3	0	0	0	0	0.1	18.1
HF_1		0	0	0	9.7	0	34.4	0	32.3	36.9	0	3.3	0	0
MG_1		0	0	0	0.4	1.6	1.3	0.4	0	2.8	0	0	1.7	0
$HF_{n>1}$		0	0	0	23.6	0	0	32.7	0	0	0	0	0	44.7
$MG_{n>1}$		0	0	0	19.3	0	0	26.9	0	0	0	0	0	36.6

688 | *React. Chem. Eng.*, 2018, **3**, 676–695

This journal is © The Royal Society of Chemistry 2018

Table 3 Energy and utility consumption of the heat integrated OME_{3-5} production process

| Unit | Duty [MWh a^{-1}] | Utility | | NG [MWh a^{-1}] | Share [%] | Relative share [MWh t$_{OME_{3-5}}$$^{-1}$] |
		HP steam [kt a^{-1}]	Cooling water [10^4 m^3 a^{-1}]			
HTXR						
Heating	5477			5477	2.36	0.15
Cooling	16 598		135		7.16	0.47
Distillation						
Heating	80 004	200			34.51	2.30
Cooling	76 158		619		32.85	2.196
Reactors						
Heating	25 552			25 552	11.02	0.73
Cooling	10 085		82		4.35	0.29
Electricity						
Pumps	16				0.01	0.00
Compressors	17 924				7.73	0.51
					100%	

Process energy efficiency

The energy efficiency relates the energy content of the final products to that of the feed and also accounts for the process energy $E_{process}$ required performing the conversion of certain feed to a final product. For the considered process, three different energy efficiencies are evaluated. First, the thermal energy efficiency $\eta_{eff,th}$ where only the heating load is considered as the $E_{process}$ and accounting for OME_{3-5} as the only product. For the overall process energy efficiency $\eta_{eff,overall}$, the $E_{process}$ accounts for the heating load and the electricity consumption. The last category is the overall energy efficiency $\eta_{eff,overall}^{H_2}$ considering the side products H_2 and CO and the $E_{process}$ constituting of the heat and electricity. A generic equation for calculating the energy efficiency can be written as follows:

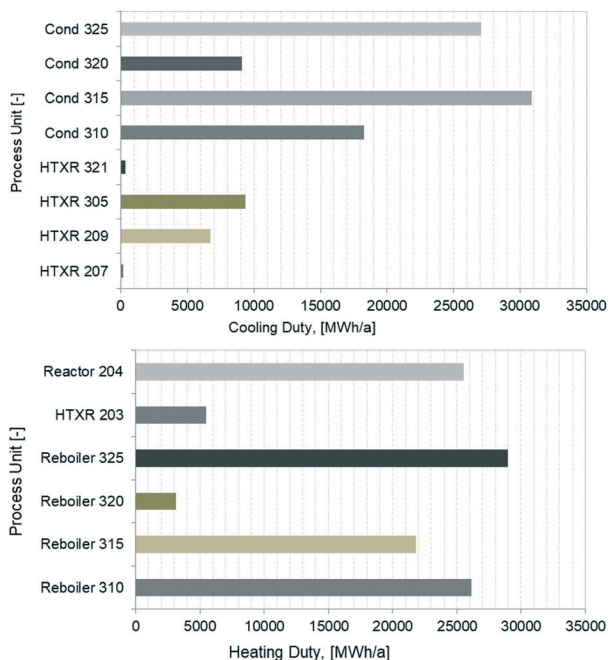$$\eta_{eff} = \frac{\left(\dot{m}_i \, LHV_i\right)_{product}}{\left(\dot{m}_i \, LHV_i\right)_{feed} + E_{process}} \quad (19)$$

where η_{eff} is process efficiency, $\dot{m}_i$ is the mass flow rate of component i, LHV_i is the lower heating value of component i and $E_{process}$ is the energy consumption in the process as previously defined. Thermochemical properties required for process energy evaluation are given elsewhere.[10,70]

The evaluated process energy efficiency $\eta_{eff,overall}^{H_2}$ based on the hybrid model results is 71.7%. With MeOH as the starting material, the described process efficiency is *ca.* 25% higher than the state of the art process in China with overall process efficiency of 45%.[71] Also the process presented by Schmitz *et al.* based on TRI/OME_1 synthesis route was evaluated at 52.6% overall efficiency which is significantly less than the direct synthesis process efficiency described in this work.[67]

Key performance indicators

From the results of the hybrid process model, several process material and energy streams are determined. From these figures process characteristic KPIs are defined (Table 5). A very important process characteristic is the overall process yield where the raw material cost is a major component of the OME production cost (Fig. 7). This indicator illustrates the potential of process enhancement regarding selective synthesis steps and minimizing target product losses in the separation steps. With 80.3% MeOH to OME_{3-5} product yield, the process represents a selective route in comparison with the process described by Schmitz *et al.* (considering OME_{3-6} while here only OME_{3-5} are considered).[67,68] Figures as recycle ratio reflects on the CAPEX of the reaction equipment and the OPEX due to the electrical power consumed for recycling. Specific energy and utility consumption figures

Fig. 6 Breakdown of the energy consumption for the process units.

This journal is © The Royal Society of Chemistry 2018

React. Chem. Eng., 2018, **3**, 676–695 | **689**

Table 4 Distillation columns operational conditions and technical data

Unit	*LKC/HKC	LKC in distillate [wt%]	HKC in distillate [wt%]	n-stages	Feed stage	T_{feed} [°C]	$T_{distillate}$ [°C]	T_{bottom} [°C]	Condenser specification	Reboiler specification
									Reflux ratio	Bottom temp [°C]
SCDS 310	OME_2/OME_3	99.99	0.02	22	11	133	79	264	1	264.4
SCDS 315	H_2O/OME_2	100.00	1.77	80	23	115	53	126	4	126.4
SCDS 320	$MeOH/H_2O$	98.93	<1	21	10	80	13	108	1	107.7
SCDS 325	OME_5/OME_6	94.29	0.00	41	20	264	174	354	7	353.5

*LKC: light key component; HKC: heavy key component.

reflect on the process energy efficiency. The evaluated energy efficiency is significantly higher than literature investigated processes as aforementioned.

A simple cost evaluation was done based on the method discussed in our previous work.[34] In this basic evaluation, the capital costs (CAPEX) and the operational costs (OPEX) (constitutes mainly of variable cost of production (VCP) and fixed cost of production (FCP)) are evaluated as follows. Regarding CAPEX, a capital investment of 1000 kt annual capacity plant which was used by Schmitz *et al.* was adopted in this work.[67] To adjust the CAPEX to the considered capacity in this work, a power law with a capacity factor, also called six-tenths rule due to the regression coefficient of 0.6 was used. For the OPEX, VCP are basically MeOH raw material cost (354 US$ per t, Methanex.org, 01/10/2017 until 31/12/2017) and the process energy cost. The former is provided by the material balance while the latter is calculated from the

process energy demand as evaluated in this work. The process energy is supplied by high pressure steam (24 US$ per t),[72] natural gas (0.03 US$ per kWh),[73] cooling water (0.04 US$ per m³)[74] and electricity (0.08 US$ per kWh).[75] The FCP are evaluated using a factorial method as discussed previously by Baerens.[57]

A breakdown of the OPEX is depicted in Fig. 7. Increasing the production capacity significantly enhance the production cost of OME due to the non-linear relation of CAPEX and production capacity. For OME_{3-5} annual production capacity of 1000 kt, the production cost of the described process is 598.7 US$ per t (at MeOH feed cost of 300 US$ per t, which was considered by Schmitz *et al.*[67] for evaluating same production capacity). Also the MeOH feed cost has a major impact on the OME product cost (*i.e.* a 47% share as shown in Fig. 7). With MeOH costs at 300 US$ per t the OME production cost is 882.79 US$ per t (at 35 kt per annum) with a breakeven point with diesel production cost (at a price of crude oil of *ca.* 83 US$ per barrel[67]) at MeOH feed cost of 126 US$ per t. Important to be noted that the CAPEX in this investigation is derived from rather a complicated synthesis technology, with more detailed CAPEX evaluation for the described process, OME production cost can be considerably reduced.

Another significant production cost enhancement potential is the synergy potential of coupling the OME synthesis plant with the MeOH synthesis plant; a case under investigation using the hybrid model which preliminary shows energy saving potential. The MeOH plant distillation unit and the OME reactor are operating at close T levels with integration potential. Same integration effect is possible considering the MeOH synthesis reactor and OME product work up units. The by-products H_2 and CO of the OME synthesis are also a suitable feed for the MeOH synthesis.

One of the main process energy consuming steps is the feed heating for MeOH dehydrogenation reactor unit operated at *ca.* 700 °C. This feed stream consists mainly of carrier gas N_2 and CO (>90 vol%) where the major heating energy shares is consumed for the enthalpy rise of the inert carrier gas. Additionally to the change in thermal energy demand the electricity demand of the compressor is influenced significantly, which is directly reflected on the costs for electricity. Therefore, research and development for new catalyst system for selective FA synthesis with higher MeOH concentrations in the feed can enhance the process energy efficiency and the production cost (Fig. 8). Increasing MeOH concentration up

Table 5 Technological indicators for the production of OME_{3-5} from MeOH

Technological indicators		
Material balance	[t a⁻¹]	[t $t_{OME_{3-5}}$⁻¹]
Inlet MeOH	43211.5	1.246
Outlet CO	2563.2	0.07
Outlet H_2	2029.2	0.06
Outlet H_2O	3948.4	0.11
		[g g⁻¹ product]
Outlet OME_{3-5}	34687.9	OME_3: 0.38
		OME_4: 0.33
		OME_5: 0.27
Overall yield [g g⁻¹]	[OME_{3-5}/MeOH]	80.3%
R1 yield [g g⁻¹]	[FA/MeOH]	57.2%
R1 feed ratio [mol mol⁻¹]	[FA/MeOH]	1.9
R2 yield [g g⁻¹]	[MeOH/OME_{3-5}]	0.45
Recycle ratio R2	[$g_{OME_{3-5},product}$ $g_{recycled}$⁻¹]	0.25
Energy balance	[kt a⁻¹]	[MWh $t_{OME_{3-5}}$⁻¹]
Steam consumption	200.4	2.31
Natural gas		0.89
Electricity		0.53
$\eta_{eff,th}$		53.9%
$\eta_{eff,overall}$		51.2%
$\eta_{eff,overall}^{H_2}$		71.7%
Economic indicators		
CAPEX	33424298.22 US$	
OPEX	[US$ per a]	[US$ per $t_{OME_{3-5}}$]
VCP	23532361.04	678.4 (69.8%)
FCP	9474968.00	273.1 (30.2%)
Total	33007329.04	951.5

690 | *React. Chem. Eng.*, 2018, **3**, 676–695

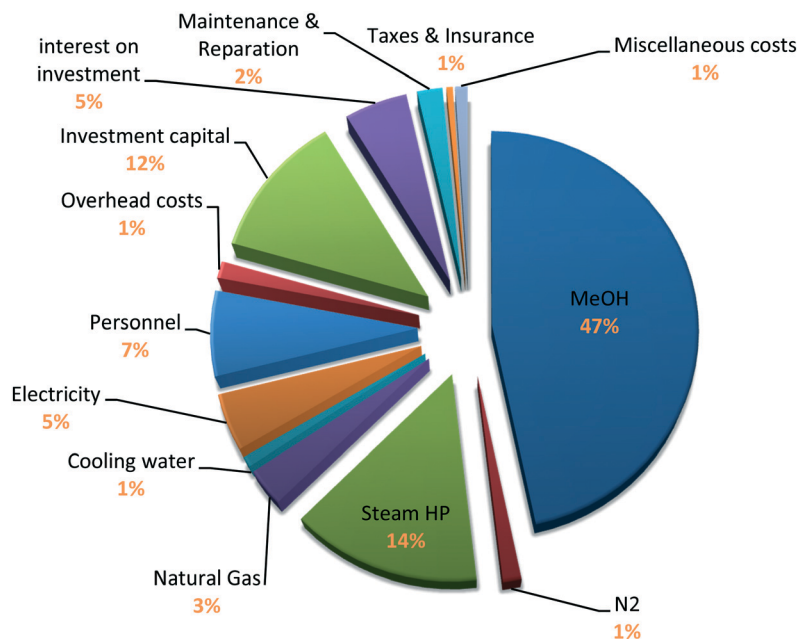This journal is © The Royal Society of Chemistry 2018

Fig. 7 OPEX break down for the OME direct synthesis. **VCP** composed of (1) raw materials: MeOH and N_2; (2) energy cost: steam HP, natural gas, cooling water, electricity. **FCP** composed of: personnel, overhead costs, investment capital with 10 years depreciation period and 3% interest on capital investment, maintenance and reparation, taxes and insurance and miscellaneous costs.

to 20 vol%, a production cost reduction of *ca.* 4.6% and synthesis efficiency of *ca.* 2.8% increase are potential.

For the MeOH dehydrogenation step the high temperature energy required is supplied by natural gas. One of the synergies that can significantly enhance the presented OME synthesis process is coupling the synthesis plant with industries where high temperature waste heat might be available. A concept being considered in the steel industry from steel mill exhaust gas valorisation perspective and also from the energy integration perspective.[76] Considering this integration can supply the high T energy needed for the feed preparation for the endothermic MeOH dehydrogenation, the process energy efficiency significantly increases by 6.6% to reach 78.3%.

The water management and separation from the desired OME product is challenging and indeed energy consuming in this synthesis concept. The distillation apparatus for water separation from the product mixture represent a major energy consumption share (19.6% of the total heat energy consumption). As previously mentioned, other R&D contributions are investigating several water separation alternatives than the energy consuming distillation. With the developed tool and considering an adsorption based water separation alternative as described by Schmitz *et al.*,[35] the potential of this solution is identified. Assuming two scenarios were the adsorption unit requires 50% and 20% of the distillation unit reboiler heat duty, the energy efficiency and the production cost calculated are 74% and 932.7 US$ per t for the former case and 75.3% and 921.5 US$ per t for the latter.

Conclusions

A "direct" OME synthesis based on the endothermic dehydrogenation of MeOH as the only feed is presented. In the described process presented in this paper, MeOH undergoes selective catalytic dehydrogenation at high temperatures to yield FA and H_2. The non-converted MeOH and produced anhydrous FA are converted directly with high yield to the desired OME_{3-5}. The described process was implemented in a hybrid simulation model where own developed reactor models using Matlab® are coupled with process units in the commercial software CHEMCAD®. A global kinetic reactor model based on experimental and literature data was developed in Matlab® for describing the anhydrous FA synthesis reactor. The OME synthesis reactor was described also in Matlab® using a Gibbs minimisation approach for multicomponent reaction equilibrium. The interface between the two platforms was implemented using an Excel® unit in
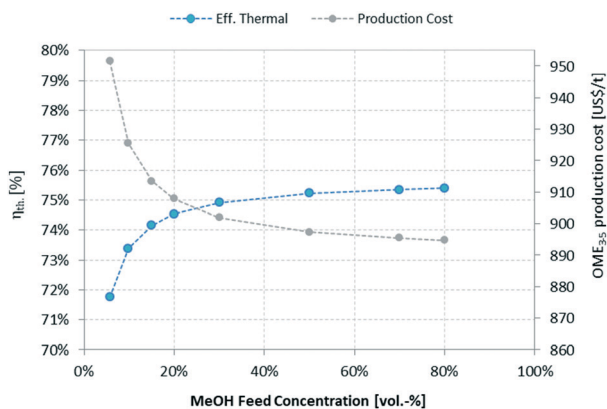

Fig. 8 Effect of MeOH feed concentration on the process energy efficiency and the production cost of OME_{3-5}.

This journal is © The Royal Society of Chemistry 2018

React. Chem. Eng., 2018, **3**, 676–695 | 691

CHEMCAD® software in which a VBA node can open, run and call the results from the Matlab® platform. With all process units implemented and after the hybrid model convergence in CHEMCAD®, a heat integration was conducted using the software PinCH 2.0 with maximum process heat recovery as the objective function. The process flow diagram was subsequently updated in CHEMCAD® and the convergence was repeated accordingly.

Due to its importance in the overall process scheme, endothermic dehydrogenation of MeOH over a Na_2CO_3 catalyst was also experimentally investigated in a specially developed reactor (ACCR) to meet the described reaction system prerequisites. At low MeOH concentrations in the feed (<10 vol%), FA selectivity of 90% with MeOH conversion of 40% were reached at 690 °C. However, the behaviour of this catalyst under the applied conditions is still under investigation and will be discussed further in a forthcoming publication. Nonetheless, given its abundance and indeed low relative price, the use of the Na_2CO_3 catalyst systems represents a promising basis for further development, although further investigations are still required.

The process energy integration in the hybrid model was also evaluated. The material streams and energy duties were extracted and used to define the process KPIs. An overall process OME_{3-5} yield of 80.3 wt% was calculated which is almost 10% higher than the current state of the art process (e.g. in China). From the computed heating duties and electricity consumption the process overall energy efficiency was calculated as 71.7% with 200.4 kt per annum steam consumption and 18.4 GWh annual electricity consumption. The energy integration task led to reduction of the steam consumption by 16.1% less than the non-heat integrated process. The working up of the product stream was done in four distillation units implemented as rigorous columns in CHEMCAD®. The technical characteristics of the columns were given which showed the complexity of the water separation column representing 19.6% share of the total process thermal energy consumption. This emphasizes that new innovative water management solutions are essential for enhancing the OME synthesis chain technical and economic performance.

A basic production cost model was applied where the following are the main results of this evaluation:

• OME_{3-5} production cost of the 35 kt per annum facility was calculated as 951.5 US$ per t.

• The main cost influencing components are the MeOH feed cost with 47% of the production cost share, the energy cost with 22.13% share and the production capacity.

• At high annual production capacity of 1000 kt, the production cost per tonne OME_{3-5} was evaluated at 598.7 US$.

Several scenarios where also considered with the aim to enhance the described process economics from which:

• Catalyst developments for the endothermic MeOH dehydrogenation reaction to operate at higher concentrations showed significant energy efficiency and production cost improvement. A production cost reduction of 5.9% was calculated with increasing the MeOH feed concentration from 5 to 50 vol%.

• Coupling the existing technology with high temperature industries (e.g. steel production facilities) could lead to significant production cost reductions with 6.6% process overall energy efficiency enhancement potential.

• Further process improvements could relate to separation of H_2O from the OME product mixture, for example using adsorption technology rather than distillation, whilst increasing the MeOH concentration in the feed to 20 vol% based on a MeOH feed price of 300 US$ per t, would result in a production cost of 820.3 US$ per t OME_{3-5} (with process energy efficiency of 76.9%).

The production cost evaluated in this investigation might not show direct competitiveness for OME in the fuel market. However, it is based on small production capacity and relatively conservative evaluation conditions. On the other hand the considered production capacity and cost could be attractive for OME as a solvent or for other applications in the chemical industry.

In conclusion, the developed hybrid process model is capable of robust process technical and preliminary economic metrics evaluation once the process is correctly defined. For more detailed process evaluation the following improvements are to be considered. Regarding the anhydrous FA synthesis, saturating the MeOH feed in circulating gas (consisting of CO and H_2 as described by Schweers et al.[66]), including the absorption model of this product in the recycle stream and more detailed kinetic description of the catalytic reaction are important improvements. Also, the so far ideally considered separation of N_2, CO and H_2 is to be further investigated in more detail. On the OME synthesis block side, improving the physical and thermodynamic property models for the HF_n and MG_n can allow more detailed reactive distillation modelling. Furthermore, improving the developed OME reaction equilibrium model towards kinetic modelling is a foreseen enhancement for detailed reactor sizing and costing. An exact process unit operations sizing and CAPEX evaluation for the specific described process and implementing the costing model in the hybrid model are under development for improved process description.

Funding sources

Nomenclature

Abbreviations

Abbreviations	Full Name
ACCR	Annular counter current reactor

Symbol	Name
EGR	Exhaust gas recycle
FA	Formaldehyde
GA	Gas analyser
GC	Gas chromatograph
GHGE	Green house gas emissions
HF	Polyoxymethylene hemiformals
LHV	Lower heating value
CH_3OH/MeOH	Methanol
MFC	Mass flow controller
MG	Polyoxymethylene glycols
NO_x	Nitrous oxides
OME/POMDE	Polyoxymethylene dimethyl ethers
OME_n	OME of chain length n
pFA	Para formaldehyde
PM	Particulate matter
SGO	Stochastic global optimizer
TCD	Thermal conductivity detectors
VBA	Visual Basics for Applications
SEM	Scanning electron microscope

Symbols and indices

Symbol or Indice	Name
C_A	Concentration of component A
C_P	Heat capacity
γ_i	Activity coefficient of component i
E	Energy
G_f	Gibbs free energy of formation
G^t	Gibbs free energy
η	Efficiency
ΔH_R	Enthalpy of reaction
$K_{eq.}$	Equilibrium constant
K_j	Reaction rate constant of reaction j
m_i	Mass of component i
n	Order of the reaction
N	Number of species present in the reacting mixture
n_i	Molar amount of component i
P	Pressure
r_j	Reaction rate of reaction j
R	Gas constant
T	Temperature
t	Time
τ	Residence time
V	Volume
$\dot{V}$	Volume flow
w_i	Mass fraction of component i
X_i	Molar fraction of component i in the liquid phase
U_{MeOH}	Methanol conversion
S_{FA}	Formaldehyde selectivity

Conflicts of interest

There are no conflicts to declare.

Acknowledgements

References

1 *CO2 to Fuels – Chemical Perspectives: 193–264, 37*, ed. R. Schlögl, Internationales Wiener Motorensymposium, Vienna, 2016.
2 R. Schlögl, *Angew. Chem.*, 2017, **129**(37), 11164.
3 E. Jacob and W. Maus, *MTZ Worldw.*, 2017, **78**(3), 52.
4 European Commission, *White paper: Roadmap to a Single European Transport Area - Towards a competitive and resource efficient*, Brussels, Belgium, 2011.
5 O. Deutschmann and J.-D. Grunwaldt, *Chem. Ing. Tech.*, 2013, **85**(5), 595.
6 B. Niethammer, S. Wodarz, M. Betz, P. Haltenort, D. Oestreich, K. Hackbarth, U. Arnold, T. Otto and J. Sauer, *Chem. Ing. Tech.*, 2018, **90**(1–2), 99.
7 Bundesministerium für Verkehr und Bau und Stadtentwicklung, *The Mobility and Fuels Strategy of the german government (MFS): New pathways for energy*, 2013.
8 S. Schemme, R. C. Samsun, R. Peters and D. Stolten, *Fuel*, 2017, **205**, 198.
9 M. Bertau and F. Asinger, *Methanol: The basic chemical and energy feedstock of the future Asinger's vision today*, Springer, Heidelberg, 2014.
10 M. Härtl, K. Gaukel, D. Pélerin and G. Wachtmeister, *MTZ Worldwide*, 2017, **78**(2), 52.
11 P. Haltenort, K. Hackbarth, D. Oestreich, L. Lautenschütz, U. Arnold and J. Sauer, *Catal. Commun.*, 2018, **109**, 80.
12 L. Lautenschütz, D. Oestreich, P. Seidenspinner, U. Arnold, E. Dinjus and J. Sauer, *Fuel*, 2016, **173**, 129.
13 *Synthetic Fuels–OME1: A Potentially Sustainable Diesel Fuel: 325–347, 35*, ed. E. Jacob and W. Maus, Wiener Motorensymposium, Vienna, 2014.
14 G. Richter and H. Zellbeck, *Motortech. Z.*, 2017, **78**(12), 66.
15 H. Liu, Z. Wang, J. Wang, X. He, Y. Zheng, Q. Tang and J. Wang, *Energy*, 2015, **88**, 793.
16 J. Liu, H. Wang, Y. Li, Z. Zheng, Z. Xue, H. Shang and M. Yao, *Fuel*, 2016, **177**, 206.
17 M. Bohner, R. Fischer and R. Gscheidle, *Fachkunde Kraftfahrzeugtechnik*, Verl. Europa-Lehrmittel Nourney, Vollmer, Haan-Gruiten, 2001.
18 A. Feiling, M. Münz and C. Beidl, *Springer Fachmedien Wiesbaden ATZextra Worldwide*, 2016, **21**(11), 16.
19 *The Fuel OME2: An Example to Pave the Way to Emission-Neutral Vehicles with Internal Combustion Engine: 224–252, 37*, ed. M. Härtl and E. Jacob, Internationales Wiener Motorensymposium, Vienna, 2016.
20 M. Härtl, P. Seidenspinner, E. Jacob and G. Wachtmeister, *Fuel*, 2015, **153**, 328.

This journal is © The Royal Society of Chemistry 2018

React. Chem. Eng., 2018, **3**, 676–695 | 693

21 S. E. Iannuzzi, C. Barro, K. Boulouchos and J. Burger, *Fuel*, 2016, **167**, 49.

22 W. Sun, G. Wang, S. Li, R. Zhang, B. Yang, J. Yang, Y. Li, C. K. Westbrook and C. K. Law, *Proc. Combust. Inst.*, 2016, 1269–1278.

23 L. Tong, H. Wang, Z. Zheng, R. Reitz and M. Yao, *Fuel*, 2016, **181**, 878.

24 K. D. Vertin, J. M. Ohi, D. W. Naegeli, K. H. Childress, G. P. Hagen, C. I. McCarthy, A. S. Cheng and R. W. Dibble in *International Fuels & Lubricants Meeting & Exposition*, SAE International, 400 Commonwealth Drive, Warrendale, PA, United States, 1999.

25 H. Yang, X. Li, Y. Wang, M. Mu, X. Li and G. Kou, *Sci. Rep.*, 2016, **6**, 37611.

26 H. Yang, X. Li, Y. Wang, M. Mu, X. Li and G. Kou, *Aerosol Air Qual. Res.*, 2016, **16**(10), 2560.

27 W. Sun, G. Wang, S. Li, R. Zhang, B. Yang, J. Yang, Y. Li, C. K. Westbrook and C. K. Law, *Proc. Combust. Inst.*, 2017, **36**(1), 1269.

28 J. Liu, H. Shang, H. Wang, Z. Zheng, Q. Wang, Z. Xue and M. Yao, *Fuel*, 2017, **193**, 101.

29 L. P. Lautenschütz, Neue Erkenntnisse in der Syntheseoptimierung oligomerer Oxymethylendimethylether aus Dimethoxymethan und Trioxan, *PhD*, Inaugural-Dissertation, Ruprecht-Karls-Universität Heidelberg, 2015.

30 C. J. Baranowski, A. M. Bahmanpour and O. Kröcher, *Appl. Catal., B*, 2017, **217**, 407.

31 M. Schappals, T. Breug-Nissen, K. Langenbach, J. Burger and H. Hasse, *J. Chem. Eng. Data*, 2017, 4027–4031.

32 J. Burger, E. Ströfer and H. Hasse, *Ind. Eng. Chem. Res.*, 2012, **51**(39), 12751.

33 Y. Zhao, Z. Xu, H. Chen, Y. Fu and J. Shen, *J. Energy Chem.*, 2013, **22**(6), 833.

34 M. Ouda, F. K. Mantei, M. Elmehlawy, R. J. White, H. Klein and S.-E. K. Fateen, *React. Chem. Eng.*, 2018, **534**(7609), 631.

35 N. Schmitz, E. Ströfer, J. Burger and H. Hasse, *Ind. Eng. Chem. Res.*, 2017, **56**(40), 11519.

36 D. Oestreich, L. Lautenschütz, U. Arnold and J. Sauer, *Chem. Eng. Sci.*, 2017, **163**, 92.

37 N. Schmitz, J. Burger and H. Hasse, *Ind. Eng. Chem. Res.*, 2015, **54**(50), 12553.

38 N. Schmitz, F. Homberg, J. Berje, J. Burger and H. Hasse, *Ind. Eng. Chem. Res.*, 2015, **54**(25), 6409.

39 J. Zhang, D. Fang and D. Liu, *Ind. Eng. Chem. Res.*, 2014, **53**(35), 13589.

40 J. Zhang, M. Shi, D. Fang and D. Liu, *React. Kinet., Mech. Catal.*, 2014, **113**(2), 459.

41 M. Ouda, G. Yarce, R. J. White, M. Hadrich, D. Himmel, A. Schaadt, H. Klein, E. Jacob and I. Krossing, *React. Chem. Eng.*, 2017, **2**(1), 50.

42 U. Arnold, L. Lautenschutz, D. Oestreich and J. Sauer, Verfahren zur Herstellung von Oxymethylenethern und deren Verwendung, EP2987781, 2015.

43 S. Su, P. Zaza and A. Renken, *Chem. Eng. Technol.*, 1994, **17**(1), 34.

44 J. Sauer and G. Eming, *Chem. Eng. Technol.*, 1995, **18**, 284.

45 G. Reuss, W. Disteldorf, A. O. Gamer and A. Hilt in *Ullmann's Encyclopedia of Industrial Chemistry*, Wiley-VCH Verlag GmbH & Co. KGaA, Weinheim, Germany, 2000.

46 J. Burger, *A novel process for the production of diesel fuel additives by hierarchical design*, Techn. Univ, Kaiserslautern, 2012.

47 J. Burger, E. Ströfer and H. Hasse, *Chem. Eng. Res. Des.*, 2013, **91**(12), 2648.

48 M. Albert, B. Coto García, C. Kuhnert, R. Peschla and G. Maurer, *AIChE J.*, 2000, **46**(8), 1676.

49 C. Kuhnert, M. Albert, S. Breyer, I. Hahnenstein, H. Hasse and G. Maurer, *Ind. Eng. Chem. Res.*, 2006, **45**(14), 5155.

50 N. Schmitz, A. Friebel, E. von Harbou, J. Burger and H. Hasse, *Fluid Phase Equilib.*, 2016, **425**, 127.

51 I. Hahnenstein, M. Albert, H. Hasse, C. G. Kreiter and G. Maurer, *Ind. Eng. Chem. Res.*, 1995, **34**(2), 440.

52 M. Albert, I. Hahnenstein, H. Hasse and G. Maurer, *AIChE J.*, 1996, **42**(6), 1741.

53 Y.-Q. Liu, H. Hasse and G. Maurer, *AIChE J.*, 1992, **38**(11), 1693.

54 H. Du, J. Li, J. Zhang, G. Su, X. Li and Y. Zhao, *J. Phys. Chem. C*, 2011, **115**(47), 23261.

55 H. Kister, *Distillation Design*, McGraw-Hill Education, 1992.

56 E. Henley and J. Seader, *Equilibrium-stage separation operations in chemical*, John Wiley and Sons Ltd, 1981.

57 *Rules of thumb for chemical engineers*, ed. C. Branan, Elsevier, 2002.

58 M. Albert, I. Hahnenstein, H. Hasse and G. Maurer, *AIChE J.*, 1996, **42**(6), 1741.

59 S. Su, Catalytic dehydrogenation of methanol to formaldehyde on sodium carbonate, *PhD*, Dissertation, 1991.

60 Fogler, *Elements of chemical reaction engineering*, Prentice-Hall of India, 2004.

61 L. M. Naphtali and D. P. Sandholm, *AIChE J.*, 1971, **17**(1), 148.

62 L. Weise and D. Seidl, *Shortcut simulation*.

63 G. Towler and R. Sinnott in *Chemical Engineering Design*, Elsevier, 2013, p. 1047.

64 *CHEMCAD Version 6: SpringerReference, User Guide*, Springer-Verlag, Berlin/Heidelberg, 2011.

65 J. F. Walker, *Formaldehyde*, Reinhold Publ. Corp, New York, 1964.

66 E. Schweers, T. Kaiser, M. Haubs and M. Rosenberg, *Apparatus for the preparation of Formaldehyde from Methanol*, US006472566B2, 2002.

67 N. Schmitz, J. Burger, E. Ströfer and H. Hasse, *Fuel*, 2016, **185**, 67.

68 S. Su, M. R. Prairie and A. Renken, *Appl. Catal., A*, 1992, **91**, 131.

69 G. Towler and R. Sinnott in *Chemical Engineering Design*, Butterworth-Heinemann, Boston, 2nd edn, 2013, p. 103.

70 L. Lautenschütz, D. Oestreich, P. Seidenspinner, U. Arnold, E. Dinjus and J. Sauer, *Fuel*, 2016, **173**, 129.

71 H. Shang, Z. Hong, Z. YE, J. Xiang and Z. Xue, *Method for producing polyoxymethylene dimethyl ethers from feedstock of concentrated formaldehyde*, US20160168307A1, 2016.

72 M. Baerns, A. Behr, A. Brehm, J. Gmehling, H. Hofmann, U. Onken, A. Renken, K.-O. Hinrichsen and R. Palkovits, *Technische Chemie*, Wiley-VCH-Verl., Weinheim, 2013.

73 http://ec.europa.eu/eurostat/statistics-explained/index.php/File: Natural_gas_prices_for_industrial_consumers,_second_half_2016_%28EUR_per_kWh%29_YB17.png (last accessed March 2018).

74 https://www.thuenen.de/media/ti-themenfelder/Nachwachsende_Rohstoffe/Bioraffinerie/Pilotprojekt_Lignocellulose_Bioraffinerie_Schlussbericht.pdf (last accessed March 2018).

75 http://ec.europa.eu/eurostat/tgm/refreshTableAction.do;jsessionid=PFQ0ll_JhIhX0p9NIV3oixTQdNVmcuO6MsiUY79AVpd47XuQ45vh!-800505858?tab=table&plugin=1&pcode=ten00117&language=en (last accessed March 2018).

76 M. Oles, W. Lüke, R. Kleinschmidt, K. Büker, H.-J. Weddige, P. Schmöle and R. Achatz, *Chem. Ing. Tech.*, 2018, **90**(1–2), 169.

This journal is © The Royal Society of Chemistry 2018

React. Chem. Eng., 2018, **3**, 676–695 | 695

A Hybrid Description and Evaluation of Oxymethylene Dimethyl Ethers Synthesis based on the Endothermic Dehydrogenation of Methanol

Electronic Supplementary Information

Mohamed Ouda,[a,b*] Franz Mantei,[a] Kai Hesterwerth,[a] Eleonora Bargiacchi,[a] Harald Klein,[b] and Robin J. White[a*]

[a] *Sustainable Catalytic Materials Group, Division Hydrogen Technologies, Fraunhofer Institute for Solar Energy Systems, Heidenhofstr. 2, 79110 Freiburg, Germany*

Email: mohamed.ouda@ise.fraunhofer.de / Email: robin.white@ise.fraunhofer.de

[b] *Institute of Process and Plant Technology, Technical University Munich, Boltzmannstr. 15, 85748 Garching, Germany*

Keywords
Oxymethylene Ethers; anhydrous formaldehyde; Gibbs minimisation; Process design and optimisation

Experimental results for equilibrium constant evaluation for Na_2CO_3 catalyst at 690 °C
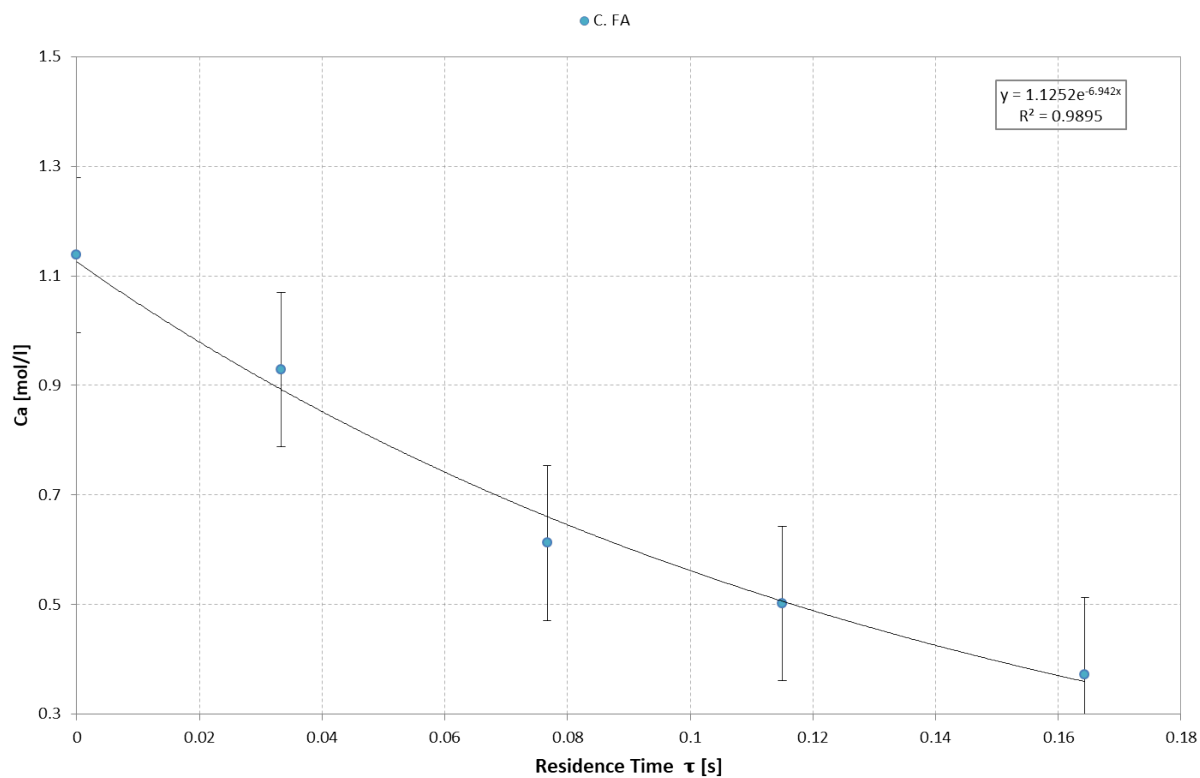
Fig. S1 Dependency of MeOH concentration consumed for FA production on residence time at 690 °C, a first order reaction fitting is illustrated
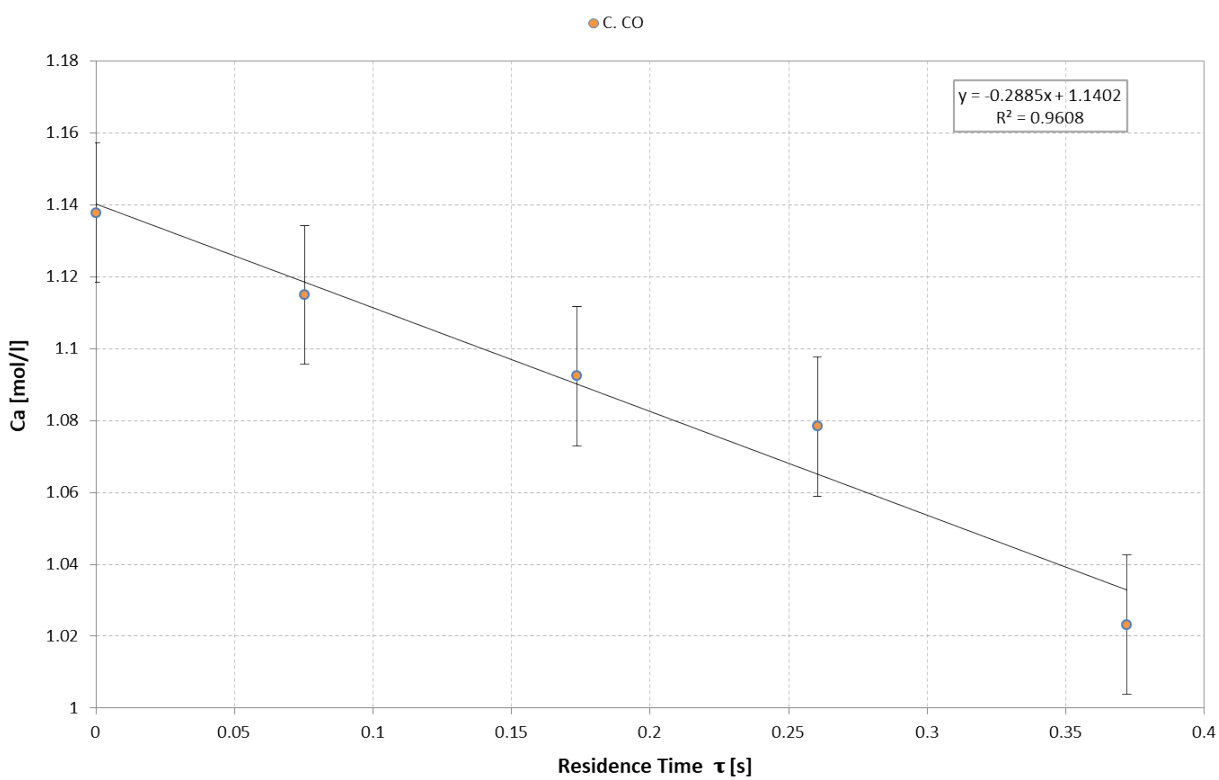
Fig. S2 Dependency of MeOH concentration consumed for CO production on residence time at 690 °C, a zero order reaction fitting is illustrated.

Kinetic model results for endothermic selective methanol dehydrogenation to formaldehyde reaction over Na_2CO_3 catalyst
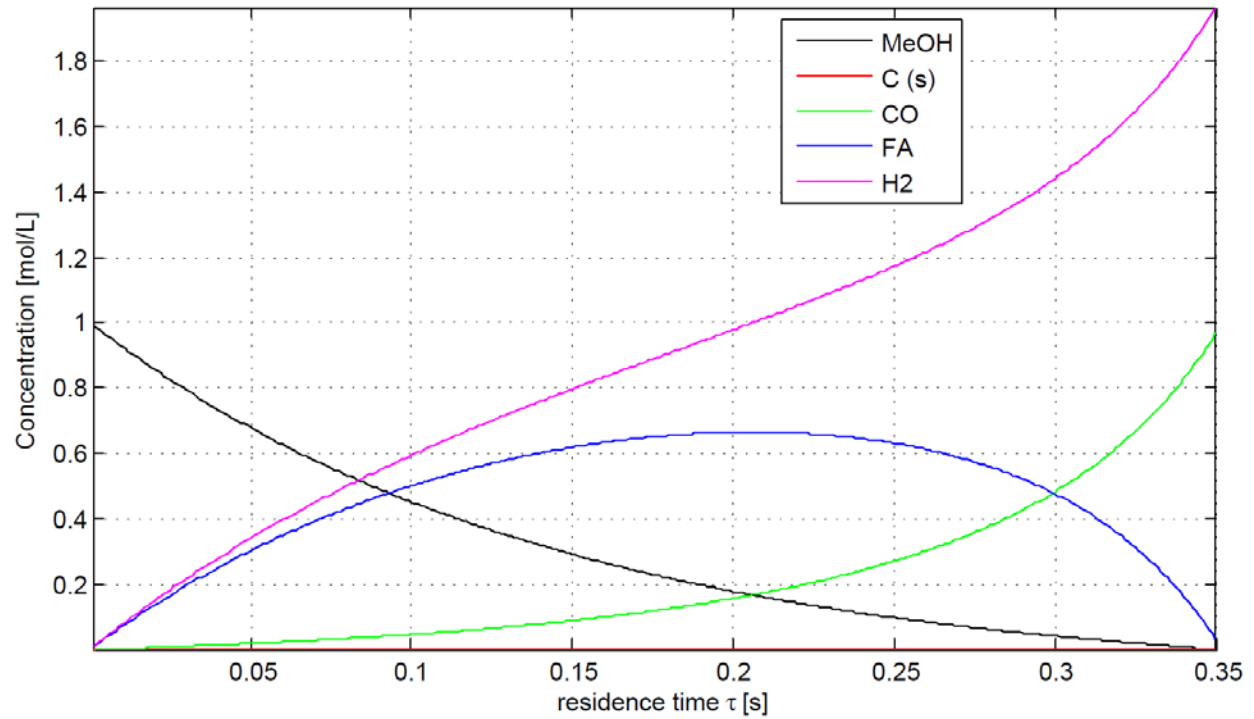
Fig. S3 Concentration curves of MeOH, C, CO, FA and H_2 over residence time for C_{A0} = 1 mol/L, T = 690 °C from kinetic FA reactor model
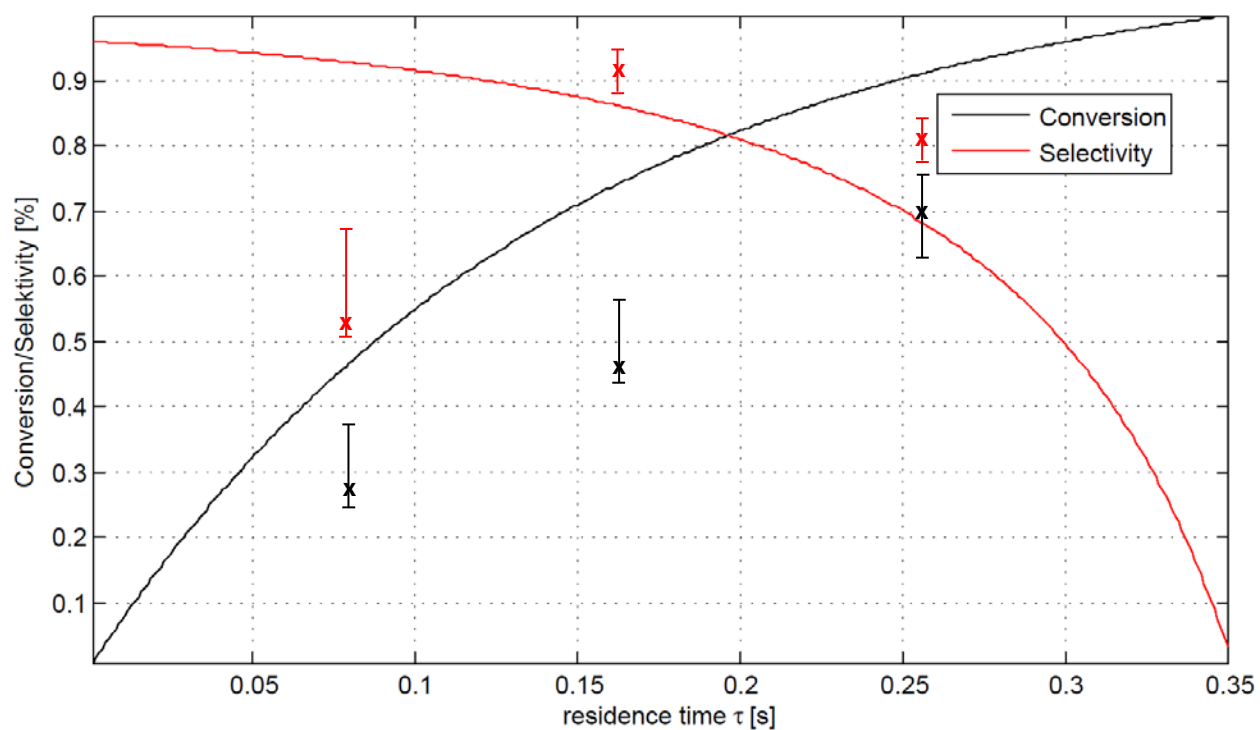
Fig. S4 Conversion of MeOH and Selectivity of MeOH regarding FA over residence time for C_{A0} = 1 mol/L, T = 690 °C from kinetic FA reactor model. **X:** measured conversion; **X:** measured selectivity.

Chemical Equilibrium composition using different reaction models
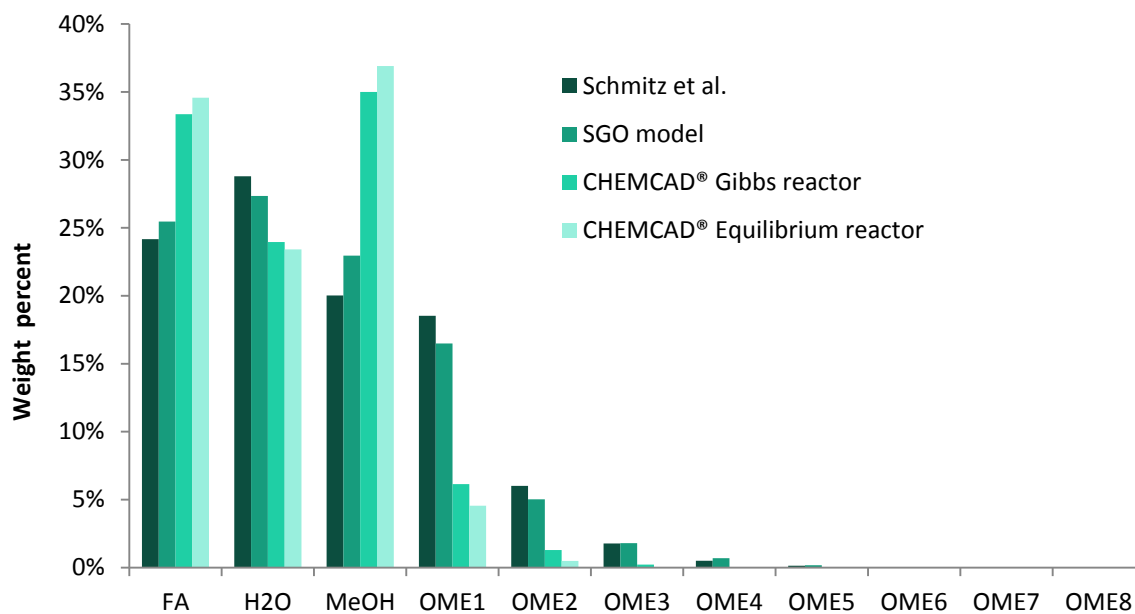
Fig. S5 Comparison of chemical equilibrium composition of experimental results from Schmitz *et al.*[1] at T = 348 K, P = 2 bar with a feed composition of FA/MeOH = 0.89 and H_2O/MeOH = 0.54, with the results obtained from the Stochastic Global Optimizer model and the CHEMCAD®, Gibbs and equilibrium reactors modules
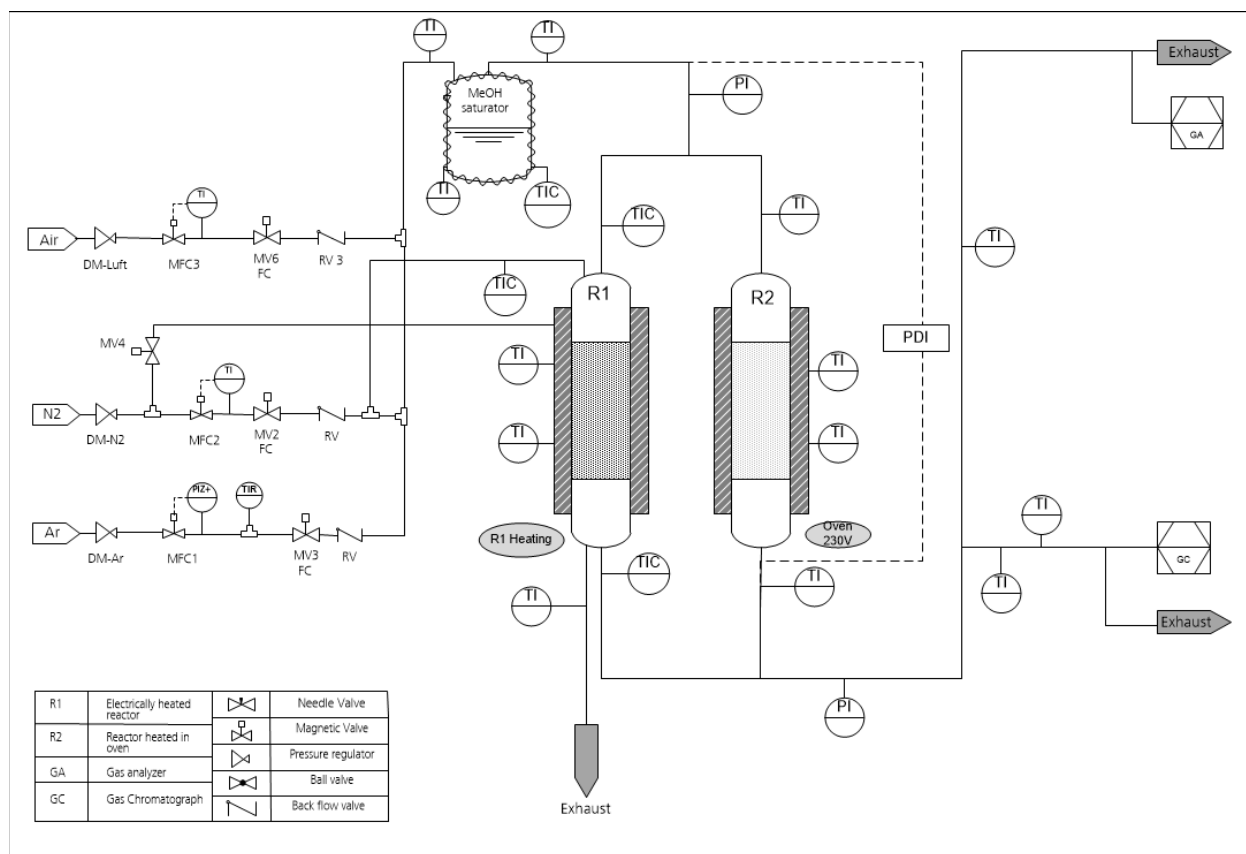
Results and HEN from PinCH 2.0
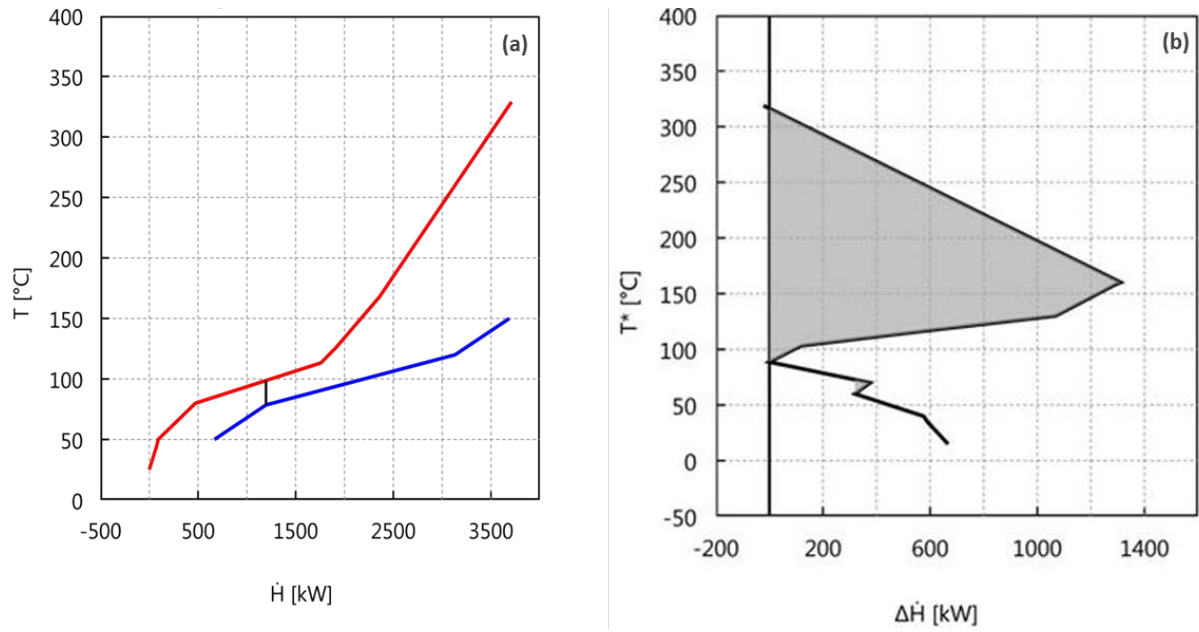
Fig. S6 (a) Composite curves and (b) Grand composite curve from PinCH 2.0 for generating the HEN
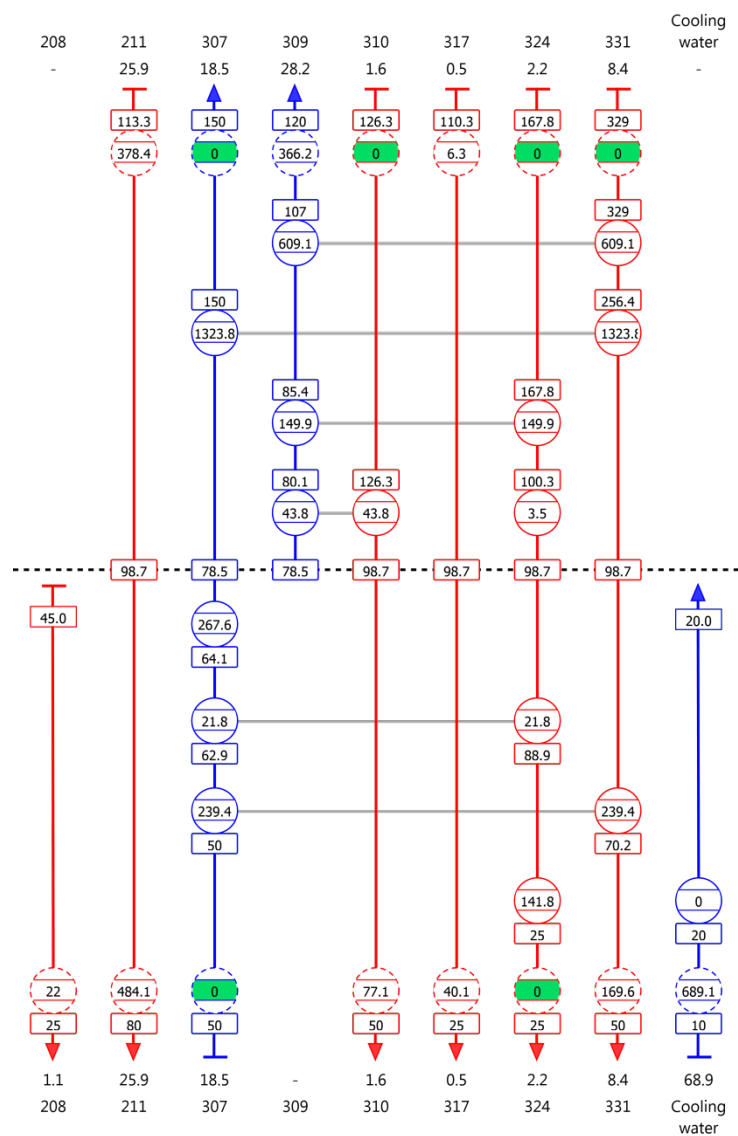
Fig. S7 HEN designed using PinCH 2.0 for the OME$_{3\text{-}5}$ production process

Test stand for endothermic MeOH catalytic dehydrogenation to FA

Fig. S8 Simplified Process Flow Diagram for the laboratory test stand used for anhydrous FA synthesis.

Ergun's Equation for pressure drop evaluation in ACCR[2]

$$P = P_0 \times (1 - \frac{2 \times \beta_0 \times z}{P_0})^{0.5} \qquad \qquad \textit{Equation S1}$$

With $\qquad \qquad \beta_0 = \frac{G(1-\Phi)}{\rho_0 D_P \Phi^3} \times [\frac{150 \times (1-\Phi) \times \mu}{D_P} + 1.75 \times G]$

P = pressure [Pa]

z = Length of the catalyst bed [m]

G = Superficial velocity [kg/(m min)]

Φ = Porosity
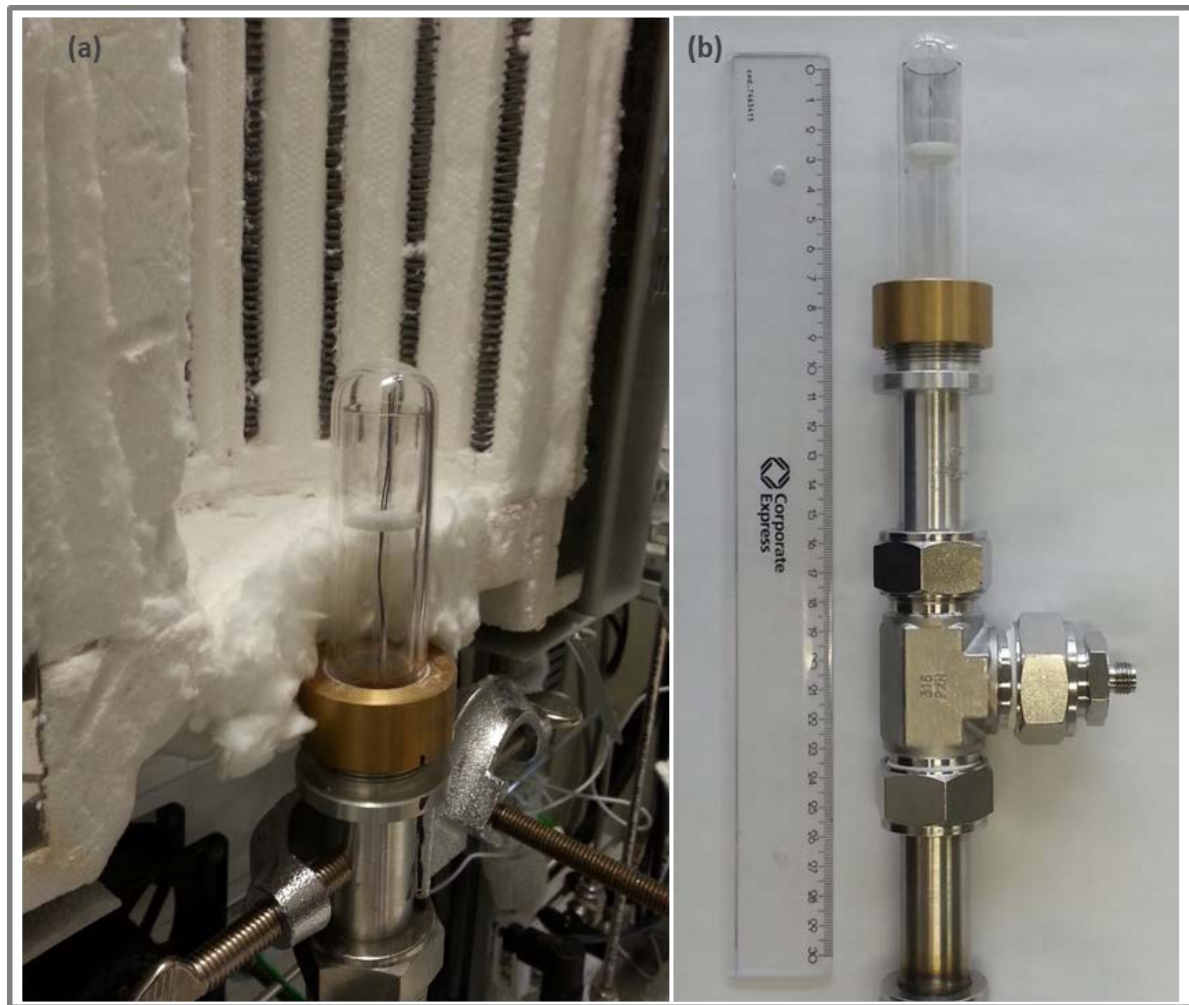
ρ = Density [kg/(m^3)]
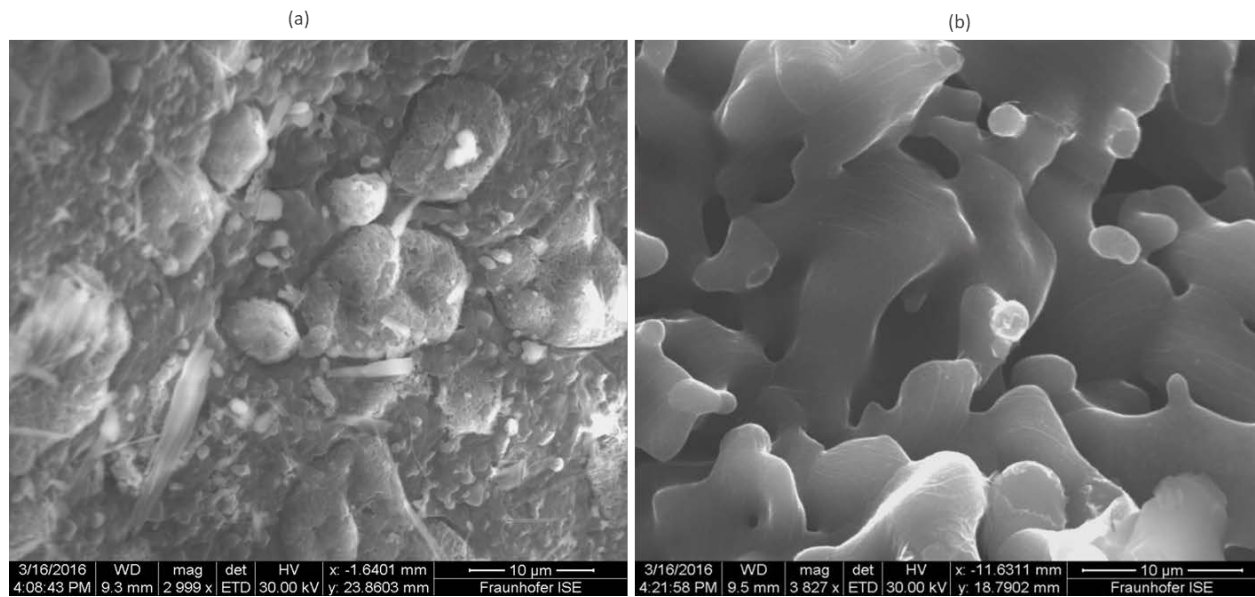
D$_p$ = Lower limit of catalyst particle size [m]

μ = Viscosity [kg/(m min)]

Photographs of the ACCR with relative dimensions

Fig. S9 Demonstration of the ACCR as installed in the electrically heated oven (a) and with relative dimensions as shown in (b)

Na₂CO₃ Catalyst Characterization

Fig. S10 SEM analysis for Na$_2$CO$_3$ catalyst with D_p = 400-800 µm (a) before test; (b) After test

References

1. N. Schmitz, F. Homberg, J. Berje, J. Burger and H. Hasse, *Ind. Eng. Chem. Res.*, 2015, **54**(25), 6409.
2. K. Schwister and V. Leven, eds., *Verfahrenstechnik für Ingenieure*, 2012.